(2)

SHOCK WAVE/TURBULENT BOUNDARY LAYER INTERACTION IN HIGH-REYNOLDS-NUMBER HYPERSONIC FLOWS

M.S. Holden
Calspan-UB Research Center

A.G. Havener
SUNY at Binghamton, NY

C.H. Lee
SUNY at Buffalo, NY

AFOSR-TR- 87-1587

July 1987

Annual Report

Approved for Public Release;
Distribution Unlimited

Prepared for:

USAF/AFSC/AFOSR
Directorate of Aerospace Sciences
Bolling AFB, DC 20332-6448

UNCLASSIFIED
SECURITY CLASSIFICATION OF THIS PAGE

REPORT DOCUMENTATION PAGE

1a. REPORT SECURITY CLASSIFICATION UNCLASSIFIED	1b. RESTRICTIVE MARKINGS
2a SECURITY CLASSIFICATION AUTHORITY	3 DISTRIBUTION / AVAILABILITY OF REPORT Approved for Public Release Distribution is Unlimited
2b. DECLASSIFICATION / DOWNGRADING SCHEDULE	
4. PERFORMING ORGANIZATION REPORT NUMBER(S) CUBRC REPORT NO. 86681	5. MONITORING ORGANIZATION REPORT NUMBER(S) AFOSR-TR- 87-1587
6a. NAME OF PERFORMING ORGANIZATION Calspan-UB Research Center 6b OFFICE SYMBOL (If applicable)	7a. NAME OF MONITORING ORGANIZATION AFOSR/Directorate of Aerospace Sciences
6c. ADDRESS (City, State, and ZIP Code) 4455 Genesse Street Buffalo, NY 14225	7b. ADDRESS (City, State, and ZIP Code) Building 410 Bolling AFB, DC 20332-6448
8a. NAME OF FUNDING / SPONSORING ORGANIZATION AFOSR 8b. OFFICE SYMBOL (If applicable) NA	9. PROCUREMENT INSTRUMENT IDENTIFICATION NUMBER F49620-85-C-0130
8c. ADDRESS (City, State, and ZIP Code) AFOSR/ NA Bolling AFB, DC 20332	10. SOURCE OF FUNDING NUMBERS PROGRAM ELEMENT NO. 61102F PROJECT NO. 2307/A1 TASK NO. A1 WORK UNIT ACCESSION NO.

11 TITLE (Include Security Classification)
Shock Wave/Turbulent Boundary Layer Interaction in High-Reynolds-Number Hypersonic Flows

12 PERSONAL AUTHOR(S)
M.S. Holden, Calspan-UB Research Center; A.G. Havener, SUNY at Binghamton, N.Y.; C.H. Lee, SUNY at Buffalo, N.Y.

13a. TYPE OF REPORT	13b. TIME COVERED	14. DATE OF REPORT (Year, Month, Day)	15. PAGE COUNT
Annual	FROM 1/9/85 TO 30/9/86	~~86,6,30~~ July 87	116

16. SUPPLEMENTARY NOTATION

17. COSATI CODES			18. SUBJECT TERMS (Continue on reverse if necessary and identify by block number)
FIELD	GROUP	SUB-GROUP	3D flow separation, hypersonic flow, laser holography

19. ABSTRACT (Continue on reverse if necessary and identify by block number)

a 96 inch

This report summarizes the research conducted under contract F49620-85-C-0130 for USAF/AFSC/AFOSR from 1 August 1985 through 30 August 1986. We investigated fundamental aerothermal phenomena in hypersonic flow, with particular emphasis on viscous/inviscid interaction phenomena. The experimental studies were conducted to examine the changes in the structure at the base of a hypersonic turbulent boundary layer as it is subjected to a strong self-induced pressure gradient in regions of shock wave/boundary layer interaction. The initial phase of the theoretical program was directed toward summarizing existing techniques for obtaining Navier/Stokes solutions for laminar flow over flat plates in hypersonic flow. In the experimental program, surface and flow field measurements were made to examine the detailed flow mechanics associated with turbulent boundary layer separation over a large cone flare model at Mach numbers 11, 13 and 16 and Reynolds numbers up to 100×10^6. Holography measurements were used to examine the flow field regions of hypersonic shock wave/turbulent boundary layer interaction. In this preliminary investigation of the application of holography in Calspan's 96" Shock Tunnel, holographic interferograms were obtained for viscous/inviscid interactions at Mach numbers of 11 and 13 and Reynolds numbers up to 30×10^6, nominally. Flow field studies were made for flat plate/wedge, cone/flare and incident shock configurations. The quantitative results presented offer new information as well as a potential to obtain density measurements in other types of hypersonic flows; however, they also reveal important concerns which need to be resolved before the interferometric data can be claimed to give accurate measurements of these flows. Two papers (Appendices A and B) were written and presented at international meetings during the past year including an invited review paper on aerothermal problems associated with hypersonic flight, which was supported in part by contracts through CUBRC.

20. DISTRIBUTION / AVAILABILITY OF ABSTRACT	21. ABSTRACT SECURITY CLASSIFICATION
☒ UNCLASSIFIED/UNLIMITED ☐ SAME AS RPT ☐ DTIC USERS	UNCLASSIFIED
22a NAME OF RESPONSIBLE INDIVIDUAL DR JAMES WILSON	22b TELEPHONE (Include Area Code) 202-767-4935 22c. OFFICE SYMBOL AFOSR/NA

DD FORM 1473, 84 MAR 83 APR edition may be used until exhausted
All other editions are obsolete.

SECURITY CLASSIFICATION OF THIS PAGE
UNCLASSIFIED

TABLE OF CONTENTS

LIST OF FIGURES

LIST OF FIGURES (Cont.)

LIST OF FIGURES (Cont.)

LIST OF TABLES

Section 1
INTRODUCTION

Regions of shock wave/turbulent boundary layer interaction, in which large pressure gradients, flow separation and turbulent nonequilibrium flows are generated, have traditionally been the testing ground of prediction techniques, particularly based on the solution of the full Navier-Stokes equations where the recirculating flow can be handled "more exactly." However, despite the significant advances in computational techniques during the past decade, there remain significant gaps in our understanding and ability to predict regions of shock wave/turbulent boundary interactions in hypersonic flows. At the heart of the problem lies the difficulty of describing the generation and development of turbulence in the extremely large pressure gradients developed across hypersonic interaction regions. However, many of the problems that have been blamed on poor turbulence modeling may in fact stem from the grid selection or nature of the numerical scheme. In the rush to demonstrate that the Navier-Stokes codes can be successfully applied to describe a variety of interaction problems, very little emphasis has been placed on the demonstration that the numerical schemes are indeed an accurate representation of the equations upon which they are based. At a minimum, the sensitivity to grid size should be examined, and, particularly for turbulent interacting flows, an analysis of the characteristic scale lengths, like that employed in triple deck theory, should be performed to aid in grid positioning.

The complexity of turbulent interaction regions makes it essential that detailed information from experiments be used to construct realistic models of the turbulent transport mechanisms. The harsh aerothermal environment in hypersonic turbulent interacting flows makes delicate probing of these flows difficult, and because the typical natural frequencies in these flows are of the order of 500 kHz, the instrumentation and recording requirements for capturing fluctuating features of the flow are far from simple. While skin friction and heat transfer measurements are useful in the evaluation of turbulence modeling techniques, employing comparisons with surface pressure data to support the models used in a Navier-Stokes code is a weak verification.

The complexity of the flow field in regions of shock wave/turbulent boundary layer interaction is such that it is unrealistic to expect to describe such regions in any detail within the framework of the boundary layer equations. Indeed, there are some who would question whether the time- or mass-averaged Navier-Stokes equations capture

the basic fluid mechanics associated with the intrinsically unsteady nature of separated regions. In hypersonic flows, the effects of compressibility on the structure and development of turbulence must also be considered.

While there have been strenuous efforts to obtain predictions of two-dimensional and three-dimensional turbulent interaction regions, it is currently recognized that "successes" with the "Navier-Stokes" code in describing some three-dimensional turbulent interaction regions are a result of the dominance of the pressure and inertial terms in these flows. In two recent studies,[1,2] it was shown that turbulence modeling could be changed signficantly without significantly changing the numerical solution for a three-dimensional interaction region. For two-dimensional interactions, it appears that turbulence modeling is more critical. To obtain good agreement for these latter flows, some very gross assumptions must be made in the turbulence model. Shang and Hankey[3], for example, chose to apply an empirical relationship (selected by matching the length of the separated region) to rapidly decrease the turbulent scale size through the interaction region. Horstmann[4], however, found the best agreement with Settles[5] measurements in wedge-induced separated regions using a two-equation model for turbulence scale size and vorticity. Working with this same turbulence model, however, Horstmann was unable to predict the occurrence of separation on two incident shock/turbulent boundary layer configurations studied by Holden[6] at Mach 11.2. In the latter studies, for flows which were clearly separated, the numerical solution failed to predict the characteristic plateaus in either the heat transfer or pressure distributions. The modeling of turbulence in separated interaction regions at hypersonic Mach numbers should account for the effects of compressibility and the generation of turbulence by the unsteady movement of the incident and induced shocks as they traverse and interact with a major region of the turbulent boundary layer and the unsteady movement of the separated region. Clearly, further detailed experimental work on insightful theoretical modeling is required to develop numerical prediction techniques which are capable of describing separated turbulent interaction regions in hypersonic flow.

In this report, Section 2 describes the use of "parabolized" (or "thin-layer") Navier-Stokes equations to solve turbulent flow equations and existing differing schemes to solve Navier-Stokes equations. Section 3 describes how models and instruments were developed and used to obtain detailed measurements of the profile characteristics of a turbulent boundary layer ahead of and through regions of flow separation induced by shock wave/boundary layer interaction over a cone/flare configuration. Section 4

presents the results of the application of laser holography to measure viscous flow interactions in hypersonic shock tunnel flows. Section 5 summarizes the research conducted under the current contract to investigate fundamental problems associated with flight at hypersonic speeds with emphasis placed on aerothermal effects of viscous/inviscid interactions and boundary layer transition. Section 6 provides a list of references. Two appendices provide copies of papers on aerothermal problems associated with hypersonic flight that were presented by Dr. M.S. Holden at the AIAA 24th Aerospace Science Meetings.

Section 2
SUMMARY OF EXISTING SOLUTION TECHNIQUES

2.1 INTRODUCTION

While the Navier-Stokes equations were formulated nearly 140 years ago, only recently has computational speed increased enough to handle the entire set of simultaneous differential equations. Even with the advent of the new generation "super" computers (e.g., CRAY1, CRAYXMP, CDC7600, new generation array processors, etc.), economics remains a major consideration. Chapman[7], however, notes that the cost of these types of calculations has been decreasing by a factor of ten every eight years. It may be just a matter of time before these types of large numerical simulations are of some consequential value to practical engineering problems.

In most turbulent flow applications, the Navier-Stokes equations are simplified by Reynolds time averaging. We are then faced with the difficult task of developing a model for turbulence. There have been many approaches to the turbulent closure problem, from simple algebraic closure to various two-equation models (e.g., k-e, k-w, see Anderson and Tannehill[8], Tennekes and Lumley[9], Jones and Launder[10]), and the Reynolds stress equations. The lack of progress is threefold. One, we lack the physical understanding to model these complex turbulent flows. Two, we lack the computational resources to deal with so-called higher order turbulence models, which add nine more unknowns (in an incompressible flow) and two or three more equations. Three, we still lack the ability to solve the laminar portion of the Navier-Stokes equations in an efficient and accurate manner. Most existing differencing schemes (which will be discussed here) are second-order accurate with various restrictions applied by the numerical stability.

There are several levels of complexity of Navier-Stokes equations which fall between a full Navier-Stokes equation (Figure 1) and a boundary layer equation. Common names for these types of equations are "parabolized" Navier-Stokes equations and "thin-layer" Navier-Stokes equations. These sets of equations are characterized by their applicability in both viscous and inviscid flow regions; they all contain the normal pressure terms which are usually dropped in any boundary layer formulation.

To arrive at the thin layer approximation shown in Figure 1, a scaling argument is used (see Anderson and Tannehill[8]), and terms on the order of $1/Re_L$ and smaller are neglected. All viscous terms containing derivatives parallel to the wall are dropped because they are substantially smaller than those viscous terms normal to the wall. If this same argument were to be used for the normal (y) direction, the equation could be reduced to dp/dy=0. For this approximation to handle a possible flow reversal, it is necessary to retain all terms in the momentum equations except for the viscous terms parallel to the flow (the upstream diffusion terms). The final set of equations is as shown in Figure 1, in the Cartesian coordinate system. This mixed set of hyperbolic-parabolic partial differential equations is solved instead of the elliptic-hyperbolic partial differential equations, using a "time-dependent" approach. The overall complexity of the equations is reduced, but the difficulty of solving a hyperbolic system still remains.

The parabolized Navier-Stokes equations are derived using an argument similar to that employed to derive the thin-layer equations. An asymptotic expansion (see Karvorkin and Cole[11]) is performed (Rudman and Rubin[12]) with the Navier-Stokes equations, and all of the terms exhibiting characteristic order of magnitude of $(1/\delta^{*2})$ or higher are retained. The normal pressure gradient terms are deleted from the x-momentum equation, which restricts the solutions of the flows without upstream influences. The most commonly used form of the parabolized Navier-Stokes equations (formulated by Cheng[13]) contains the streamwise pressure gradient term. Thus, the most common form of this type of equation is obtained by assuming that only the streamwise viscous derivative terms and the heat flux terms are negligible compared to the normal transverse viscous derivative terms. The parabolized Navier-Stokes equations are derived by dropping all viscous and heat flux terms containing partial derivatives with respect to the streamwise direction, from a steady Navier-Stokes equation. A set of parabolized Navier-Stokes equations is shown in Figure 1.

2.2 COMPARISONS WITH MEASUREMENTS IN HYPERSONIC FLOW

The majority of the efforts made in the numerical simulations at CUBRC were geared toward understanding and utilizing existing differencing schemes for solving the Navier-Stokes equations. The initial efforts included obtaining a code that utilized an explicit type of differencing scheme and running it to simulate a set of laminar shock/boundary layer interaction problems. The MacCormack-Shang-Hankey code was obtained from J. Shang of Wright-Patterson AFB. It is a straightforward application

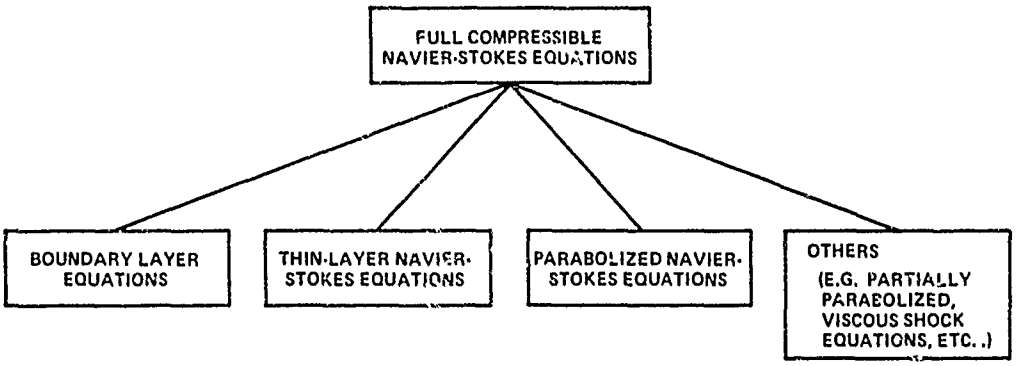

COMPRESSIBLE NAVIER-STOKES EQUATIONS*

$$\frac{\partial U}{\partial t} + \frac{\partial E}{\partial x} + \frac{\partial F}{\partial y} = 0$$

$$U = \begin{matrix} \rho \\ \rho u \\ \rho v \\ E_t \end{matrix}$$

$$E = \begin{matrix} \rho u \\ \rho u^2 + P - \tau_{xx} \\ \rho uv - \tau_{xy} \\ (E_t + P)u - u\tau_{xx} - v\tau_{xy} + q_x \end{matrix}$$

$$F = \begin{matrix} \rho v \\ \rho uv - \tau_{yy} \\ \rho v^2 + P - \tau_{yy} \\ (E_t + P)v - u\tau_{xy} - v\tau_{yy} + q_y \end{matrix}$$

$$\tau_{xx} = \frac{2}{3}\mu\left(2\frac{\partial u}{\partial x} - \frac{\partial v}{\partial y}\right)$$

$$\tau_{yy} = \frac{2}{3}\mu\left(2\frac{\partial v}{\partial y} - \frac{\partial u}{\partial x}\right)$$

$$\tau_{xy} = \tau_{yx} = \mu\left(\frac{\partial v}{\partial y} + \frac{\partial u}{\partial x}\right)$$

$$q_y = -K\frac{\partial T}{\partial y}$$

$$q_x = -K\frac{\partial T}{\partial x}$$

$$E_t = \left(P + \frac{U^2 + v^2}{2}\right)$$

THIN-LAYER NAVIER-STOKES EQUATIONS*

$$\frac{\partial U}{\partial t} + \frac{\partial E}{\partial x} + \frac{\partial F}{\partial y} = 0$$

$$U = \begin{matrix} \rho \\ \rho u \\ \rho v \\ E_t \end{matrix}$$

$$E = \begin{matrix} \rho u \\ \rho u^2 + P \\ \rho uv \\ (E_t + P)u \end{matrix}$$

$$F = \begin{matrix} \rho v \\ \rho uv - \mu\frac{\partial u}{\partial y} \\ \rho v^2 + P - \frac{4}{3}\mu\frac{\partial v}{\partial y} \\ (E_t + P)v - u\left(\mu\frac{\partial u}{\partial y}\right) \\ \quad - v\left(\frac{4}{3}\mu\frac{\partial v}{\partial y}\right) - K\frac{\partial T}{\partial y} \end{matrix}$$

– ASSUMPTION MADE WAS THAT ALL VISCOUS TERMS CONTAINING DERIVATIVES PARALLEL TO THE WALL ARE DROPPED.

PARABOLIZED NAVIER-STOKES EQUATIONS*

$$\frac{\partial E}{\partial x} + \frac{\partial F}{\partial y} = 0$$

$$E = \begin{matrix} \rho u \\ \rho u^2 + P \\ \rho uv \\ (E_t + P)u \end{matrix}$$

$$F = \begin{matrix} \rho v \\ \rho uv - \mu\frac{\partial u}{\partial y} \\ \rho v^2 + P - \frac{4}{3}\mu\frac{\partial v}{\partial y} \\ (E_t + P)v - u\left(\mu\frac{\partial u}{\partial y}\right) \\ \quad - v\left(\frac{4}{3}\mu\frac{\partial v}{\partial y}\right) - K\frac{\partial T}{\partial y} \end{matrix}$$

– PARABOLIC TYPE OF EQUATIONS WILL NORMALLY DROP $\left(\frac{\partial P}{\partial x}\right)$ TO ACHIEVE PARABOLIC NATURE, BUT IT WAS LATER ADDED TO ACHIEVE MORE GENERAL FORMULATION.**

– NORMALLY WRITTEN IN A FORM WHERE THE VISCOUS AND INVISCID TERMS ARE SEPARATED.**

*ALL EQUATIONS ARE WRITTEN IN TWO-DIMENSIONAL FORM.

**SEE TANNEHILL (1984) FOR FURTHER DETAIL.

Figure 1 CLASSIFICATION OF NAVIER-STOKES EQUATIONS

SCHEME PROPOSED TO DATE

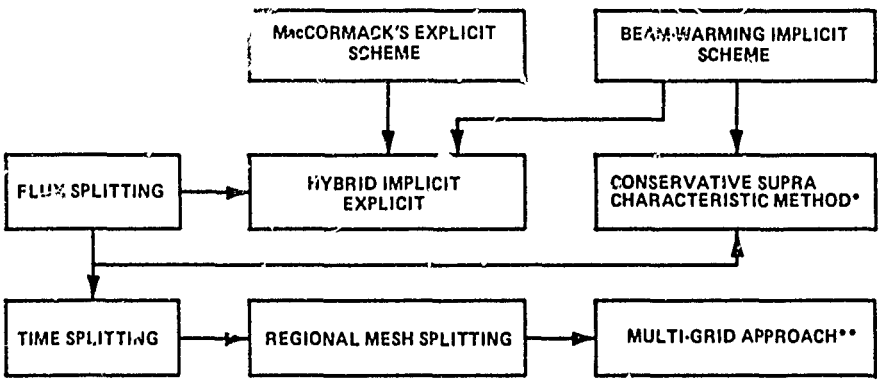

*ONLY KNOWN APPLICATION TO DATE WAS FOR THE PNS.

**APPLIED AS EULER SOLVER BY JAMESON (1986); NOT DISCUSSED IN PRESENT REPORT

***ALL METHODS ARE APPLICABLE TO BOTH FULL COMPRESSIBLE N-S EQUATIONS AND ANY OTHER SIMPLER VERSIONS OF N-S.

Figure 1 CLASSIFICATION OF NAVIER-STOKES EQUATIONS (Cont.)

of the MacCormack explicit differencing scheme, which was vectorized to use the CRAY's high-speed vector processing (Shang[14]). There were some modifications made on the pressure damping terms to handle the sharp leading edge problem.

The governing equations are in vector form:

$$\frac{\partial u}{\partial t} + \frac{\partial E}{\partial x} + \frac{\partial F}{\partial y} = 0$$

where

$$u = \begin{pmatrix} \rho \\ \rho u \\ \rho v \\ E_t \end{pmatrix} \qquad E_t = C_v T + \frac{q^2}{2}$$

$$q_x = -K\frac{\partial T}{\partial x}, \; q_y = -K\frac{\partial T}{\partial y}$$

$$E = \begin{pmatrix} \rho u \\ \rho u^2 + P - \tau_{xx} \\ \rho uv - \tau_{xy} \\ (E_t + P)u + q_x - u\tau_{xx} - v\tau_{xy} \end{pmatrix} \qquad F = \begin{pmatrix} \rho v \\ \rho uv + P - \tau_{xy} \\ \rho v^2 - \tau_{xy} \\ (E_t + P)v + q_y - u\tau_{xy} - v\tau_{yy} \end{pmatrix}$$

Then the governing equations are transformed into an orthogonal coordinate system based on generalized transformation, as proposed by Viviand[15], which made it easier to handle arbitrary geometry.

$$m = m(x, y), \; \xi = \xi(x, y)$$

$$\frac{\partial u_1}{\partial t} + \frac{\partial E_1}{\partial m} + \frac{\partial F_1}{\partial \xi} = 0$$

$$u_1 = \frac{u}{J}$$

$$E_1 = \frac{1}{J}\left(\frac{\partial m}{\partial x} E + \frac{\partial m}{\partial y} F\right)$$

$$F_1 = \frac{1}{J}\left(\frac{\partial \xi}{\partial x} E + \frac{\partial \xi}{\partial y} F\right)$$

$$J = \text{Jacobian} = \frac{\partial(m, \xi)}{\partial(x, y)} = \frac{\partial m}{\partial x}\frac{\partial \xi}{\partial y} - \frac{\partial \xi}{\partial x}\frac{\partial m}{\partial y}$$

$$= m_x \xi_y - \xi_x m_y$$

The numerical scheme applied is, as noted previously, MacCormack's[16] explicit scheme.

Predictor:
$$\overline{U}^{m+1}_{ij} = U^{m}_{ij} - \frac{\Delta t}{\Delta \eta_1}\, m_x\left(E^{m}_{i+1j} - E^{m}_{ij}\right) - \frac{\Delta t}{\Delta \xi}\, s_y\left(F^{m}_{ij+1} - F^{m}_{ij}\right)$$

Corrector:
$$U^{m+1}_{ij} = \frac{1}{2}\left[\overline{U}^{m+1}_{ij} + U^{m}_{ij} - \frac{\Delta t}{\Delta \eta}\, m_x\left(\overline{E}^{m+1}_{ij} - \overline{E}^{m+1}_{i-1j}\right) - \frac{\Delta t}{\Delta \xi}\, s_y\left(\overline{F}^{m+1}_{ij} - \overline{F}^{m+1}_{ij-1}\right)\right]$$

The numerical stability condition proposed by MacCormack[16] is also utilized by this code.

$$(\Delta t)_{CFL} \le \mathrm{Min}\left[\left|\frac{u_m}{\Delta m}\right| + \left|\frac{u_s}{\Delta s}\right| + C\sqrt{\left(\frac{m_x}{\Delta m}\right)^2 + \left(\frac{s_x}{\Delta s}\right)^2 + \left(\frac{m_y}{\Delta m}\right)^2 + \left(\frac{s_y}{\Delta s}\right)^2}\right]^{-1}$$

$$C = \sqrt{\frac{\gamma p}{\rho}}$$

The fourth-order pressure damping was used to add a dissipative control to the numerical instabilities as proposed by Shang[17].

$$< \Delta t\, \Delta m_m \frac{\partial}{\partial m_m}\left[\frac{u_m + C}{4p}\, \frac{\partial^2 p}{\partial m_m^2}\right] \frac{\partial u}{\partial m_m}$$

$$m = 1, 2 \quad , \; m_1 = m \, , \; m_2 = s$$

The turbulence model used is an algebraic model proposed by Baldwin and Lomax[18].

$$\tau_{xy} = (\epsilon + \mu)\, \frac{\partial u}{\partial y} \; ; \; q_y = -c_p\left(\frac{\mu}{Pr} + \frac{\epsilon}{Pr_t}\right)\frac{\partial T}{\partial y}$$

where: $\epsilon = \rho (KYD)^2 |\omega|$ $\quad K = 0.4$ $\quad Y =$ Normal dis.

$$D = 1 - \mathrm{Exp}\left(-Y\sqrt{\rho_w \tau_w}/26\mu_w\right)$$

Thus far, we have made a considerable effort in trying to obtain a set of solutions for Holden's[19] laminar shock/boundary layer interaction problem for which a similar type of numerical study already exists (Hung and MacCormack[20]). After a considerable amount of "extra" effort, we were able to obtain a solution for the flat plate section of the problem. These "extra" efforts include applications of two new mesh systems: one mesh system near the wall to resolve the length scale problem within the viscous layer, and the second mesh system near the leading edge of the flat plate to resolve length scales near a sharp leading edge. The leading edge mesh system was on the order of 10^{-6} feet in size, and the wall mesh system was 10^{-3} feet, which proved to be small enough to resolve all required length scales within the problem. The sharp leading edge problem is especially difficult for explicit type schemes, but unless it is resolved, the explicit calculations will not be able to proceed. The explicit schemes require that the time marching is done at the smallest length scale of the problem, as stated previously, and if the smallest length scale is not resolved, time marching will cause the numerics to overshoot the physics, resulting in a numerical instability.

Once these length scales were resolved, we were able to obtain, with considerable computational time, a set of solutions for the flat plate portion of the shock boundary interaction problem. The calculated skin friction and heat transfer data are shown in Figures 2 and 3. These figures show good agreement with Holden's early experimental data.[20A]

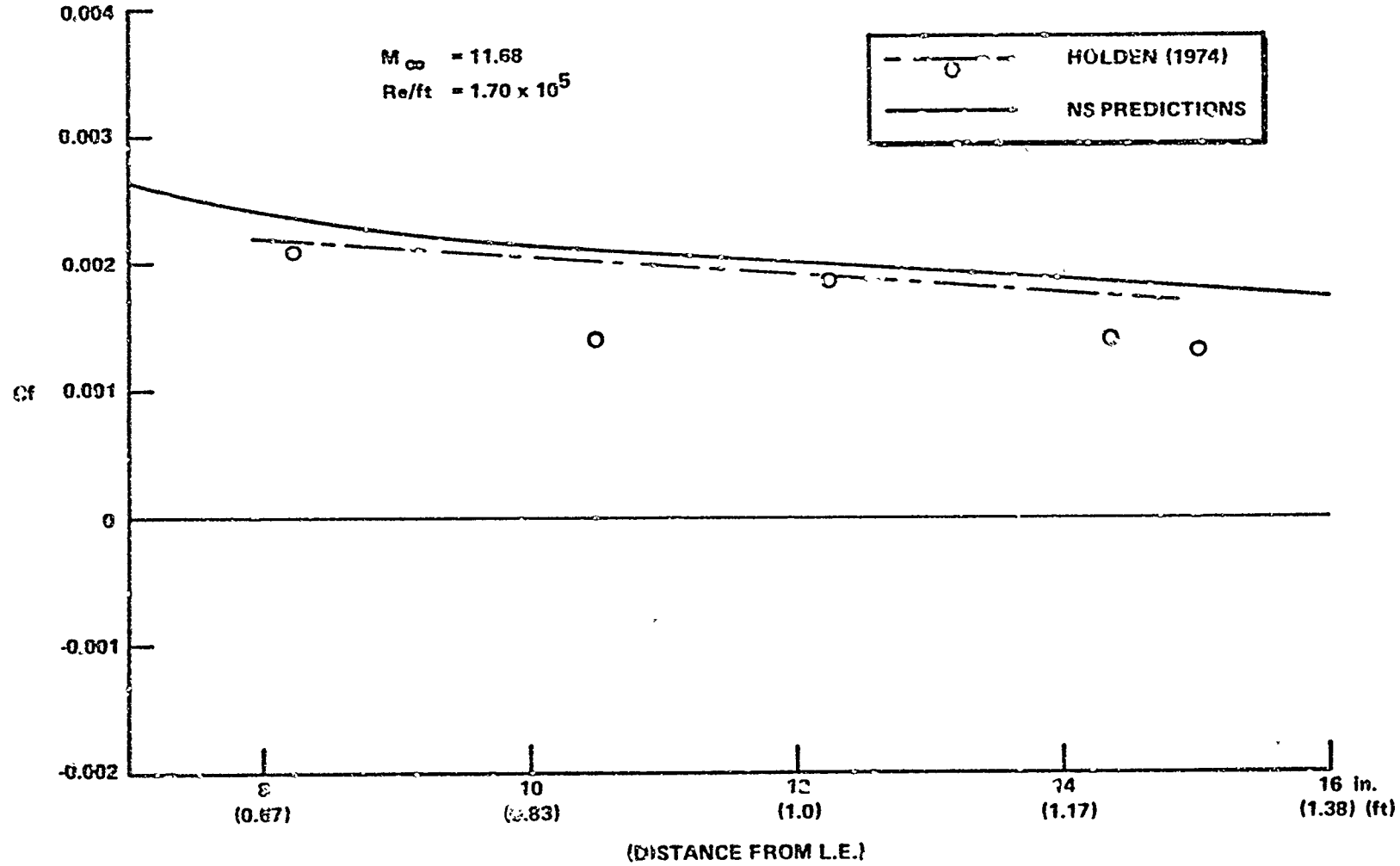

Figure 2 SKIN FRICTION COEFFICIENT DATA COMPARISON (DETAILS)

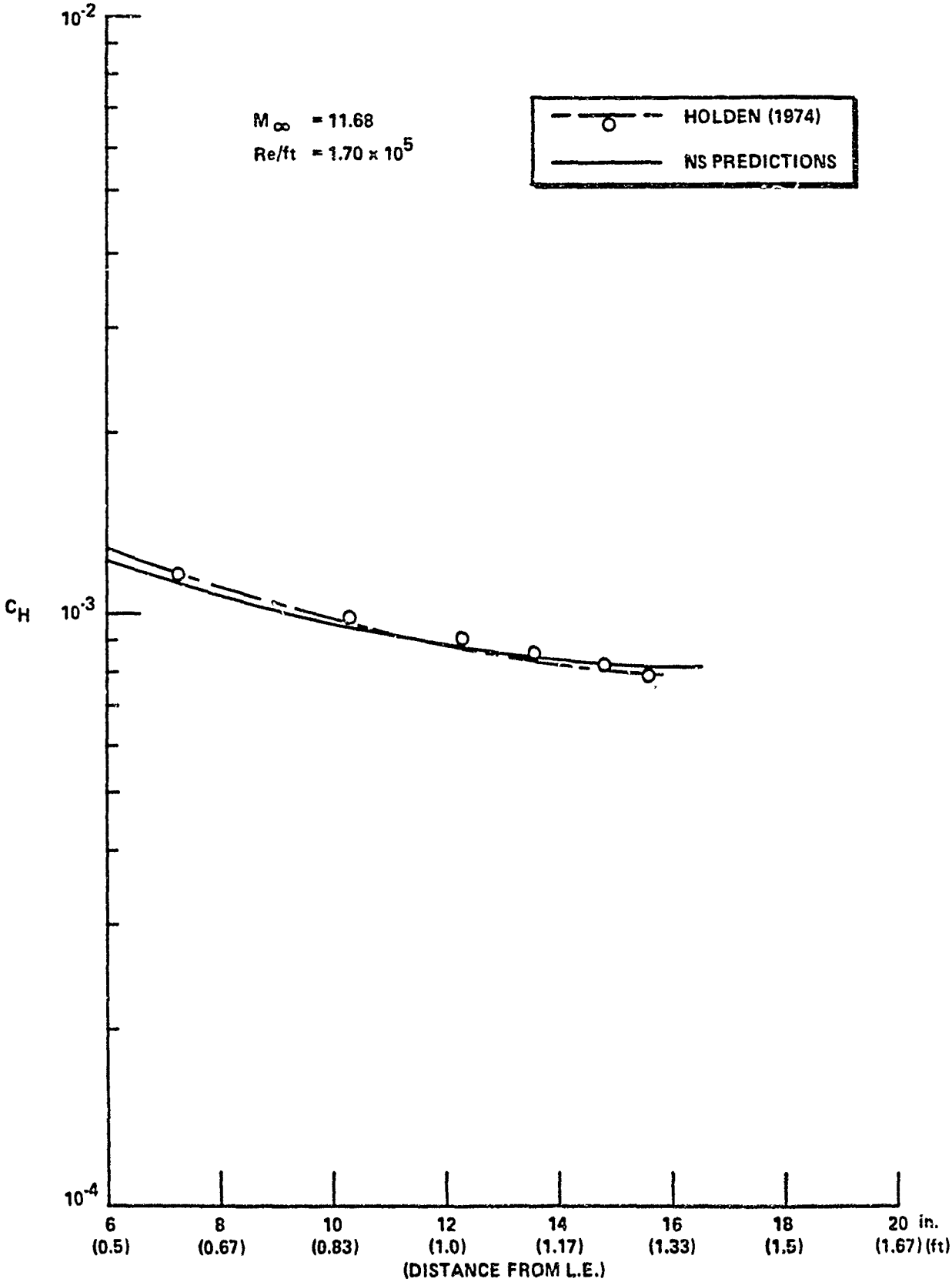

Figure 3 HEAT TRANSFER COEFFICIENT DATA COMPARISON (DETAIL)

Section 3
EXPERIMENTAL PROGRAM

3.1 PROGRAM OBJECTIVE AND DESIGN OF THE EXPERIMENTAL STUDY

The major objective of the current study was to develop and use models and instrumentation to obtain detailed measurements of the profile characteristics of a turbulent boundary layer ahead of and through regions of flow separation induced by shock wave/boundary layer interaction over a cone/flare configuration. Such measurements are of key importance in the evaluation of the theoretical modeling of the turbulent separation process in hypersonic flows. As discussed in the introduction, current turbulence models apparently are incapable of describing the d elopment of turbulence in regions of strong pressure gradients and boundary layer separation in hypersonic flow, possibly because of compressibility, shock/turbulence interaction, or unsteady effects under hypersonic highly cooled wall conditions. In hypersonic high-Reynolds-number flows over highly cooled walls, the "wall layer", in which our earlier studies have suggested separation first takes place, and which contains the principal information on the character of the boundary layer, is very thin. Consequently, boundary layer thicknesses of over one inch are required to enable this layer to be probed with the required resolution. While the turbulent boundary layers on the walls of hypersonic nozzles have been used as the source of thick turbulent boundary layers in experimental studies, it has been shown that significant turbulent nonequilibrium effects can exist in these nozzle flows[21]. The distortion of the structure and turbulent characteristics of the boundary layer generated through the strong expansion in the nozzle can persist well downstream of the nozzle exit plane and can significantly influence the characteristics of a separating turbulent boundary layer. For this reason, we elected to perform studies to examine the characteristics of the turbulent boundary ahead of and in regions of shock wave/boundary layer interaction on a large slender cone/flare configuration in the large contoured "D" nozzle in the 96-inch Shock Tunnel. The technique employed in the design of the "D" nozzle, and indeed, most contoured nozzles, is such that the test core is a cone-shaped region of uniform flow which originates well upstream of the exit plane. Thus, by designing a conical model so that it can be fit within this uniform conical region, it is possible to develop a constant pressure boundary layer over a large conical model that extends well into the contoured nozzle. The ultimate objective of this study was to obtain both mean and fluctuation measurements on the surface and across the turbulent layer. However, during this

phase of the study, we concentrated on obtaining measurements of the mean properties across the viscous layer, more specifically to obtain measurements of the pitot pressure, total temperature, total heat transfer rate and, using holographic interferometry, the mean density distribution.

3.2 MODELS AND INSTRUMENTATION

The experimental studies were conducted at Mach numbers of 11 and 13 in the large contoured "D" nozzle in the Calspan 96-inch Shock Tunnel. As discussed in subsection 3.1, the large conical region of uniform flow that extends well up into the contoured "D" nozzle allows us to generate a constant pressure boundary layer on a conical model which extends into the nozzle.

For these studies, we selected the large 6-degree cone with flares of 30 and 36 degrees attached at its base. The cone/flare configuration is shown in Figure 4. The cone angle and length were selected on the basis of calculations to achieve the maximum length over which uniform constant pressure flow could be established within the further constraints of tunnel blockage and sting loading. A diagram of the cone/flare model and its positioning within the "D" nozzle is shown in Figure 5. Previously,[21] we demonstrated that this large model could be used to produce the required flow, we obtained pressure and heat transfer measurements for this model equipped with both sharp and blunt nosetips. The good agreement between the measured pressure and heat transfer distribution and theory for these configurations, shown in Figures 6 through 9, demonstrates that the design and positioning of the model produced the required testing environment. Schlieren photographs of the flow field for these cases are shown in Figures 10 and 11.

3.2.1 Heat Transfer Instrumentation

Platinum thin-film instrumentation was used to obtain heat transfer measurements on the surface of the flat plate/cone model and as the sensing element of the 0.05-inch-diameter stagnation heating probes. Because this gage has a megahertz frequency response, it can be used to examine the unsteady characteristics of the turbulent boundary layer and separated region. The large gradients that are generated along the walls and in the flow in the separation and reattachment region of shock wave/boundary layer interactions make it essential that distortion of the heat transfer distribution

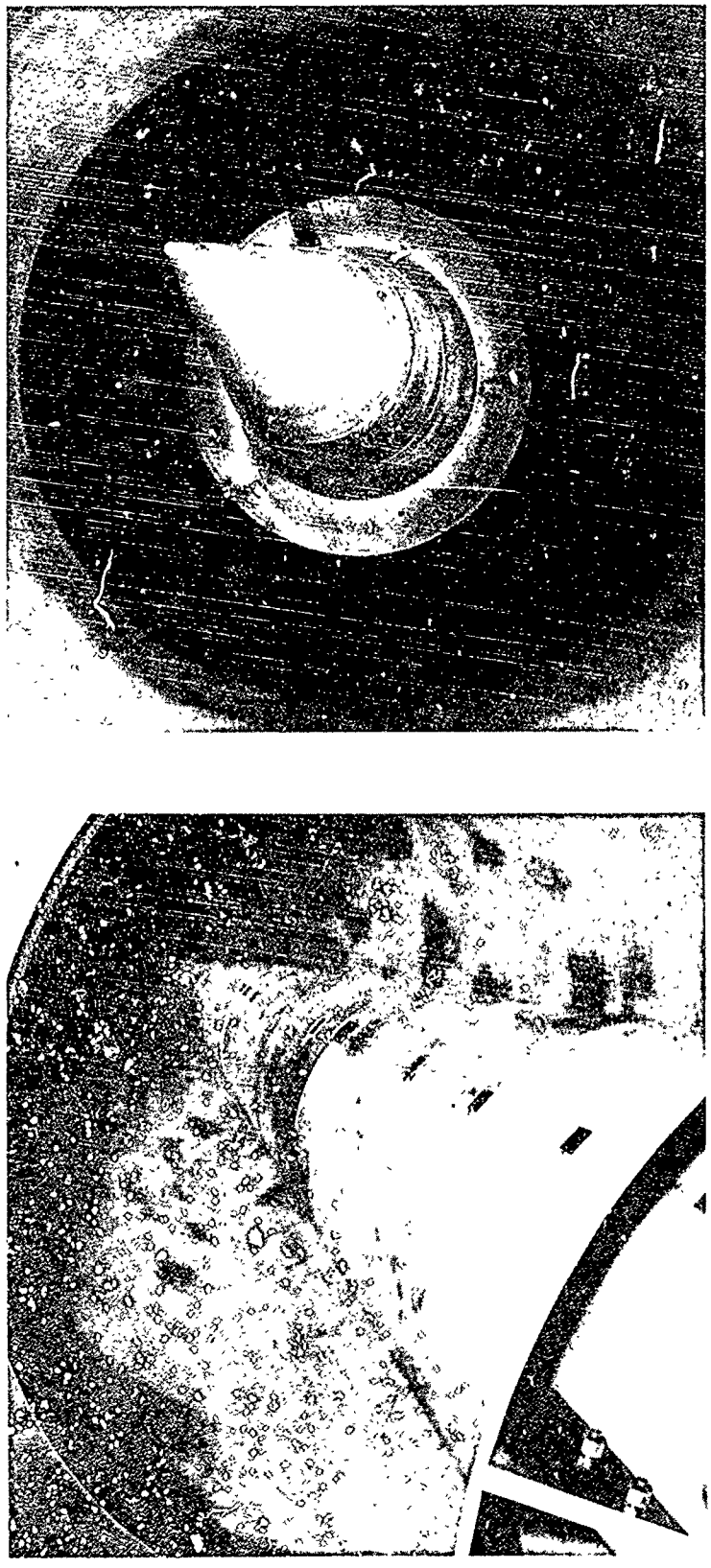

Figure 4 SHARP 6^{o} CONE/30^{o} FLARE MODEL INSTALLED IN CALSPAN'S 96" SHOCK TUNNEL

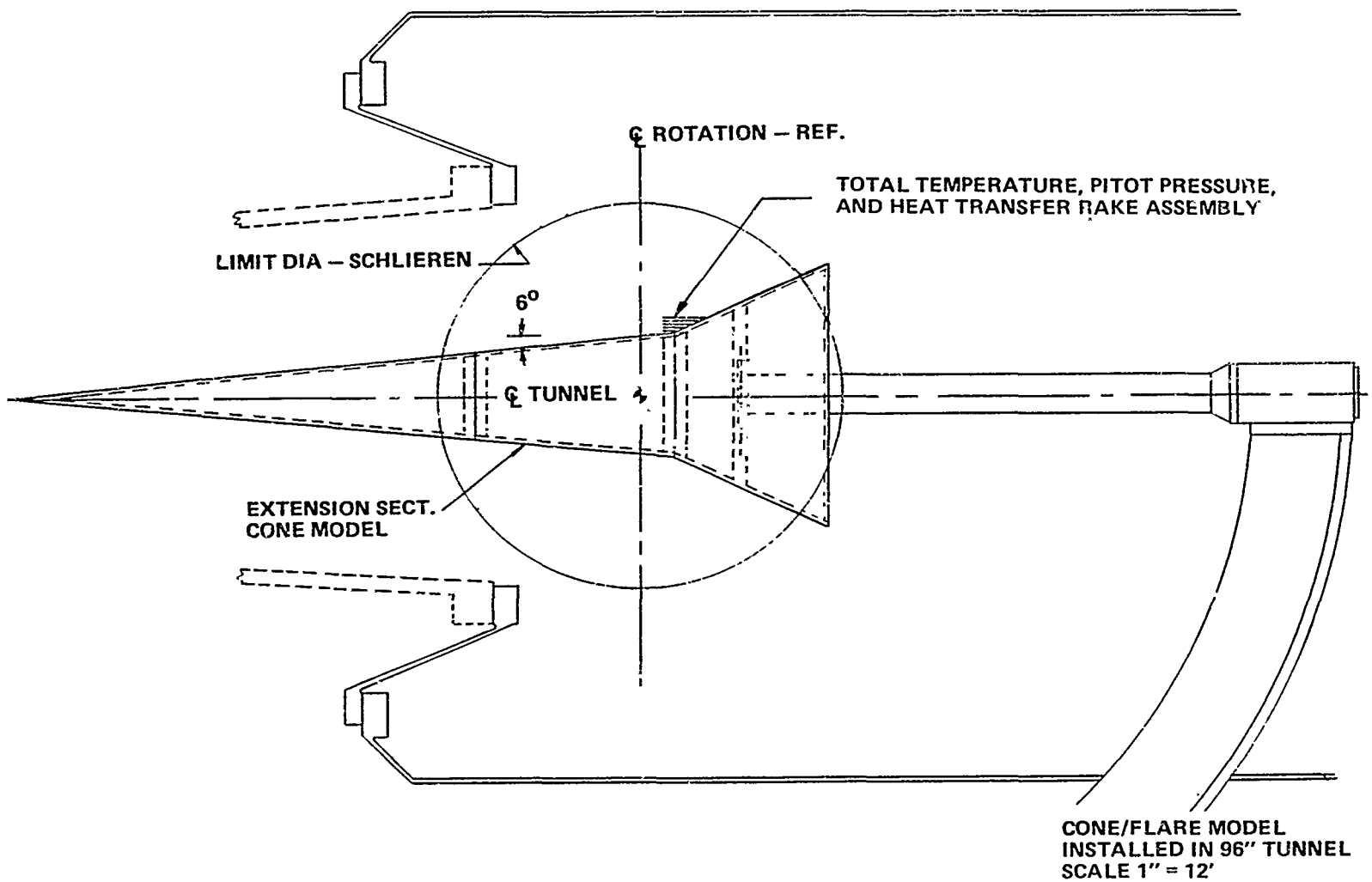

Figure 5 INSTALLATION DRAWING OF CONE/FLARE MODEL

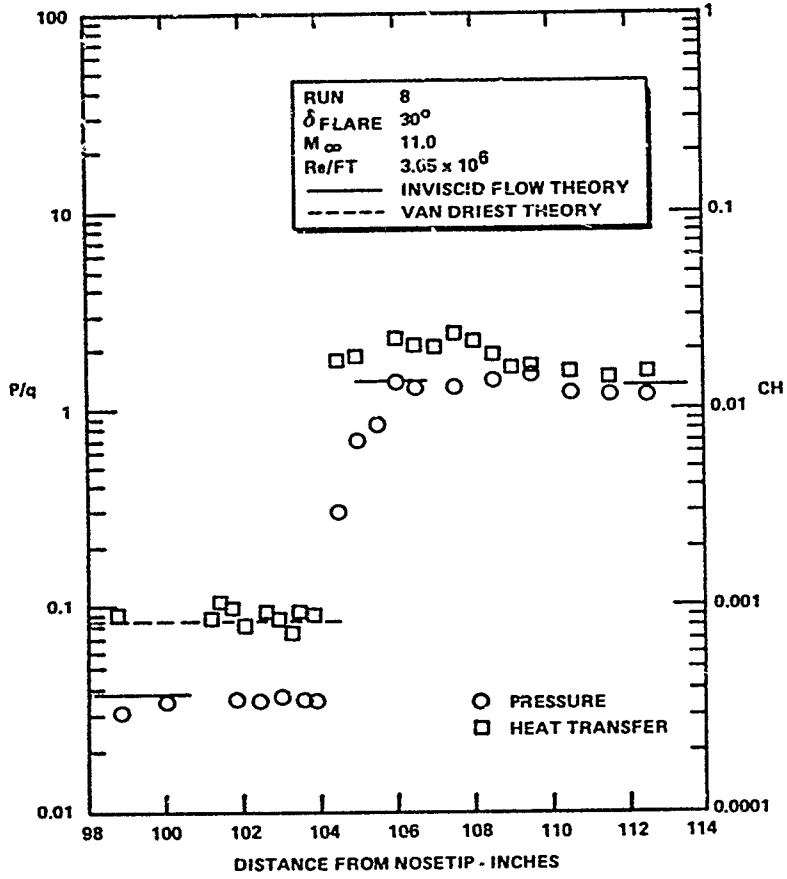

Figure 6 DISTRIBUTION OF PRESSURE AND HEAT TRANSFER IN ATTACHED FLOW OVER THE LARGE 6° CONE/30° FLARE CONFIGURATION

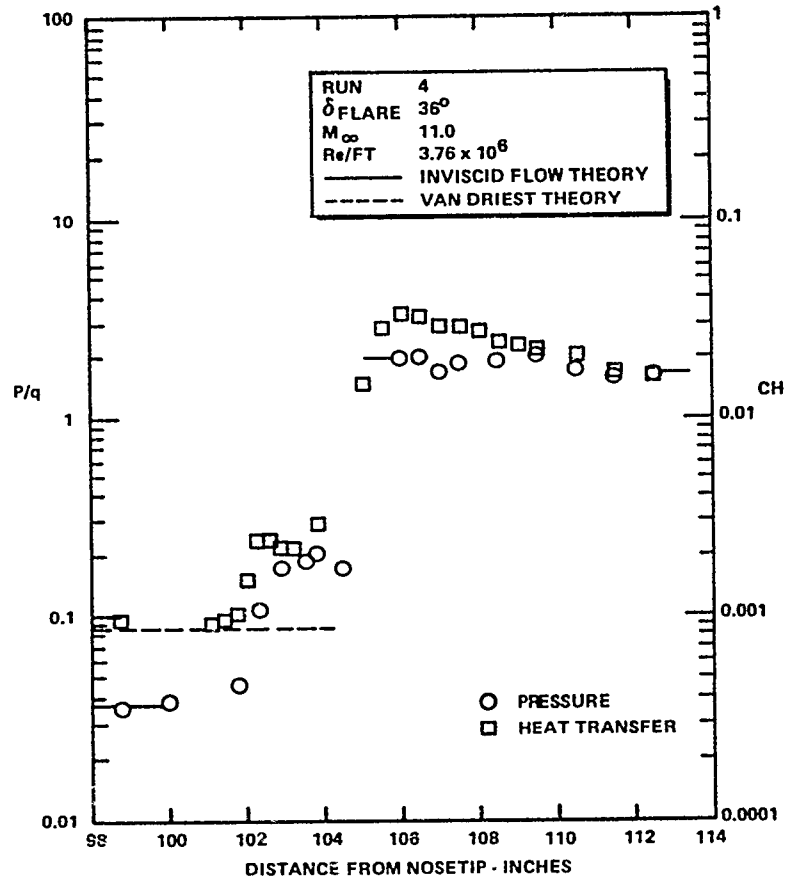

Figure 7 DISTRIBUTION OF PRESSURE AND HEAT TRANSFER IN ATTACHED FLOW OVER THE LARGE 6° CONE/36° FLARE CONFIGURATION

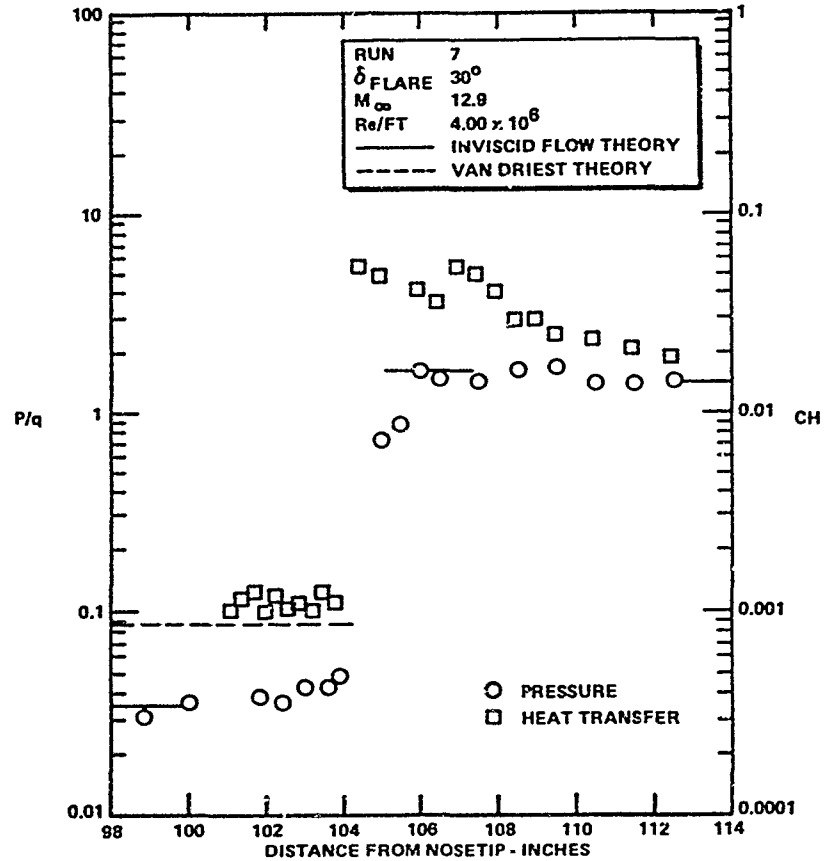

Figure 8 DISTRIBUTION OF PRESSURE AND HEAT TRANSFER IN ATTACHED FLOW OVER THE LARGE 6° CONE/30° FLARE CONFIGURATION

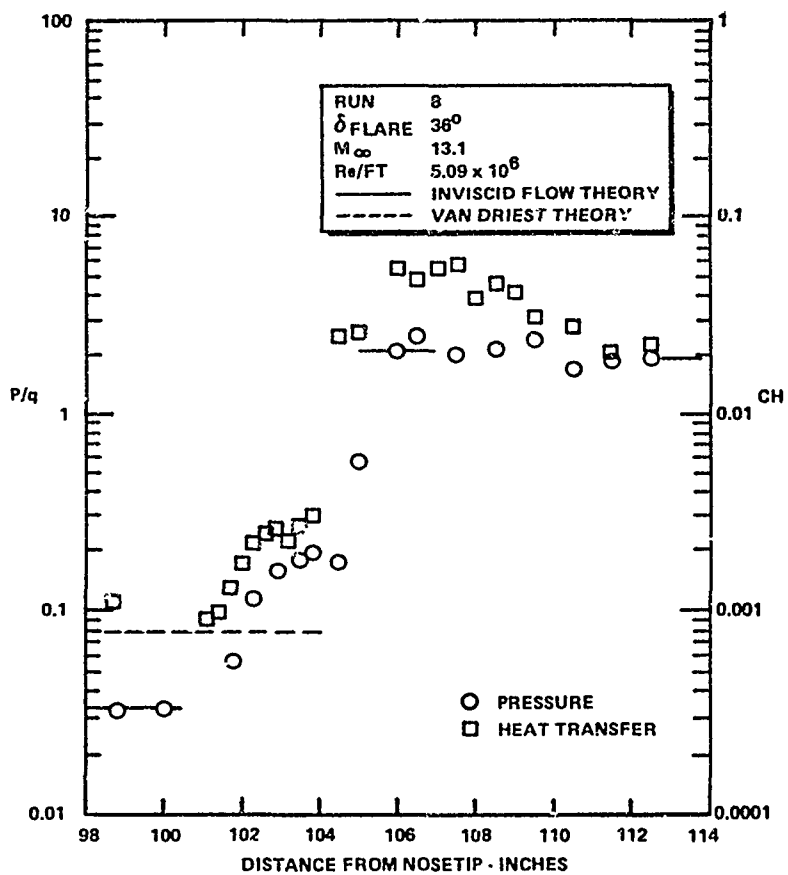

Figure 9 DISTRIBUTION OF PRESSURE AND HEAT TRANSFER IN SEPARATED FLOW OVER THE LARGE 6° CONE/36° FLARE CONFIGURATION

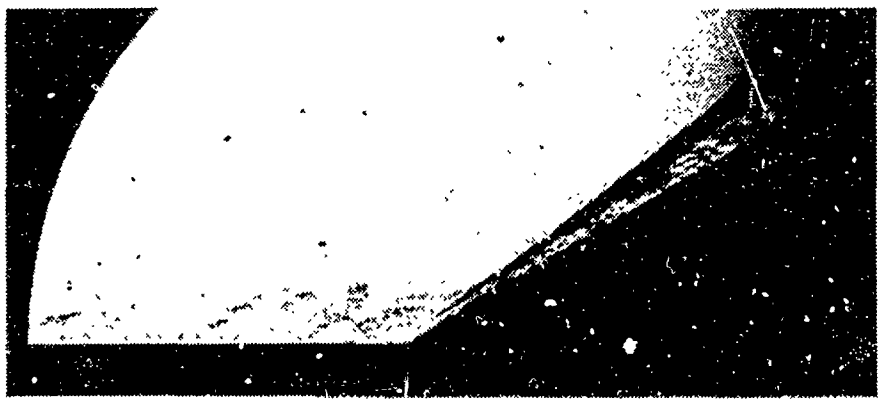

Figure 10a ATTACHED FLOW OVER CONE/FLARE CONFIGURATION, M = 11

Figure 10b SEPARATED FLOW OVER CONE/FLARE CONFIGURATION, M = 11

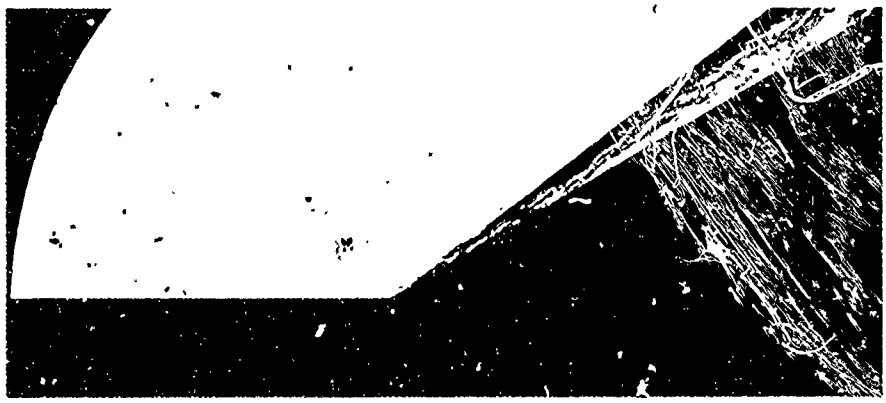

Figure 11a ATTACHED FLOW, M = 13

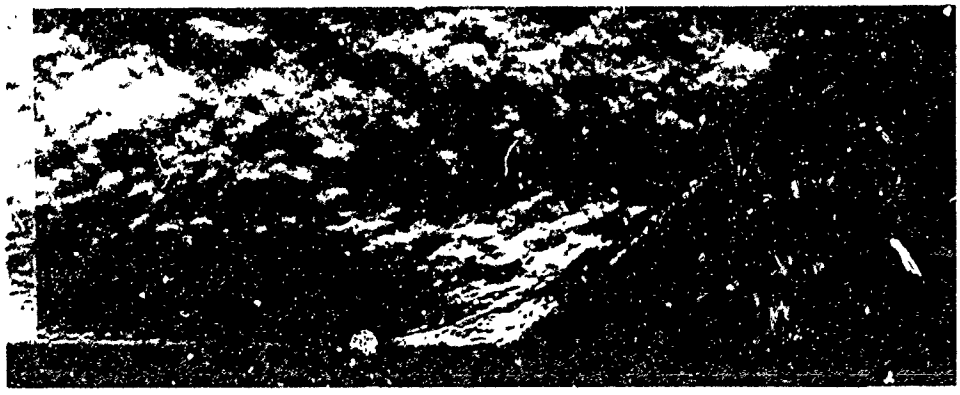

Figure 11b SEPARATED FLOW, M = 13

resulting from lateral heat conduction be minimized by employing models constructed with low conductivity materials. The pyrex-backed, thin-film gages with their high resolution, sensitivity and frequency response are almost ideal for this type of study. The platinum thin-film probes (Figure 12) were used, in conjunction with the total temperature instrumentation, to examine the structure of the turbulent boundary layer and shear layer.

3.2.2 Pitot and Static Pressure Instrumentation

We used Calspan piezoelectric pressure transducers mounted in pitot pressure rakes, beneath orifices in the model surface, to obtain the mean pitot pressure through the boundary layer and along the surface. The pitot pressure gages (Figure 12) had 0.030-inch orifices and were staggered to achieve a transverse spacing of 0.010 inch at the base of the boundary layer.

3.2.3 Total Temperature Instrumentation

A significant effort was devoted to the design and development of a total temperature gage which responded within 3 milliseconds, withstood the large static and dynamic pressures generated in regions of shock/boundary layer interaction in the shock tunnel flows, and was small enough to resolve the total temperature in the wall layer. The result of this development was a gage 0.030 inch in diameter which used a 0.0005-inch, butt-welded iron/constantin thermocouple in the arrangement shown schematically in Figure 13. The typical response of one of these gages (Figure 14) clearly shows that we have adequate time to obtain accurate measurements. A small amount ($\sim$2%) of radiation is applied and this factor is checked for measurements in the freestream where the total temperature is known accurately. The gages are deployed in a staggered array (Figure 12) similar to that employed for the pitot pressure gages.

3.2.4 Test Conditions and Model Configurations

The experimental studies were conducted at Mach 11, 13 and 16 for Reynolds numbers from 30×10^6 to 80×10^6. Under these conditions, the boundary layer is fully turbulent well upstream of the cone/flare junction and, as discussed in the following sections, the measurements of heat transfer were in good agreement with prediction

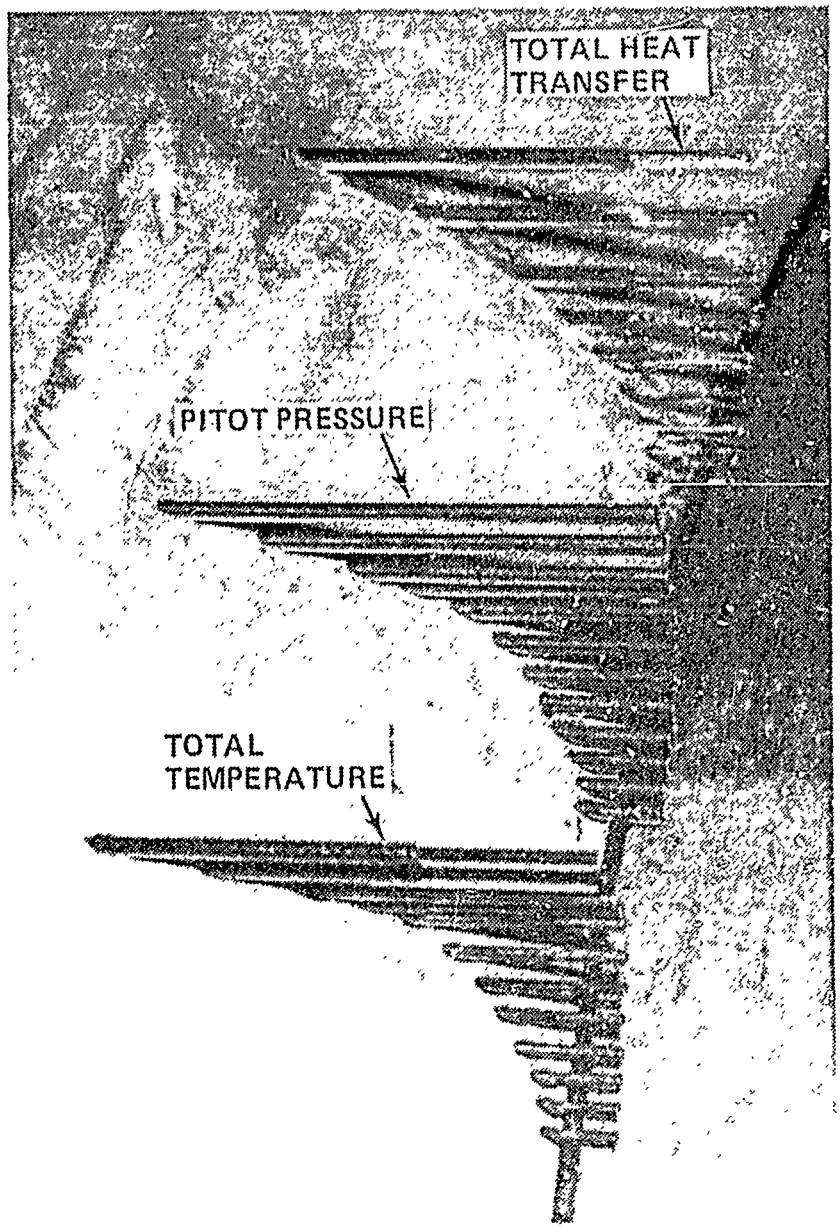

Figure 12 RAKE ASSEMBLY

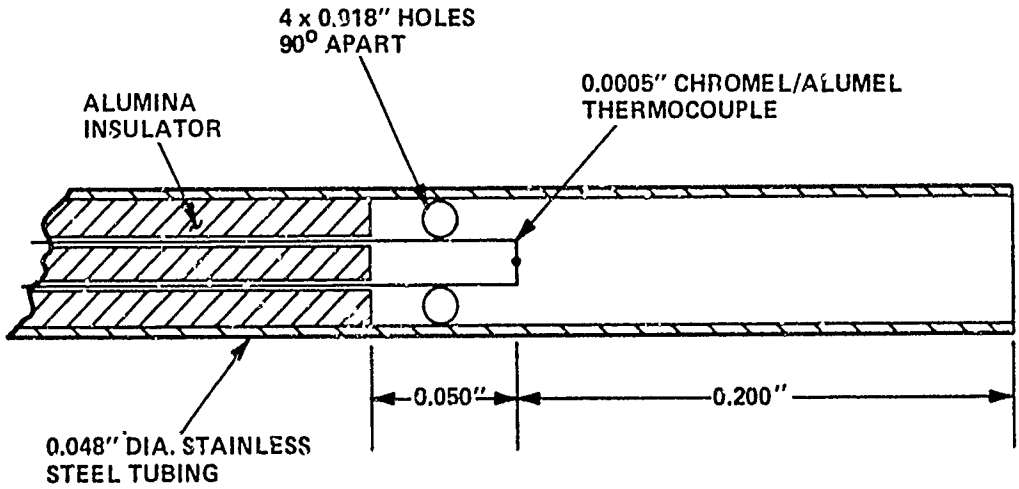

Figure 13 SCHEMATIC DIAGRAM OF TOTAL TEMPERATURE GAGE

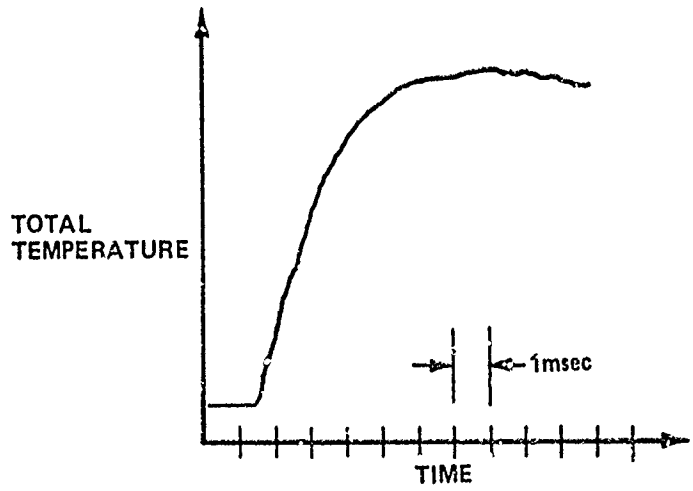

Figure 14 TYPICAL RESPONSE OF TOTAL TEMPERATURE GAGE

techniques based on a large amount of measurements on highly cooled walls in high-Reynolds-number hypersonic flows. The test conditions at which the studies were conducted are listed in Table 1.

3.3 RESULTS AND DISCUSSION

The experimental program had two objectives. First, we sought to generate a model and environment in which we could establish a thick, well-developed turbulent boundary layer that had developed under constant pressure conditions. We then sought to design, develop and use instrumentation to obtain profile measurements--first, in the constant pressure boundary layer, and then, in regions of strong adverse pressure gradient in regions of shock wave/boundary layer interaction generated at a cone/flare junction. We planned to use two cone/flare junctions: one (a 30-degree flare) which promoted a flow close to incipient separation, and a second (a 36-degree flare) which promoted a well separated flow.

The measurements of the heat transfer and pressure distributions over the two cone/flare configurations are shown in Figures 6 through 9. The corresponding schlieren photographs are presented in Figures 10 and 11. The measurements of the pressure along the entire length of the cone were in good agreement with predictions based on Sim's solutions for a sharp cone, and the pressures at the back of the flare were in good agreement with calculations based on an inviscid shock compression from the cone to the flare (Figures 7 and 8).

Flow field surveys were made to determine the distribution of pitot pressure, total temperature and total heat at a number of stations through the interaction region at each of the flow conditions described above. Figures 15 and 16 show the pitot and total temperature measurements for the Mach 11 condition with a 30-degree flare. The profiles that were obtained at 2, 1.2, 0.8, and 0 inches ahead of the cone/flare junction indicate that there is very little upstream influence at this condition. (A similar set of measurements for the 36-degree flare is shown in Figures 17 and 18.) The Mach number and velocity profiles shown in Figures 19 and 20 were determined from the inverse relationships:

Table 1

TEST CONDITIONS, LARGE 6° CONE

	AIR			N_2
RUNS	3,4,8	6,7	9	6-15
Mi	3.345E+00	3.633E+00	4.200E+00	2.635E+00
P0 PSIA	7.216E+03	1.760E+04	1.705E+04	5.430E+03
H0 FT^2/SEC^2	1.825E+07	2.147E+07	2.795E+07	1.287E+07
T0 °R	2.717E+03	3.104E+03	3.875E+03	1.939E+03
M	1.096E+01	1.301E+01	1.543E+01	1.111E+01
U FT/SEC	5.922E+03	6.458E+03	7.404E+03	4.981E+03
T °R	1.214E+02	1.026E+02	9.574E+01	8.065E+01
P PSIA	9.172E-02	7.345E-02	1.860E-02	6.698E-02
Q PSIA	7.721E+00	8.712E+00	3.104E+00	5.800E+00
RHO SLUGS/FT^3	6.340E-05	6.038E-05	1.631E-05	6.734E-05
μ SLUGS/FT·SEC	1.021E-07	8.634E-08	8.054E-08	6.783E-08
RE/FT	3.680E+06	4.544E+06	1.499E+06	4.945E+06
PITOT PSIA	1.431E+01	1.619E+01	5.798E+00	1.070E+01

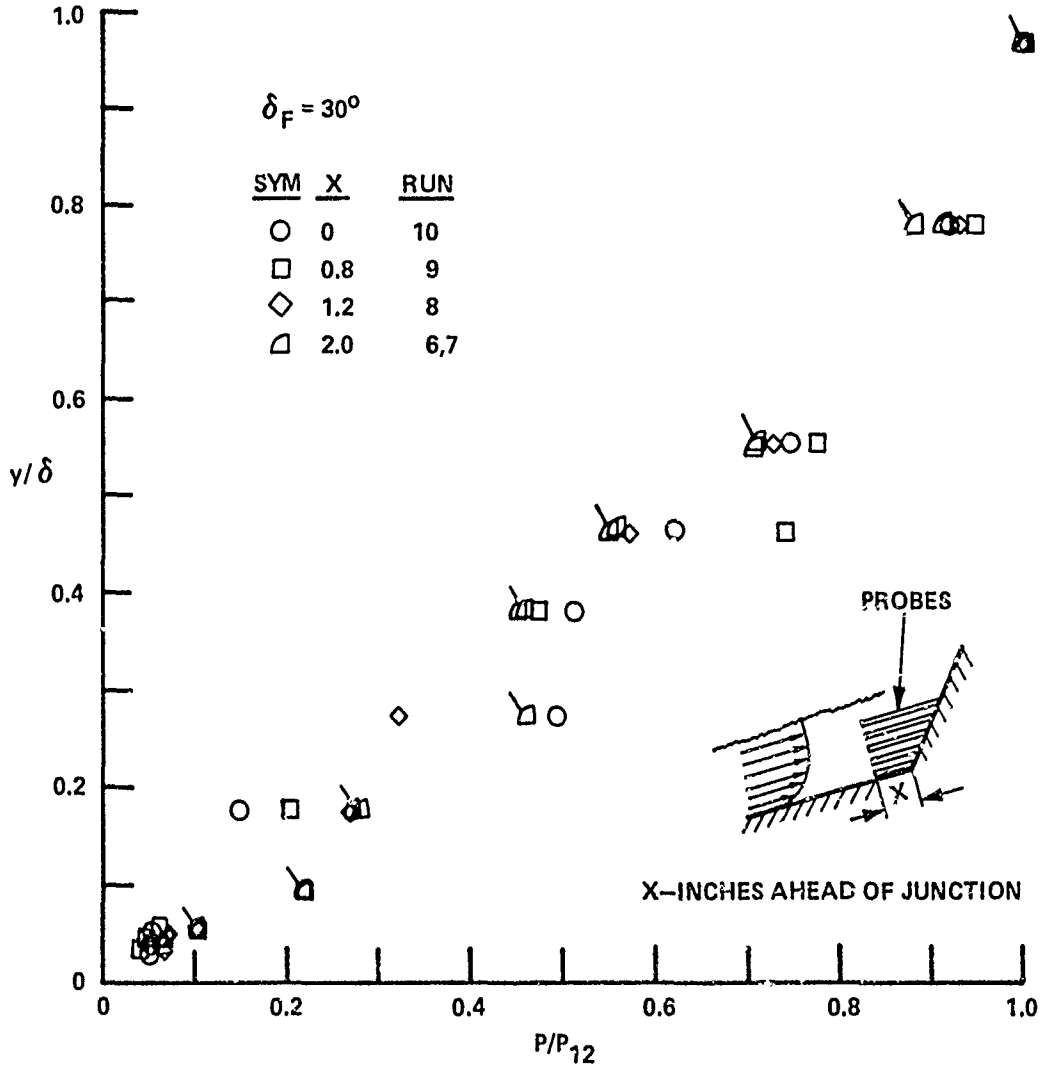

Figure 15 DISTRIBUTION OF PITOT PRESSURE ACROSS BOUNDARY LAYER UPSTREAM OF CONE/FLARE JUNCTION, 30° FLARE

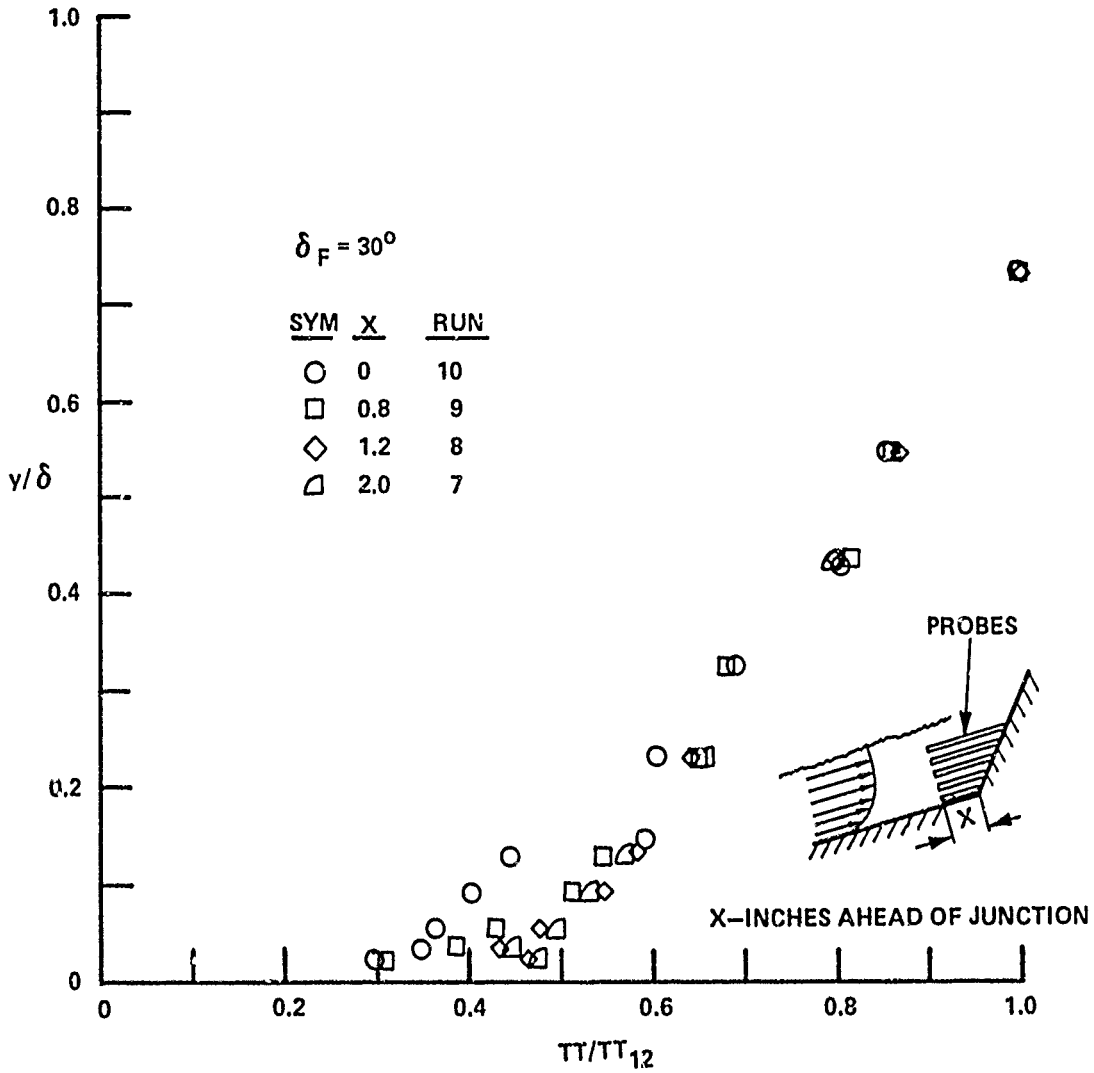

Figure 16 DISTRIBUTION OF TOTAL TEMPERATURE ACROSS BOUNDARY LAYER UPSTREAM OF CONE/FLARE JUNCTION, 30° FLARE

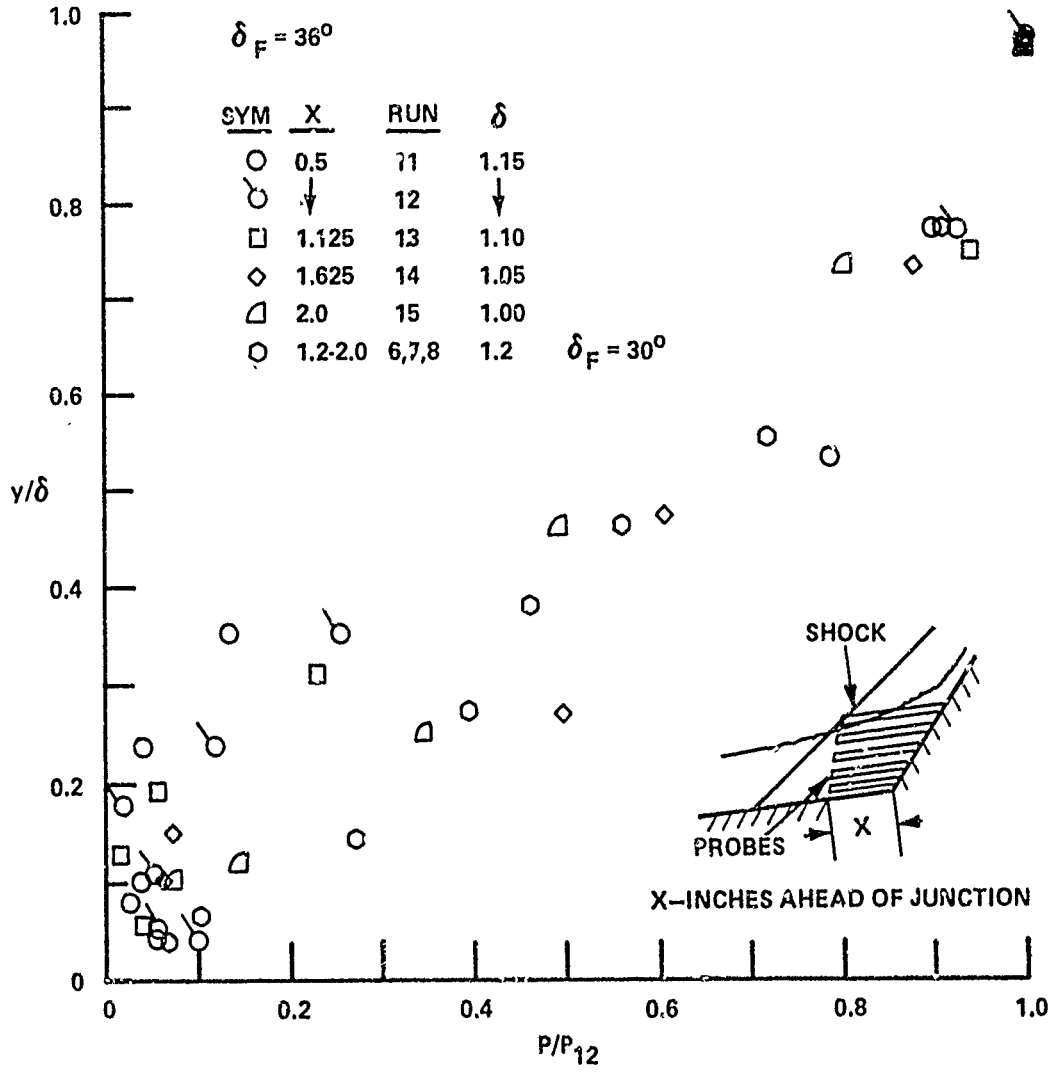

Figure 17 DISTRIBUTION OF PITOT PRESSURE ACROSS BOUNDARY LAYER UPSTREAM OF CONE/FLARE INTERACTION, 36° FLARE

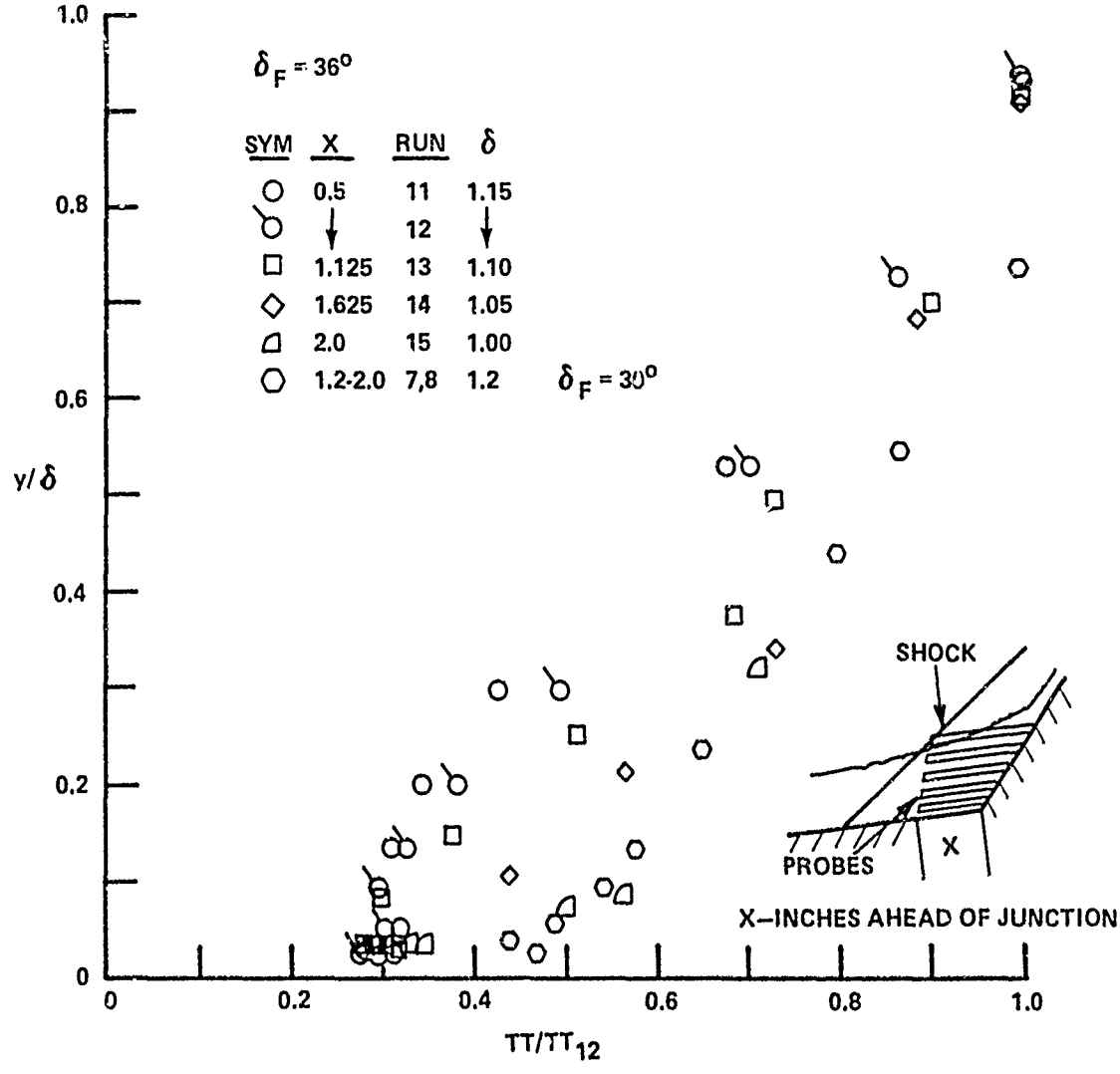

Figure 18 DISTRIBUTION OF TOTAL TEMPERATURE ACROSS BOUNDARY LAYER UPSTREAM OF CONE/FLARE JUNCTION, 36° FLARE

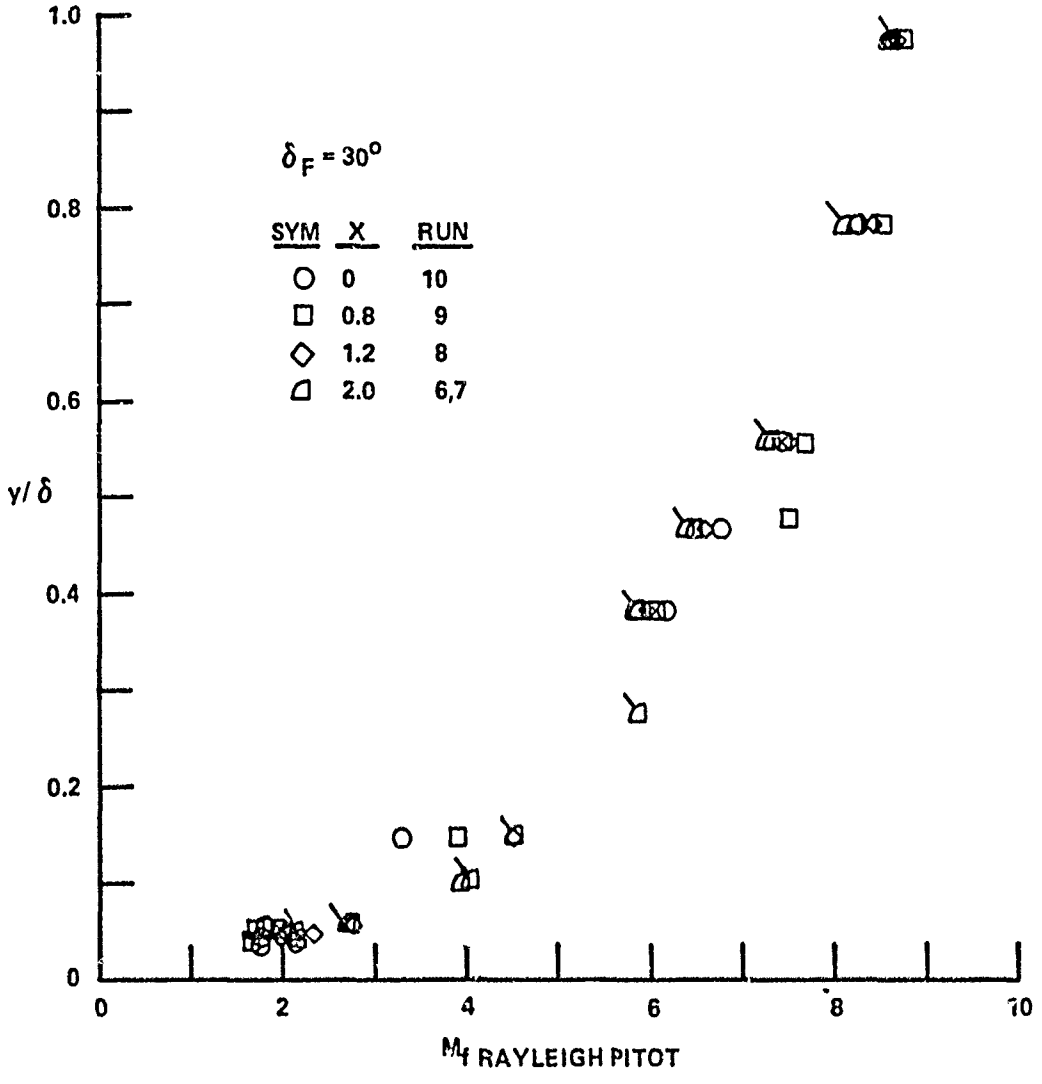

Figure 19 DISTRIBUTION OF MACH NUMBER ACROSS BOUNDARY LAYER

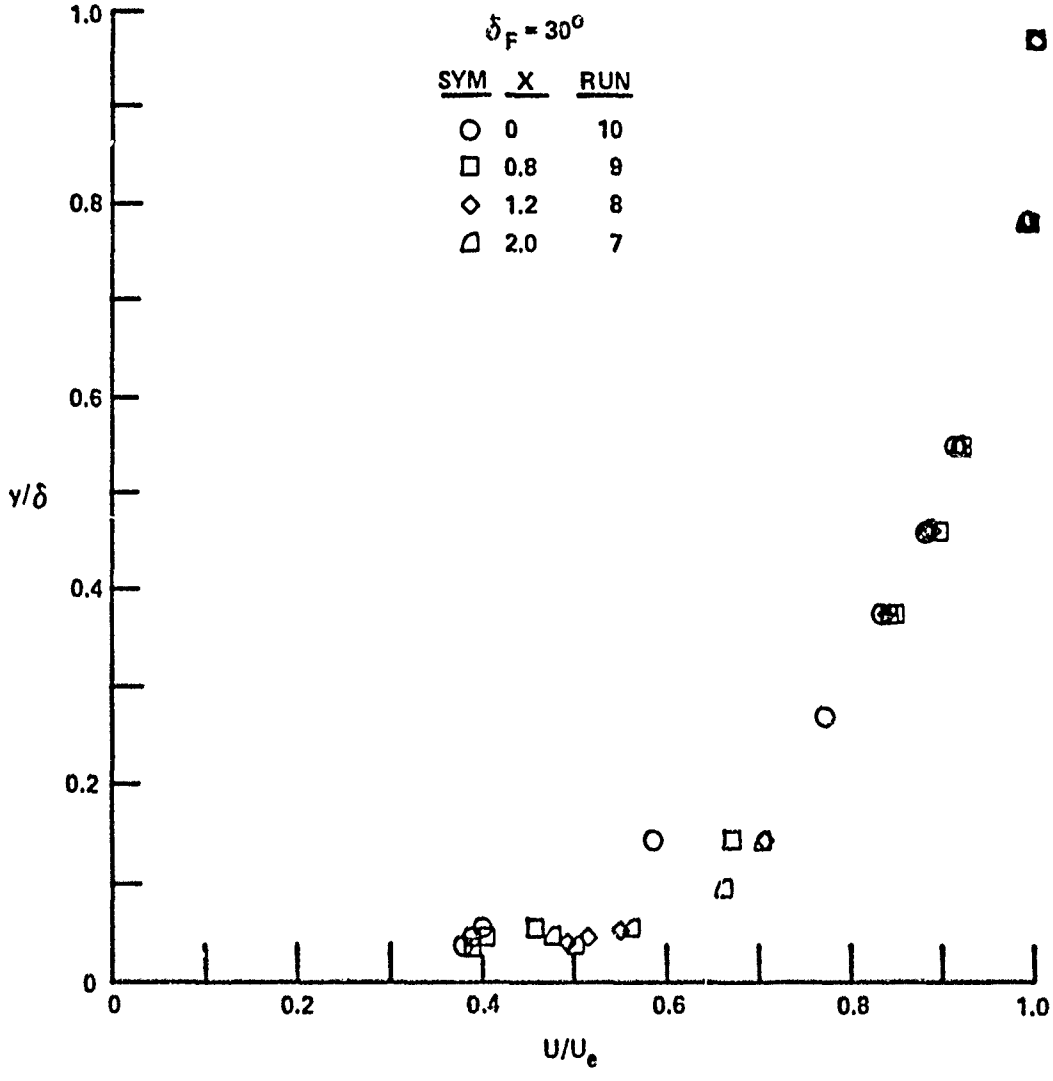

Figure 20 DISTRIBUTION OF VELOCITY ACROSS BOUNDARY LAYER

$$\frac{\tau}{\tau_w} = 1 + \left[\left(1-C_t\right)\left(1+\left(\frac{\gamma-1}{2}\right)M_e^2\right)\frac{T_e}{T_w} - 1\right]\frac{u}{u_e} + \frac{T_e}{T_w}\left[C_t\left(\frac{1+\left(\frac{\gamma-1}{2}\right)M_e^2}{\left(\frac{\gamma-1}{2}\right)M_e^2}\right) - 1\right]\left(\frac{\gamma-1}{2}\right)M_e^2\left(\frac{u}{u_e}\right)^2$$

$0.5 < C_t < 1$; $C_t = 1$ for Crocco, $C_t = 0.5$ for quadratic

These measurements are compared with the Crocco relationship between enthalpy and velocity in Figure 21. It is clear that our measurements follow a parabolic relationship:

$$\frac{P_{rake}}{P_{meas.cone}} = \left[\frac{(\gamma+1)Mb^2}{2}\right]^{\frac{\gamma}{\gamma-1}} * \left[\frac{\gamma+1}{2\gamma Mb^2-(\gamma-1)}\right]^{\frac{1}{\gamma-1}}$$

$$\frac{u_b}{u_e} = \frac{M}{Me}\sqrt{\frac{T_{ob}}{T_{oe}}}\sqrt{\frac{1+\left(\frac{\gamma-1}{2}\right)M_e^2}{1+\left(\frac{\gamma-1}{2}\right)M_b^2}}$$

rather than Crocco's linear relationship:

$$\frac{T_d}{T_w} = 1 + B\left(\frac{u}{u_e}\right) - A^2\left(\frac{u}{u_e}\right)^2$$

where:

$$A = \left[r\left(\frac{\gamma-1}{2}\right)M_e^2\frac{T_e}{T_w}\right]^{0.5}$$

$$B = \left[\left(1+r\left(\frac{\gamma-1}{2}\right)M_e^2\right)\frac{T_e}{T_w} - 1\right]$$

In the past, it has been assumed that the "fuller than Crocco" velocity profile obtained in studies over tunnel walls was associated with turbulent nonequilibrium effects associated with the strong favorable pressure gradient upstream on the nozzle wall;[21] however, no such explanation can be advanced to explain our results.

Of the transformation techniques that have been postulated to cast the compressible flow measurements into an equivalent incompressible form, the relationships derived by Van Driest have received the greatest support. Van Driest starts with the assumption that the Crocco relationship is valid and uses the mixing length theory to calculate the Reynolds stresses in the flow. By inspection, the transformation, is

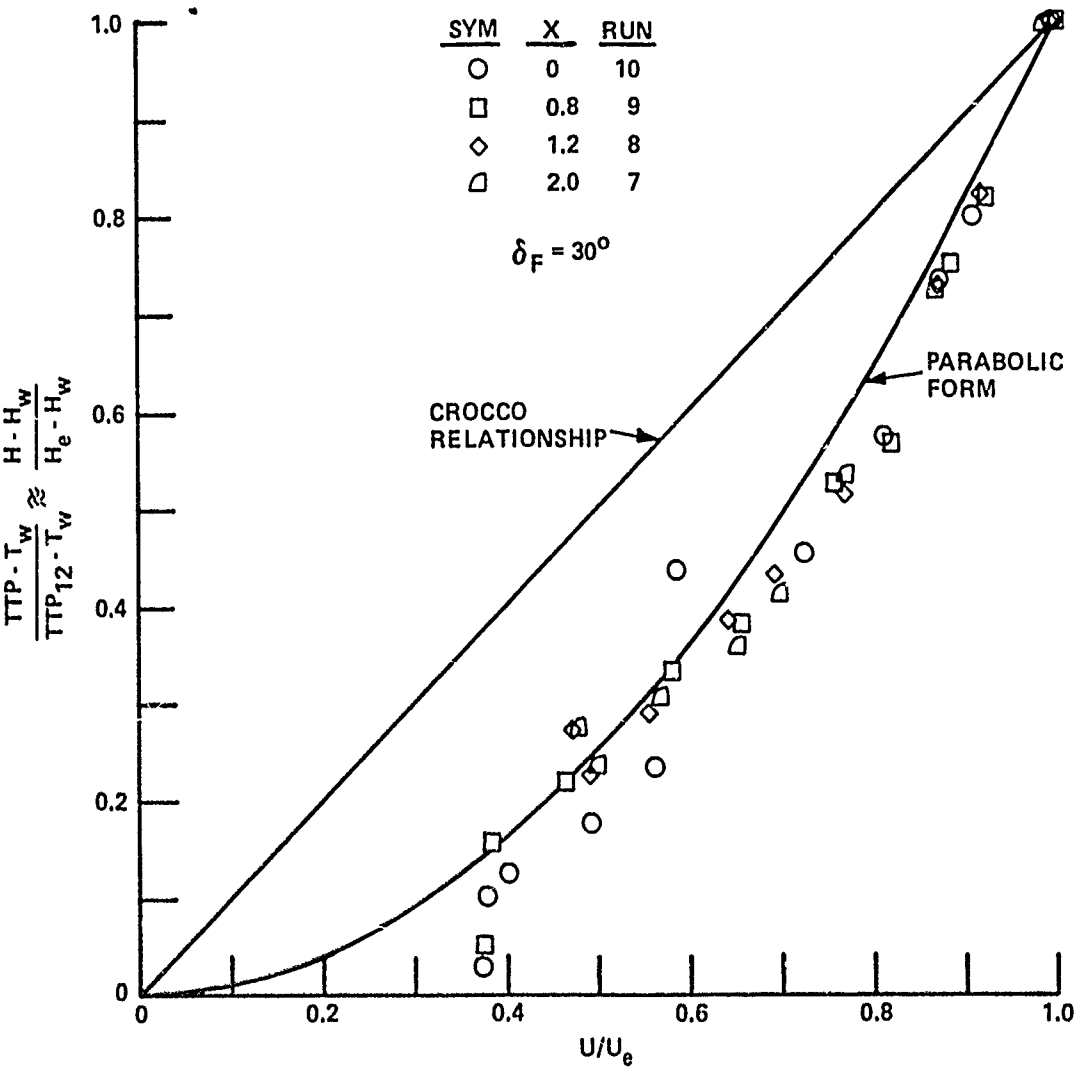

Figure 21 TOTAL TEMPERATURE AND VELOCITY MEASUREMENTS PRESENTED IN CROCCO FRAMEWORK

$$\frac{u^*}{u_e} = \frac{1}{A}\sin^{-1}\frac{2A^2\left(\frac{u}{u_e}\right)-B}{(B^2+4A^2)^{1/2}} + \frac{1}{A}\sin^{-1}\frac{B}{(B^2+4A^2)^{1/2}}$$

where: $$A^2 = r\frac{\gamma-1}{2}M_e^2\frac{T_e}{T_w}$$

$$B = \left(1+r\frac{\gamma-1}{2}M_e^2\right)\frac{T_e}{T_w}-1$$

The appropriate form of the incompressible law of the wall relationship is

$$u^+ = \frac{u^*}{u_t} = \frac{1}{K}\ln y^+ + C$$

However, because the wake region of the flow is so extensive, Maise and McDonald[22] have suggested that Coles[23] wake function be included:

$$u^+ = \frac{u^*}{u_t} = \frac{1}{K}\ln y^+ + C + \frac{\bar{\pi}}{K}w\left(\frac{y}{\delta}\right)$$

They, in fact, suggest a defect form of this relationship:

$$\frac{u_\infty^* - u^*}{u_t} = f\left(\frac{y}{\delta}\right) = \frac{1}{K}\ln\left(\frac{y}{\delta}\right) + C(2-w)$$

Comparisons between our measurements in each of the incompressible formats are shown in Figures 22 and 23. It is clear that the transform is not as successful at these high Mach numbers as it has been below Mach 5. Comparisons between the measurements and these prediction techniques in the compressible plane are shown in Figure 24. It can be seen that this is a relatively insensitive way of examining the measurements.

We are concerned with the differences between the current set of measurements and the prediction techniques. We will attempt to check our measurements against more sophisticated prediction techniques and density measurements obtained with holographic interferometry. We also plan further refinement of the instrumentation to more effectively probe the wall layer.

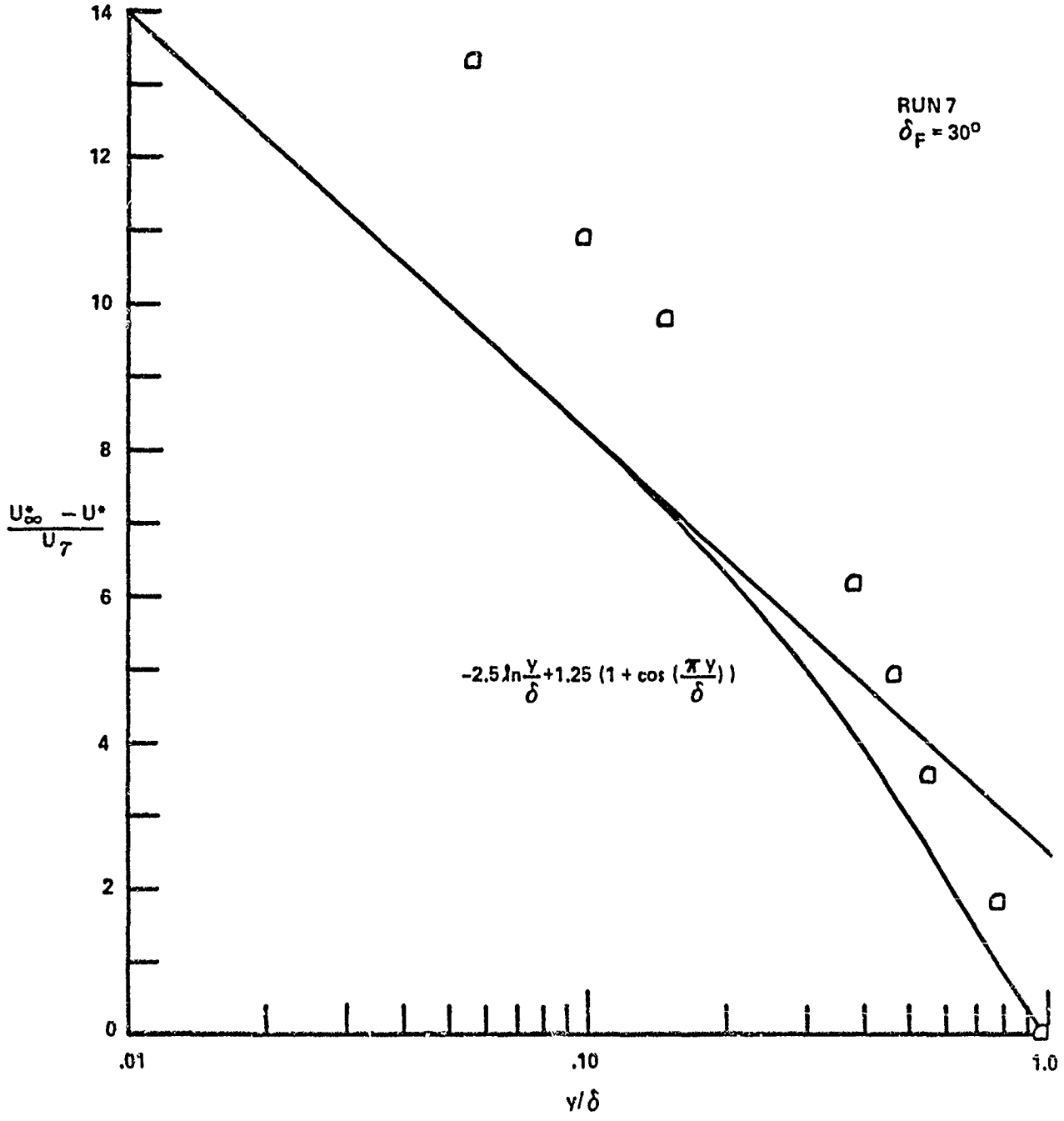

Figure 22 INCOMPRESSIBLE VELOCITY PROFILE MEASUREMENTS IN DEFECT FORM

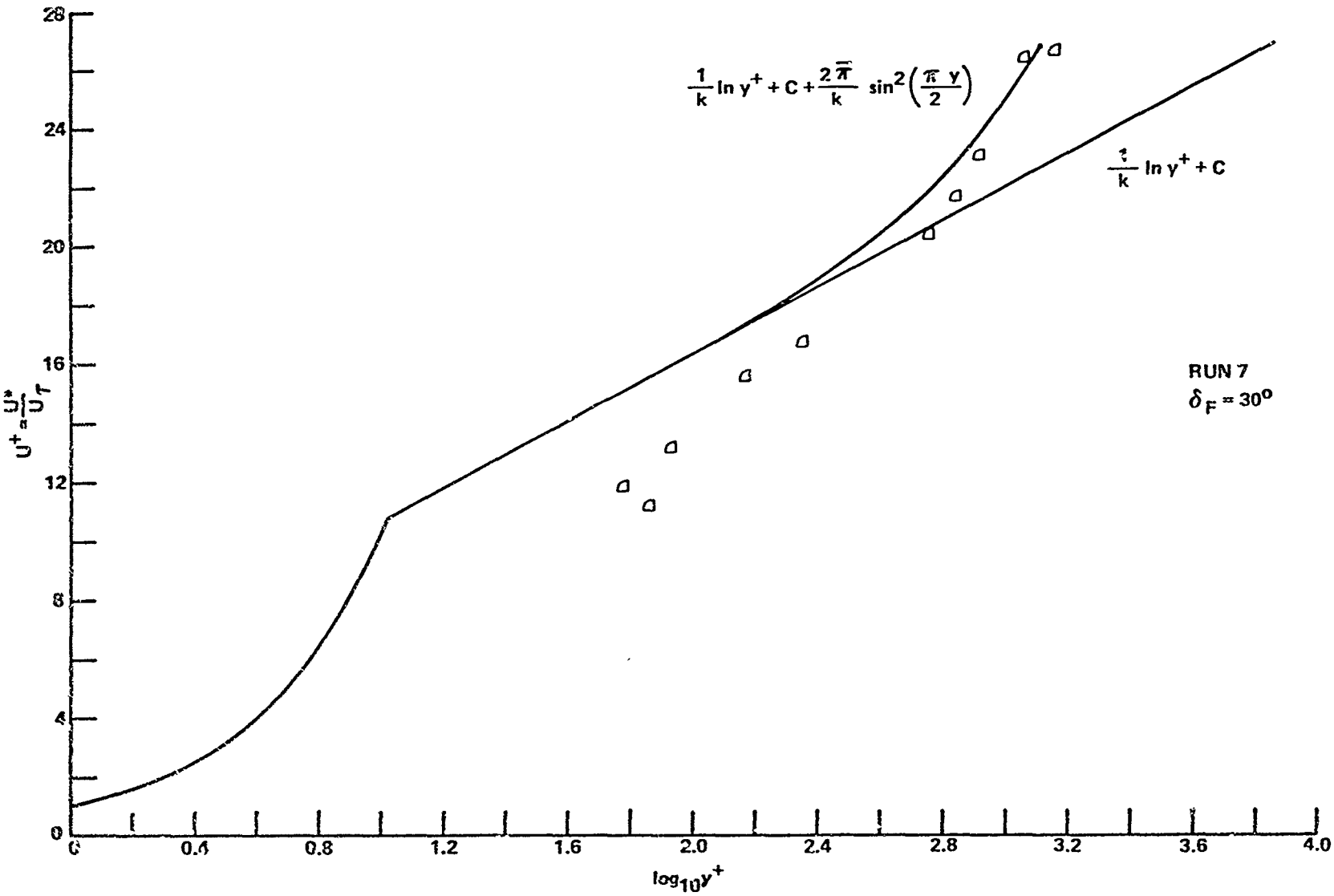

Figure 23 VELOCITY PROFILE MEASUREMENTS IN INCOMPRESSIBLE WALL COORDINATES

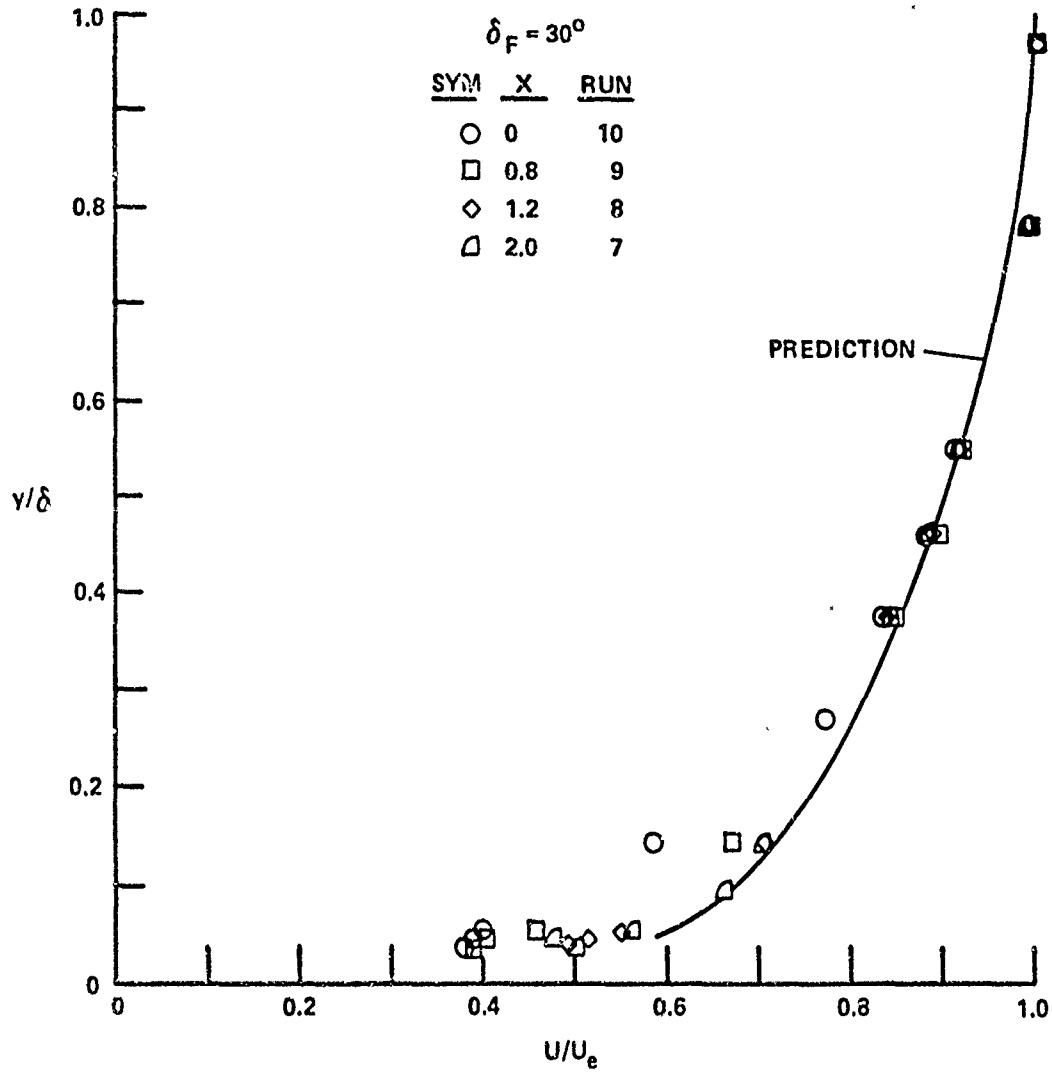

Figure 24 COMPARISON BETWEEN MEASURED AND PREDICTED VELOCITY DISTRIBUTION

Section 4

PRELIMINARY APPLICATIONS OF HOLOGRAPHIC INTERFEROMETRY TO STUDY HYPERSONIC REGIONS OF SHOCK WAVE/ BOUNDARY LAYER INTERACTION

4.1 INTRODUCTION

This section documents the findings of an initial application of pulse laser holography to study hypersonic turbulent boundary layer interactions, especially in regions of strong pressure gradients. One important objective is to provide detailed information on the mechanism of flow separation in regions of shock wave/ boundary layer interaction in hypersonic flows. In previous studies, miniature probes were developed and used to examine the structure of turbulent boundary layers in high Mach number, high Reynolds number hypersonic flows. The extremely large heat transfer rates and stresses developed on the tiny probes in these flows make this task difficult, and wall interference problems near the model surface present important concern for the accuracy of the measurements. Hence, exploring these flows with non-intrusive, optical techniques is very desirable.

Holographic interferometry is a potentially worthwhile measuring technique, because it is nonintrusive and offers the potential to capture information of the entire flow field in a single instantaneous exposure. To the uninitiated, the term "holographic" in holographic interferometry might be thought to imply that this technique is capable of measuring densities in streamwise slices of the flow. However, this is not the case, because the fringe shifts result from an integration of the density changes along the path traversed by the laser light waves. Thus, as in conventional Mach-Zehnder interferometry, distortions resulting from two-dimensional effects, surface refraction, diffraction and more importantly, the intrinsic unsteady three-dimensional structure of a turbulent flow can result in uncertainty in the interpretation of the optical measurements. Edge effects are of special concern when this technique is used to examine separated flows over two-dimensional models, because three-dimensional effects are induced by the separated region at the edges of the model.

4.2 LASER HOLOGRAPHIC SYSTEM

The holographic recording system[24] (Figure 25) was loaned to CUBRC (Calspan-UB Research Center, Buffalo, NY) by the Air Force Flight Dynamics Laboratory (AFFDL), Wright-Patterson Air Force Base, Ohio.

4.2.1 Basic System

The holograms obtained during this study are made with a pulsed ruby laser that is Q-switched passively with a dye cell to produce single 25-nanosecond (nominal) light pulses. Both single plate and dual plate techniques are required to record holograms, which are subsequently used in the playback step to obtain shadowgrams, schlieren photographs and interferograms of the shock tunnel tests. The optical reference conditions are taken for both atmospheric and tunnel "pump down" conditions; the latter condition is needed to assess the optical effect of loading the test chamber windows. During the actual recording of the holograms, the shock tunnel test section is nearly at vacuum condition, which means that the windows are stressed by atmospheric pressure.

4.2.2 Shock Tunnel Installation

The holographic system is positioned and aligned with the Toepler schlieren system of the shock tunnel facility. A 20-power microscope objective is used to expand the laser beam to fill a 15-inch diameter parabolic mirror. A pin hole is not required to spatially filter the laser beam. A collimated beam reflected from the parabolic mirror is directed through the windows of the shock tunnel, captured by a second parabolic reflector on the opposite side of the tunnel, and directed toward the hologram recording plane. The holographic reference beam is split from the output beam of the ruby laser by a 30 to 70 percent beam splitter. Thirty percent of the incident radiation is reflected from the front surface of the beam splitter; this light is used to establish the scene beam, and the remaining 70 percent is directed over the shock tunnel by specially built beam elevation towers. The holographic reference beam is collimated by a beam expander-collimator positioned approximately 7 inches ahead of the hologram recording plane. Natural divergence of the ruby laser beam causes an approximate 50 percent reduction in the intensity of the light entering the collimator, so the net intensities of the scene and reference beams in the hologram plane are nearly equal. The AFFDL dual plate hologram holder[25] is used to hold and align the holograms, and it

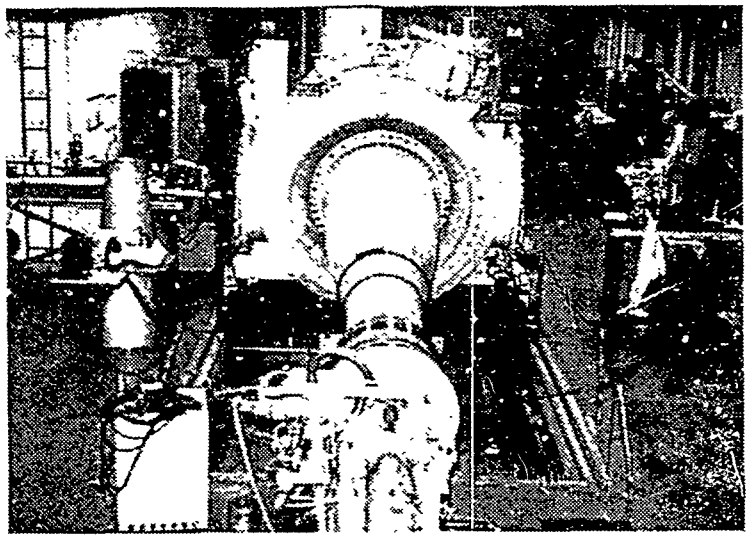

96-INCH HYPERSONIC SHOCK TUNNEL WITH LASER HOLOGRAPHIC SYSTEM INSTALLED

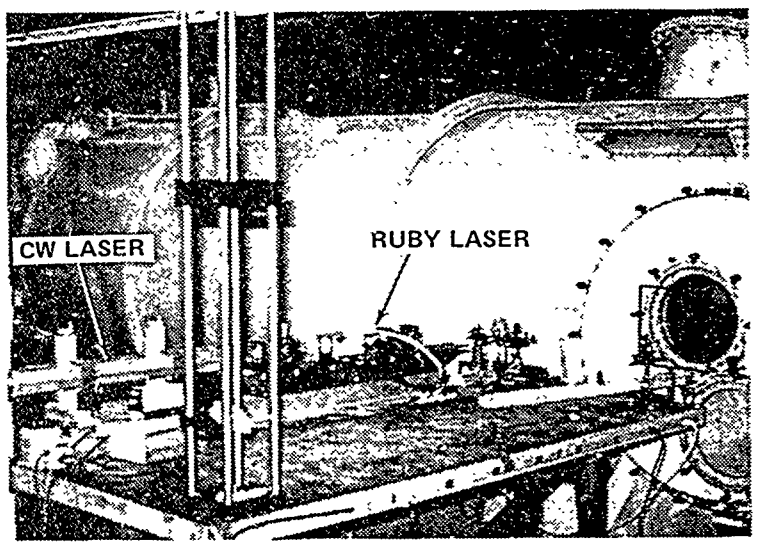

SENDING OPTICS

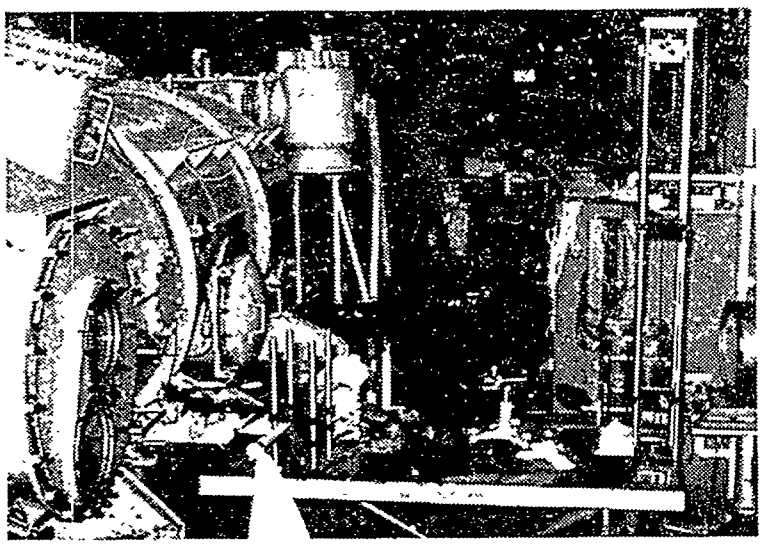

RECEIVING OPTICS

Figure 25 LASER HOLOGRAPHIC SYSTEM

is positioned so that the converging light waves of the scene beam illuminate a 1-inch circular area in the hologram plane; the collimated reference waves illuminate a 2-inch circular area, and both beams are aligned relative to the hologram recording plane so that the light waves of the scene beam are centered upon the light waves of the reference beam. Further, the holder is positioned so that the incident angles of both beams are 20 degrees relative to normal to the holograms. The path length of each beam is approximately 53 feet, and both path lengths are adjusted to be equal to within 2 inches.

The ruby laser in the recording system is a Korad, single-oscillator system that is passively Q-switched with a Kryptocine dye cell. The bank voltage applied to the flash lamp and the dye concentration in the dye cell are adjusted so that the laser emits a single pulse energy of 25 millijoules in 25 to 50 nanoseconds, nominally. The output beam is 0.06 inch in diameter at the front reflector of the ruby laser cavity. The laser is remotely charged, and once armed, the laser firing circuit is triggered from a voltage spike induced by the rupture pressure at the end of the driver section of the shock tunnel. The duration of usable flow in the shock tunnel for these tests is approximately 5 milliseconds, and the triggering circuit is adjusted to cause the laser to fire near the center of this period (2.7 to 2.8 ms, typically). A 15-milliwatt, continuous-wave (CW), helium neon laser is mounted behind the rear reflector of the ruby laser cavity and is aligned so that both laser beams are coaxial. The CW laser is used to align all the components in the recording system, and to preview the holograms in situ prior to analyzing them in detail using a separate playback system.

Figure 26 shows the hologram playback system.[24] A duplication of the holographic reference beam is established by directing the output of an argon ion, CW laser into a beam expander-collimator similar to the one used in the recording system. The same dual hologram holder is used to position the holograms, and a positive, f/8 lens is used to image the reconstructed object light waves directly into the field of a 20X telescope. The 20X telescope is the imaging component of an x-y microcomparator. This system is used to measure the interferometric fringe shifts for both single plate and dual plate applications, as well as to obtain photographic enlargements of selected apertures for the flow fields. This latter feature is especially valuable, because it allows details of the flow, which are otherwise invisible, to be observed and studied. Alternatively, a Graflex camera with a 4 x 5 Polaroid film holder is used in place of the microcomparator to photograph the full-aperture views of the flow fields. During hologram playback,

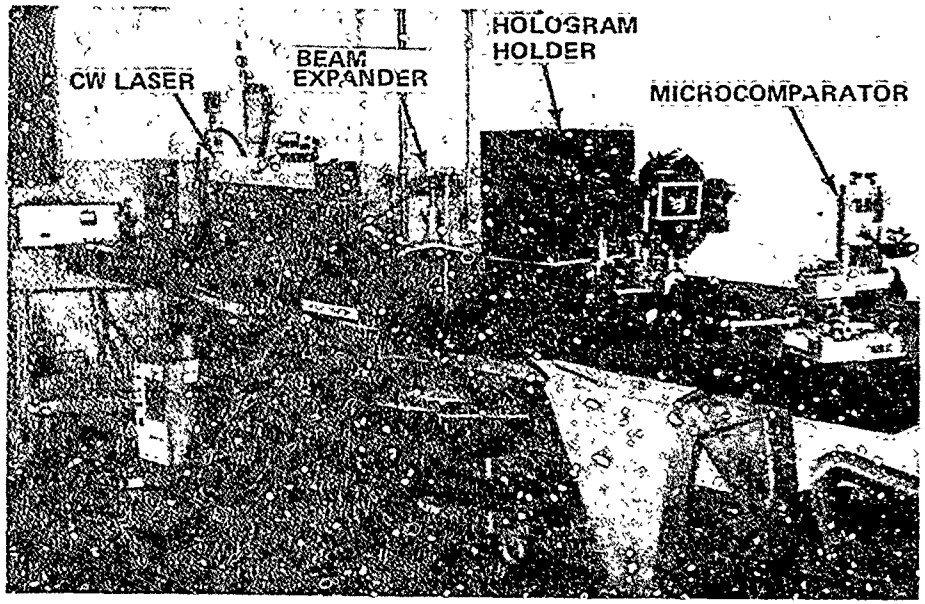

Figure 26 HOLOGRAPHIC PLAYBACK SYSTEM

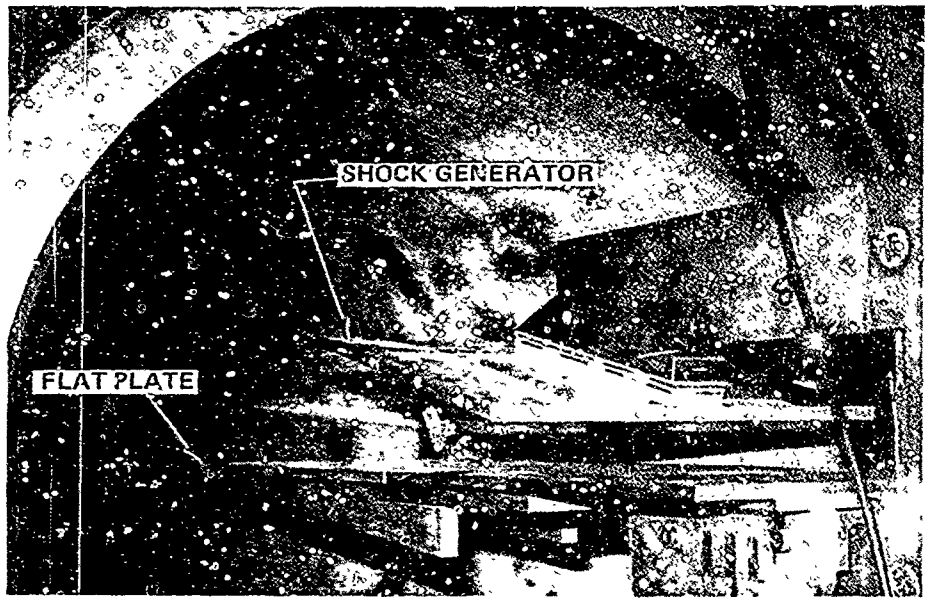

Figure 27 2-D SHOCK GENERATOR MODEL

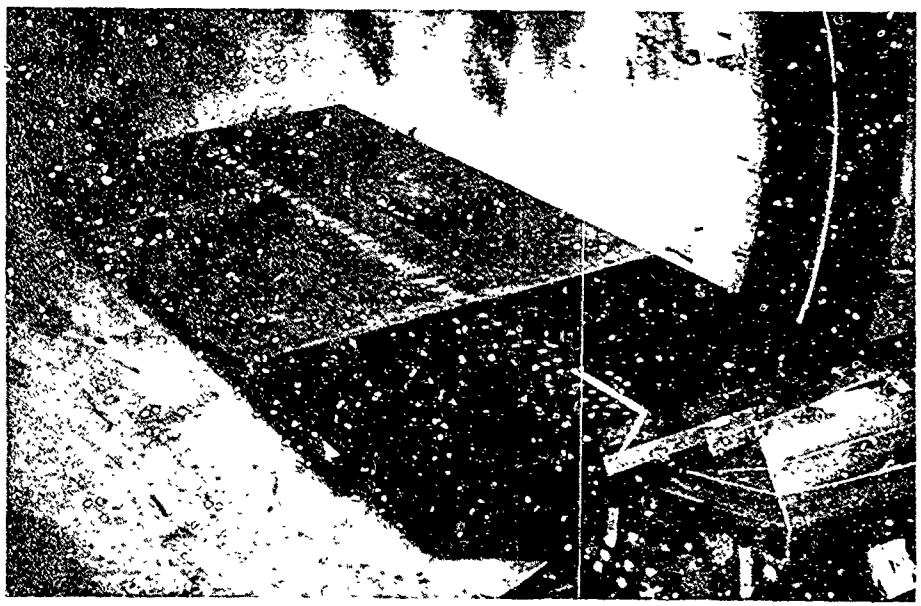

Figure 28 2-D COMPRESSION-RAMP MODEL

the reconstructed light waves converge from the holograms to form a duplication of the true focus of the second parabolic reflector in the recording system, permitting schlieren studies to be accomplished at leisure.

With the exception of one test for the 2-D compression ramp configuration, dual hologram interferometry[25] is the primary optical process used in this study. Interferograms of the flows are obtained by interfering light waves produced simultaneously from a test hologram and a reference state hologram; shadowgrams and schlieren results are obtained directly from the test holograms. A test hologram is a recording of a specific shock tunnel test, while a reference state hologram is a recording of a no-flow, model-out condition in the test section for either atmospheric or pump-down states. The test section of the shock tunnel is pumped to near vacuum levels for each test, and the pump-down reference state hologram is used to negate the effects of stress in the test section windows. A one-atmosphere pressure loading is supported by each window during a test. For these tests, window stress appears to have a negligible effect on the optical measurements, because the reference waves of both types of reference state holograms produce identical interferograms. For this study, the reference state holograms are the lead holograms in the dual plate alignment so that during the hologram playback step, the reconstructed reference waves are generated first and pass through the test hologram. This alignment allows the reconstructed test waves to propagate freely from the hologram into the data recording/analyzing system. Glass compensators, which would correct the lateral shift of the reference light waves, are not placed in front of the test holograms during the recording step, because this ray shifting is small enough to be corrected by the final alignment of the holograms during the playback step.

4.3 MODELS, INSTRUMENTATION AND TEST CONDITIONS

The models and instrumentation used in this investigation, and the conditions at which the experiments are conducted, are selected on the basis of the knowledge accumulated from a large number of studies over the past 15 years. The flow fields over the configurations selected are known to exhibit definitive features in the separation and reattachment regions as well as definitively formed separated regions.

Studies of the characteristics of incident shock-induced turbulent boundary layer separation have been made at Mach numbers from 6 to 13 (Ref. 26) with the model

shown in Figure 27. The strength of the interaction is controlled by the angle of the shock generator, and the boundary thickness is varied by changing the length of the flat plate. The flat plate, which is 18 inches wide, is extensively instrumented with heat transfer and pressure gages along the centerline and also along selected spanwise rays. A shock generator angle of 15 degrees and a flat plate length of 38 inches ahead of the interaction is the basic configuration used in these tests. This configuration gives a well separated region and well defined heat transfer and pressure distributions.

Studies of the flow over the compression surface are conducted using the flat plate/wedge model shown in Figure 28. This model, which has been used in a number of studies of laminar and turbulent interacting flows[27], uses a major part of the instrumentation from the shock generator model described above. A wedge angle of 36 degrees is selected for the current measurements, again to obtain a well separated flow.

The large cone flare model shown in Figure 4 is used for measurements over an axisymmetric configuration for which the transverse curvature effects are small. A 9-foot long, 6° half-angle cone with a 36° flare is used in these studies. This configuration is selected so that the flow field surveys made through the boundary layer and separated region just ahead of the flare can be compared to the results in a complementary study.

These experimental studies are conducted in Calspan's 96" Shock Tunnel at Mach numbers 11 and 13 and at the respective Reynolds numbers listed in Table 2. The boundary layers are completely turbulent well upstream of the interactions.

Table 2
TEST CONDITIONS FOR EXPERIMENTAL STUDIES

	Flat Plate/ Wedge	Incident Shock	Cone/ Flare
Mach Number	11.34	11.34	13.06
Reynolds Number	1.7017E7	1.039E7	5.071E6
Reservoir Temperature (^{o}R)	2.564E3	2.585E3	3.005E3
Reservoir Pressure (psia)	1.739E4	1.721E4	1.836E4
Freestream Velocity (ft/s)	5.079E3	5.5735E2	6.340E3
Freestream Density (slugs/ft^{3})	1.662E-4	1.621E4-4	6.593E-5
Freestream Temperature (^{o}R)	1.053E2	1.064E2	9.797E1
Freestream Pressure (psia)	2.085E-1	2.056E-1	7.696E-2
Pitot Pressure (psia)	3.481E1	3.428E1	1.709E1

4.4 RESULTS AND DISCUSSION

4.4.1 Comparison to Flat Plate Theory

To evaluate the accuracy of deducing density from the interferograms, detailed fringe shift measurements are made for the turbulent boundary layer approximately 4 inches upstream of the corner interaction (Figure 29). These results are compared with simple prediction methods for hypersonic turbulent boundary layers over a flat plate with a sharp leading edge. To maintain the greatest accuracy, the measurements are made by directly viewing the holographically reconstructed image with an x-y microcomparator. These measurements are compared with predictions based on the Van Driest compressibility transformation of the Clauser/Cole incompressible velocity profiles and a modified Crocco relationship.[28]

4.4.2 Reduction of Interferometer Measurements

The reduction of interferometric measurements to density for a 2-D flow field is a linear relationship between density and fringe shift which is written as,

$$S = \frac{K_{DG}}{\lambda} \ell \, (\rho - \rho_{ref}) \qquad (1)$$

where: S = measured fringe shift, dimensionless

K_{DG} = Dale Gladstone constant

λ = wavelength of light

ℓ = extent of 2-D field traversed by light waves

$\rho - \rho_{ref}$ = relative change in density between the reference point and the point where S is measured

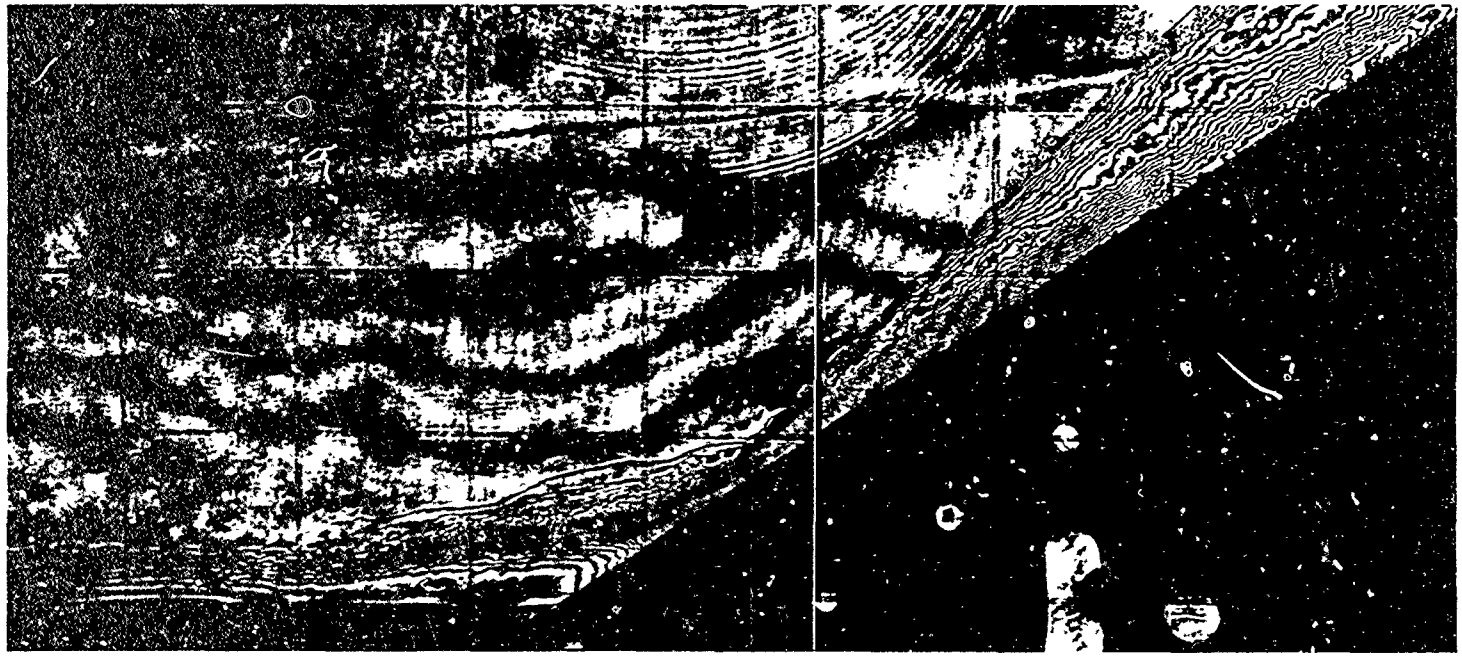

Figure 29 FLOW STRUCTURE IN A TWO DIMENSIONAL CORNER FLOW (M=11 $R_{e_L} = 30 \times 10^6$)

Normally, ℓ is assumed to be the geometric length of the field in the direction of the light waves, but rarely is this the case for wind tunnel applications. When the model is bounded by vertical sidewalls, the extent of the 2-D field is less than the geometric width of the model, and the numerical value for ℓ in Equation (1) is reduced usually by an estimation for the boundary layer displacement thickness of the sidewall boundary layers. The opposite is true for models placed in the core of a free jet, as is the case here. Because the flow is unconstrained in the lateral direction (no sidewalls), the density has to be continuous around the surfaces of the model. The model develops boundary layers along its sides similar to the boundary layer developed on the testing surface. In the absence of shock waves, all fluid properties, as well as the streamlines in these boundary layers, are continuous around the edges of the model, because the boundary layers are connected. This condition makes the extent of the 2-D field wider than the geometric length of the model, and the precise increase in ℓ is unknown. In the present case, a theoretical maximum fringe shift across the boundary layer (S_{max}) of 10.2 is computed from Equation (1) using the $\rho_\infty - \rho_w$ as prescribed by shock tunnel flow field conditions, but the maximum S measured from the interferogram is 10.59. The density of the freestream and the flow at the wall are known from other data, and the optical constants are known from physics. The additional 0.39 fringe shift is believed to be due to the influence of the edge conditions. To have agreement between the theoretical and measured S_{max}, ℓ has to be 0.56 inch longer than the 18 inch width of the flat plate. If the 0.56 inch increase in ℓ is ignored, and the fringe data are reduced using the freestream conditions, the interferometric measurements predict T_w = 643°R, which is impossible! At the start of a test, the model temperature is nearly the same as the ambient temperature--531 to 540°R, typically--and even for extreme heat transfer rates, the model temperature remains constant for the 5-ms duration of the test. Hence, the additional 0.39 fringe shifts are likely due to edge effects.

As an initial treatment, ℓ in Equation (1) is assumed to be 0.56-inch longer than the plate width so that there is agreement in the S measurements from the freestream to the model surface. Although incorrect, this simple choice for ℓ provides a starting point to show the general trend of the density distribution, as well as a starting point from which the influence of the edge effects might be determined; more realistic corrective methods are being studied as reduction and analyses of these data continues. For now, with both S_{max} and $\rho_\infty - \rho_w$ specified, the quantity $(K_{DG}/\lambda)\ell$ in Equation (1) is known, and, hence, the density at all measured S locations is

$$\rho = \rho_\infty - \frac{s}{s_{MAX}} \cdot (\rho_\infty - \rho_w) \tag{2}$$

Equation (2) is used to compute the experimental density distribution shown in Figure 30. For a steady flow, the distribution would be a reasonably smooth, monotonic function. The small anomalies in the actual distribution are believed to result from the instanteous measurements of the unsteadiness in the flow.

The comparisons between theoretical and experimental data are shown in Figure 31. The difficulty in the accurate reduction of the measurements close to the wall is reflected in densities that are larger than the wall value just above the flat plate. For a constant pressure boundary layer, this would result in temperatures at the base of the boundary layer which are lower than the wall temperature, which would result in heat transfer from the wall to the flow. This result is impossible for this case, and the heat transfer measurements show this is clearly not true.

Using the Van Driest compressibility transformation

$$\frac{u^*}{u_e} = \frac{1}{A} \sin^{-1} \frac{2A^2\left(\frac{u}{u_e}\right) - B}{(B^2 + 4A^2)^{1/2}} + \frac{1}{A} \sin^{-1} \frac{B}{(B^2 + 4A^2)^{1/2}} \tag{3}$$

where

$$A^2 = m_e \frac{T_e}{T_w}, \quad B = (1 + m_e)\frac{T_e}{T_w} - 1 \quad \text{and} \quad m_e = r \cdot \frac{\gamma - 1}{2} M_e^2$$

together with Coles modification of the Clauser incompressible relationship

$$\frac{u}{u_\tau} = \frac{1}{K} \log \frac{(u_\tau y)}{\nu_w} + c + \frac{\pi}{K} w\left(\frac{y}{\delta}\right)$$

and the generalized Crocco relationship

$$\frac{T}{T_w} = 1 + \left[(1 - c_t)(1 + m_e)\frac{T_e}{T_w} - 1\right]\frac{u}{u_e} + \frac{T_e}{T_w}\left[c_t \frac{(1 + m_e)}{m_e} - 1\right] m_e \left(\frac{u}{u_e}\right)^2 \tag{4}$$

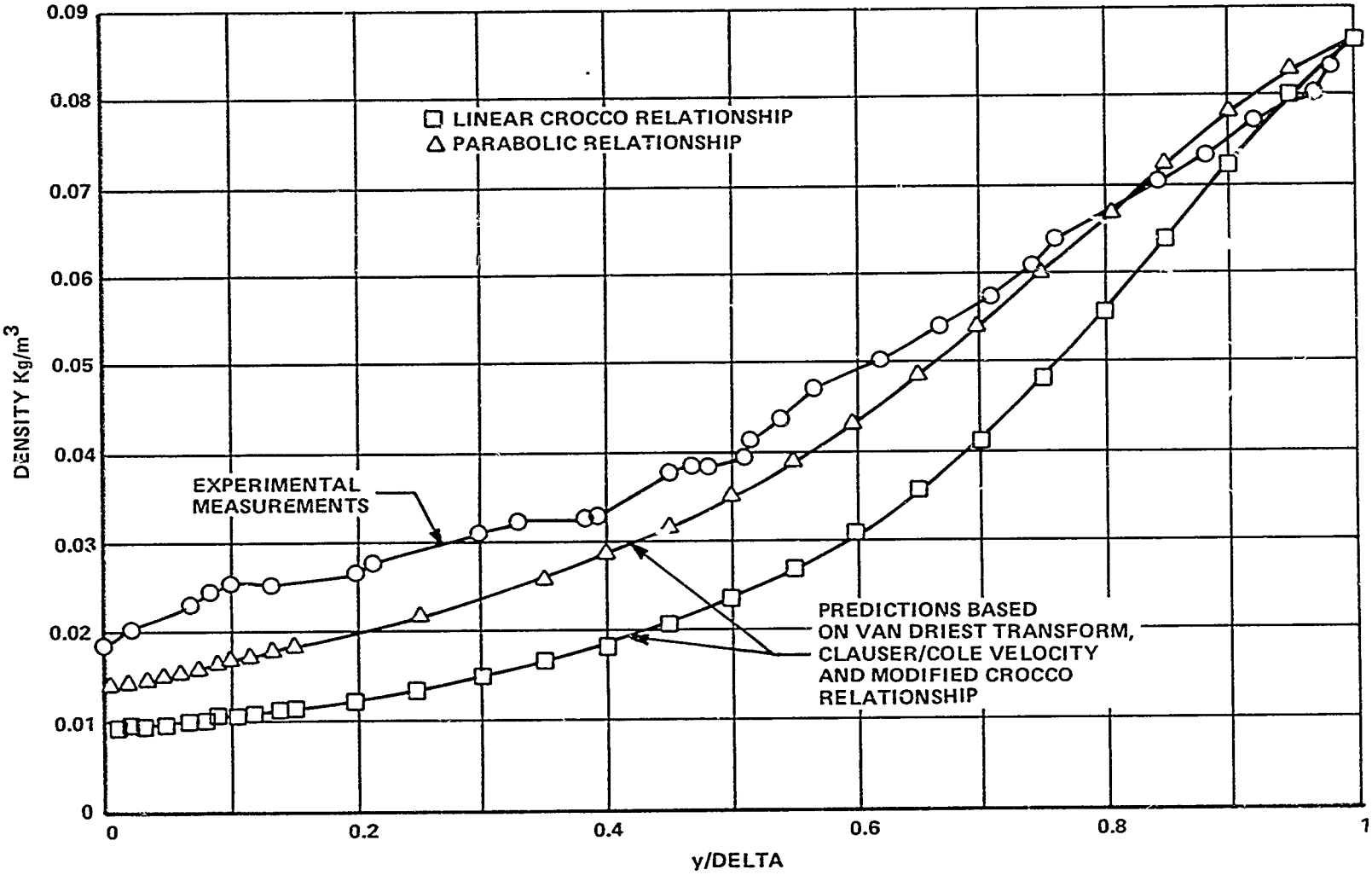

Figure 30 COMPARISON BETWEEN MEASUREMENTS OF THE DENSITY DISTRIBUTION ACROSS TURBULENT FLAT PLATE BOUNDARY LAYER AND SIMPLE PREDICTION

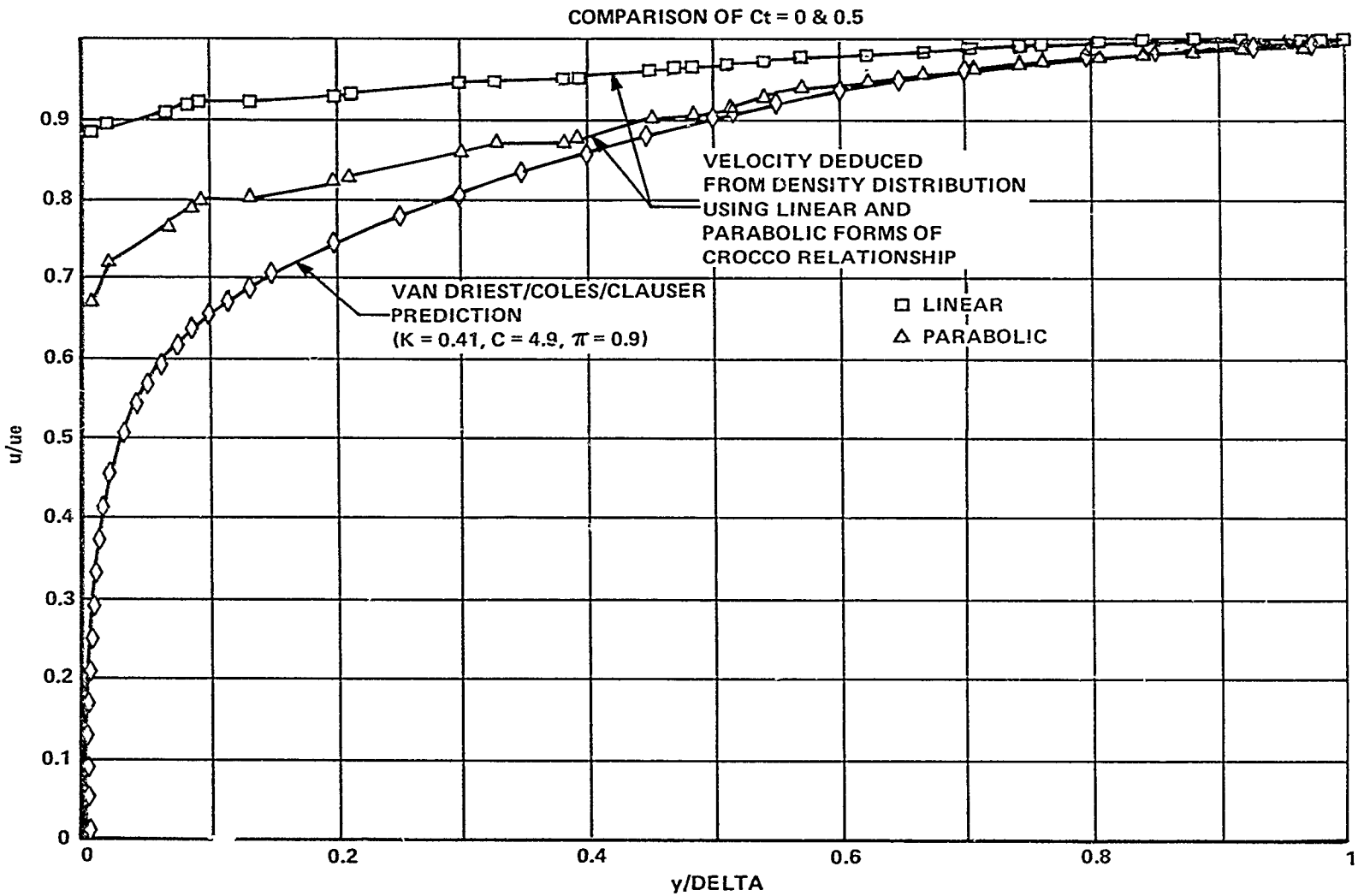

Figure 31 COMPARISON BETWEEN PREDICTED VELOCITY DISTRIBUTION AND VALUES DEDUCED FROM DENSITY MEASUREMENT

where Ct = 0 for a linear relationship and Ct = 0.5 for a parabolic form. Close to the wall, the measurements exhibit the anticipated lower values associated with a local peak in temperature close to the wall.

The distribution of velocity through the boundary layer can be calculated from the measured density distribution by using the modified Crocco relationship (Equation 4). These calculations for Ct = 0 and 0.5 together with the Van Driest transformed Clauser/Cole relationship are shown in Figure 31. The velocities deduced from the measurements are significantly larger than the predicted values and those deduced from pitot and total temperature measurements obtained in an earlier Calspan study.[28] This result is consistent with the density discrepancies.

Clearly, a closer examination of refraction and edge effects as well as the data reduction technique, are required. In retrospect, a better approach may be to examine an axisymmetric laminar flow to first evaluate the problems with the basic system. Following this, the problems associated with the intrinsic three-dimensional structure of turbulent flow and the intricacies of the flow at the edges of the two-dimensional model may be easier to resolve. Also, making independent measurements of the density in both laminar and turbulent flows using an electron beam are desirable, because this would provide redundant and independent measurements. We intend to pursue this approach to further study these flows.

4.4.3 Discussion of Qualitative Features

A single plate holographic interferogram typical of those taken during the current study is shown in Figure 29. This particular hologram is made by double-exposing a single plate, first with the reference beam just before the test, and then approximately 15 minutes later with the scene beam of the test. Here, the interferogram is fixed in the hologram. In this interferogram, the model wall appears as a solid black surface, while in the interferogram reconstructed using the dual plate technique, the model appears as a gray silhouette. The photographs shown in this paper are enlargements

of 35mm photographs of the reconstructed object waves as viewed through the eyepiece of a 20X telescope. Because this direct viewing approach is used in this study, details in the hologram can be magnified to achieve pictures of greater clarity than would otherwise be obtained. Restating the fact that all optical data shown here result from the integrated effects of density changes from the beam splitter to the recording plane, these photographs must be interpreted with care, especially in and close to regions of separated flow.

4.4.4 Turbulent Separation in a Two-Dimensional Compression Corner

The scale and properties of separated regions formed over flat plate/wedge compression surfaces are controlled by a "free" interaction between the viscous layer and the overlaying inviscid flow. Because of the intrinsic differences between the structure and properties of laminar and turbulent boundary layers, the mechanism of flow separation and the structure of the separated flows are significantly different. In laminar flows, the major mechanism controlling the flow in regions of separation is the mutual interaction between the growth of the displacement layer and the outer inviscid flows that can be described in terms of second order boundary layer theory.

Turbulent separation takes place in the sublayer from which the strong separation shock traverses the boundary resulting in strong normal pressure gradients. Such flows cannot be described by boundary layer theory and possibly not by the mass averaged Navier-Stokes equations. A schlieren photograph and distributions of heat transfer and pressure (Figure 32) are shown for separated flow over the flat plate/wedge configuration.[27] The corresponding holographic interferograms, schlieren photographs and shadowgraphs that are obtained in the current study are shown in Figures 33 and 34. The heat transfer and pressure distributions clearly indicate that the separation region occupies a fraction of a boundary layer thickness. The separation shocks that are created in this region are seen clearly in the shadowgraph and schlieren photographs, and they appear as rapid distortions of the fringe pattern in the interferogram. These shocks are highly distorted as they traverse the major part of the boundary layer. A matter of continuing debate is whether these distortions are responses to the unsteady movement of the separation point or to responses in the incoming turbulent flow. However, it is clear that significiant pressure, temperature, and, hence, density fluctuations are generated by the inflections of the separation shock in this region. The multiple shocks that are typically observed in the separation region reflect the time-

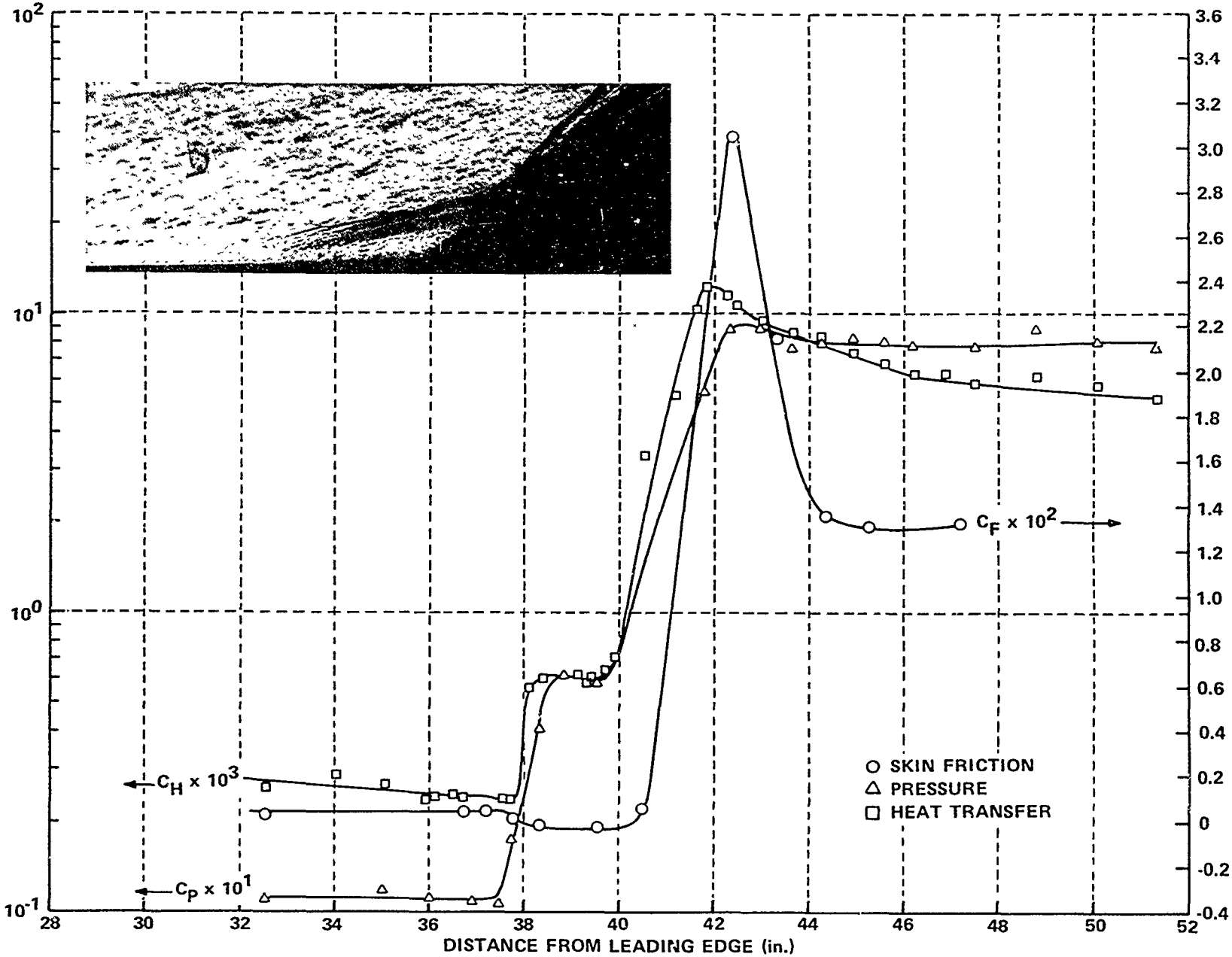

Figure 32 PRESSURE, HEAT TRANSFER AND SKIN FRICTION DISTRIBUTION IN WEDGE-INDUCED SEPARATED FLOW ($M = 11.3$ $Re_L = 33 \times 10^6$ $\theta_{WEDGE} = 36^o$) (REF. 27)

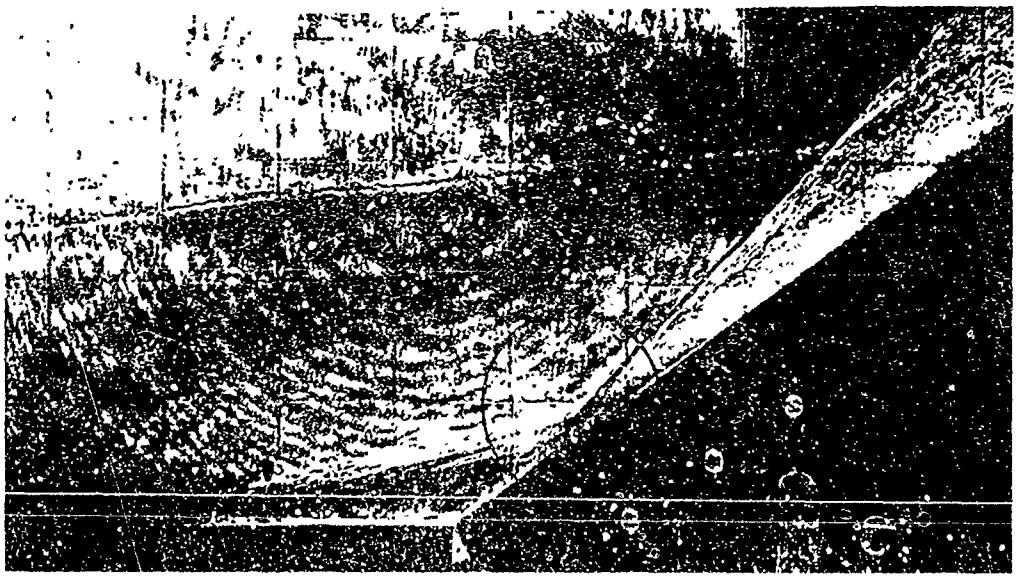

SEPARATION REGION

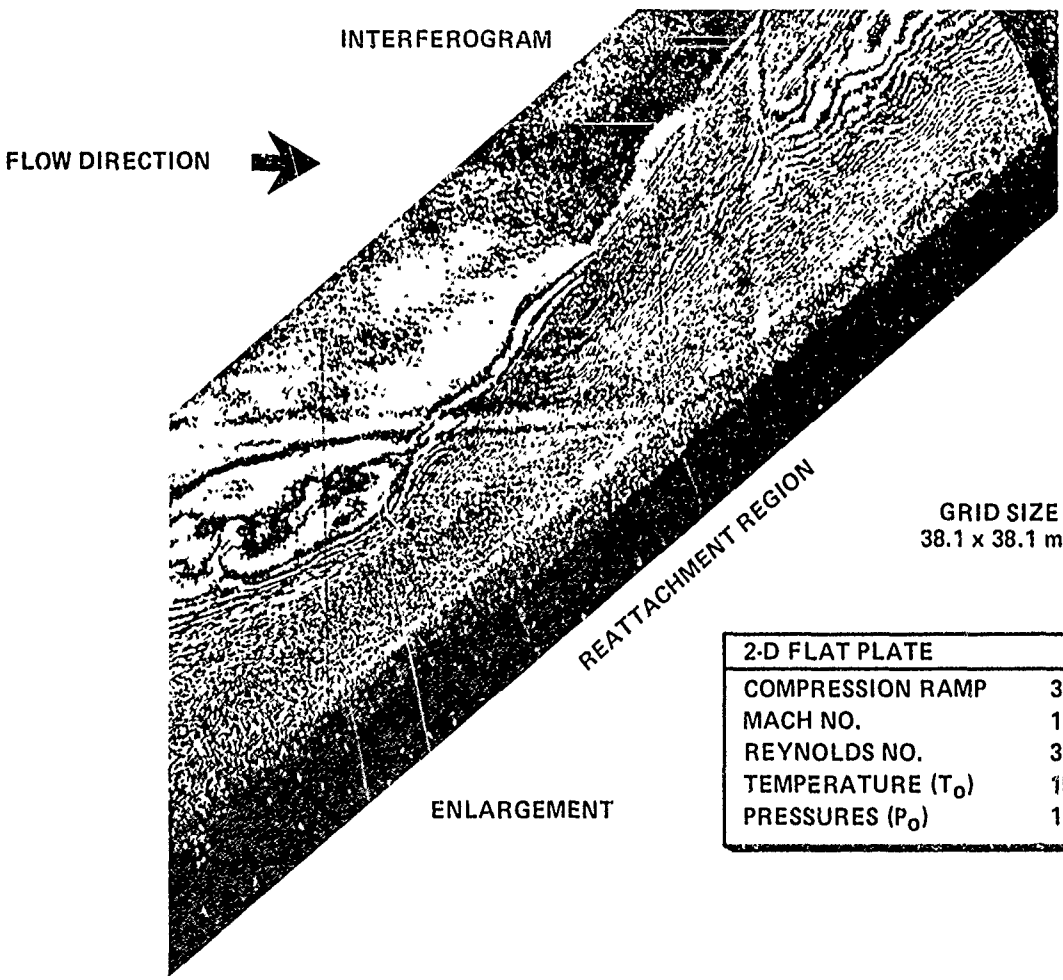

2-D FLAT PLATE	
COMPRESSION RAMP	36^{o}
MACH NO.	11.34
REYNOLDS NO.	35.4×10^{6}
TEMPERATURE (T_o)	1555°K
PRESSURES (P_o)	102.5 MPa

Figure 33 HOLOGRAPHIC INTERFEROGRAM OF COMPRESSION-RAMP INDUCED BOUNDARY LAYER SEPARATION FOR 2-D FLAT PLATE IN HYPERSONIC FLOW

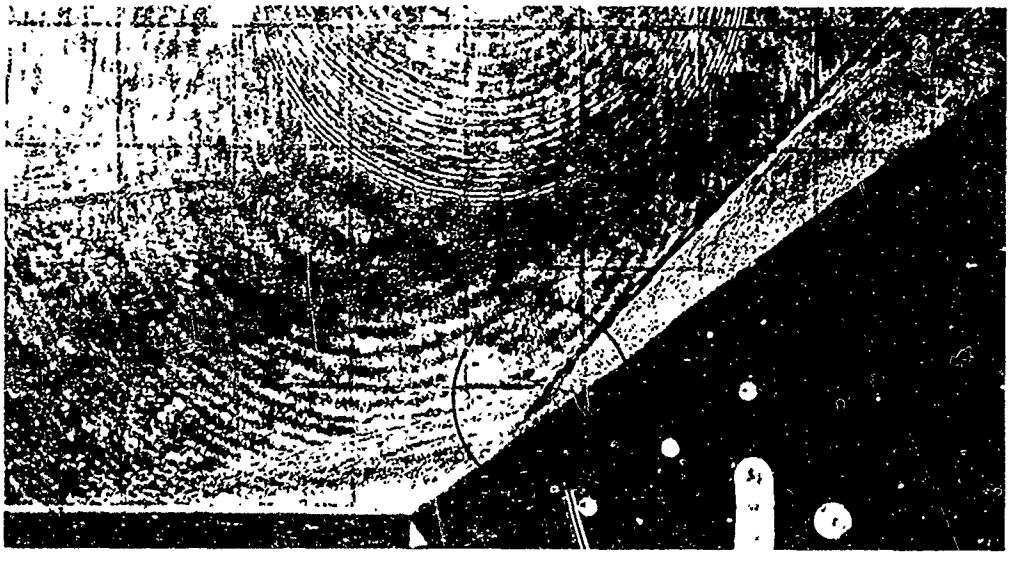

SHADOWGRAM

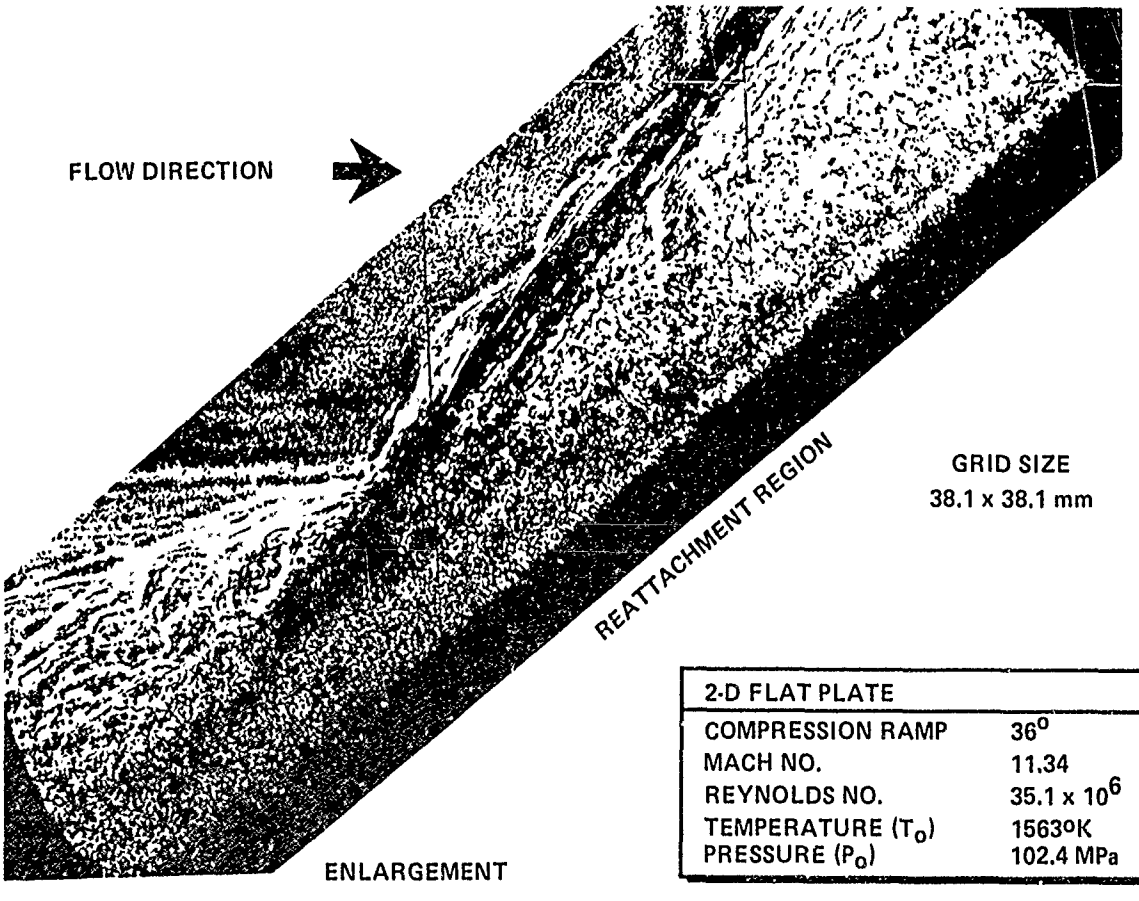

ENLARGEMENT

2-D FLAT PLATE	
COMPRESSION RAMP	36^{o}
MACH NO.	11.34
REYNOLDS NO.	35.1×10^{6}
TEMPERATURE (T_o)	1563°K
PRESSURE (P_o)	102.4 MPa

Figure 34 HOLOGRAPHIC SHADOWGRAMS OF COMPRESSION-RAMP-INDUCED BOUNDARY LAYER SEPARATION FOR 2-D FLAT PLATE IN HYPERSONIC FLOW (REFERENCE FIGURE 33)

dependent position of separation (since they are also observed on axisymmetric models) and the three-dimensional nature of the flow at the edges of the model.

A prominent feature of the interferogram is a relatively uniform high temperature structure of the constant pressure recirculation region (Figure 29). The straight shear layer can be seen to be lifted above the recirculating flow, which appears to be constructed from a single vortex sheet with some smaller cells imbedded close to the reattachment region. This feature is significant from the viewpoint of the turbulence modeling of these flows. The rapid recompression that is always observed in reattachment regions is accompanied by the formation of a reattachment shock. This shock relaxes to the wedge shock as the influence of the more efficient compression process close to the separated region disappears. Meaningful interpretation of the interferometer data obtained is difficult, if not impossible, because significant refraction effects are clearly observed in the interferogram. As observed and discussed in earlier papers, the schlieren photographs reveal an almost sinusoidal shock structure in the reattachment region, possibly reflecting a movement of the reattachment point. Such a movement indicates changes in the flow reversal in the separated region. This aspect of flow unsteadiness could significantly influence the size of the separated region, and clearly complicates a numerical description of this flow. The development of turbulence through the large pressure gradients in the reattachment region and the subsequent relaxation in the constant pressure region downstream of reattachment are important features of this flow. If refraction and edge effects can be eliminated from the fringe shift measurement, holographic interferometry will provide extremely valuable quantative measurements of this separated flow field.

The reattachment region presents additional difficulties, because the strong flow curvature and rapid thinning of the boundary layer here may be generating three-dimensional flow structures (Goertler vortices) that clearly prevent a meaningful interpretation of these interferograms. Such three-dimensional effects also may be induced in the strong flow curvature close to the separation point. Basically, the unsteady and three-dimensional characteristics of these flows must be understood to develop accurate numerical descriptions of these flows, but an understanding of the unsteady and three-dimensional effects is also needed to help interpret the optical measurements. This point further suggests a need to study less complicated flows first (e.g., axisymmetric laminar cases previously mentioned).

4.4.5 Incident Shock Wave/Turbulent Boundary Layer Interaction

As in the flow over the flat plate/wedge compression corner, the size and flow structure in a region of incident shock impingement is controlled by the mutual interaction between the viscous and inviscid flow. However, the disturbances are generated outside the boundary layer, and the incident shock strength is modified by its interaction with the separation shock. The measurements of heat transfer and pressure on this configuration are shown in Figure 35, together with schlieren photographs made in earlier studies.[27] The measurements made in the current studies are shown in Figures 37 through 39. The structure of the upstream disturbance generated by the incident shock is very similar to that generated over the flat plate/wedge model. The basic viscous/inviscid interaction resulting in flow separation takes place at the base of the boundary layer. Separation shock(s) traverse through a major segment of the boundary layer, interact with the incident shock, and are then turned almost parallel to the plate surface; an expansion fan is generated as the incident shock interacts with the constant pressure free shear layer. The boundary layer flow is again turned parallel to the flat plate by the formation of the reattachment shock. These features are clearly visible in the schlieren photographs and int ograms shown in Figures 36 through 38.

The structure of the recirculating region is shown in detail in Figure 36, which again suggests a basic single cell structure with a relatively uniform high temperature core. Again, however, the very large density gradients generated in the reattachment region have caused proportionately large refraction effects making the interpretation of the interferograms virtually impossible for this region. Similar to the reattachment region developed on the compression ramps, the strong flow curvature would likely cause the formation of three dimensional disturbances (Goertler vortices) in this region downstream of the incident shock. Again, the highly curved inflective shocks in the separation and reattachment regions are indicative of an unsteadiness which needs to be investigated with high frequency flow measurements to gain an understanding of these unsteady effects.

4.4.6 Separated Flows at the Cone/Flare Junction

Interferograms and shadowgrams for the axisymmetric flow fields obtained in the current study are shown in Figures 40 and 41. Measurements of the distribution

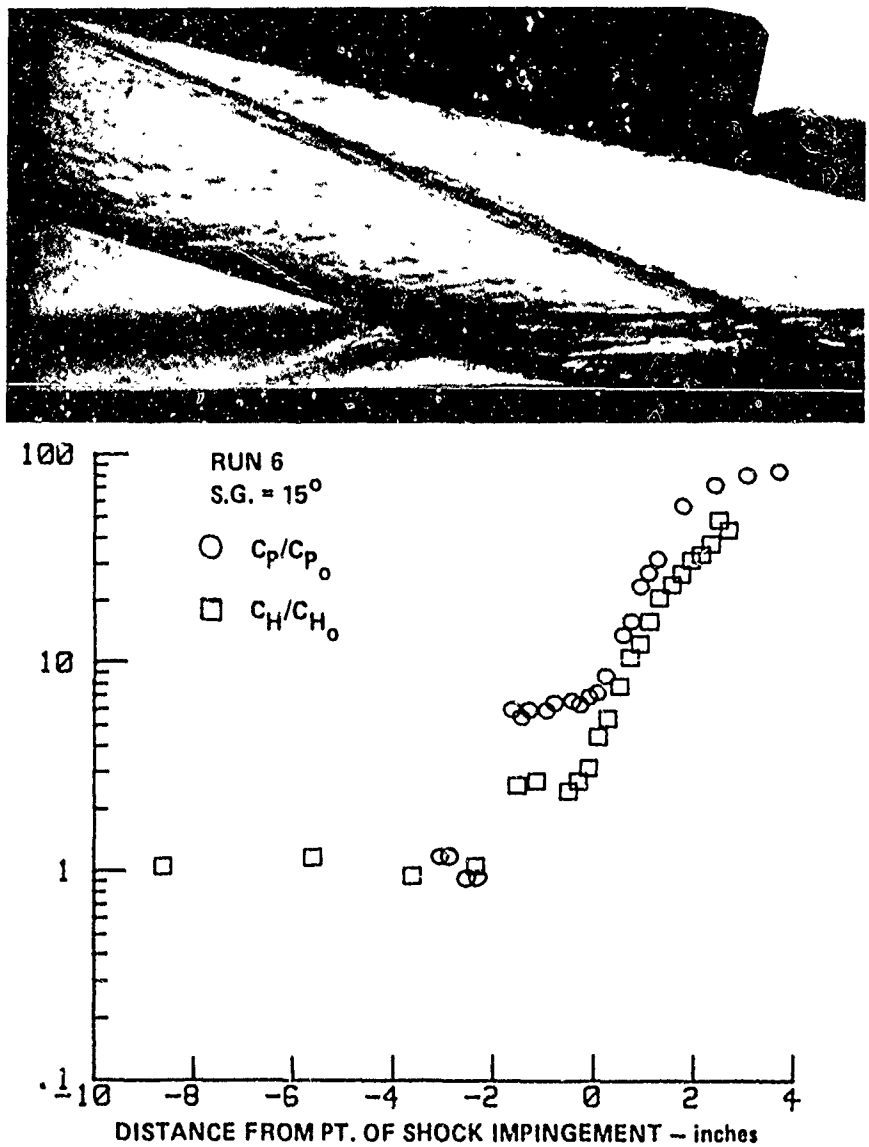

Figure 35 STREAMWISE DI: :IBUTIONS OF HEAT TRANSFER AND PRESSURE THROUGH SKEWED-OBLIQUE-SHOCK BOUNDARY LAYER INTERACTION (θ = 15° ψ = 0°)

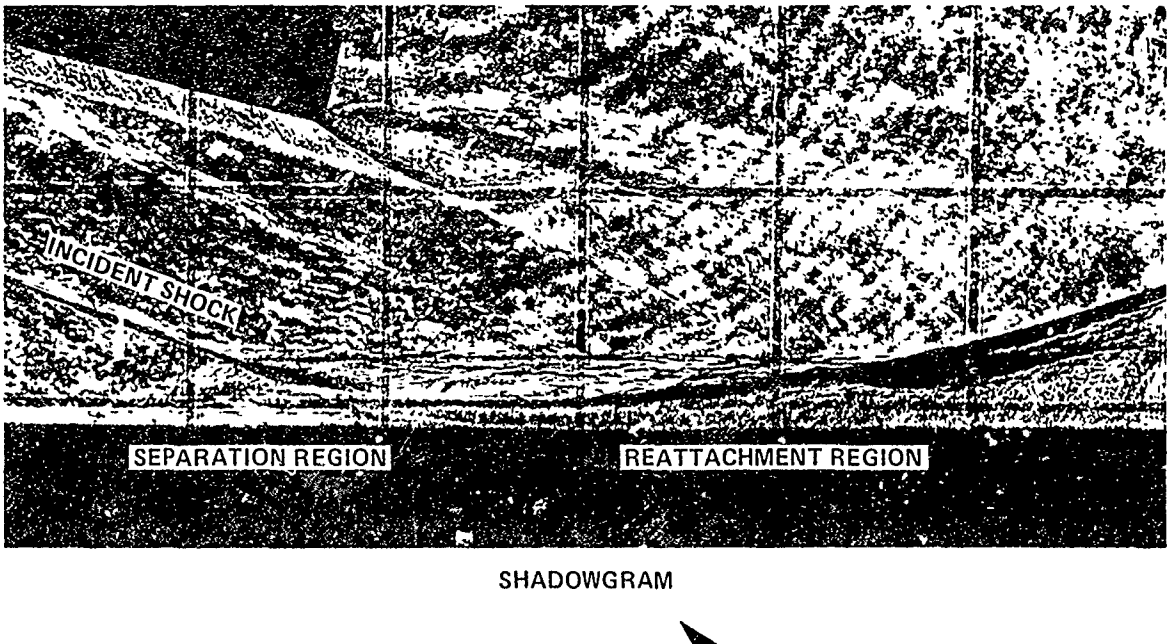

SHADOWGRAM

FLOW DIRECTION

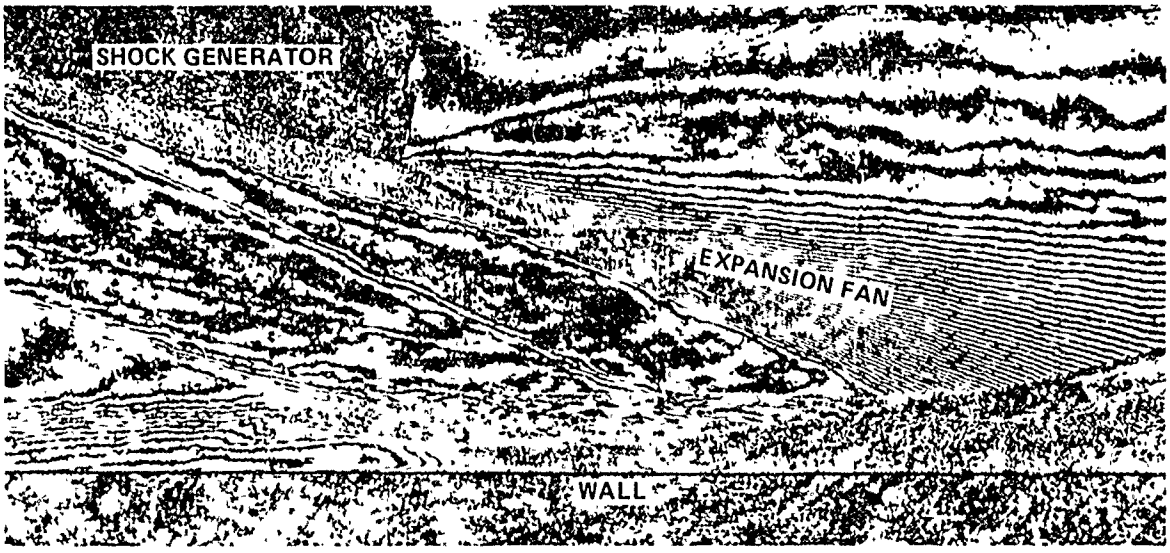

INTERFEROGRAM

GRID SIZE 38.1 x 38.1 mm

2-D FLAT PLATE	
SHOCK GENERATOR	15°
MACH NO.	11.34
REYNOLDS NO.	34.1×10^6
TEMPERATURE (T_o)	1603°K
PRESSURE (P_o)	100.2 MPa

Figure 36 HOLOGRAPHIC DEPICTION OF SHOCK-INDUCED BOUNDARY LAYER SEPARATION ON 2-D FLAT PLATE IN HYPERSONIC FLOW

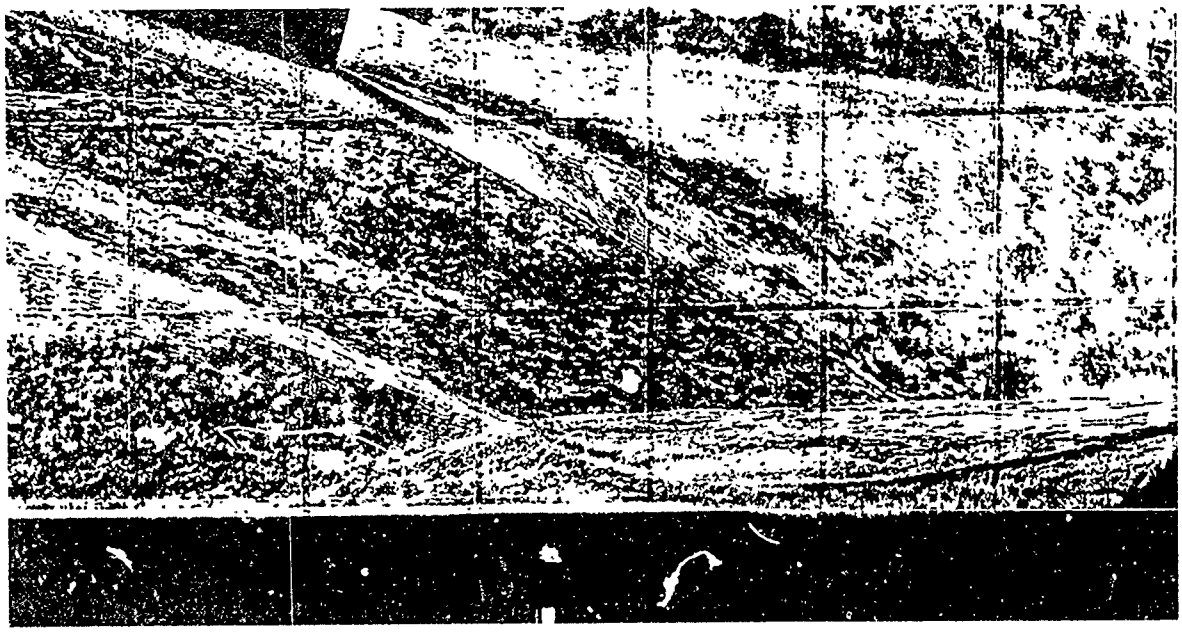

SHADOWGRAM

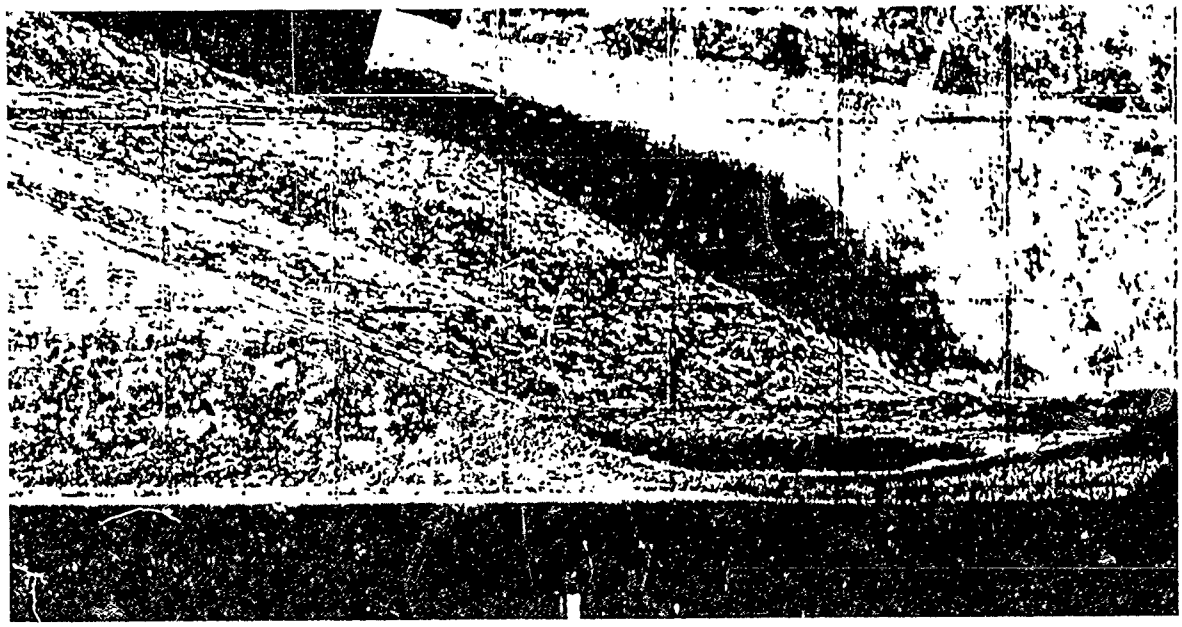

SCHLIEREN PHOTOGRAPH

2-D FLAT PLATE	
SHOCK GENERATOR	12.5°
MACH NO.	11.35
REYNOLDS NO.	35.1×10^6
TEMPERATURE (T_o)	1567°K
PRESSURE (P_o)	102.7 MPa

Figure 37 HOLOGRAPHIC DEPICTION OF HYPERSONIC BOUNDARY LAYER FLOW FIELD

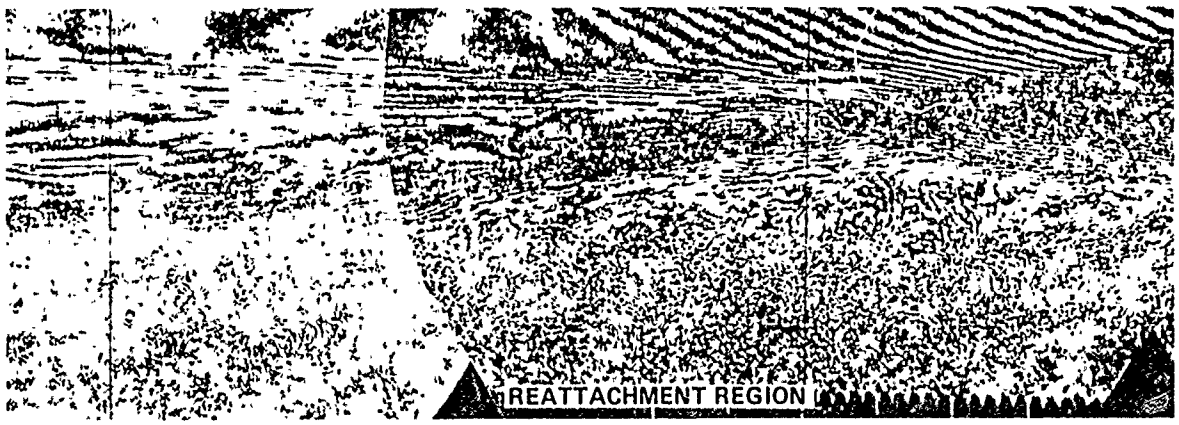

2-D FLAT PLATE	
SHOCK GENERATOR	15^{o}
MACH NO.	11.35
REYNOLDS NO.	34.1×10^{6}
TEMPERATURE (T_o)	1603°K
PRESSURE (P_o)	100.2 MPa

Figure 38 ENLARGEMENTS OF INTERFEROGRAM (REFERENCE FIGURE 36)

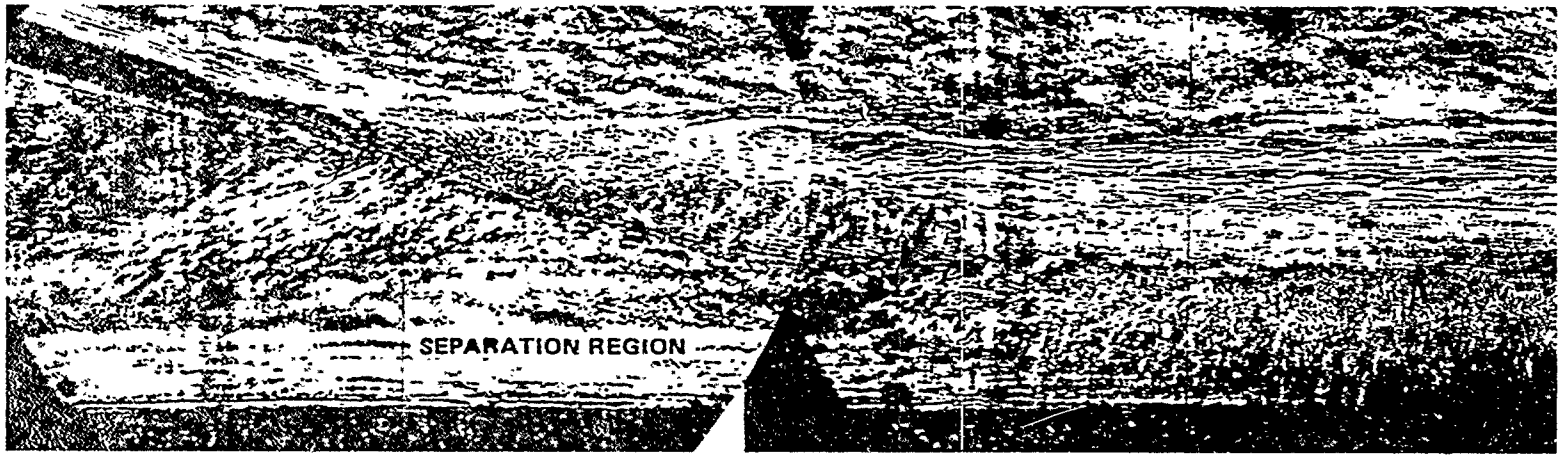

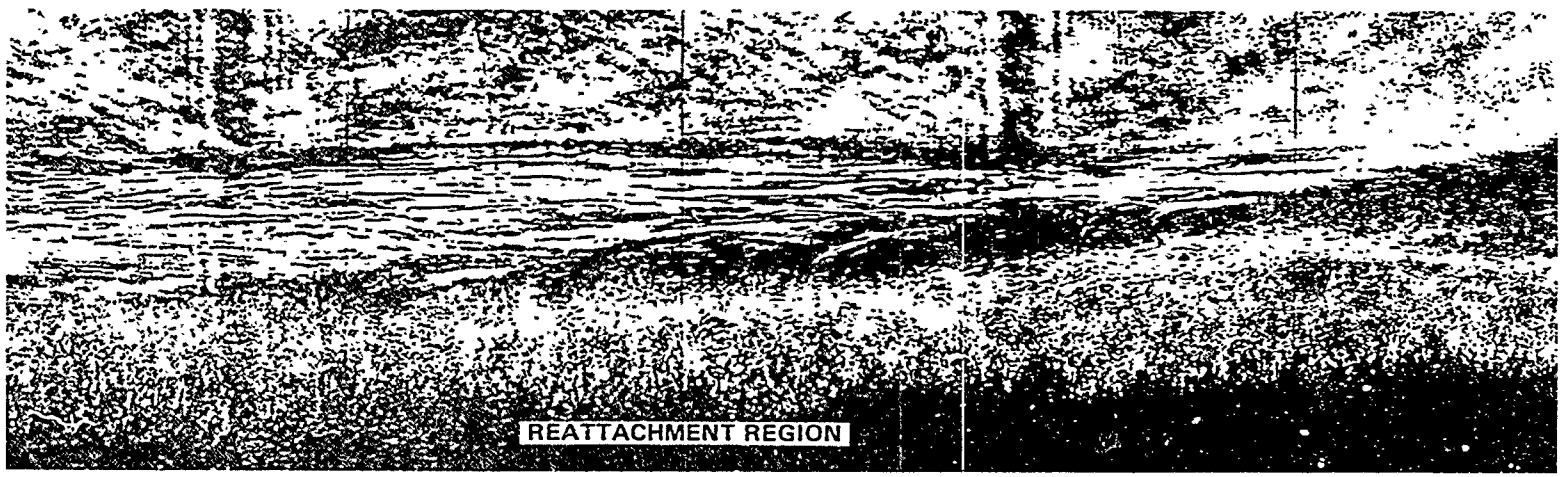

2-D FLAT PLATE	
SHOCK GENERATOR	15^{o}
MACH NO.	11.35
REYNOLDS NO.	34.1×10^{6}
TEMPERATURE (T_o)	1603°K
PRESSURE (P_o)	100.2 MPa

Figure 39 SHADOWGRAM ENLARGEMENTS OF FLOW FIELD (REFERENCE FIGURE 38)

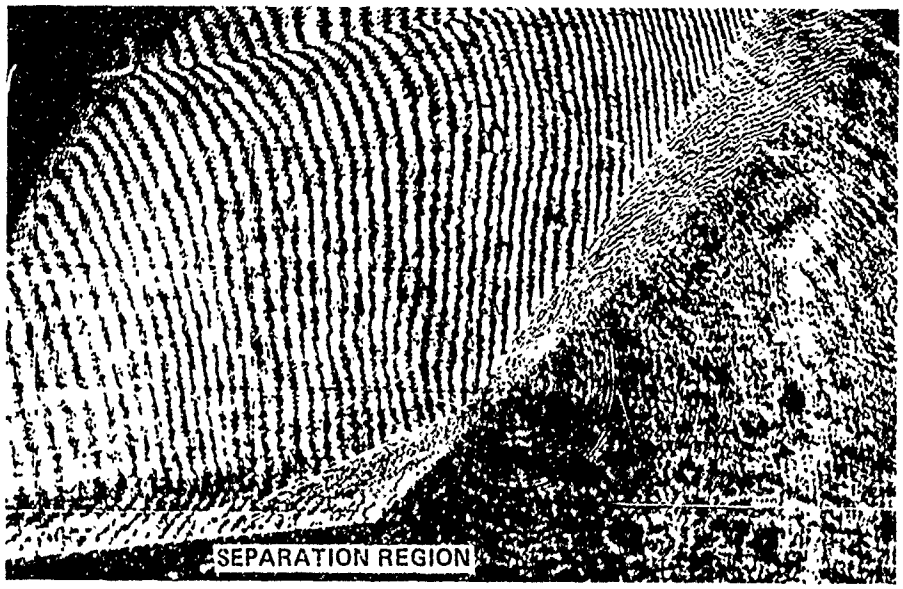

INTERFEROGRAM

FLOW DIRECTION

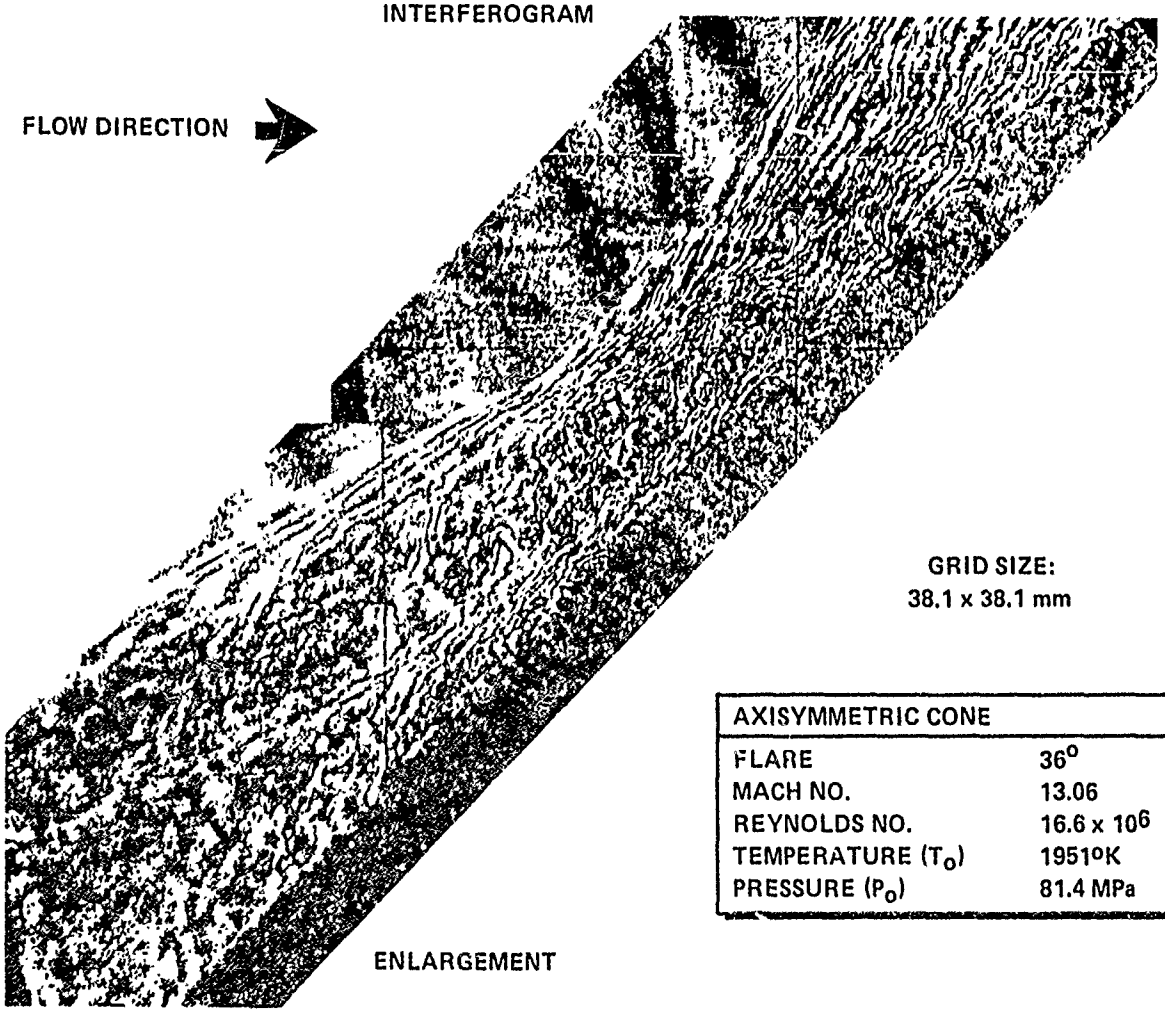

GRID SIZE:
38.1 x 38.1 mm

AXISYMMETRIC CONE	
FLARE	36^{o}
MACH NO.	13.06
REYNOLDS NO.	16.6×10^{6}
TEMPERATURE (T_o)	1951°K
PRESSURE (P_o)	81.4 MPa

ENLARGEMENT

Figure 40 HOLOGRAPHIC INTERFEROGRAMS OF AXISYMMETRIC COMPRESSION-RAMP-INDUCED BOUNDARY LAYER SEPARATION

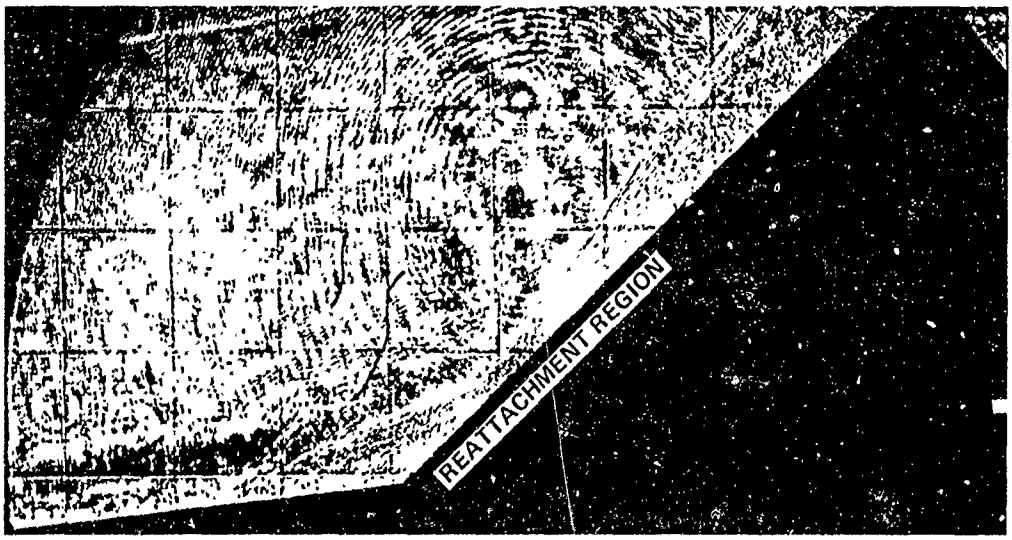

SHADOWGRAM

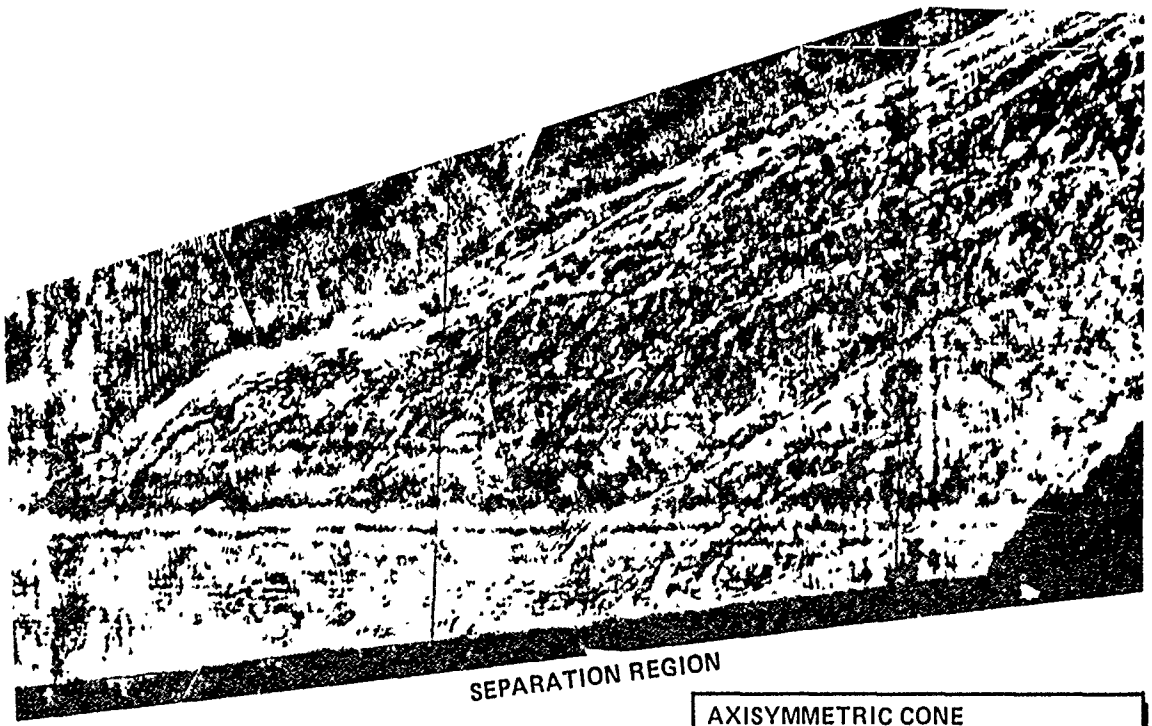

ENLARGEMENT

AXISYMMETRIC CONE	
FLARE	36^{o}
MACH NO.	13.06
REYNOLDS NO.	16.6×10^{6}
TEMPERATURE (T_o)	1951°K
PRESSURE (P_o)	81.4 MPa

Figure 41 HOLOGRAPHIC SHADOWGRAMS OF HYPERSONIC FLOW FIELD (REFERENCE FIGURE 40)

of heat transfer and pressure over this configuration made in previous studies[21] are shown in Figure 42 along with a conventional schlieren photograph. The 36° flare angle generates a large separated region which extends 2 inches ahead of the cone-flare junction. As expected, the flow in the separated region is very similar to the corresponding regions on the compression ramp and incident shock configurations. However, interpretation of the phenomena causing the shock waves in the neighborhood of the constant pressure separated region is not understood. This multiplicity of shocks is also clearly discernible in the reattachment region of the flow, again leading to speculation on the intrinsic unsteady or three-dimensional character of the flow in this region. Even though the optical path lengths of these reattachment regions are significantly shorter than those of the two-dimensional models, strong refraction appears to distort these interferograms as well. Finding the best way to reduce the interferometer measurements of these axisymmetric separated regions remains an important task. However, resolving this problem may be easier and more productive than attempting to evaluate edge effects of the two-dimensional models.

4.5 CONCLUSIONS

A preliminary investigation has been conducted into the use of holographic interferometry to study regions of shock wave/boundary layer interaction in a hypersonic shock tunnel. The interferograms of the complex flow fields generated in this investigation provide a good qualitative basis for evaluating some of the important phenomena that control the characteristics of th e flows. However, the quantitative evaluations of the interferograms are made difficult by edge effects and three-dimensional flow effects on two-dimensional models and by refraction effects in regions of high density gradients close to the wall. The disagreement between density measurements and simple prediction techniques for turbulent flat plate boundary layers indicates that further analyses and experiments are required to develop an understanding of both the refraction and three-dimensional effects. Future studies should be directed towards laminar flows over axisymmetric and two-dimensional models after which the more difficult conditions of these turbulent flows can be understood.

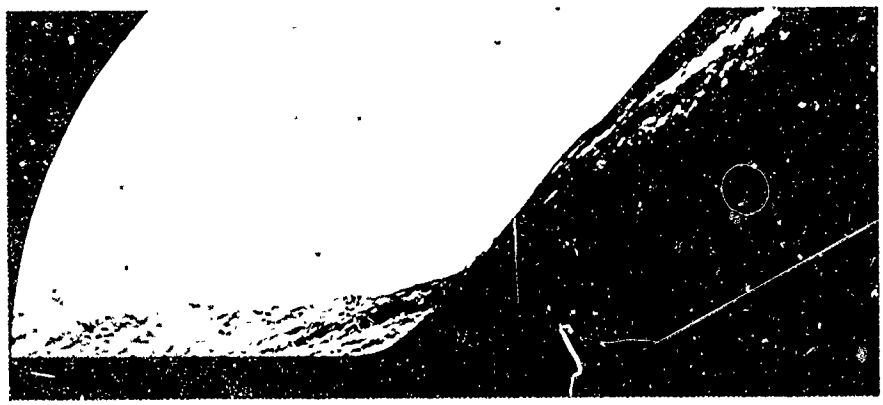

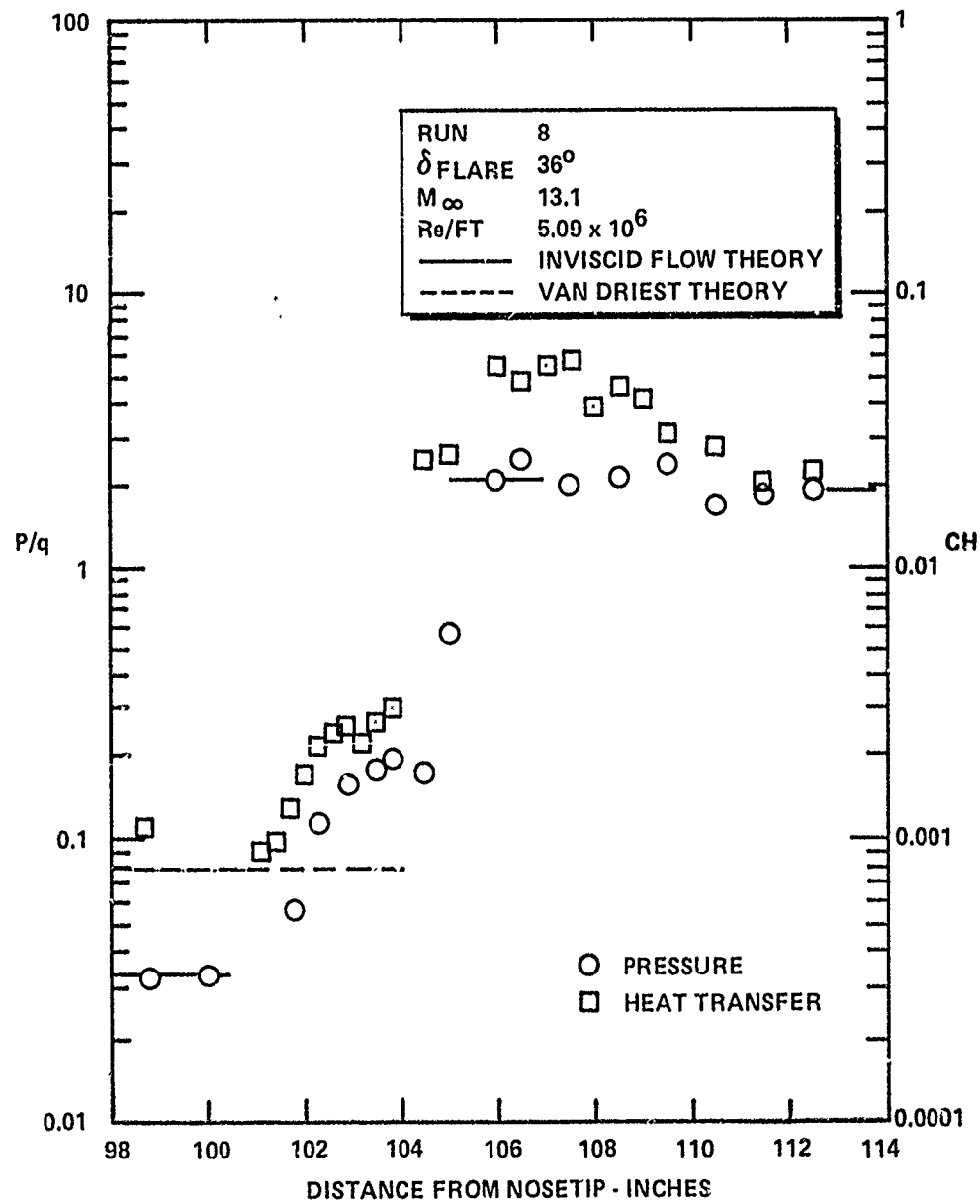

Figure 42 DISTRIBUTION OF PRESSURE AND HEAT TRANSFER IN SEPARATED FLOW OVER THE LARGE 6° CONE/36° FLARE CONFIGURATION

Section 5
CONCLUSIONS

This report summarizes the research conducted under the current contract to investigate fundamental problems associated with flight at hypersonic speeds with particular emphasis on those related to the aerothermal effects of viscous/inviscid interactions and boundary layer transition.

Solutions have been obtained to Navier-Stokes equations for the laminar flow over the leading edge of a sharp flat plate in Mach 16 flow for highly cooled wall conditions using a modified MacCormack/Shang fully explicit formulation. To obtain a stable converged solution, it was necessary to reduce the grid size close to the leading edge to the order of the mean free path, and, typically, 20,000 time steps were required to achieve convergence. However, once obtained, the solution was in good agreement with the experiment.

The experimental study conducted under the current contract was directed toward obtaining detailed flow field measurements in a separating boundary layer over a large cone/flare model. In this study, the structure of the separating boundary layer was examined with pitot, total temperature and laser holography measurements. These measurements suggest that the total temperature/velocity relationship in the cone boundary layer is quadratic rather than the usually assumed linear form suggested by Crocco. The Van Driest transformation, which has been used successfully in supersonic flows over adiabatic walls to relate the measured velocity to similar measurements in subsonic flow, is apparently not as effective in hypersonic flows over highly cooled walls. The measurements in the separation region demonstrate a rapid change in the structure of the sublayer as separation takes place and the formation of strong shock waves in the turbulent shear layer.

In addition to experimental studies of turbulent boundary layer separation in hypersonic flow, during the past year, further analysis has been performed of measurements made during earlier studies for AFOSR. This work has resulted in two AIAA publications during the course of this current contract. We investigated the aerothermal characteristics of nosetips and leading edges as transition moves onto the nosetip. In these studies, it was shown that heat transfer rates significantly larger than the stagnation value can be generated near the sonic line close to the end of the

transition region, and such large heat transfer rates can cause serious indentations of an ablative nosetip. The results of these studies for transitional flows over hemispherical and indented noseshapes were reported at the annual AIAA meeting in January 1986 (see Appendix A). Finally, an invited paper reviewing the status of research in aerothermal problems in hypersonic flight with emphasis on those associated with boundary layer transition, and viscous/interaction and flow separation, was presented at the Annual AIAA Meeting in January 1986 (Appendix B).

Section 6
REFERENCES

1. Knight, D.D., "Problems in Reconciling Computation and Experiment," 1985 Princeton University Workshop on the Structure of High-Speed Turbulent Boundary Layers.

2. Knight, D., Horstmann, C.C., Shapey, B., and Bogdonoff, S., "The Flowfield Structure of the 3-D Shock Wave Boundary Layer Interaction Generated by a 20 Degree Sharp Fin at Mach 3," AIAA-86-343, Jan. 6-9, 1986.

3. Shang, J.S., Hankey, W.L., and Petty, J.S., "Three-Dimensional Supersonic Interacting Turbulent Flow Along a Corner," AIAA Paper 78-1210, July 1978; also AIAA Journal, Vol. 17, No. 7, July 1979, pp. 706-713.

4. Horstmann, C.C. and Hung, C.M., "Computations of Three-Dimensional Turbulent Separated Flows at Supersonic Speeds," AIAA Paper 79-2, January 1979.

5. Settles, G.S. and Hortsmann, C.C., "Flowfield Scaling of a Swept Compression Corner Interaction -- A Comparison of Experiment and Computation," AIAA-84-0096, 22nd Aerospace Sciences Meeting, January 9-12, 1984.

6. Holden, M.S., "Preliminary Studies of Shock Wave-Turbulent Boundary Layer Interaction in Hypersonic Flow," AIAA Paper 72-74, 17-19 January 1972, 10th Aerospace Sciences Meeting, San Diego, CA.

7. Chapman, D.R. "Computational Aerodynamic Development Outlook," AIAA Journal, Vol. 17, pp. 1293-1313, 1979.

8. Anderson, D.A., Tannehill, J.C., and Pletcher, R.H., Computational Fluid Mechanics and Heat Transfer, 1984, McGraw Hill.

9. Tennekes, H., and Lumley, J.L., A First Course in Turbulence, 1985, MIT Press.

10. Jones, W.P., and Launder, B.E., "The Prediction of Laminarization with Two-Equation Model of Turbulence," Int. J. of Heat Mass Transfer, Vol. 15, pp. 301-314, 1972.

11. Karvorkin, J., Cole, J.D., Perturbation Methods in Applied Mathematics, Spring-Verlag, 1981.

12. Rudman, S. and Rubin, S.G., "Hypersonic Viscous Flow over Slender Bodies with Sharp Leading Edge," AIAA Journal, Vol. 16, pp. 1883-1889, 1968.

13. Cheng, H.K., Chen, S.Y., Mobley, R., Huber, C.R., "The Viscous Hypersonic Slender Body Problem: A Numerical Approach Based on a System of Composite Equations," The Rand Corporation, Report No. RM-6193-PR, Santa Monica, CA, 1970.

14. Shang, J.G., Buning, P.G., Hankey, W.L., "Performance of a Vectorized Three-Dimensional Navier-Stokes Code on the CRAY-1 Computer," AIAA Journal, Vol. 18, pp. 1073-1079, 1980.

15. Viviand, H.," Conservative Forms of Gas Dynamic Equations," La Recherche Aerospatiale, No. 1971-1, pp. 65-68, 1974.

16. MacCormack, R.W., and Baldwin, B.S., "A Numerical Method for Solving the Navier-Stokes Equations with Applications to Shock-Boundary Applications," AIAA Paper 75-1, Pasadena, CA, 1975.

17. Shang, J.G. "Numerical Solution of the Compressible Navier-Stokes Equations for a Three-Dimensional Corner," AIAA Paper 77-169, Los Angeles, CA, 1977.

18. Baldwin, B.S., and Lomax, H., "Thin-Layer Approximation and Algebraic Model for Separated Turbulent Flows," AIAA Paper 78-257, Huntsville, AL, 1978.

19. Holden, M.S., "Experimental Studies of the Effects of Asymmetric Transition on the Aerothermal Characteristics of Hypersonic Blunted Slender Cones," AIAA Paper 85-0325, 1985.

20. Hung, C.M., MacCormack, R.W., "Numerical Solutions of Supersonic and Hypersonic Laminar Compression Corner Flows," AIAA Journal, Vol. 14, pp. 475-481, 1976.

20A. Holden, M.S., "A Study of Flow Separation in Regions of Shock Wave-Boundary Layer Interaction in Hypersonic Flow," AIAA Paper 78-1169, Seattle, WA, 1978.

21. Holden, M.S., and Lee, Jhinho, "Viscous Interactions at Hypersonic Speeds", CUBRC Report No. 86611, October 1986.

22. Maise, G. and McDonald, H., "Mixing Length and Kinematic Eddy Viscosity in a Compressible Boundary Layer," AIAA Paper 67-199, January 1967.

23. Coles, D., "Measurements in the Boundary Layer on a Smooth Flat Plate in Supersonic Flow," Ph.D. Thesis, California Institute of Technology, 1953.

24. Havener, A.G., "Users Guide on Pulsed Laser Holography for Wind Tunnel Testing," ARLTR 75-0213, Aerospace Research Laboratories, Wright-Patterson AFB, Dayton, OH, AD/A017710, June 1975.

25. Havener, A.G. and Radley, R.J., "Turbulent Boundary Layer Flow Separation Measurements Using Holographic Interferometry," AIAA Journal, Vol. 12, August 1974, pp 1071-1075.

26. Holden, M.S., "Experimental Studies of Quasi-Two-Dimensional and Three-Dimensional Viscous Interaction Regions Induced by Skewed-Shock and Swept Shock Boundary Layer Interactions," AIAA Paper 84-1677, AIAA 19th Thermophysics Conference, Snowmass, CO, June 25-27, 1984.

27. Holden, M.S., "Shock Wave Turbulent Boundary Layer Interaction in Hypersonic Flow," AIAA Paper 77-45, AIAA 15th Aerospace Sciences Meeting, Los Angeles, CA, January 24-25, 1977.

28. Holden, M.S. and Havener, A.G., "Shock Wave/Turbulent Boundary Layer Interaction in High-Reynolds-Number Hypersonic Flow, USAF/AFSC/AFOSR Directorate of Aerospace Sciences, Bolling AFB, DC, 20332-6448, June 1987.

APPENDIX A

AIAA-86-0384

"Studies of the Heat-Transfer and Flow Characteristics
of Rough and Smooth Indented Noseshapes
Part I. Steady Flows"

By:

M.S. Holden
Calspan Corporation

AIAA 24th Aerospace Sciences Meeting
January 6-9, 1986
Reno, Navada

AIAA'86

AIAA-86-0384

Studies of the Heat-Transfer and Flow Characteristics of Rough and Smooth Indented Noseshapes Part I. Steady Flows

M.S. Holden
Arvin/Calspan Corporation
Buffalo, NY

AIAA 24th Aerospace Sciences Meeting
January 6-9, 1986/Reno, Nevada

STUDIES OF FLOWS OVER INDENTED NOSE SHAPES

PART I - STEADY FLOWS

MICHAEL S. HOLDEN*
CALSPAN CORPORATION
BUFFALO, NY 14225

Supported by AFOSR and Calspan Corporation

ABSTRACT

Experimental studies have been conducted to examine the flow structure and distribution of heat transfer and pressure over indented noseshapes. Measurements were made to examine the influence of boundary layer trips; surface roughness; and Mach number and Reynolds number of the freestream, on the size and structure of the shock/turbulent boundary interaction over the nosetips. It was demonstrated that Mach number and surface roughness are of key importance in the correct simulation of these flows, and it is essential in the correct simulation of these flows, and it is essential that the boundary be fully turbulent upstream of the body shock/boundary layer interaction. In similar studies of the flow over the recovered NRV noseshape at conditions which duplicated the flight Mach number and Reynolds number, it was demonstrated the flow was intrinsically three-dimensional and that the distribution of heat transfer and pressure were also controlled by boundary layer transition and shock/boundary layer interaction. In a study performed specifically for code validation, detailed measurements of heat transfer and pressure were made in laminar flows over two indented noseshapes. Navier-Stokes solutions for one of these case obtained by Widhopf and Victoria exhibited unsteady flows. Experiment showed the flow to be stable; however, it was observed that the heat transfer measurements were in agreement with the time averaged predictions.

I. INTRODUCTION

Wind tunnel studies using ablating models have demonstrated that "slender" concave nose shapes, over which separated regions and gross flow instabilities are observed, can be formed under certain free stream conditions and nosetip properties. While an explanation of this behavior using sophisticated shape change codes awaits the development of accurate models of regions of transition and shock wave/turbulent boundary layer interaction the simple equilibrium solutions obtained by Welsh[1] provide an important insight into the development of ablated nose shapes. Welsh's analysis predicts the occurrence of the well known "blunt" self-preserving nose shape for fully laminar or fully turbulent boundary layers; however, for flows where transition occurs ahead of the sonic point on the nosetip (and under certain fully turbulent conditions) this approach predicts the occurrence of slender nose shapes similar to those shown in Figure 1. This result has been verified in wind tunnel tests of camphor models where shapes similar to those shown on Figure 2 can be developed under transitional conditions. The existence of slender ablated nose shapes have been demonstrated in many experimental studies[2,3,4,5] in general, however, these shapes exhibit marked asymmetric characteristics. Asymmetric nose shapes can give rise to large de-stabilizing moments and side forces. Highly indented nose shapes, under conditions similar to that shown in Figure 3 were generated on camphor models, and over such shapes the viscous and inviscid flow fields interact in such a way that the flow became oscillatory.

In studies of ablated nose shapes, it has become customary to describe the nosetip geometry in terms of the BI-CONIC or TRI-RADIUS configuration. Schematic representations of these shapes are shown in Figure 4a. The form of a highly ablated nose shape which is to be characterized by these models is shown in Figure 5. The increased heating resulting from boundary layer transition close to the sonic region is believed responsible for the initial development of the identation in ablating nose shapes. Because transition in such a situation is almost certainly three-dimensional in character, the initial indenting of the nosetip will also reflect the asymmetric characteristics of the transition process. Subsequently the large heating rates which are developed in the recompression region resulting from shock-boundary layer interaction at the base of the indentation can cause grossly indented nose shapes. While it is possible to predict the initial indenting using relatively simple shape change code, when significant ablation occurs the computation of heating over the rough surface for flows with embedded regions of shock wave-boundary layer interaction are subject to considerable uncertainties. To calculate the effects of surface roughness on heating and surface recession, the magnitude of the surface roughness and the roughness augmented heating in the presence of blowing must be predicted. The prediction of the heating to the embedded regions of shock wave turbulent boundary layer interaction, some involving separated flows, over a rough surface represents one of the most difficult configurations to calculate with precision. Although there have been a number of experimental studies[2,3,5] to examine the distribution of heating to non-indented nose shapes and investigations with a major emphasis on examining the gross stability of flows over highly indented nose shapes, little detailed information is available for indented nosetips where attached or slightly separated regions of shock wave-turbulent interactions occur. Such studies are required to provide a method of evaluating and developing the prediction methods, and obtaining better insights into the basic phenomena leading to nosetip indentation.

This paper is composed of three experimental studies designed to provide fundamental information on the characteristics of the flow over indented nose shapes. In the first study we examined the parameters which control the correct simulation of the flow over a non-ablating axisymmetric indented nosetip. Detailed measurement of heat transfer, pressure and flow field structure were made on rough and smooth configurations for a range of Mach numbers and Reynolds numbers. We describe a study using a 4X replica of the recovered NRV nosetip, in which

*Member, AIAA

detailed heat transfer, pressure and flow field measurements were made for Mach numbers and Reynolds number conditions which duplicated those obtained in flight. Finally the results of a study of laminar flows over two indented nose shapes are reported to provide a basis for evaluating solutions obtained using the full Navier Stokes equations.

II. STUDIES TO INVESTIGATE THE SIMULATION OF FLOWS OVER INDENTED NOSE SHAPES

Introduction

Because the initiation and development of nosetip indentation is so strongly influenced by the occurrence and position of boundary layer transition on the nosetip, experimental studies to simulate these flows must be very carefully constructed. To correctly simulate the flow over a mildly indented nose shape, it is of fundamental importance that the Reynolds number be of a sufficient magnitude to move transition relatively close to the stagnation region and preserve turbulent flow through the strong expansion which precedes the model concavity. To correctly simulate the flow field and the distribution of heating beneath the embedded region of shock wave/turbulent boundary layer interaction, the Mach number, Reynolds number and wall-to-free stream stagnation temperature ratio must be correctly simulated as well as the surface roughness of the model.

In this segment of the study we examined the flow field and distribution of heating to the indented nosetip at high Mach numbers for unit Reynolds numbers large enough to establish turbulent boundary layers over the model without tripping. We wished to investigate the effects of trips and free stream Mach number on the heating distribution for a fully turbulent condition. We then wanted to determine the effects of surface roughness on the distribution of heating and flow field properties for both high and low Reynolds number free stream conditions.

Models and Instrumentation

The model used in this study was as tri-radius representation (see Figure 4b) of an ablated indented nosetip. This configuration is one of a family of nose shapes, a number of which have been examined experimentally in earlier studies conducted at Calspan to examine the stability boundaries for the flow over indented nosetips. From the earlier studies[3] conducted at Calspan, we would predict that provided the boundary layer remained turbulent over the nosetip ahead of the concave section of the nosetip, the boundary layer should remain attached or slightly separated from the base of the body shock. Our earlier studies with rough and smooth 45 degree biconic nosetips[4] suggested that a fully turbulent boundary layer could be anticipated for free stream Reynolds numbers of 10 x 10^6/ft and 5 x 10^6/ft at Mach 11 and 13, respectively, while for Reynolds numbers of 2 x 10^6/ft, the upstream of the body shock would be laminar or transition. In this latter case, we would expect laminar separation to occur and spread forward to the tip causing the flow field to differ markedly from the equivalent fully turbulent case.

The model of the indented nosetip used in these experimental studies is shown in both its smooth and rough configuration in Figure 6. The rough model had 15 mil sand grain roughness bonded to its surface with pressure-sensitive adhesive and was instrumented with rough calorimeter heat transfer gages (see Ref. 6). The gage positions were selected to provide detailed coverage in the area of greatest interest--the recompression/reattachment region beneath the body shock. The gradients of heating in this area are such that isolated gages, or gages placed on a low diffusivity substrate are required to prevent inaccuracies which will result from streamwise heat conduction. Employing "thin skin" heat transfer techniques with a non-segmented model could lead to serious inaccuracies in the heat transfer measurements in the shock interaction region on the model (Ref. 7). We used a single pass schlieren system with a focal length of 10 feet for flow visualization in this study., the knife edge was set parallel to the conical segment which precedes the concave section of the model, and adjusted to give a 15 percent cut-off.

Results and Discussion

In this study the effects of the Mach and Reynolds number of the freestream were investigated first on the smooth indented nose shapes. We then coated same nosetip with 15 mil roughness and again examined the effect of Mach number and Reynolds number. Heat transfer and schlieren measurements were made on both configurations to examine the flow mechanisms upstream and in the regions of body shock-boundary layer interaction over the nosetip. Particular emphasis was placed in these studies on examining how the scale of the body shock-boundary layer interaction and the distribution and peak heating is influenced by the freestream Mach number and the ratio of roughness height to momentum thickness (K/θ) upstream of the interaction region.

Studies with the Smooth Nose shapes

The first set of measurements were made at Mach 11 for a Reynolds number (Re_D.) of 12 x 10^6 based on body diameter. Here the emphasis was first on determining whether we could obtain a fully turbulent boundary layer over the model without employing boundary layer trips. We then examined the effects of boundary layer trips on the properties of the body shock interaction region. The effects of Mach number and Reynolds number were then studied.

The distribution of heat transfer to the completely smooth model and a schlieren photograph of the flow at M=11 $Re_d=10^7$, are shown in Figures 7 and 8. The heat transfer measurements demonstrate that the boundary layer remains turbulent as it expands onto the short conical section of the model upstream of the body shock-boundary layer interaction. The severity of the shock interaction is such that a small turbulent separated region is induced ahead of the body shock, its presence being marked by separation shocks in the schlieren photographs and indicated by the characteristic rise and plateau region in heat transfer distribution upstream of the body shock. A steep rise in the heating rate occurs in the re-compression region downstream of the body shock resulting in peak heating rates of over three times those measured at the stagnation point. The inviscid flow above the boundary layer downstream of the body shock is dominated by the interaction between the nosetip, body and separation and reattachment shocks. The vorticity generated in the inviscid flow behind the body shock is reflected in the large density variations which can be observed in the schlieren photographs. The complexity of interacting flow in this important region just downstream of the body shock makes a numerical analysis of these flows very difficult.

We then examined whether employing an annular 15 mil trip ring around the sonic point on the nosetip would

disturb the flow structure and distribution of heating to the model under the fully turbulent conditions found in Run 1. The schlieren photographs and distribution of heating for this tripping experiment are shown in Figure 8. There is little difference between the flow patterns obtained in Runs 1 and 2; and the comparisons between the measured heating distributions shown in Figure 7 indicates that with the exception of the region immediately ahead and behind the trips, the distribution of heating is relatively uninfluenced by the presence of the trips. The effects of freestream Mach number were explored by repeating the studies at Mach 13. The schlieren photographs and distribution of heating obtained are shown in Figures 9 and 10. Both the schlieren photographs and the heat transfer distribution indicate that the flow remains attached upstream of the body shock. Comparing the distribution of heat transfer coefficients for the Mach 11 and 13 flows (shown in Figure 9), it is clear that the peak heat transfer coefficients for the Mach 13 flow are almost twice those at Mach 11. We believe this results from a greater severity of the compression process in the interaction region of the Mach 13 flow. It is clear from the levels of heating through the body shock-boundary layer interaction region that the boundary layer was fully turbulent in both the Mach 11 and 13 flows over the nosetip.

Studies with the Rough Nosetip

The distribution of heating to and the flow pattern of the rough nosetip at Mach 11 for RE_d=11 x 10^6 are shown in Figures 11 and 12. While the position of the body shock remains essentially unchanged by surface roughness, separation has spread further forward than on the smooth model at the same freestream conditions. We believe this forward moment of separation results principally from a significant thickening of the boundary layer upstream of the interaction combined with the decreased velocity adjacent to the wall both of which result from surface roughness. The heat transfer measurements on the rough and smooth configurations, which are compared in Figure 11, show that while the position of the region of peak heating remains unchanged by surface roughness, the recompression heating is nearly doubled by roughness effects. The measurements made on the nosetip at Mach 13 are shown in Figures 13 and 14. As we observed in the smooth wall studies, increasing Mach number increases the nondimensional heating rate, and the comparison shown in Figure 18 indicates that this is also true for rough walls.

It is clear from these studies that the scale of the body shock-boundary layer, as well as the peak interaction heating, are strongly controlled by the scale of the surface roughness and the freestream Mach number. We measured increases in the heating coefficients of close to 100 percent from either increasing Mach number or adding surface roughness, resulting in a combined enhancement effect of close to 300 percent. Because of the formation of separated embedded interaction regions on these indented noseshapes, the blunt body Mach number independence principal cannot be expected to apply directly to these flows.

This study underlined the importance of careful selection of the scale of the surface roughness, in addition to testing at the highest Mach number for which fully turbulent conditions can be generated. The large gradients generated in the interaction region makes it imperative that streamwise heat transfer conduction along the model surface be minimized to obtain accurate heat transfer measurements by using isolated gages or a poorly conducting model.

STUDIES OF THE FLOW OVER RECOVERED NOSE SHAPES

Objective

The Nose Tip Recovery Vehicle (NRV) and the Role Torque Experiment Vehicle (RTE) nosetips are two of the few nosetips which have been recovered from flight during re-entry[8]. These nosetips are of particular interest because they were "caught" during the portion of the trajectory where transition was spreading over the nosetip, and a non-similar shape change was occurring. The nosetips shown in Figure 15, display two characteristics which are of key importance to the nosetip designer. The first is that the nosetip is indented to the point where three-dimensional separated regions of significant proportions must have been formed. The second feature is the distinctive three-dimensional grooved shape of the NRV and RTE nosetips, shapes which could not have been predicted from shape change codes.

The purpose of the present study was to obtain detailed heat transfer and pressure measurements on a model of the NRV nosetip at a Mach number and Reynolds number which duplicated flight conditions. The model was highly instrumented to examine the heat transfer and pressure in the re-attachment compression regions and close to the axial ridges. We wished to examine whether the flow was steady, to look for evidence of the streamwise vortices, and to determine the sensitivity to changes in Reynolds number.

Model and Instrumentation

A 4X scale model of the NRV nosetip was constructed for this program so that we could obtain detailed spatially resolved measurements and the ability to duplicate the Reynolds numbers obtained in the flight tests. The model was constructed using a precision three-dimensional pantagraph milling machine with a epoxy replica of the recovered nosetip as the original. The model was instrumented with 100 heat transfer gages and 43 pressure gages. The model is shown mounted in the 96-Inch Shock Tunnel in Figure 16.

Results and Discussion

A schlieren photograph of the flow over the NRV model is shown in Figure 17. This photograph illustrates the two classes of flow with embedded shocks which are typical of the flow over indented nose shapes. The flow over the top of the model separates as it expands downstream of the spherical cap and a small three-dimensional separated region is formed in the cavity formed by the grooves. The compression waves generated in the reattachment region coalesce to form a single shock--the re-compression shock. The bow shock and re-compression shock interact with the formation of a single shock and a shear layer. The flow over the bottom of the model remains attached: however, the flow over the roughly conical section of the nosetip was again characterized by a re-compression process. Here, however, re-compression takes place through a series of oblique shocks as a wall jet is formed. It is the structure and development of the boundary layer at the base re-compression processes which controls the large heat transfer rates which are developed in these regions.

The distributions of heat transfer and pressure over the NRV nosetip made in this study are shown in Figures 18 through 21. A typical heat transfer distribution for free stream conditions closest to those encountered in flight are shown in Figure 18a. The heat transfer measurements on the sperical cap indicate that the boundary layer remains laminar over this part of the model, with transition occurring in the free shear layer downstream of the shoulder expansion. While the heat transfer rates drop below the stagnation point value in the separated regions just downstream of the shoulder, heat transfer rates in the reattachment and re-compression regions over the model can rise to close to three times the stagnation point value. This increase is influenced by transition, the increased density and thinning of the boundary layer in the re-compression region and entropy swallowing. However, the measurements clearly indicate that the surface recession would be largest on the conical frustum of this nosetip. The pressure distribution over the nosetip for the conditions discussed is shown in Figure 18b. As we would anticipate from our observations on the schlieren photographs and the heat transfer measurements, the pressure rises along the roughly conical portion of the nosetip as a result of the re-compression process and reaches close to 89 percent of the stagnation pressure toward the base of the nosetip. However, there is a significant variation in the pressure around the conical segment of the nosetip as a result of the different re-compression processes associated with the circumferential variations in surface geometry.

During the design of this experiment, it was speculated that the flow over the NRV nosetip would be very sensitive to the Reynolds number and Mach number of the freestream, because boundary layer transition and separation were intrinsic features of the flow field. Therefore, a large scale replica of the NRV nosetip was constructed so that the flight Reynolds number could be duplicated in the Shock Tunnel. Thus, it was of interest to examine the effects of Reynolds number on the flow structure and the distribution of heat transfer and pressure over the nosetip. Figures 19a and 19b show the distribution of heat transfer and pressure over the NRV nosetip for conditions where we have lowered the Reynolds number to 1×10^6. This results in an increase in the size of the separated region and the aft movement of the re-compression regions. It also results in a decrease in pressure rise (relative to the stagnation point pressure) on the conical segment of the nosetip and a dramatic reduction (a factor of 3 relative to the stagnation point heat transfer) in the heat transfer to the conical frustum. These results underline the importance of conducting experimental studies of the flow over complex indented nose shapes at Reynolds numbers and Mach numbers as close to the flight conditions as possible. Further measurements made at Mach 11 and 13 with Reynolds numbers of 5×10^6/ft, which are shown in Figures 20 and 21, demonstrate that the heat transfer and pressure distribution are sensitive to the position of the boundary layer transition and the flow pattern, which are again controlled by the Mach number and Reynolds number of the freestream.

The measurements made in this study clearly demonstrate that the flow field and the distribution of properties on "real" ablated nose shapes differ significantly from the idealized biconic configurations assumed by many analysts. The flow over NRV configuration is intrinsically three-dimensional with regions of embedded separated flows as well as embedded shocks. Experimental studies of the flows over such configurations must be conducted at Reynolds numbers and Mach numbers which come close to duplicating those encountered in flight for meaningful results to be obtained.

LAMINAR FLOWS OVER INDENTED NOSE SHAPES

Introduction

When indented nose shapes occur on ablating nosetips they do so because the flow over the major segment of the nosetip is transitional and turbulent. However, there have been a number of theoretical studies in which predictions have been made of laminar flow over indented nose shapes. It was for this reason that the measurements made in this segment of the study were obtained to provide a detailed set of measurements in laminar flows with which to examine the validity of such solutions. We studied the laminar flow over two ablated nose shapes for which Widhopf and Victoria[9] obtained detailed numerical solutions to the complete flow field using the time-dependent Navier-Stokes equations. These nose shapes termed the 1-10-10 and 1-10-1 in the tri-radius terminology, (or the Widhopf 1 and 2) are shown in Figure 22.

Model and Instrumentation

Detailed heat transfer and pressure measurements were made over both of these configurations at Mach 10 for a Reynolds number (Re_N) of 300. The instrumentation and recording equipment were designed to enable frequencies up to 1 Mz to be recorded with little attenuation. Widhopf's calculations for the 1-10-10 configuration showed a high frequency instability occurred in the flow field close to the point of surface inflexion on this body. This localized oscillation was predicted to have a major frequency of approximately 600 KHz. Thus, the heat transfer gages were constructed so that their physical dimensions were smaller than the wavelength of the oscillation.

Results and Discussions

The heat transfer distribution to the 1-10-10 configuration is shown in Figure 23 together with the predictions from the Navier-Stokes solutions of Widhopf. Although the measurements are in good agreement with the mean values from these calculations, we were unable to detect the flow instabilities observed by Widhopf in his numerical solutions. Measurements were made at a different Mach number and Reynolds number to determine whether an oscillation could be induced at slightly different flow conditions, but again we found a stable flow. However, one of the most interesting aspects of the aerodynamics of this configuration is the large heating rates generated at the inflexion of the concave surface at the base of the embedded shock (see Figure 24). Studies of shock wave-turbulent boundary layer interaction on concave bodies suggest that an even larger increase in heat transfer would occur on the 1-10-10 configuration if the boundary layer were transitional or turbulent. An ablating body upon which these heating levels were impressed would tend to become more highly indented and possibly develop onto the shape of the 1-10-1 configuration.

Heat transfer, pressure and schlieren records from measurements made on the 1-10-1 configuration at Mach 10 demonstrate that the flow is fully pulsating in the E oscillation mode.[3] The schlieren photographs, shown in Figure 25 indicate the oscillation is symmetric with a frequency which gives a Strouhal number ($FD/\mathcal{V}$) of 0.19. The heat transfer and pressure to the model (shown in

igure 26) undergoes a cyclic variation with the heat transfer varying between a value which is approximately equal that to the stagnation point on a flat faced cylinder with the same body diameter, to a level six times as large. This later condition is attained during the part of the cycle where the separated shear layer impinges onto the almost vertical face of the afterbody. A small angle of attack can induce a second asymmetric oscillational mode during which a circumferential movement of the separated region occurs. While in laminar flows, the basic frequency of the E oscillational mode and the higher harmonics appear to be little influenced by the Mach number or Reynolds number of the freestream, for turbulent flows over configurations which are close to the oscillation boundaries these effects do become of importance. In Part II of this study, we describe an investigation of the occurence and structure of unsteady flows over symmetrical and asymmetric indented noseshapes.

CONCLUSIONS

Experimental studies have been conducted to examine the structure and properties of steady flows over indented nosetips. In this three-part study we first investigated the influence of boundary layer trips, surface roughness and the Mach number and unit Reynolds number on the flow field and distribution of heat transfer and pressure over an axisymmetric indented noseshape. At Mach 11 it was found that the surface properties and flow field was uninfluenced by tripping, but introducing uniform surface roughness increased the size of the separated region at the base of the body shock and doubled the maximum heating rate in this region. Both on the rough and smooth configuration the maximum heat transfer coefficient was doubled when the Mach number was increased from 11 to 12. It is clear that to correctly simulate the characteristics of the flow over indented noseshapes, the surface roughness of the nosetip, the Mach number and Reynolds number of the freestream, the incidence of the nosetip must be closely duplicated.

In the second investigation, in which a 4X replica of the recovered NRV nosetip was studied at conditions which duplicated those obtained in-flight, it was demonstrated that the flow field and distribution of pressure and heating differed significantly from the axisymmetric analog. The flow over the NRV nosetip is intrinsically three-dimensional and contains regions of embedded separated flows and complex viscous/inviscid interaction.

The study of the laminar flow over indented noseshapes was performed specifically for a validation of a solution generated by Widhopf and Victoria using their Navier-Stokes code. While we did not find the high frequency oscillation predicted by the numerical solution, the time averaged predictions were in good agreement with the experimental measurements made in the current studies.

In part two of this study we will examine the occurrence and properties of unsteady flows over indented noseshapes.

REFERENCES

1. Welsh, W.E. "Shape and Surface Roughness Effects on Turbulent Nose Tip Ablation" AIAA Journal Vol. 8 No. 11 November 1970, pp. 1983-1989.

2. Abott, M.J., et al "Unsteady Flow on Ablated Nosetip Shapes--PANT Series G Test and Analysis Report" Aerotherm Report 73-87, Project 7040, December 1973.

3. Holden, M.S. "Studies of the Effects of Transitional and Turbulent Boundary Layers on the Aerodynamic Performace of Hypersonic Re-Entry Vehicles in High Reynolds Number Flow" Calspan Report No. AB-5834-A-2.

4. Holden, M.S. "Studies of Transitional Flow, Unsteady Separation Phenomena and Particle Induced Augmentation Heating on Ablated Nose Tips" AFOSR TR 76-1066, October 1975.

5. Abbett, M.J., Cooper, T.J., Dahm, T.J. and Jackson, M.D. "Flow Characteristics about Concave Conic Forebodies at High Mach Numbers" AIAA Paper 75-153.

6. Holden, M.S. "Experimental Studies of Surface Roughness Shape and Spacing Effects on Heat Transfer and Skin Friction in Supersonic and Hypersonic Flows" AIAA-84-0016, Paper presented at the AIAA 22nd Aerospace Sciences Meeting, Reno, Nevada, 9-12 January 1984.

7. Hiers, R.S and Loubsky, W.J. "Effects of Shock-Wave Impingement on the Heat Transfer on a Cylindrical Leading Edge" NASA TN D-3859, Feb. 1967.

8. English, E.A. "Nosetip Recovery Vehicle Postflight Development Report" SAND75-8059, Sandia Laboratories, Livermore, CA, January 1976.

9. Widhopf, G.F. and Victoria, K.J. "Numerical Solutions of the Unsteady Navier-Stokes Equations for the Oscillatory Flow over a Concave Body" 4th International Conference on Numerical Methods, Boulder, Colorado, June 1974.

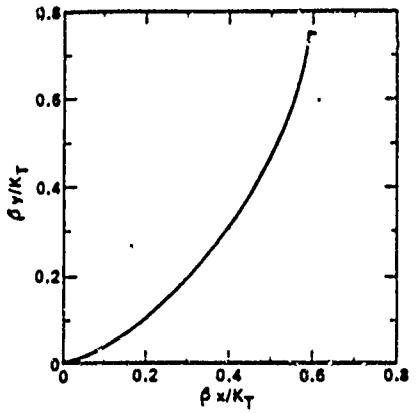

Figure 1 SLENDER EQUILIBRIUM SHAPE DEVELOPED UNDER PURELY TURBULENT BOUNDARY LAYER CONDITIONS

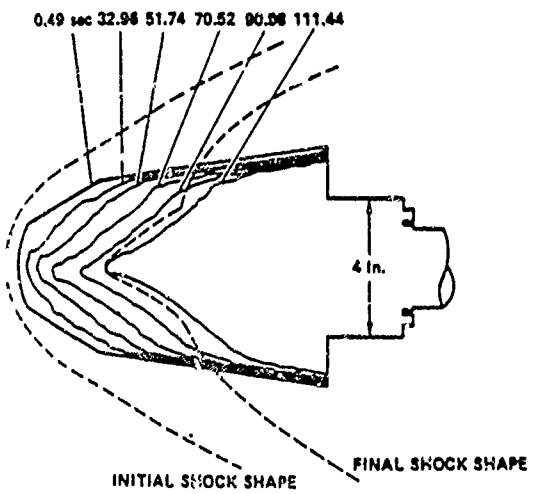

Figure 2 VARIATION OF PROFILE SHAPE WITH TIME FOR AXISYMMETRIC CAMPHOR MODELS

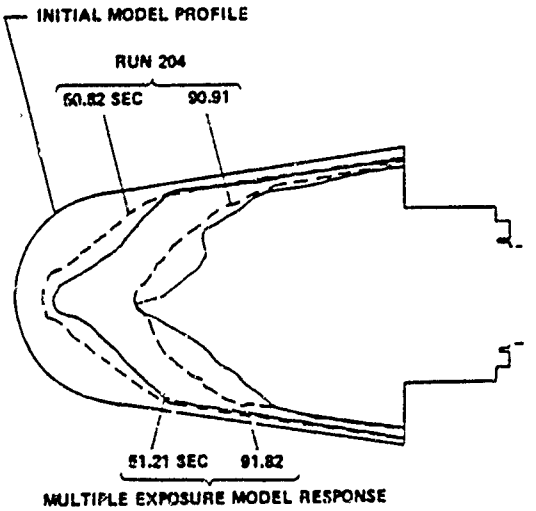

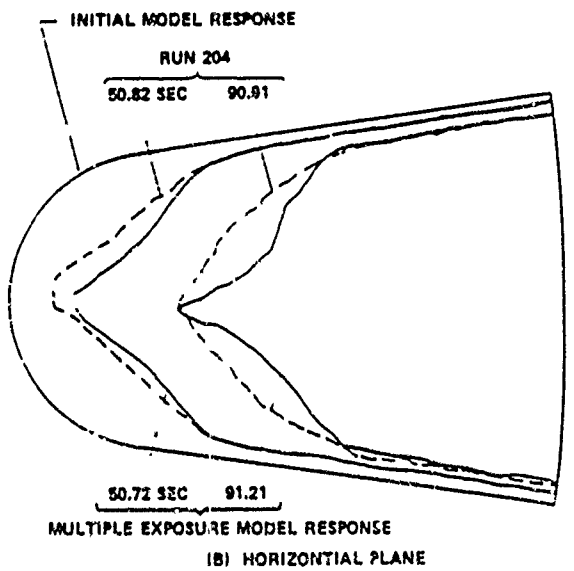

Figure 3 THE DEVELOPMENT OF ABLATED NOSE SHAPES OVER WHICH FLOW INSTABILITIES CAN OCCUR

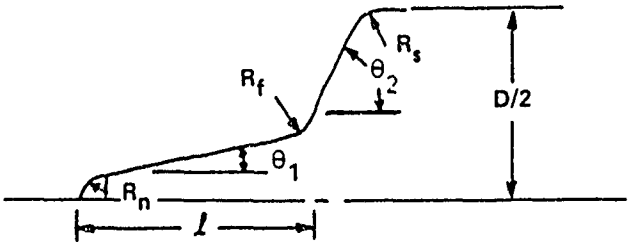

Figure 4a BI-CONIC REPRESENTATION FOR ABLATED NOSE SHAPE

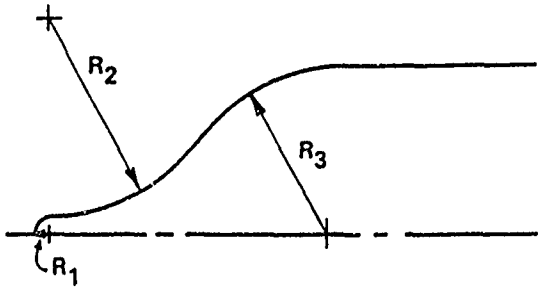

Figure 4b TRI-RADIUS REPRESENTATION FOR ABLATED NOSE SHAPE

Figure 5 TYPICAL HIGHLY INDENTED ABLATED SHAPE

(a) SMOOTH MODEL

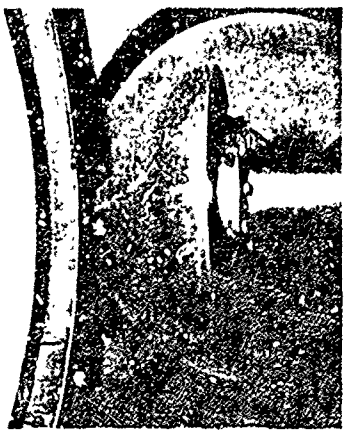

(b) MODEL COATED WITH 15-MIL-GRIT ROUGHNESS

Figure 6 ROUGH AND SMOOTH INDENTED MODELS INSTALLED IN 96" SHOCK TUNNEL AT CALSPAN

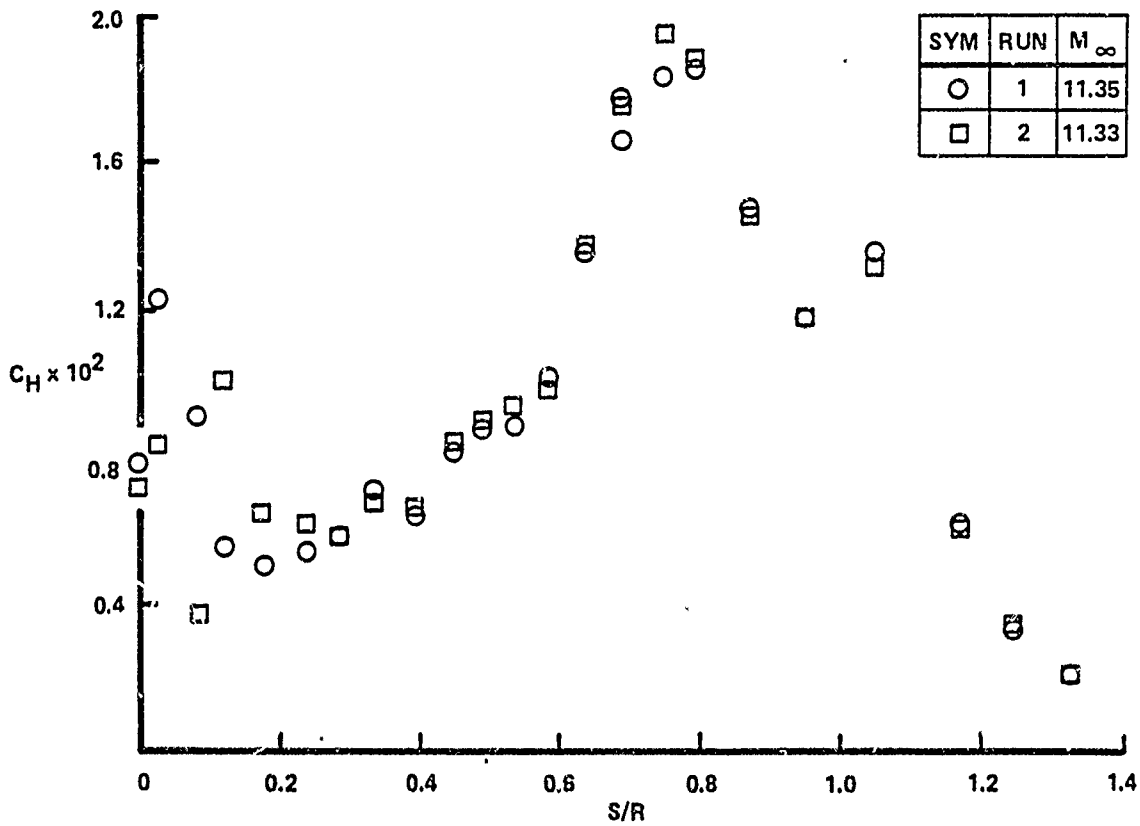

Figure 7 EFFECT OF BOUNDARY LAYER TRIPS ON DISTRIBUTION OF HEATING ($M = 11.3$ $Re_D \approx 12 \times 10^6$)

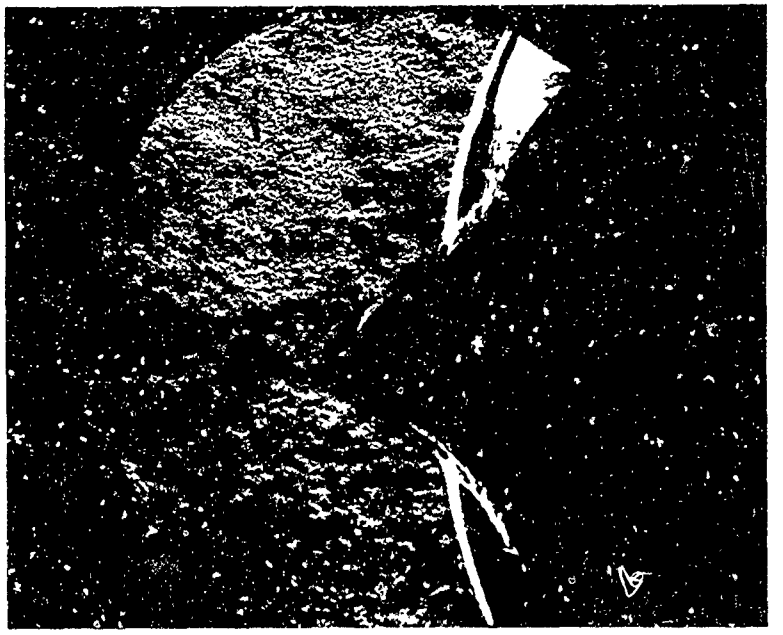

(a) SMOOTH MODEL

(b) MODEL WITH TRIP

Figure 8 SCHLIEREN PHOTOGRAPHS OF FLOW OVER THE SMOOTH AND TRIPPED CONFIGURATION ($M = 11.3$, $Re_D = 12 \times 10^6$)

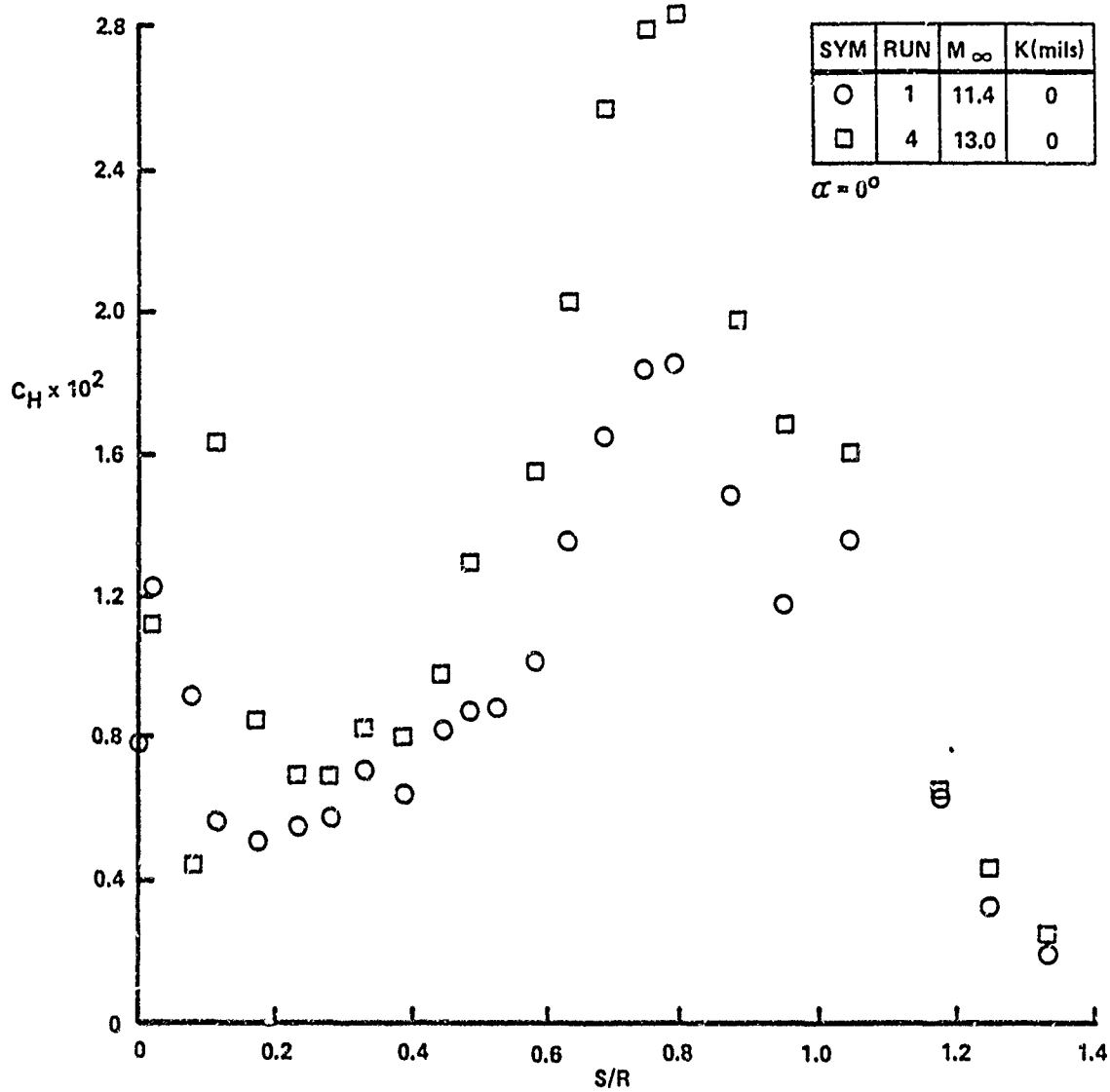

Figure 9 INFLUENCE OF MACH NUMBER ON THE DISTRIBUTION OF HEATING TO THE SMOOTH MODEL

(a) MACH 11

(b) MACH 13

Figure 10 EFFECTS OF MACH NUMBER ON FLOW PATTERN OVER THE INDENTED NOSETIPS

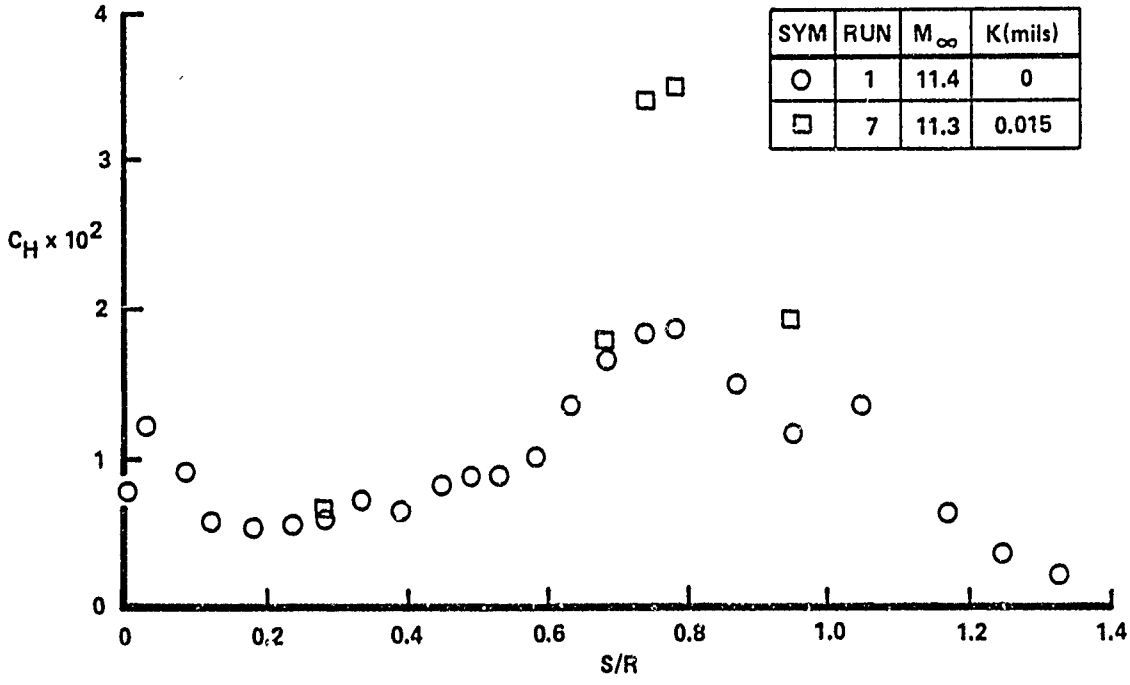

Figure 11 INFLUENCE OF SURFACE ROUGHNESS ON THE HEATING DISTRIBUTION ($M = 11.4 \quad Re_D = 12 \times 10^6$)

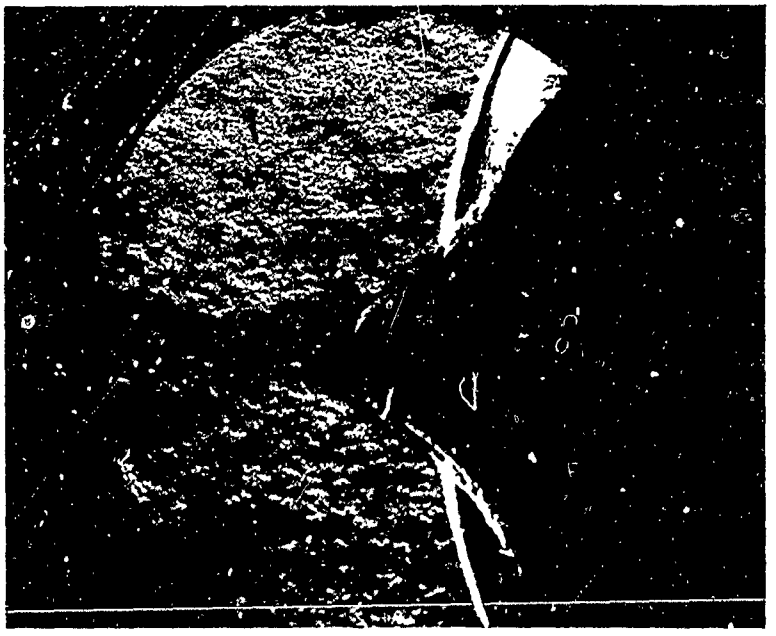

(a) K = 0

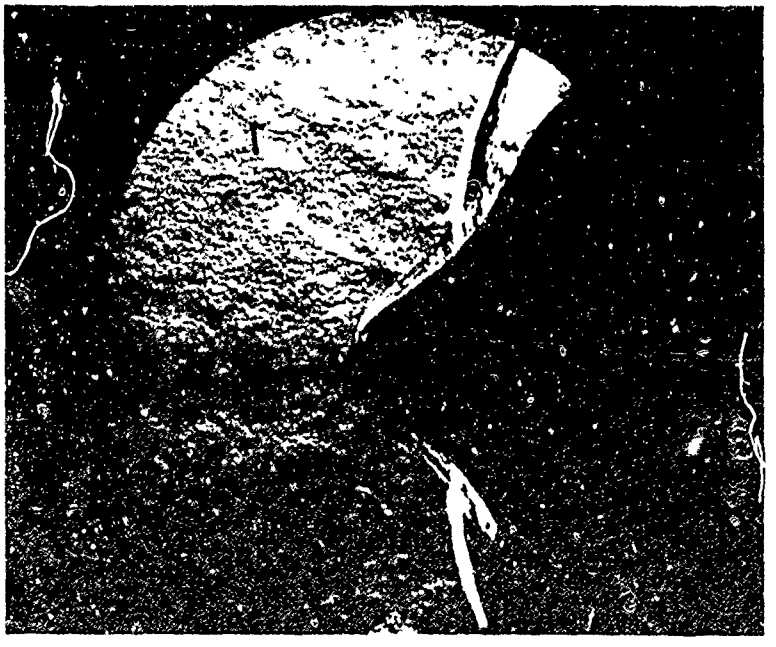

(b) K = 15 MILS

Figure 12 INFLUENCE OF SURFACE ROUGHNESS ON THE FLOW FIELD ON INDENTED NOSETIPS

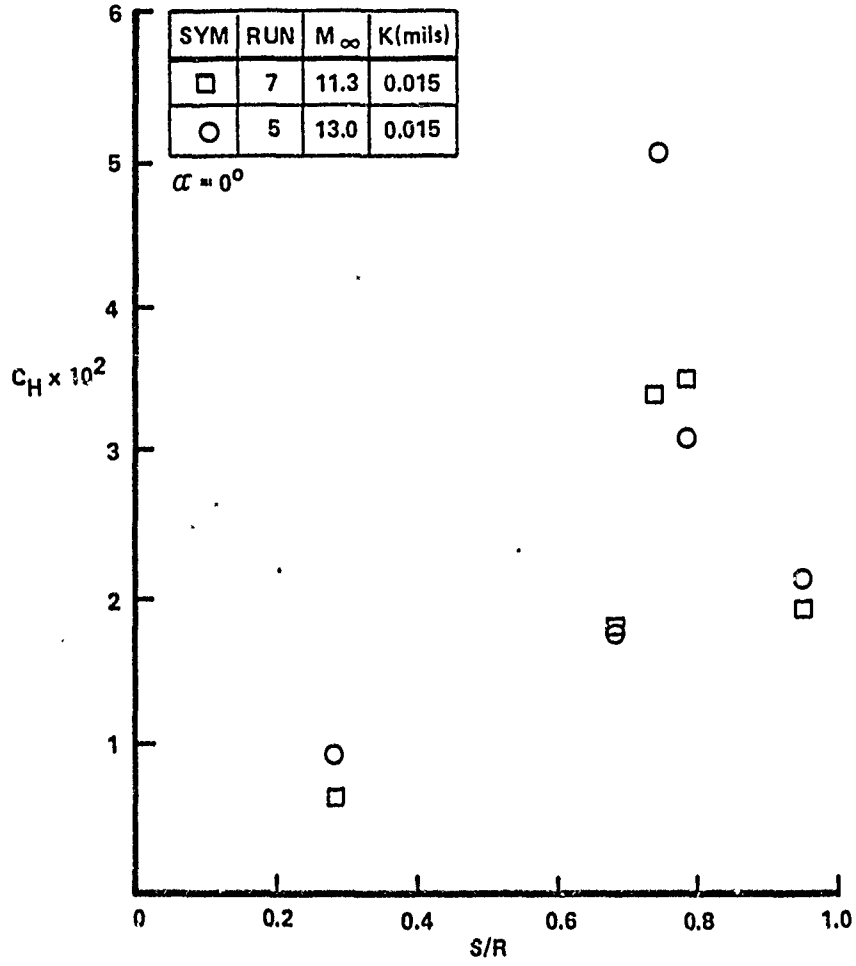

Figure 13 INFLUENCE OF FREESTREAM MACH NUMBER ON THE HEATING TO THE ROUGH NOSETIP

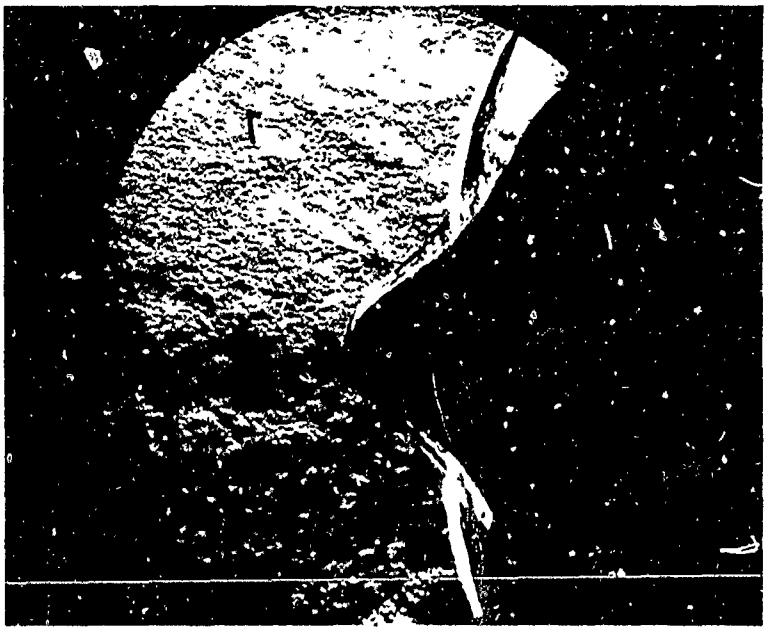

(a) MACH 11

(b) MACH 13

Figure 14 INFLUENCE OF FREESTREAM MACH NUMBER ON THE FLOW FIELD OVER ROUGH INDENTED NOSETIP

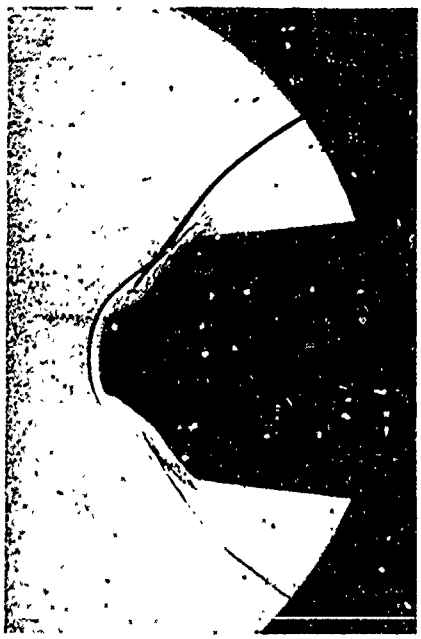

NRV NOSE TIP

RTE NOSE TIP

Figure 15 SCHLIEREN PHOTOGRAPHS OF THE FLOW OVER THE NRV AND RTE NOSE TIPS EXHIBITING REGIONS OF BODY SHOCK – BOUNDARY LAYER INTERACTION

Figure 16 INSTALLATION OF NRV HEAT TRANSFER AND PRESSURE MODEL IN 96" SHOCK TUNNEL

Figure 17 SCHLIEREN PHOTOGRAPH OF THE FLOW OVER THE NRV HEAT TRANSFER AND PRESSURE MODEL (M = 11.3 Re/FT = 10 x 10^6)

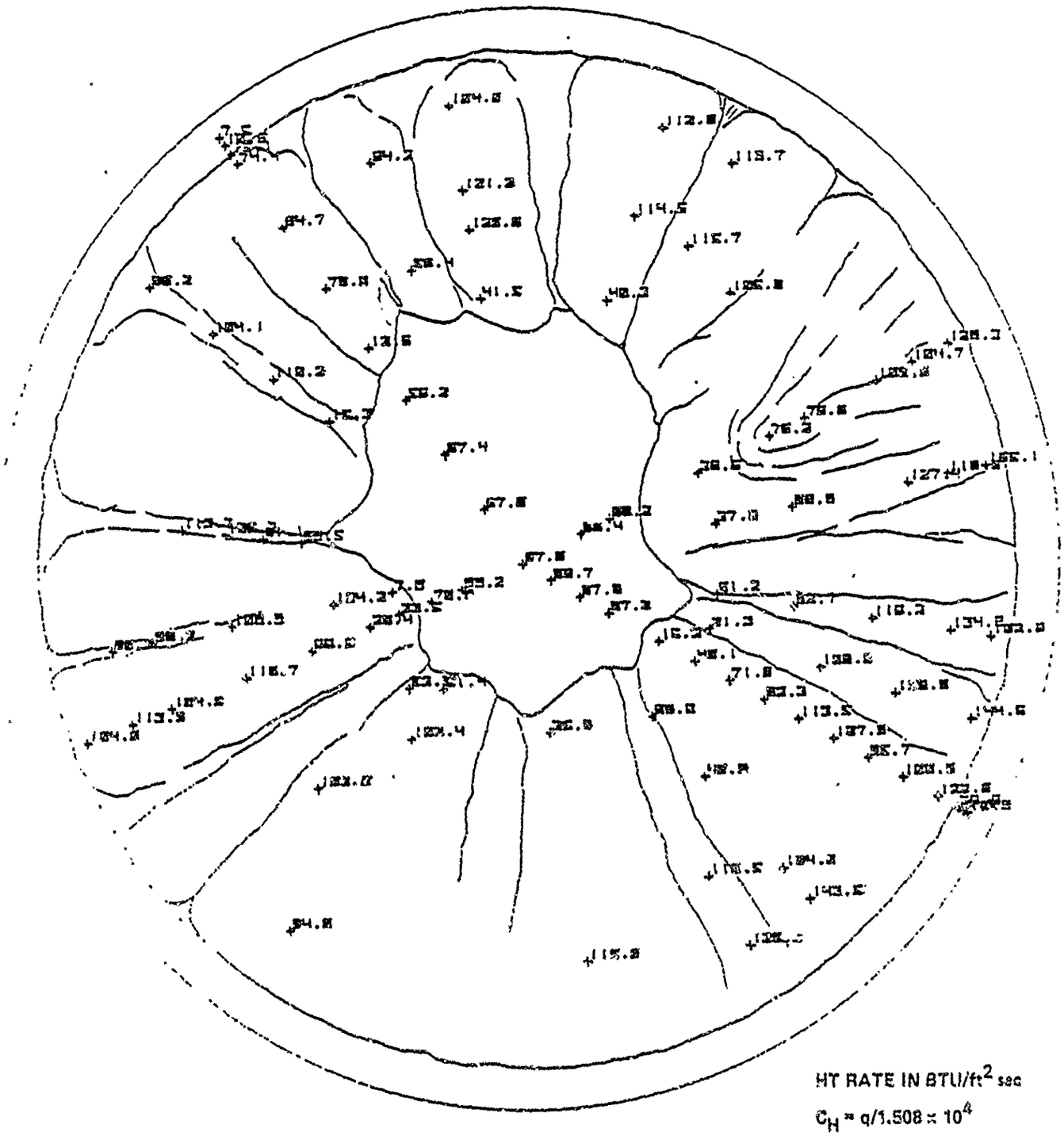

Figure 18a HEAT TRANSFER DISTRIBUTION OVER THE NRV CONFIGURATIC) – M = 11, Re/FT = 10 X 10^6, $\alpha = 0^o$

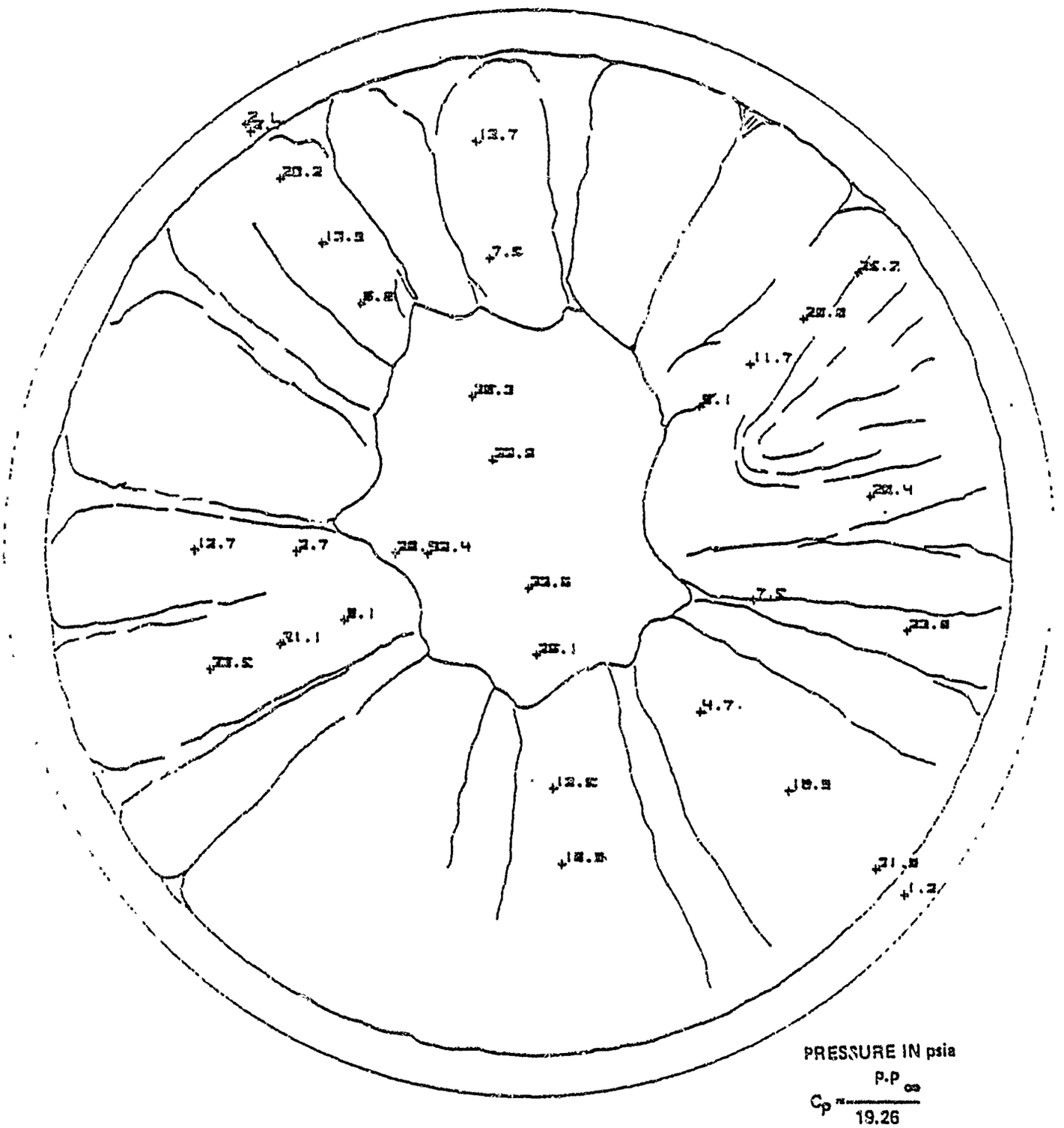

Figure 18b PRESSURE DISTRIBUTION OVER THE NRV CONFIGURATION – M = 11, Re/FT = 10 X 10^6, $\alpha = 0^o$

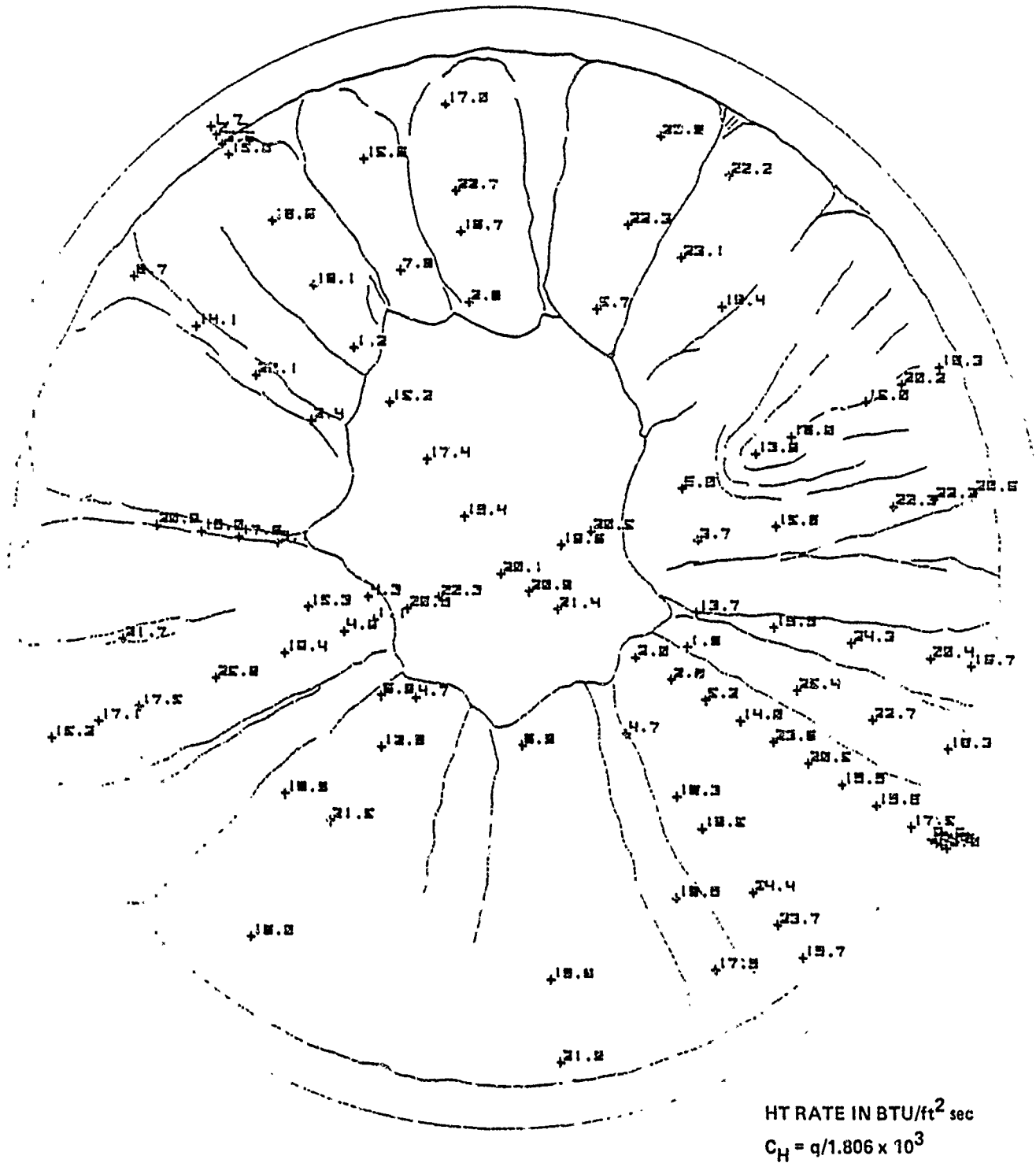

Figure 19a HEAT TRANSFER DISTRIBUTION OVER THE NRV CONFIGURATION – M = 11, Re/FT = 1 X 10^6, $\alpha = 0^o$

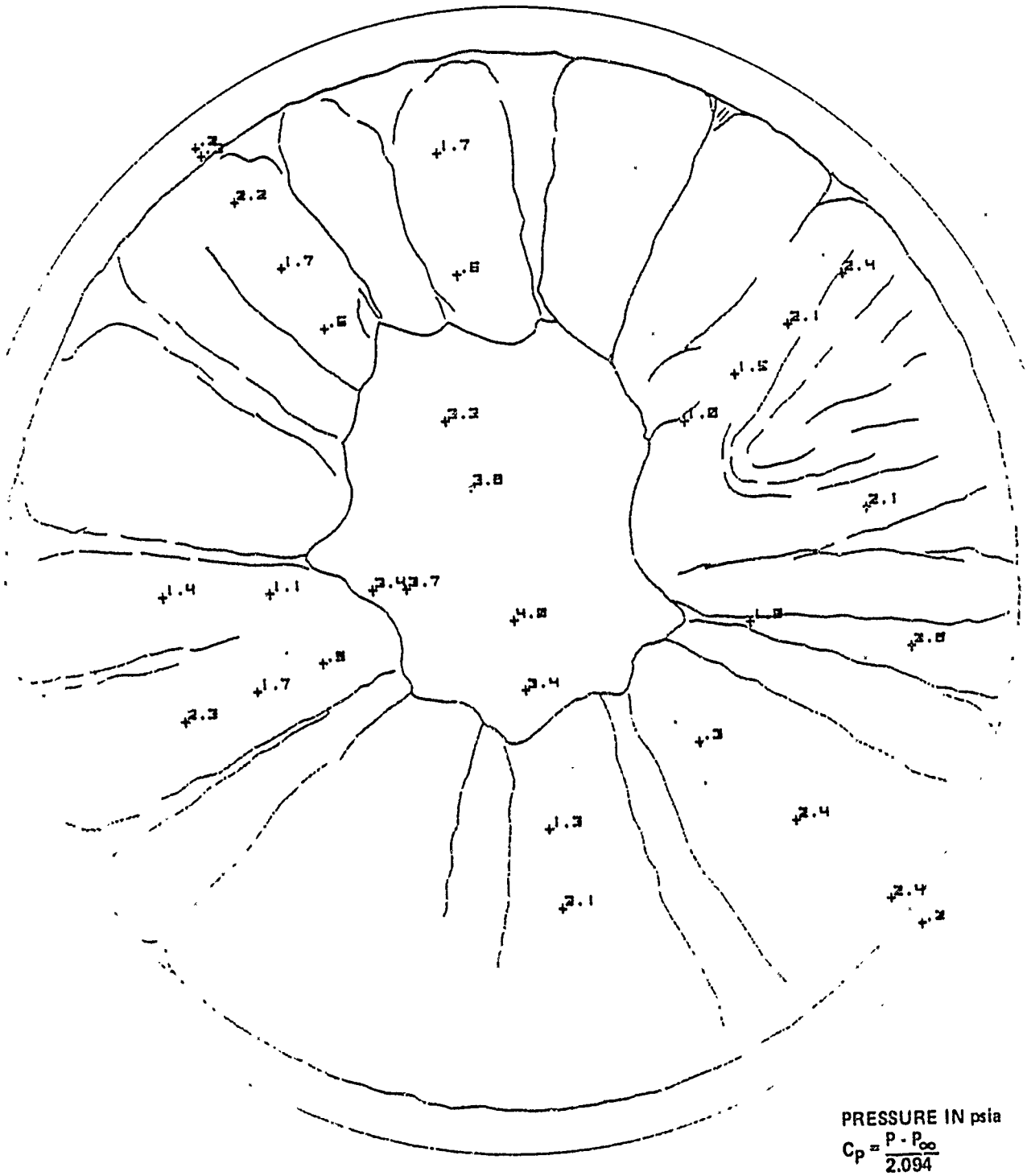

Figure 19b PRESSURE DISTRIBUTION OVER THE NRV CONFIGURATION – M = 11, Re/FT = 1 X 10^6, $\alpha = 0^o$

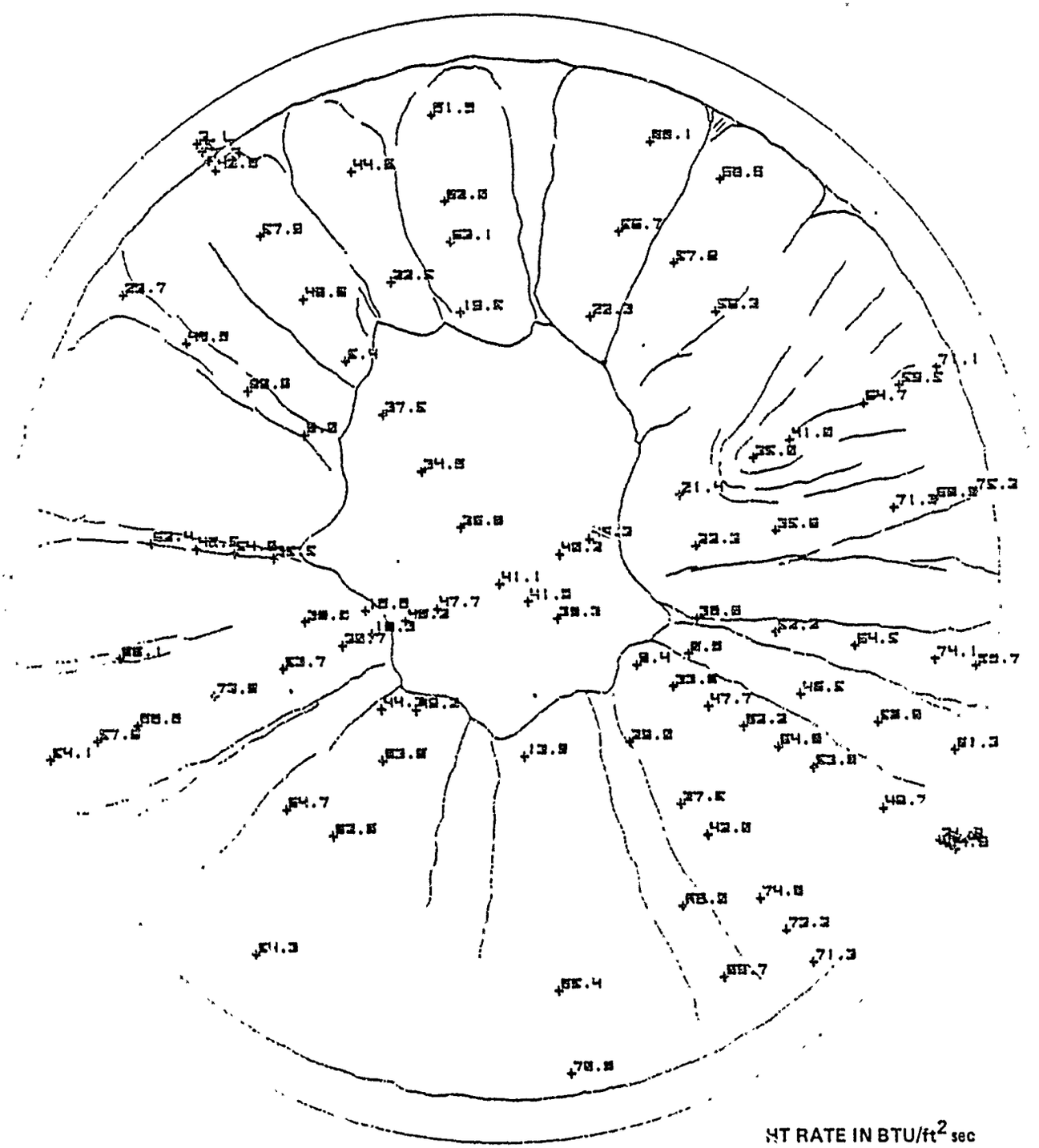

Figure 20a HEAT TRANSFER DISTRIBUTION OVER THE NRV CONFIGURATION – M = 11, Re/FT = 4.6 X 10^6, $\alpha = 0^o$

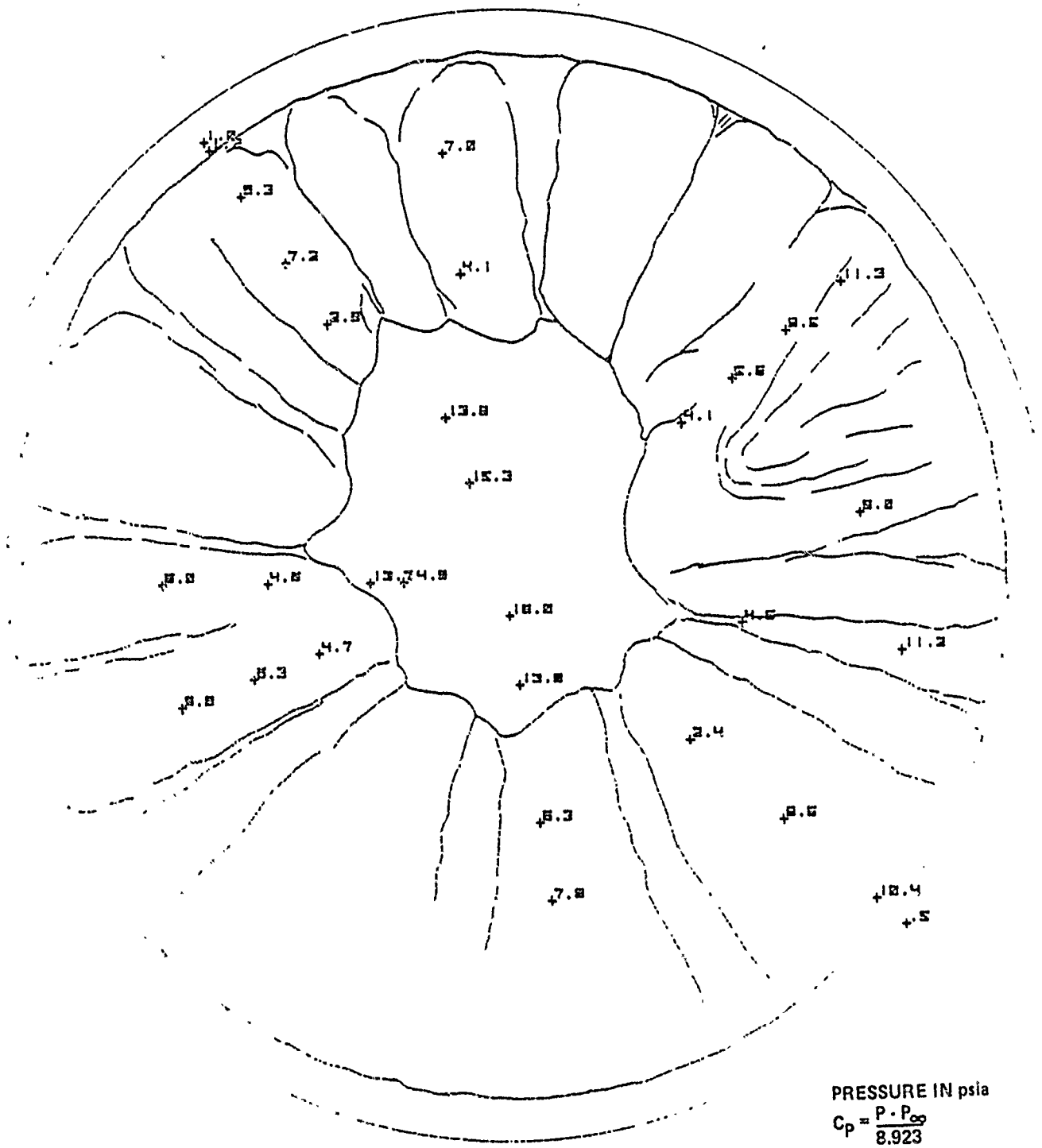

Figure 20b PRESSURE DISTRIBUTION OVER THE NRV CONFIGURATION – M = 11, Re/FT = 4.6 X 10^6, $\alpha = 0^o$

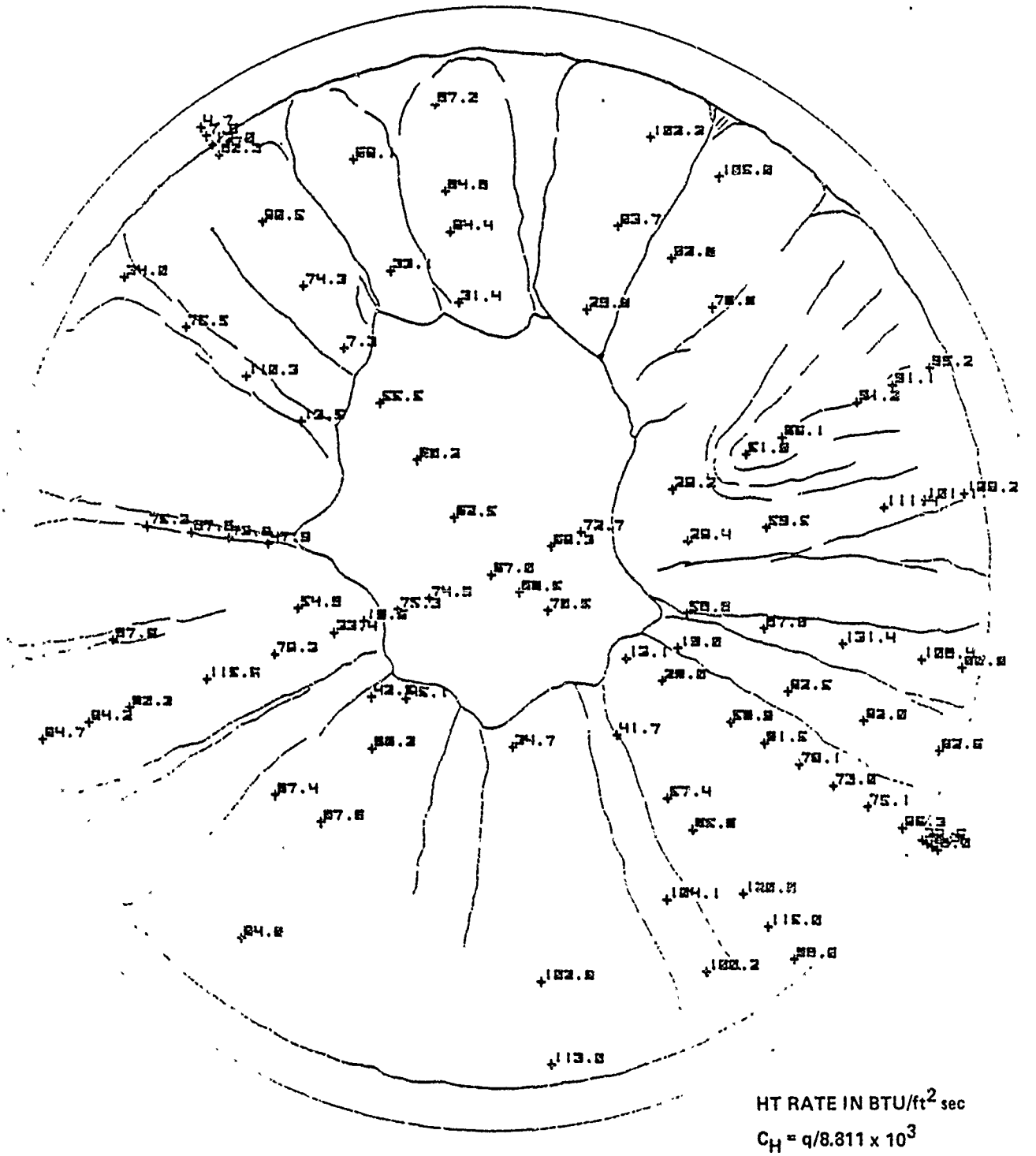

Figure 21a HEAT TRANSFER DISTRIBUTION OVER THE NRV CONFIGURATION – M = 13, Re/FT = 4.8 X 10^6, $\alpha = 0^0$

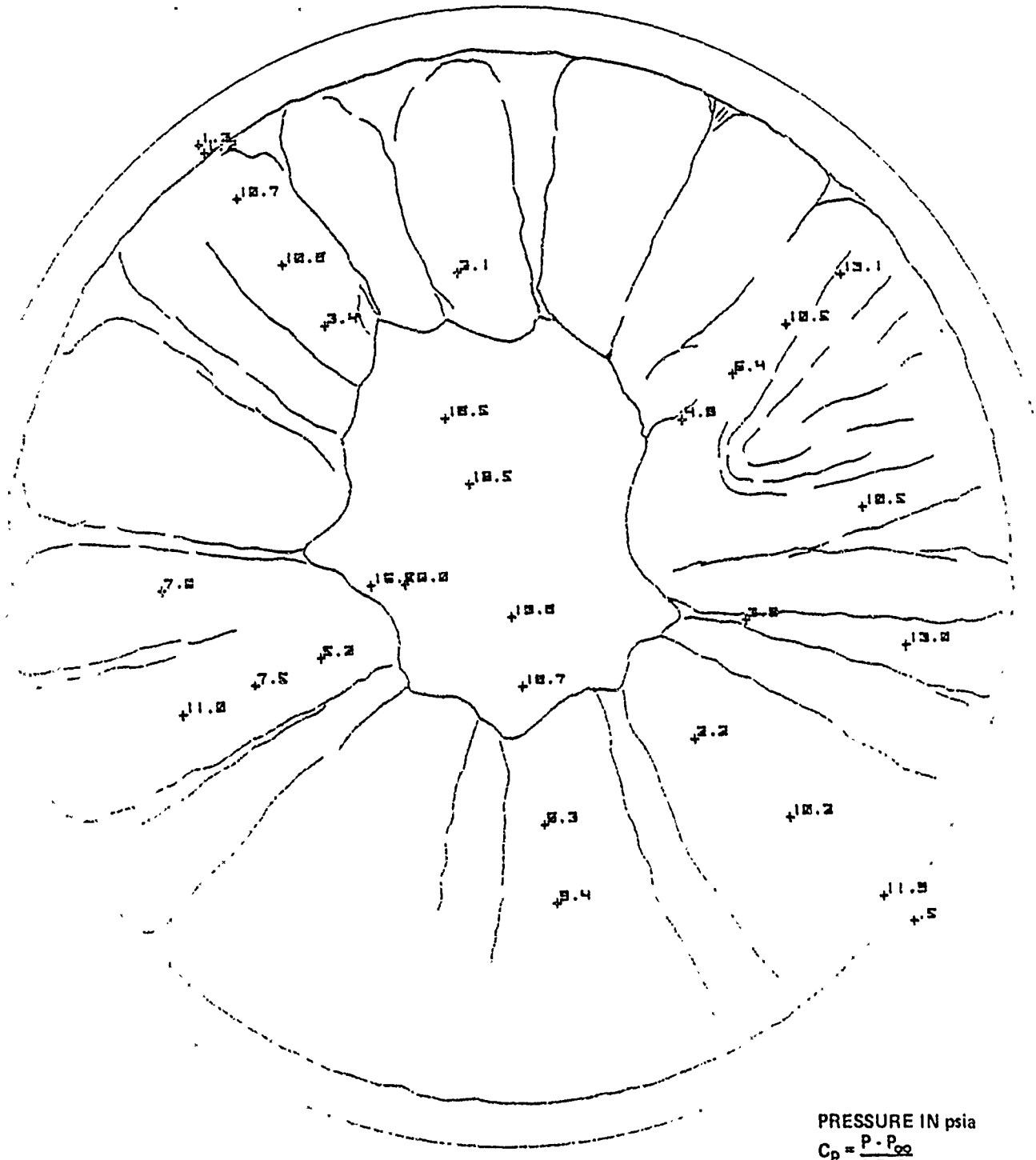

Figure 21b PRESSURE DISTRIBUTION OVER THE NRV CONFIGURATION — M = 13, Re/FT = 4.8 X 10^6, $\alpha = 0^o$

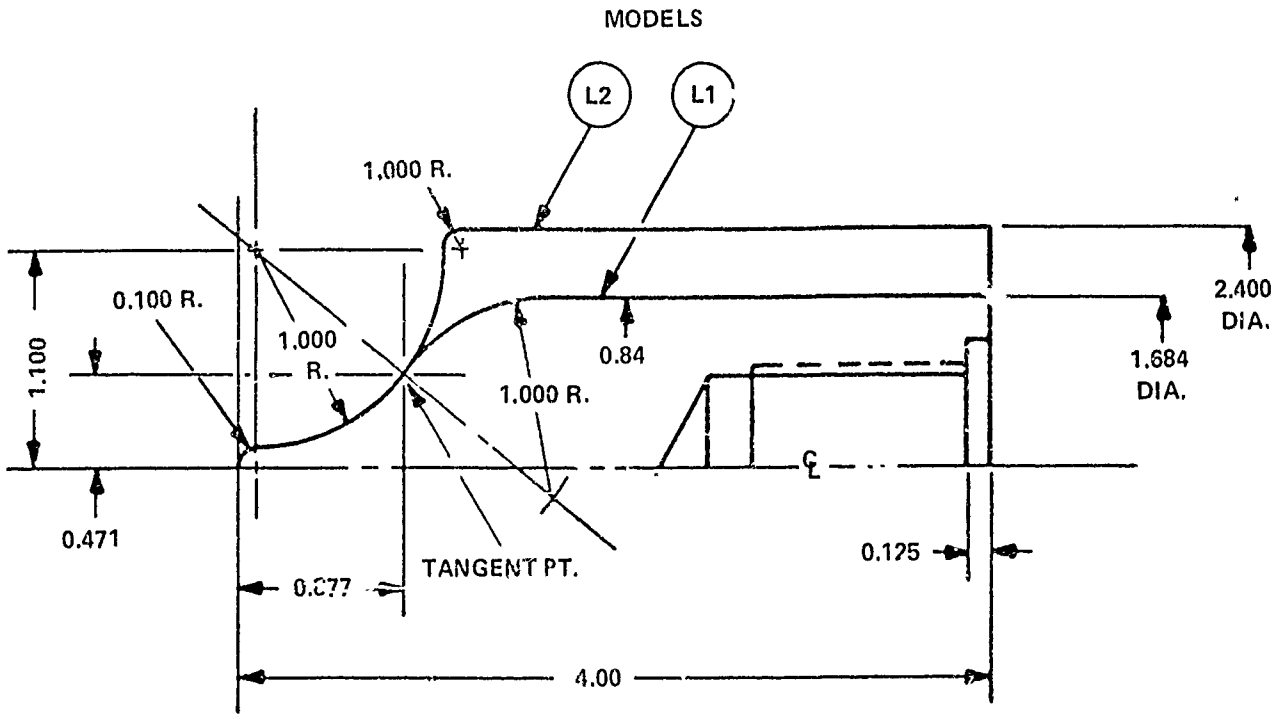

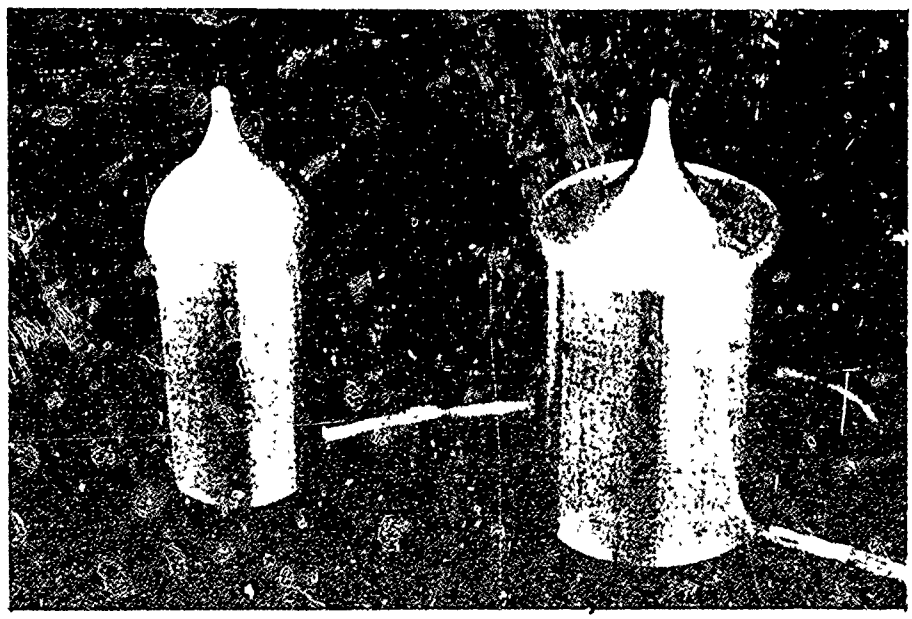

Figure 22 WIDHOPF CONFIGURATIONS 1 AND 2

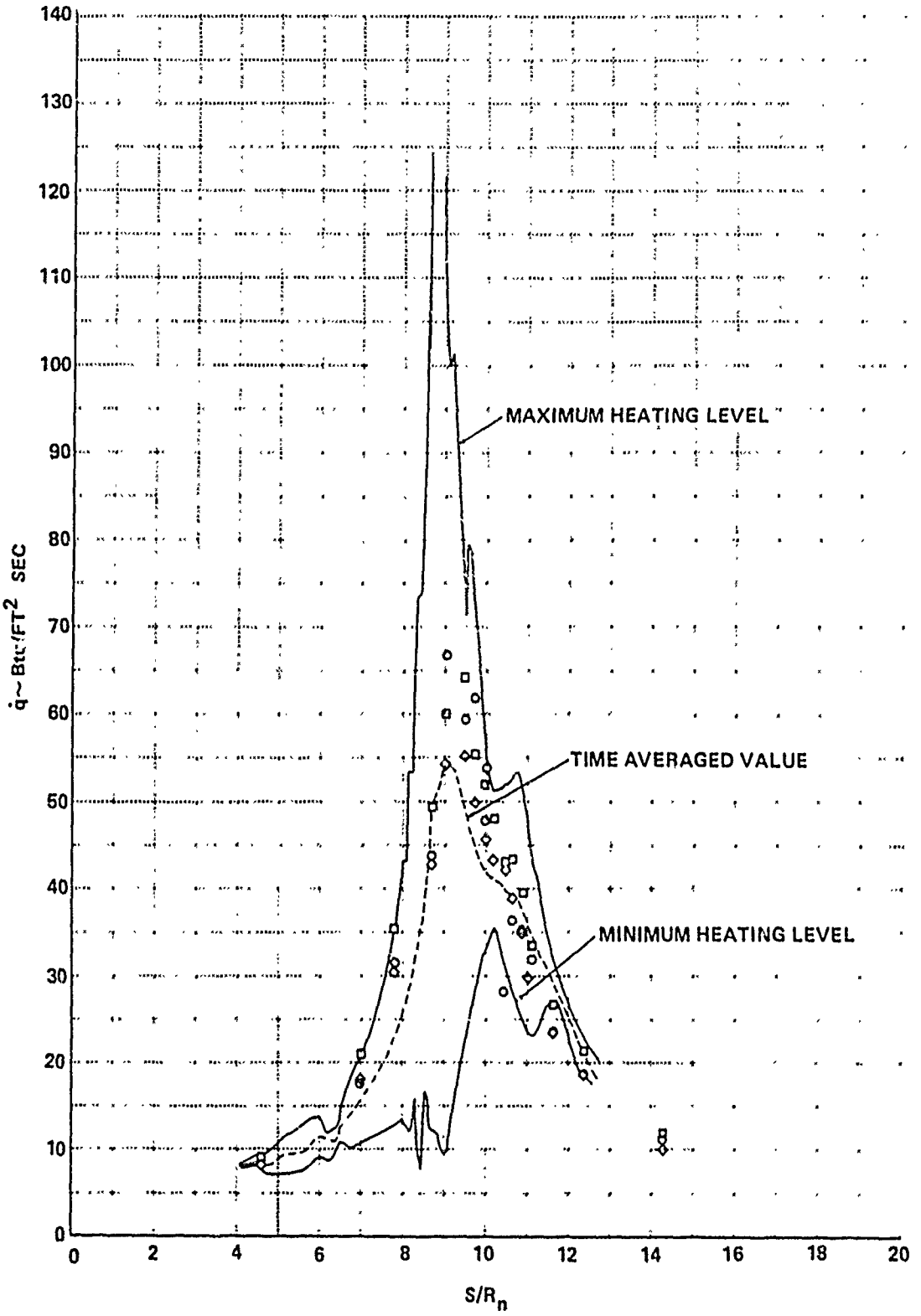

Figure 23 COMPARISON BETWEEN THEORY AND EXPERIMENT FOR THE WIDHOPF 1 CONFIGURATION (1-10-10)

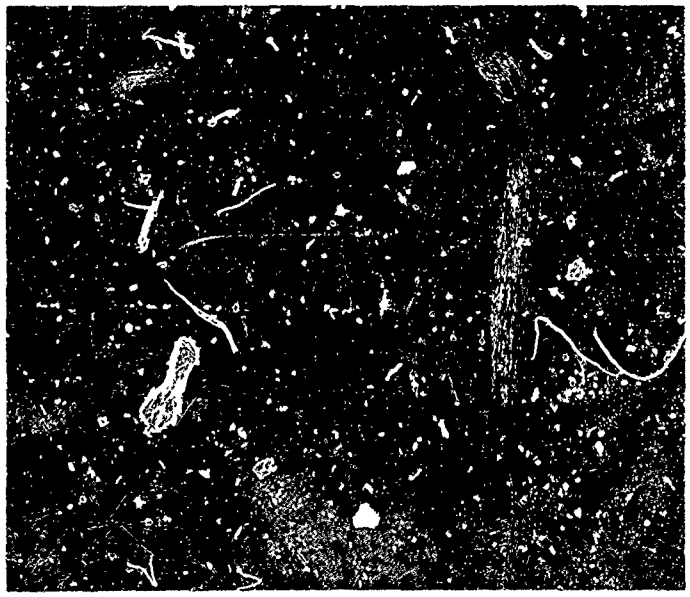

Figure 24

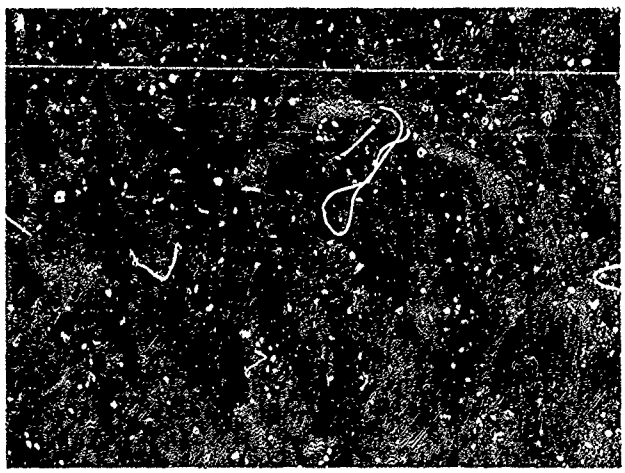

Figure 25a

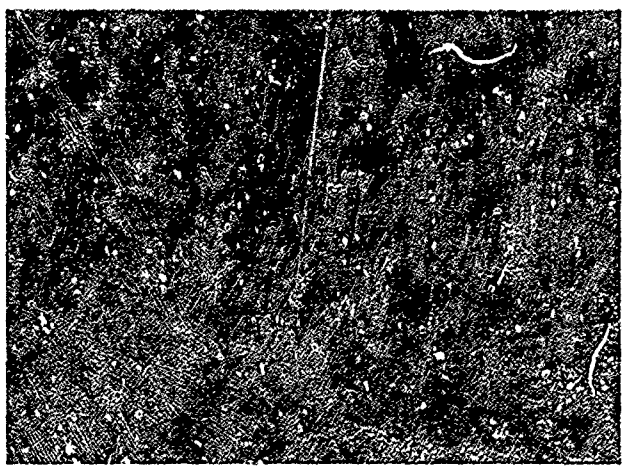

Figure 25b

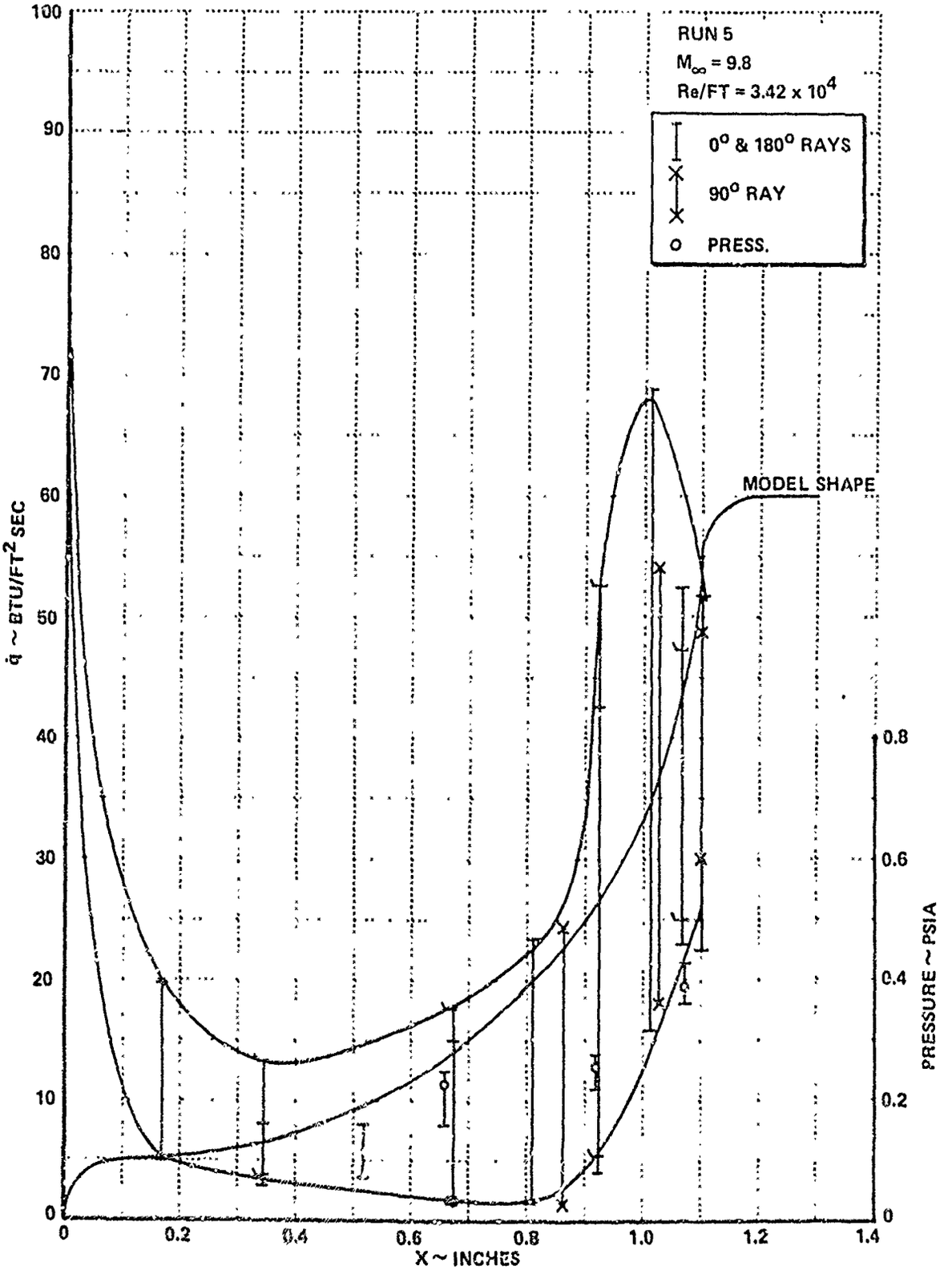

Figure 26a HEAT TRANSFER AND PRESSURE MEASUREMENTS ON THE WIDHOPF 2 CONFIGURATION

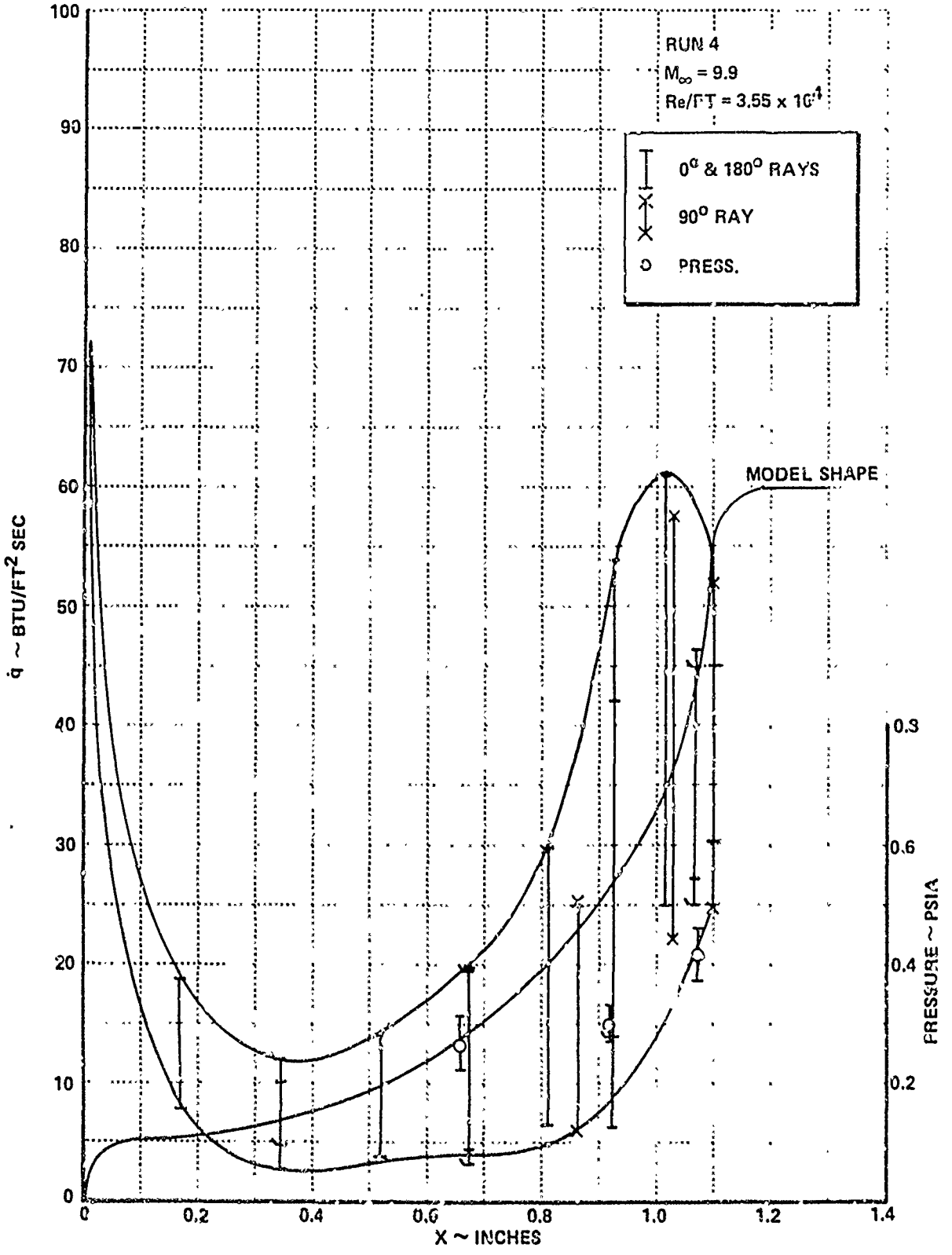

Figure 26b HEAT TRANSFER AND PRESSURE MEASUREMENTS ON THE WIDHOPF 2 CONFIGURATION

APPENDIX B

AIAA-86-0267

"A Review of Aerothermal Problems Associated with Hypersonic Flight"

By:

M.S. Holden
Calspan Corporation

AIAA 24th Aerospace Sciences Meeting
January 6-9, 1986
Reno, Navada

AIAA'86

AIAA-86-0267

A Review of Aerothermal Problems Associated with Hypersonic Flight

M. S. Holden, Calspan/Univ. of Buffalo Research Center, Buffalo, NY

AIAA 24th Aerospace Sciences Meeting
January 6-9, 1986/Reno, Nevada

Index of Sections

A REVIEW OF AEROTHERMAL PROBLEMS ASSOCIATED WITH HYPERSONIC FLIGHT

Michael S. Holden*
Calspan/UB Research Center
Buffalo, NY 14225

ABSTRACT

A review is presented of some important aerothermal problems associated with hypersonic flight with emphasis on those involved with viscous/inviscid interaction. The flow regimes of importance to hypersonic vehicles of current interest are discussed and the performance of experimental facilities currently available to study real gas phenomena associated with hypervelocity flight are briefly reviewed. Viscous interaction and real gas effects in hypervelocity flight at high altitudes are discussed with reference to the measurements which are required to support the development of improved prediction capabilities in this regime. Theoretical and experimental research on 2D and 3D shock wave/laminar boundary layer interaction relevant to the performance of control surfaces and inlets in hypersonic flight at high altitudes is reviewed. The characteristics of transition regions in hypersonic flows are discussed with particular reference to transitional flows over nosetips and swept leading edges. Studies of shock interaction phenomena on indented nosetips are discussed, followed by a review of the surface roughness and blowing effects. Research to describe the characteristics of 2D and 3D regions of shock wave/turbulent boundary layer interaction in hypersonic flow is reviewed with particular reference to intrinsic unsteadiness and potential compressibility effects in these flows. This review is concluded with a brief discussion of observations suggesting a decrease in the spreading rate in shear layer mixing in hypersonic flow.

I. INTRODUCTION

With the current interest in the design of trans-atmospheric vehicles, maneuvering re-entry vehicles, orbital transfer vehicles and smaller space shuttles, there has been an increased interest within the aerospace community in aerothermodynamic problems associated with hypersonic flight. Following the extensive programs conducted in the sixties and early seventies most subsequent research in hypersonic flows has been limited to the support of specific and very conservatively designed systems such as the Space Shuttle, the Jovian entry vehicle, and ballistic and maneuverable re-entry vehicles. With the advent of interest in the more complex, sophisticated, and by necessity, more efficient vehicles such as terminally guided maneuvering re-entry vehicles, has come the realization that our current predictive capability is not able to support the design of such systems. Some of the fundamental problem areas which must be addressed are: the fundamental understanding and prediction of flows in the low density transition regime in the presence of real gas effects and surface catalysis; the control of laminar viscous/inviscid interaction regions of non-equilibrium airflows on inlets and on control surfaces of high flying hypersonic vehicles; the prediction of transition on complex (and simple) vehicle configurations; the prediction of regions of shock wave/turbulent boundary interaction, chemically reacting turbulent shear flows and the structure of plasmas in the turbulent boundary layer over an ablating or transpiration-cooled vehicle.

Hypersonic flow regions of viscous/inviscid interaction in laminar and turbulent flows represent one of the most taxing group of aerothermal problems for the designer and certainly are the most difficult to predict in detail with any accuracy. The severity of the gradients in heat transfer and pressure, coupled with the intrinsic unsteadiness of separated, turbulent regions of shock wave/boundary layer interaction make the computation of such flows one of most challenging in high speed flows. During the past two decades there has been significant advances resulting from fundamental theoretical and experimental research in shock wave-boundary layer interaction in supersonic and hypersonic flows. Prediction techniques have been successfully developed to describe laminar separated flows, first using integral techniques to solve the boundary layer equations and then through use of the full Navier-Stokes equations, solutions to these equations have yet to be obtained for laminar separated flow with non-equilibrium chemistry. However, two-dimensional turbulent separated flows induced in regions of shock wave boundary layer interaction have not yet yielded to a detailed numerical analysis using the full Navier-Stokes equations. In many cases the severe heating loads and gradients generated in regions of shock/boundary layer interaction mandate the use of thermal protection systems employing ablative or transpiration cooling. In each case surface roughness is intrinsically a factor resulting from either surface structure of the ablated surface or the geometric design of the transpiration-cooled surface. The effects of surface roughness and blowing will have a large effect on the size and characteristics of regions of shock wave-turbulent boundary layer interaction in hypersonic flow.

In the following paper we review some important aerothermal problems associated with flight at hypersonic speed, with particular emphasis on regions of viscous/inviscid interaction in hypersonic flows. We first discuss the flow regimes which are of importance for the hypersonic vehicles of current interest and facilities which are currently available to study hypervelocity airflows. Viscous interaction and real gas effects in the high altitude transition regime are briefly reviewed. Studies of laminar 2D and 3D viscous interaction regions are then discussed with emphasis on comparisons between computational methods and experimental measurements. Research on boundary layer transition and transitional flows over nosetips and leading edges at hypersonic speeds are briefly reviewed. The regions of shock/boundary layer interaction which control the nose shaping of

*Member, AIAA

Supported by the US Air Force and NASA under Contracts F49620-85-C-0130 and NAS1-177-21 respectively

ablating nosetips are described with particular reference to the importance of Mach number and Reynolds number simulation in experimental studies of these flows. The characteristics of 2D and 3D shock wave/turbulent interactions in hypersonic flows are then described again with particular reference to solutions obtained to the Navier-Stokes equations. We conclude with discussion of compressibility and unsteady effects in hypersonic flows.

II. FLIGHT REGIMES AND PHENOMENA OF INTEREST AND GROUND TEST SIMULATION CAPABILITIES

While the accurate prediction of three-dimensional turbulent regions of shock wave/boundary layer interaction with embedded separated regions over rough blowing surfaces represents one of the most difficult problems from the viewpoint of analysis, it is the occurrence of extensive laminar and transitional regions of viscous/inviscid interaction which may present the designer of high flying hypersonic vehicles with the greatest design problems. A plot of the Mach number/Reynolds number and altitude/ velocity capabilities of a number of high performance hypersonic facilities are shown together with the flight envelopes of a number of proposed vehicles in Figures 1 and 2. Because of the increased stability of the laminar boundary layer at high Mach numbers, the trans-atmospheric and the orbital transfer vehicles will be immersed in laminar boundary layers for a significant part of their flight. Laminar viscous/inviscid interaction regions for large values of the viscous interaction parameter $M\sqrt{C^*/Re}$ will cause a significant reduction in the control forces that can be developed by elevons or reaction jet controls. As illustrated in Figure 3, extensive regions of laminar attached or separated flow can, in essence, "fair-in" the compression surface, reducing their effectiveness. Likewise, the boundary displacement effects may significantly modify the effective shape of the compression ramp on a hypersonic intake. Because of the intrinsic structure of hypersonic laminar boundary layers over cooled surfaces it may be extremely difficult to develop an effective boundary layer control.

For at least two concepts currently under study, the orbital transfer vehicle and the trans-atmospheric vehicle, designed to operate at very high altitudes, it has yet to be established that the Navier-Stokes codes will successfully handle flows on the boundaries of continuum flow. Because of the high re-entry velocities associated with these missions it is clear that the airflows over the vehicles will be in chemical non-equilibrium, and again incorporating non-equilibrium chemistry into the Navier-Stokes has yet to be accomplished successfully for the hypersonic flow regime. Surface catalysis must be considered, and here errors of up to 300 percent can result from uncertainties in the current prediction techniques for heat transfer.

The prediction of boundary layer transition remains one of the most important and difficult problems in hypersonic flow. The theoretical studies have failed to provide either definitive prediction methods or the framework within which to correlate the results from the experimental studies. Of the many ways which have been suggested to correlate transition measurements from flight and ground test facilities, describing the beginning of transition in terms of a local Reynolds number based on either the local momentum thickness or streamwise distance and a local Mach number remains the most popular. A typical example of a transition correlation of flight and ground test measurements is shown in Figure 4. The ground test measurements, specifically those made on swept cylinders, are in surprisingly good agreement with those made in flight, plotted in this format. This good agreement may result in part from the relative insensitivity of stagnation line transition to facility-related disturbances. In many cases surface roughness can play an important role in controlling transition on flight vehicles, and correlations employing the Reynolds number based on momentum thickness and the roughness height in a form similar to that shown in Figure 5 can be used to extrapolate ground test data to flight. On more complex aerodynamic configurations however, where adverse pressure gradients are generated in viscous interaction regions over controls or inlets, transition can be expected to occur within these regions at Reynolds numbers of an order of magnitude less than those presented above.

The largest and most difficult to predict aerothermal loads which are experienced by an advanced hypersonic vehicle are encountered under low altitude, turbulent flow conditions. The severity of the heat transfer rates and gradients encountered in regions of shock/shock and shock/boundary layer interaction make it essential for the designer to have prediction techniques available which will describe these regions. As discussed later in the context of flows over indented nosetips, to obtain an accurate simulation of shock/boundary layer interaction phenomena in a ground test facility, it is important that both the Mach number and Reynolds number be simulated. However, if the boundary layers and shear layers in the experiments are fully turbulent (without resorting to tripping) the characteristics of the interaction regions do not appear to exhibit a strong Reynolds number dependence. There is, however, a strong effect of Mach number on the structure of viscous interaction regions and Mach number independence is not valid for blunt bodies with embedded shock systems. Also for the correct simulation of hypervelocity flows, the effects of real gas chemistry must be included.

For velocities above 10,000 ft/sec where oxygen is fully dissociated and nitrogen dissociation and ionization start to occur, surface related reactions will begin to influence heating, and real gas effects will start to influence the structure and characteristics of regions of shock wave/boundary layer interaction. The first order effects of air chemistry are to change the specific heat of the gas and thus the pressure/Mach relationships in the viscous and inviscid flow equations. It can be seen from Figures 1 and 2 that with the exception of Shock Tunnels most of the high Reynolds Number hypersonic facilities employ nitrogen as a test gas and cannot generate velocities above 6000 ft/sec.

There are very few facilities which are currently operational in which detailed studies can be performed to study real gas effects in hypersonic flows. With the exception of ballistic ranges, the shock tunnels at Calspan and piston driven shock tunnel (or Stalker Tube) in Australia are the only operational high Mach number facilities which can be used to generate clean airflows at the temperatures of above 7000°K (see Figure 6) necessary to excite both nitrogen and oxygen. The tremendous power that is being expended during the running time of these facilities (typically a million horsepower) underscores why the construction of a facility to operate at similar conditions with test times of over 1 second is a formidable, if not unrealistic, task. However, there is a clear need for facilities capable of generating high enthalpy airflows with low ambient freestream dissociation levels and sufficient test time for combustion and transpiration cooling processes to become established. Our experience suggests that most simple boundary layer flows are established in a fraction

of a millisecond while more complex flow fields, involving blowing and flow separation, can take up to 3 milliseconds to establish. A high enthalpy facility with run times of up to 10 milliseconds would handle most flows of interest with ease.

Employing an isentropic compression process to compress the test gas (rather than a reflected shock) results in a reservoir which has a lower level of dissociation, and for large drive pressure ratios can lead to higher stagnation pressures and temperatures. The isentropic compression tube was one of the concepts under study in the late sixties along with the MHD augmented shock tunnel[1], and the free piston driven shock tunnel and expansion tube[2]. It was initially hoped that stagnation temperatures of up to 10,000°K could be generated in the Gun and Longshot tunnels, where the gas is compressed by a free piston motion rather than a program piston trajectory for the isentropic tube (see Figure 7). The aerothermal loads on the piston have been such that neither facility has achieved its potential. Currently stagnation temperatures of less than 2000°K are obtained in Gun Tunnels and the Longshot facilities (see Figures 8 and 9); their value lies in their ability to generate relatively high Mach number/high Reynolds number with little cost. While interest in the development of high enthalpy hypersonic facilities dwindled in the U.S. during the late sixties and early seventies, Stalker continued work on a facility to generate real gas flow at temperatures up to 9000°K. As shown in Figure 10, the Stalker tunnel is in essence a shock tunnel with a compression tube used to supply the driver gas. This feature eliminates the problems with operating a high temperature, high pressure driver section at the expense of a more complex device and one with shorter run times than the shock tunnel, which at the high enthalpy conditions are less than 1 millisecond. Judicious use of current facilities can provide insight to many of these nonequilibirum problems, but it is clear that further inventive development of hypervelocity facilities are required if vehicles like the hypersonic transport are to be actively developed. However, in the short term, problems with real gas effects, similar to those discussed in the following section, can at best be addressed with the limited results achievable in flight tests.

III. VISCOUS INTERACTION AND REAL GAS EFFECTS IN HYPERVELOCITY FLIGHT

The recent interest in hypersonic flight at the edges of the atmosphere has rekindled interest in hypervelocity low density flows where viscous/inviscid interaction and chemical non-equilibrium effects are important. The success of a hypersonic air breathing propulsion system designed to operate at very high altitudes, and the aerothermal performance of the AOTV will depend on how well viscous interaction, real gas and surface blowing effects can be predicted and controlled. Within the past decade great strides have been made in the prediction of free molecular flows and work in this area has recently been reviewed by Bird[3]. For continuum flows the tremendous increase in computational power has allowed boundary layer displacement and leading edge bluntness effects to be computed with the full Navier-Stokes equations. For temperatures up to 6,000 °K the reaction rates of air are known with sufficient accuracy[4] to permit solutions to the full Navier-Stokes equations for laminar flows with non-equilibrium air chemistry to be obtained; however, there remains some significant numerical problems associated with the finite rate chemistry. Shock layer and boundary layers solutions with finite rate chemistry are now being routinely obtained[5]. However, until there is significant improvement in the understanding of surface catalysis, such solutions will be valid only for either fully catalytic or non-catalytic surfaces, and the differences in heat transfer between these cases can amount to factors of up to 2. One case in point is current anomalies associated with measured and computed heat transfer rates from STS flights 1, 2 and 3. While for altitudes above 150,000 feet the codes predict nonequilibrium effects associated with a lag in the nitrogen recombination rate (oxygen remains fully dissociated), the best comparisons have been obtained with calculations based on equilibrium air properties[6] (see Figure 11). Since in hypersonic flows the windward pressures reflect the momentum of the incident molecules (Newtonian theory) and not their chemical state, they are only weakly influenced by nonequilibrium effects. When such effects become large they are generally associated with regions of strong expansion or smooth compression process where their effects on δ' are important. Under such circumstances the pressure is also strongly influenced by viscous/invisicid interaction effects as illustrated by wedge/flat plate shock tunnel studies of Vidal and Stoddard[7] where the pressures on the flat plate downstream of a strong expansion were influenced by viscous effects to a greater extent than by chemical non-equilibrium. For the flows over the Space Shuttle, in the absence of viscous interaction, real gas effects would result in higher pressures on the leeside and slightly lower pressures on the windward side. However, the flow over the control surfaces are significantly influenced by viscous interaction effects as are those on the leeside, and to reconcile the differences between force measurements made in wind tunnels and flight solely on the basis of an equilibrium inviscid code to correct for real gas chemistry (as suggested by Maus and Griffith[8]) might be an interesting but slightly misleading first step. It is of interest to note that the greater-than-expected positive pitching moment experienced in flight could also be explained directly in terms of a loss in flap effectiveness as a result of increased size of the interaction region at the lower Reynolds numbers encountered in flight. The force measurements made on the shuttle model at low Reynolds numbers in the Calspan Shock Tunnel, but apparently not included in the design data book (shown in Figure '2) add support to this contention.

While in principle it is possible to describe laminar non-equilibrium interacting flows exactly within the framework of the Navier/Stokes equations once catalytic wall effects are understood, at the higher altitudes where wall slip effects become important the governing equations are not as well defined. However the general success obtained with extending simple viscous layer methods into the transition regime using simple slip models[9] (see Figure 13) suggests that extending the Navier/Stokes codes to describe transitional flows using a similar approach could be productive. It is in this flow regime where nonequilibrium, viscous interaction and wall slip effects are important that there is a significant need for detailed theoretical and experimental research. While there are surface measurements of pressure and heat transfer available[10] there is a clear need for measurements in high velocity airflows of the detailed flow structure, particularly near the wall, to aid in modeling the slip flow. These measurements must be made in high enthalpy airflows, where real gas effects are important, to capture some of the essential physics needed to check the modeling. Complementary studies employing NASA's proposed Entry Research Vehicle and high enthalpy Shock Tunnels and Plasma Jets could provide the required information on catalytic wall, viscous interaction and slip effects in non-equilibrium airflow that is required to obtain an accurate predictive capability for hypervelocity flight at high altitudes.

IV. LAMINAR VISCOUS/INVISCID INTERACTION IN HYPERSONIC FLOW

In high Mach number, low Reynolds number flows, the interaction between the growth of the laminar boundary layer and the outer inviscid flow over the nosetip or leading edge, and subsequent interaction over control surfaces or inlets can play an important role in determining the aero-thermodynamic performance of a high flying hypersonic vehicle. Also, because most practical vehicle designs employ blunt leading surfaces, the entropy layer can have a strong influence on the structure of the boundary layer upstream of the interaction, and on the pressures and heating rates on the compression surfaces. As illustrated in the schlieren photographs shown in Figures 14 and 15 for flow over flat plate/wedge and curved compression surface, at high Mach numbers it is difficult to distinguish between the separation shock and the edge of the viscous layer, while in supersonic flow these features are distinct. An important feature of the structure of a hypersonic laminar boundary layer over a cooled wall is that most of the mass and momentum is contained at the outer edge of the boundary layer, thus making it difficult to employ boundary layer control.

The importance of viscous interaction and leading edge bluntness on the flow over a two-dimensional compression corner are illustrated by the measurements of heat transfer, skin friction and pressure shown in Figure 15. Here on the configuration with the sharp leading edge, the viscous interaction extends 20 boundary layer thicknesses downstream of the corner, at which point the pressure has risen two orders of magnitude to the inviscid wedge value. In contrast, the flap pressure (and heat transfer) on the configuration with the blunt leading edge are dominated by entropy swallowing effects and rise to no more than five times the values just upstream of the corner interaction. In this study it was found that while bluntness was found to decrease the size of the reverse flow embedded within the interaction region, flow separation occurred at approximately the same wedge angle. In a subsequent study it was also shown that, in contrast with turbulent flows, the angle through which the flow could be turned without inducing separation could not be changed by radiusing the corner until the corner radius approached at least 15 initial boundary thicknesses. While, as discussed below, Holden[11] was able to obtain predictions in reasonable agreement with measurements made in these studies employing boundary layer equations modified to incorporate the normal pressure gradient, it is clear that such predictions are now best obtained with numerical solutions to the full Navier-Stokes equations. However, without the massive computational facilities currently available, the devisors of earlier prediction methods employed the boundary layer equations, coupled through equation describing a displacement surface, to the "outer inviscid" flow.

Laminar Two-Dimensional Viscous Interaction

The increased stability of the laminar boundary at high Mach numbers, and the ease with which laminar boundary layers separate, coupled with interest in high altitude hypersonic flight, has made laminar flow separation in two- and three-dimensional interacting flows of considerable practical importance. Experimental studies and flight tests show that the very large heat transfer rates and gradients generated in the reattachment regions of laminar separated flows in high speed flight are of considerable importance to the heat shield designer. The simple viscous interaction flow models that have been developed to describe laminar two-dimensional separated regions have their origins in the earlier studies of Howarth[12], Lighthill[13] and Oswatitsch and Wieghardt[14], who proposed models for the mechanism of upstream influence and boundary layer separation. It was then shown that upstream influence and flow separation could be described with good accuracy by a model in which the viscous layer grew by mutual interaction with the outer inviscid flow. Glick[15], using a semi-empirical modification of the Crocco-Lees[16] method based on this "free interaction" model, was able to describe successfully the properties of a complete shock-induced separated region. Honda[17] and later Lees and Reeves[18] added a third equation, the moment of momentum equation and obtained generally good agreement with measurements in supersonic separated flows over adiabatic walls. To describe separation in laminar viscous interaction regions under highly cooled wall conditions and to predict reattachment heating, Holden[19] added the integral form of the energy equation to the equations for mass, momentum, and moment of momentum employed by Honda, using Cohen and Reshotko's[20] similar solutions as proposed by Lees and Reeves. Good agreement was found between theory and experiment at Mach numbers in the low hypersonic range; however, for highly cooled flow above Mach 11 the laminar boundary layer exhibited a "supercritical response". At high Mach numbers, Holden[11] showed that the normal pressure gradients must be included in the description of hypersonic interaction regions to describe such flows correctly. A comparison between Holden's theory and the measurements of skin friction, pressure and heat transfer made on the flat-plate, 18°-wedge is shown in Figure 16. Incorporating $\partial p/\partial y$ into the formulation enabled a solution to be obtained where previously artifices, such as the super-subcritical jump, would have to be employed to overcome the problems inherent in conventional boundary layer theory for cooled wall hypersonic flows.

While Carter[21] obtained one of the first solutions to the Navier-Stokes equations for separated flows, the technique developed by Hung and MacCormack[22] represents the first relatively efficient method devised to predict the characteristics of laminar separated flows. Using the Navier-Stokes code developed by Hung and MacCormack, laminar solutions were obtained for comparison with the experimental measurements at Mach 16. Comparisons between the Navier-Stokes solutions and measurements in attached, incipient separated flows are shown in Figures 17a, b, and c. For attached flow over the flat-plate wedge configuration (Figure 17a), the theoretical predictions are in excellent agreement with the experimental data. In particular, the form of the heat transfer and skin friction in the region of minimum heat transfer is well reflected by the theoretical predictions. Both theory and experiment display a minimum skin friction downstream of the corner or the wedge. As the strength of the interaction is increased to obtain a small separated region, the heat transfer dips sharply ahead of the corner, displaying a cusp-like form in the presence of a separated region (See Figure 17b). Again, the skin friction distribution is well predicted by theory. For the well-separated flow (Figure 17c), the Navier-Stokes solution significantly underpredicts the size of the separated region. While the form of the distributions and the absolute levels in the plateau and reattachment region are well predicted, the separated region is approximately 0.6 of the length found in the experiment.

Laminar Three-Dimensional Interactions

Most studies of three-dimensional interaction have been conducted to examine flow in the corner of two intersecting wedges with sharp leading edges aligned at an angle of 90 degrees with each other. Stainback[27,28] made detailed heat transfer and pressure measurements in laminar flow over such a configuration at Mach 5, and later at Mach 8, for a range of Reynolds number to identify transition. These experiments led Stainback to distinguish between two flow regions: the near corner with which most previous theoretical work had been concerned and the far corner which had been studied experimentally (see Figure 19). The near corner was a region of mutual interaction of two boundary layers and resulted in lower heating. The far corner was the region of mutual interaction of the two inviscid flow fields caused by the intersection of the two flat plates forming the corner. In subsequent studies, Stainback and Weinstein[29] further observed that interaction between the mutual boundary layers in the corner results in a decrease in heat transfer in the very near corner. Away from the corner, the vortex system and reattachment of the boundary layer downstream of the shock induced separation (see Figure 19) results in an increase of heat transfer outboard of the near corner region. The basic structure of laminar interacting flows was defined in studies by Charwat and Redekeopp[30] at Mach 2 to 4. Studies in hypersonic flow by Watson and Weinstein[31] demonstrated similar features. Figure 20 shows the flow structure established from pitot pressure and flow visualization measurements. The shock waves generated by each wedge are joined by a third shock wave, bordering Zone I and the freestream flow. Slip surfaces pass from the ends of this third shock towards the corner. Shock legs extend to the surface -- a curved shock between Zones II and III and a spread of the corner disturbance outside of the inner shocks. Kutler et al.,[32] have shown that shock capturing techniques describe the inviscid flow with good accuracy; however, viscous characteristics, particularly with laminar flows, where viscous interaction is important, are predicted with significantly less accuracy.

V. TRANSITION TO TURBULENCE IN HYPERSONIC FLOWS

While boundary layer transition is one of the most important parameters in the design of hypersonic vehicles, there remains a considerable gap between "engineering" efforts to correlate the occurrence of transition and fundamental theoretical studies. The engineering studies have concentrated on correlating experimental measurements of transition obtained in flight tests, ballistic ranges, and wind tunnels against almost every conceivable parameter, while the fundamental studies have been aimed principally at exploring the modes of instability of the laminar boundary. The basic problem is that boundary layer transition is controlled by the detailed aerodynamic environment as well as the Reynolds number as demonstrated by Osborn Reynolds[33] in his classic studies.

Both theoretical and experimental studies of transition in incompressible flows have suggested that, in the absence of large freestream disturbances or disturbances from within the boundary layer, the two-dimensional Tollmien-Schlichting[34] model is a good representation of the initial breakdown of laminar flow. However, when velocity fluctuations of over 10 percent are introduced into the freestream, "by-pass" modes involving the generation of three-dimensional, streamwise, vortex-like instability may be the principal mechanisms involved in the transition process. Mack[35] among others, has speculated that a helical instability mode should be the dominant feature of the flow upstream of the non-linear breakdown into turbulence of a laminar boundary layer in supersonic flow. However, the lack of direct evidence to support this prediction has slowed theoretical developments of this nature. An understanding of how disturbances in the freestream influence transition requires knowledge of the coupling mechanisms between the laminar boundary and the outer, inviscid flow. While, in most instability problems, it is necessary only to calculate the conditions for the existence and growth of a disturbance, transition prediction using linear stability theory rests almost completely on the ability to trace the origin of the instability[36].

Experimental studies of transition are of little general value unless it can be shown that the instability modes in the boundary layer remain unexcited by disturbances in the freestream or respond to stronger disturbances generated within the boundary layer, for example, by surface roughness. As discussed earlier, the author remains openly skeptical of the general usefulness of any transition data gathered in any wind tunnel. However, the agreement between the measurements of transition Reynolds number made in large, high Mach number facilities, like the Calspan Shock Tunnel, with free flight measurements suggest a low level of tunnel noise. Studies at AEDC[37] and NASA-Langley[38] have demonstrated that, in conventional supersonic wind tunnels, the Reynolds number at which transition occurs is strongly influenced by the fluctuating pressure level in the freestream. Pate and Schueler[37] have demonstrated that the level of pressure fluctuation can be related to the geometric features of the tunnel used and to the characteristics of the boundary layer on the tunnel walls, and a decrease in tunnel size for the same freestream conditions should result in a decrease in the transition Reynolds number. Comparing measurements made in the Calspan Shock Tunnel, shown in Figure 21, we observed $Re_\theta^{0.2}$ variation and not a jump in Re_θ with tunnel size.

Correlations of the transition measurements made on sharp cones and flat plates in studies at Calspan, flight measurements reported by TRW, and measurements in the ballistic ranges at AEDC and NSWC are shown in Figure 22. A further comparison between tunnel measurements and those made in the more recent studies of Reda[39], plotted in terms of the unit Reynolds number, are shown in Figure 23. We find relatively good agreement between the two sets of measurements, and, in common with the studies of Potter[40], Sheetz[41] and Reda, we observe a unit Reynolds number effect. The source and significance of the unit Reynolds number effect have been the subject of extensive debate. The analyses of Morkovin[42] and Reshotko[43] have suggested that the unit Reynolds number effects may be traced to a sensitivity to the non-dimensional frequency (U_e^2/ν_e) or to the wavelength of the disturbance (U_e/ν_e); however, in reality, the disturbance-inducing transition may stem from superposition of a number of different mechanisms.

A composite of the schlieren-photograph and heat transfer records obtained at Mach 13, shown in Figure 24, presents a "good picture" of the general structure of the transition region. The "spikes" in the laminar heat transfer trace, which mark the beginning of the transition process, can be described as turbulent bursts, which are fairly well structured, and which travel at very close to

the velocity of the inviscid flow. As these bursts are convected downstream, they begin to break up into large-scale instabilities. The convection of these large-scale eddies past a thin-film gage gives rise to the intermittent characteristics shown in Figure 24. As the spectrum of turbulent scale sizes fills out, the heating to the surface approaches the turbulent heating range. Photographic examples of "wave-like" instabilities which preceded the large-scale breakdown into turbulence are shown in Figure 2. In many cases, wave trains would be a more accurate description for, as shown in Figure 25, there were many instances where these instabilities did not undergo a significant change in structure as they were convected along the cone. High-speed photographs obtained with the Cordin camera indicate that, in fact, these instabilities "twisted" as they were convected downstream, suggesting a helical structure. Following the region of "wave-like" instability, the laminar boundary layer began to develop large-scale instabilities at an edge (see Figure 26); then, transition began. Photographic examples of the development of the transition region following the "wave-like" instabilities discussed in the previous paragraph are shown in Figures 26a and b. In Figures 26c and 26d, we see the gross instabilities developing as they were swept downstream, culminating in some very-large-scale turbulent bursts. These disturbances traveled down the cone at convective velocities between 0.5 and 0.8 of the freestream velocity. The gross size of the eddies generated in this region is of the same order as the boundary layer thickness. In Figures 27a and 27b, are shown examples of the gross mixing in the transition region which precedes the development of the turbulent boundary layer. These photographs show the "wave-like" instability, followed by by the gross instability, followed by a region in which there is large-scale turbulent mixing. In the latter region, it appears that the scale of the turbulence exceeds that in the following, fully turbulent boundary layer; it is in this region that the heat transfer overshoot occurs. In a large number of studies in hypersonic flows, it takes many boundary layer thicknesses before the scale sized of the turbulence generated in the transition process are no longer of importance. Figure 28 shows a compilation of measurements made of the velocity exponent (n) in the relationship $\frac{U}{U_e} = (\frac{y}{\delta})^{1/n}$ obtained downstream of the transition region in hypersonic flow. Immediately downstream of transition n reaches a peak, reflecting the existence of a predominance of large scale eddies in the boundary layer. These eddies break into smaller eddies as they are transported downstream. However transition lengths from 50 to 100 boundary layer thickness are required before the turbulent boundary layer approaches equilibrium.

VI. TRANSITIONAL AND INTERACTING FLOWS OVER NOSETIPS AND LEADING EDGES

The occurrence of boundary layer transition and the subsequent turbulent flow in stagnation regions or on the attachment line of a highly swept leading edge of a wing or intake will have important impact on the design and aerothermal performance of hypersonic vehicles. In fact the trajectory flown by such vehicles may be selected in part on the basis of transition criteria. In general the application of the measurements of the occurence and mechanism of boundary layer transition made in hypersonic facilities to predict transition on flight vehicles has in fact met with little success except where transition is tripped by roughness or a disturbance induced on the surface of the body. Recently, however, it has been shown by Poll[44] and others[45] that transition on the surfaces of flight vehicles like the Space Shuttle, with highly swept leading edges, may be predicted with good accuracy from transition measurements made in ground test facilities. One explanation for the success of the wind tunnel based predictions in this instance may lie in understanding that the underlying mechanisms of transition is a "by-pass" disturbance that is generated on he body rather than external to it. For models whose surface roughness generates disturbances large enough to exceed those generated externally, transition may be controlled principally by the unit Reynolds number of the freestream and the models geometric characteristics rather than those of the tunnel in which the measurements were made.

While there have been a number of correlations suggested over the years to correlate[47-52] the occurrence of boundary layer transition on rough surfaces, the most recent work by Batt and Legner[53] appears to be one of the most comprehensive and useful. As shown in Figure 5 the occurrence of transition was found to be best correlated in terms of a Reynolds number based on momentum thickness at the start of transition and non-dimensional roughness height K'/ϕ', where $k' = k\,(1 + 350 * k/R_n)$ and $\phi' = \phi * T_w/T_e$. This correlation is supported by range measurements made by Reda[46] who however suggests a transition criteria in terms of a roughness Reynolds number $\rho_K U_K K/\mu_K$, based on the local properties at the edge of the roughness. Using either criteria it is easily shown that for a significant part of the trajectories proposed for a transatmospheric vehicle, surface irregularities of the order of 1/1000 inch would trip transition.

As shown by Poll[54], the junction between a highly swept wing or intake and forebody can act as a large trip forcing transition to turbulence on the attachment line of a leading edge at relatively low freestream Reynolds numbers. For these flows it has been found that $\eta_w = ((dU_e/dy)/\nu^*)^{0.5}$ is a characteristic dimension, and the crossflow Reynolds number $\eta^* D/\nu = 210$ at which transition occurs is independent of Mach number (see Figure 29). Clearly further studies in hypersonic flows are required to examine the validity of this relationship and determine Mach number and wall cooling effects. However, as shown in Figure 30, the Mach number dependence suggested by this relationship is not inconsistent with the transition measurements on sharp cones and rough nosetips in hypersonic flow. One of the most severe aerothermal loading conditions could arise if a strong shock, from an external component or from an engine or pod mounted on the swept wing, is incident on the turbulent boundary layer over the attachment line as discussed in Section VIII. Currently the only measurements available in regions of shock/shock interaction have been made for laminar flow over smooth surfaces. As in the case of shock/shock interaction on the indented nose shapes discussed in the following section, we believe that the largest heat loads are generated in turbulent interaction regions over rough surfaces.

Shock/Boundary Layer Interactions on Indented Nosetips

Measurements made in full-scale flight tests and ground test facilities with ablating nosetips have demonstrated that under many re-entry conditions concave or indented noseshapes can be developed[55] as the nosetip ablates. The increased heating resulting from boundary layer transition close to the sonic region is responsible for the initial development of the indentation. Subsequently, the large heating rates which are developed in the recompression region resulting from shock-

blowing are not additive, in most codes the magnitude of rough-wall heating and surface blowing are calculated by essentially superimposing calculations based on models of these two effects considered separately. In these codes the assumption that surface roughness plays the primary role in controlling heating augmentation may be significantly in error when applied to highly ablating surfaces. If, as we deduce from the experimental studies, surface blowing effectively smooths the rough surfaces, then selection of an effective roughness height as the single correlating parameter connecting flight measurements with code predictions may be in error. Also, since most predictive techniques employ an effective sand-grain roughness as the single length scale characterizing roughness size, there continues to remain a key problem in defining the surface topography of a rough hypersonic vehicle.

The experimental studies of Nikuradse[62] and Schlichting[63], both hydraulic pipe flow studies, were principally responsible for the selection of sand-grain roughness as the standard against which to measure relative effects of other types of roughness. Although this standard has been frequently employed, the topographical characteristics of a sand-grain surface have yet to be defined. In fact, because of the experimental difficulties involved in the preparation and inspection of rough surfaces inside a small-diameter pipe, it is surprising that Nikuradse's results are as consistent as reported. For fully developed pipe flows, Nikuradse established that the parameter controlling the similitude of the flows is the roughness Reynolds number ($U_t K/\nu_w$). This parameter ($\widetilde{Re}_K$) was selected in many subsequent studies to characterize boundary layer flows where other non-dimenstional groupings (such as $K_s/\delta^*, K_s/\theta$, etc.) might have been considered more valid. The Schlichting studies, conducted with roughness of well-defined geometric shapes, provided the first set of measurements which could be reproduced in both experimental and theoretical studies. The results from these studies, together with those from a number of subsequent investigations in subsonic adiabatic flows, were correlated by researchers to yield relationships between an "effective sand-grain height" and parameters which describe the geometric features of the surface--a step which further perpetuated the use of sand-grain roughness as a standard. The Dirling correlation, see (Figures 39 and 40) is one such plot, from which an effective sand-grain roughness height can be determined from knowledge of peak-to-valley roughness height together with the shape and spacing of the roughness elements. While there is little direct supporting experimental evidence, the "lambda" form of the correlating curve is assumed to reflect a sudden change in flow structure from an "open" to a "closed" cavity flow around (between) the roughness elements as the spacing between the roughness elements is varied. Do open and closed cavity flows really exist on rough surfaces constructed from three-dimensional roughness elements? Is not the structure of the flow around the elements also dependent upon the local Reynolds number, a parameter not taken into account in any such correlations? If an effective roughness height can be accurately determined from a 'bump curve', this dimension must be combined with key fluid dynamic properties to yield a non-dimensional parameter or groups of parameters with which to characterize the flow. The roughness Reynolds number $\widetilde{Re}_K (U_t K/\nu_w)$ originally used by Nikuradse, and the non-dimensional roughness heights $K/\delta^*, K/\theta_m$ and K/θ_T (where δ^*, θ_m, and θ_T are the displacement, momentum, and thermal energy thickness respectively), have all been used to correlate the aerothermal effects associated with boundary layers over rough re-entry vehicles. To date, however, no single parameter or combinations of parameters (e.g., $\widetilde{Re}_K, K/\theta$) has been used with any great success to describe the general similitude of turbulent boundary layers in supersonic and hypersonic flows over rough, highly cooled walls.

The studies of Dvorak[64], Bettermann[65], Lewis[66], Simpson[67] and more recently Lin[68] and Finson[69] have provided further insight into the basic effects of roughness shape and spacing on the characteristics of the rough wall boundary layer and skin friction and heating to a rough surface. Dvorak combined the effects of roughness shape and spacing into a single parameter λ (the roughness density), defined as shown in Figure 40. He linked the downward shift in the velocity profile $\Delta U/U_t$ to a combination of roughness Reynolds number $\widetilde{Re}_K (u_t K/\nu_w)$ and λ through the relationship

$$\frac{U}{U_t} = \frac{1}{\kappa} \ln \left(\frac{y U_t}{\nu}\right) + A - \frac{\Delta U}{U_t}\left(\frac{K U_t}{\nu}, \lambda\right)$$

In incompressible flows the smooth regime, where the surface shear is entirely due to viscous shear is defined by $KU_t/\nu < 5$. At larger $\widetilde{Re}_K$, $(5 < \widetilde{Re}_K < 70)$, the surface shear is composed of form drag on the roughness elements combined with viscous shear. For $K\frac{U_t}{\nu} > 70$, the surface shear results principally from drag, and viscosity is no longer a factor in controlling the velocity profile. For fully rough flows, Equation 1 can be rewritten

$$\frac{U}{U_t} = \frac{1}{\kappa} \ln \left(\frac{y}{K}\right) + A - \left[\frac{\Delta U}{U_t} - \frac{1}{\kappa} \ln \left(\frac{K U_t}{\nu}\right)\right] \quad \ldots 2$$

where $\frac{\Delta U}{U_t} - \frac{1}{\kappa} \ln \left(\frac{K U_t}{\nu}\right) = f(\lambda)$

which is a function of the roughness density. Here it should be noted that $f(\lambda) = A$ U_R^* where U_R is the velocity close to the top of the roughness elements and $A(\pm 5)$ is the smooth wall constant. Now the definition of Nikuradse's sand-grain roughness is basically

$$\frac{U}{U_t} = \frac{1}{\kappa} \ln \left(\frac{y}{K_s}\right) + 8.5 \quad \ldots\ldots 3$$

Hence, combining equations 2 and 3 we obtain

$$f(\lambda) = -\left[3 + \frac{1}{\kappa} \ln \left(\frac{K}{K_s}\right)\right]$$

which is generally correlated by two relationships. The existence of two regions has been rationalized on physical grounds, supported by experimental studies in two-dimensional flows. There is serious debate about whether a significant change in flow structure occurs as three-dimensional roughness elements are drawn together. Certainly the measurements with stone roughness do not exhibit such a trend. This is particularly unfortunate, since Nikuradse's data falls on the line constructed principally from data obtained on roughness constructed by two-dimensional machined grooves.

Finson's engineering model based on the early concepts of Liepmann and Goddard[70] and his (Finson's) detailed numerical calculations provides a good basis for interpreting the physical phenomena of key importance in rough wall heating, as well as a relatively simple prediction technique. The shear on a rough wall can be expressed as the sum of the viscous and form drag of the rough surface:

$$C_f = C_{f_{BASE}} + \int_B^T \frac{\rho u^2}{\rho_e U_e^2} C_D B(y) \cdot \frac{d^2(y)}{D^2}\, dy$$

where $B(y)$ is the blockage factor, and $d(y)$ and D are the diameter of the roughness element and the spacing between elements, respectively. From his detailed numerical solutions, Finson showed that ρ and u were relatively constant between the base and top of the roughness element at values ρ_R, U_R close to the top of the roughness, and this equation becomes

$$C_f = C_{f_B} + \frac{\rho_R U_R^2}{\rho_e U_e^2} C_D B\left(\frac{K}{2}\right) \frac{A_p}{A_s}$$

where A_p/A_s is the ratio of projected area of the roughness element in the direction of the flow to total area of the flow on which they stand, and $B(\frac{K}{2})$ is the average value of $B(y)$.

For compressible flows Finson found that

$$U_R/U_e = 0.247 + .234 \log\left(\frac{\rho_R}{\rho_e}\frac{A_s}{A_p}\right)$$

Therefore, assuming C_{F_B} is the smooth wall heating level, it is possible to relate the rough wall skin friction to the smooth wall value in the generalized form

$$\frac{C_f}{C_{f_{SMOOTH}}}_{ROUGH} = 1 + f_1'\left(M_e, T_w, \frac{K}{\theta}\right) * f_2'\left(\lambda, B, \left(\frac{K}{D}\right), C_D\right)$$

and the relationship for heat transfer is assumed of the same form.

$$\frac{C_H}{C_H}_{ROUGH} = f_1'\left(M_e, \frac{T_w}{T_e}, \frac{K}{\theta}\right) * f_2'\left(\lambda, B\left(\frac{K}{D}\right), C_D\right)$$

If we assume that the product of the blockage factor and C_D are invarient with roughness shape and space, then for constant local free stream condition, we get the Dvorak-Simpson Parameter:

$$\frac{C_H}{C_H}_{ROUGH} = f\left(\frac{A_p}{A_s}\right)$$

A slightly different form can be obtained by the subsonic blunt body approximation

$$C_D = C_{D\,REF}\left(A_p/A_{ws}\right)$$

and using D/K rather than A_s/A_p to obtain the correlation in terms of the Dirling[71] parameter,

$$\frac{C_H}{C_H}_{ROUGH} = f\left(\frac{D}{K} \cdot \left(\frac{A_{ws}}{A_p}\right)^{4/3}\right)$$

where the various areas are illustrated in Figure 39.

In recent studies of effects of roughness shape and spacing on the heat transfer and skin friction to the roughness, nosetips, frusta and flaps of a typical MRV configuration, Holden[61] used both the Dvorak/Simpson parameter A_s/A_p and the Dirling parameter $\frac{D}{K}\left(\frac{A_{ws}}{A_p}\right)^{4/3}$ and achieved reasonable success in correlations. In these studies, the effects of roughness shape and spacing on the heat transfer and skin friction both for surfaces with sand-grain roughness and those constructed with geometrically well-defined hemispherical and conical roughness elements were examined. Also, heat transfer, skin-friction, and pressure-distribution measurements were obtained on spherical and ablated noseshapes, conical frusta, and the control surfaces of MRV vehicle in hypersonic flow. Typical measurements and correlations are shown in Figures 41, 42, 43 The results of this work have demonstrated that the low-speed measurements of Nikuradse[62], Schlichting[63], and others, and the correlations of Dirling[71]/Simpson[67], cannot be used directly to predict rough-wall heating and skin friction in supersonic and hypersonic flows over non-adiabatic surfaces. Even the more solidly founded prediction scheme developed by Finson[69], which is based upon his detailed numerical solutions, consistently overpredicts the roughness-enhanced heating levels in high-speed flows. While direct measurements of the skin friction of, and heat transfer to, geometrically well-defined rough surfaces provide the opportunity to more closely evaluate the accuracy of the current shape-change codes and the more fundamental treatments like that of Finson in high Mach number, high Reynolds number flows, there remains a basic need to define more closely the fundamentals of the fluid dynamics which control momentum and energy exchange in high-speed flows over adiabatic and non-adiabatic surfaces.

Voisinet's[60] studies of the combined effects of roughness and blowing were conducted at Mach 6 under adiabatic wall conditions. The measurements made in these studies have clearly demonstrated that the combined effects of blowing and roughness on skin friction cannot be described in a simple manner. The effects of surface roughness alone on skin friction were shown to be correlated in terms of the roughness Reynolds number $\tilde{R}e_K$; a result consistent with earlier measurements on adiabatic walls by Goddard[70] and Reda[72]. In contrast, measurements on model placed in the flow involving significant levels of heating ($H_w/H_o = 0.5$) have in general correlated better with parameters like K/δ, K/θ or K/δ_T which, as shown by the theoretical studies of Dvorak and Finson, should have greater relevance to roughness effects on re-entry vehicles. Voisinet's studies demonstrated that the effects of surface roughness and blowing on skin friction cannot be deduced from simple expressions derived from the measurements made of each of the separate effects.

The measurements made in studies with a transpiration cooled model with and without blowing is shown in Figure 44 together with measurements of the heating rates to rough and smooth non-porous hemispherical models at the same condition. The measurements on the model with zero blowing, shown in Figure 44, clearly show that the intrinsic roughness of the surface causes heating enhancement factors of over 1.7. In fact, it can be seen by comparing Figures 44 and 45 that the heat transfer measurements on the rough hemisphere are in good agreement with those obtained on the non-blowing transpiration-cooled nosetip model such that they would be biased toward the larger heating. When a small amount of blowing ($\dot{m}/\rho u c_m = 0.032$) was introduced, the heating rates over a major part of the transpiration-cooled model dropped to levels close to those recorded on the smooth model, as shown in Figure 44. It could be postulated, on the basis of these measurements, that the initial effect of mass addition from a rough ablating nosetip is to modify the flow around the roughness elements, by eliminating the cavity flows, in such a way that the momentum defect introduced by the roughness is small as illustrated in Figure 46. How does roughness shape and spacing influence the heat transfer to the surface in the presence of mass addition? Are the current relationships which have been developed from an essentially subsonic, adiabatic flow data base, to describe roughness heating on blunt nosetips applicable to the hypersonic flow transpiration-cooled vehicles? Holden's studies of roughness shape and spacing effects on non-ablating configurations suggest that not only are the subsonic studies inapplicable to the heating of heat shields in hypersonic flow, but further that the basic modeling of the roughness drag and mechanisms of heating in the theoretical models is highly questionable. In these studies it was shown that even in mildly supersonic flow, shocklets are clearly evident (see Figure 47) around each roughness element. Thus not only is the model of drag incorrect, the entropy layer associated with each shocklet contributes to a higher temperature/ lower momentum flow around the roughness elements than described in the current roughness models.

VIII. SHOCK WAVE/TURBULENT BOUNDARY LAYER INTERACTIONS IN HIGH SPEED FLOWS

Two-Dimensional Shock-Wave/ Turbulent Boundary Layer Interactions

The development of two-dimensional turbulent separated regions, induced in a compression corner, and at the base of an incident shock, with increase in interaction strength in hypersonic flow as obtained by Holden[74], are illustrated in Figures 49 and 50. Separation is first observed in the laminar sublayer and a well-defined separation bubble is clearly visible in Figure 49. The initial development of the separation region takes place by an elongation into the laminar sublayer, with the separation and reattachment shocks combining within the boundary layer to form a single shock. Only when the separation point has fed well forward of the junction is a well-defined plateau region formed. Then, in contrast to laminar interaction regions, the separation shock originates at the bottom of the boundary layer and is contained within the boundary layer until it coalesces with the reattachment compression process. In separated regions induced by an externally generated shock, separation first takes place in the region where the incident shock strikes the laminar sublayer, see Figure 50b. The separation point moves forward with increasing strength of the incident shock until the separation shock becomes visible in the inviscid flow downstream of the incident shock; as yet, separation is still downstream of the point where the incident shock passes through the edge of the boundary layer. For large incident shocks, boundary thickening occurs ahead of the incident shock in an analogous fasion to laminar flow separation. However, as in wedge-induced separated regions, viscous-inviscid interaction takes place almost entirely within the original boundary layer. The structure wedge and shock-induced turbulent interaction regions at Mach 13 are very similar to those at Mach 8; however, as we might anticipate, the viscous interaction region and the associated shocks are even more firmly embedded within the original boundary layer.

Surface measurements with high frequency instrumentation indicated that turbulent separated regions were highly unsteady, and typically the separation point would oscillate in a streamwise direction with an amplitude of approximately one-quarter to one-third of the local boundary layer thickness, at frequencies in the range from 1 to 10 kHz (see Figure 51). The unsteady character of the records from transducers in the recirculation region indicated it could be unrealistic to assume that a laminar sublayer model, in the conventional sense, could be used to describe the lower part of the recirculating region as is done in some of the triple deck calculations. The mean distribution of skin friction, heat transfer and pressure to the wall's bounding, both shock- and wedge-induced interaction region were similar for well-separated flows with identical total pressure rises. both the pressures and heat transfer distributions are characterized by well-defined plateaus in the recirculation region and large gradients in the separation and reattachment regions. The maximum heat transfer rates generated in the reattachment regions of these flows is, of course, of considerable importance. Holden[75] found that for separated interaction regions the maximum pressure and heat transfer measurements over the Mach number range from 2 to 13 could be correlated in the form shown in Figure 52.

The influence of Reynolds number on the size of two dimensional separated regions remains unresolved. Most of the early studies of shock wave-turbulent boundary layer interaction were made in the turbulent boundary layer over a tunnel wall. Major discrepancies were found between experimental facilities; for example, the measurements of Bogdonoff and Kepler[76] differed considerably from those of Gadd[77] for identical freestream Mach numbers and interaction strength, when both experimenters had indicated that there was little effect of freestream Reynolds number on the length of the separated region. However, the measurements of Green[78], Roshko and Thomke[79], Law[80], Settles, Bogdonoff and Vas[81], and Appels[82], all made under adiabatic wall conditions, indicate that increasing Reynolds number decreases the size of a turbulent separated region. In contrast, the studies of Chapman, Kuehn and Larson[83], Kuehn[84], and Holden[74], Elfstrom[85] and Appels[86] at hypersonic speeds, all conducted on "highly cooled" models mounted in the test section, have shown the opposite trend. As in the case of incipient separation, the answer may lie in changes in the equilibrium structure of a turbulent boundary layer with Reynolds number. This hypothesis is supported by present measurements of shock- and wedge-induced separated flows at Reynolds numbers of up to 3×10^7 by Holden[75].

In the experimental studies by Holden, where dynamic measurements of the skin friction in turbulent interaction regions were made, the separation conditions were defined when the time average of surface shear at one point only on the surface was zero (see Figure 51).

Comparisons with Navier-Stokes Solutions

The complexity of the flow field in regions of shock wave/turbulent boundary layer interaction is such that it is unrealistic to expect to describe such regions in any detail within the framework of the boundary layer equations. Indeed their are some who would question whether the time or mass averaged Navier-Stokes equations capture the basic fluid mechanics associated with the intrinsically unsteady nature of separated regions. In hypersonic flows the effects of compressibility on the structure and development of turbulence must also be considered.

While there have been strenuous efforts to obtain predictions of 2D and 3D turbulent interaction regions, it is currently recognized that "successes" with "Navier-Stokes" code in describing some 3D turbulent interactions regions is a result of the dominance of the pressure and inertial terms in these flows. In these latter comparisons (References 88 & 89) it was found that the modeling of turbulence could be changed without significantly changing the numerical solution. For 2D interactions it appears the modeling of turbulence is more critical. To obtain good agreement for these latter flows some very gross assumptions must be made in the turbulence model. Shang and Hankey[90], for example chose to apply an empirical relationship (selected by matching the length of the separated region) to rapidly decrease the turbulent scale size through the interaction region as shown in Figure 53. Horstmann[91], however, found the best agreement with Settles[92] measurements in wedge-induced separated regions using a two equation model for turbulence scale size and vorticity, as shown in Figure 54. Working with this same turbulence model, however, Horstmann[92] was unable to predict the occurrence of separation on two incident shock/turbulent boundary layer configurations studied by Holden[93] at Mach 11.2. As shown in Figures 55 and 56 both these flow fields are clearly separated and yet the numerical solution fails to predict the characteristic plateaus in either the heat

transfer or pressure distributions. The modeling of turbulence in separated interaction regions at hypersonic Mach numbers should account for the effects of compressibility and the generation of turbulence by the unsteady movement of the incident and induced shocks as they traverse and interact with a major region of the turbulent boundary layer. Clearly further detailed experimental work and insightful theoretical modeling are required to develop numerical prediction techniques which are capable of describing turbulent interaction regions in detail.

Three-Dimensional Shock Wave/Turbulent Boundary Layer Interaction

Many of the conceptual problems associated with the use of the boundary layer equations to describe separated regions induced by shock wave/turbulent boundary layer interaction are circumvented by the direct solution of the Navier-Stokes equations. However, in their place we find the equally thorny problem of specifying a detailed model of turbulence for flows with exceedingly large streamwise pressure gradients. Despite the lack of success in developing credible turbulence models for two-dimensional interaction regions, or perhaps because of it, three-dimensional turbulent interaction regions have become the focus of attention of the Navier-Stokes solvers.

Corner Interaction Studies

The axial corner flow or swept-shock interaction has been one of the principal configurations selected to investigate three-dimensional regions of shock wave/boundary layer interaction. The swept-shock, which is generated by a wedge or fin mounted perpendicular to a flat plate, impinges normally onto the flat plate boundary layer. The initial studies in this area by Stalker[94] and Stanbrook[95] were followed by the more detailed investigations of McCabe[96], Peake and Rainbird[97], Oskam et al[98], Cousteix and Houdeville[99], Dolling and Bogdonoff[100, 101], Dolling and Murphy[102], and Dolling[103]. The latter extensive series of studies was conducted at Mach 3 under adiabatic wall conditions. While incipient separation is relatively easy to define for two-dimensional turbulent interactions, this concept has generated considerable controversy in three-dimensional flows. While McCabe[96] suggests that separation should be defined on the basis of converging steamlines, Stanbrook[95] and others have used criteria based on the inflection points in the pressure distribution. The occurrence of separation was correlated in simple terms by Korkegi[104], who found that in low Mach number flow, deflection angle θ_{wi} for incipient separation varies as the inverse of the upstream Mach number, i.e., $\theta_{wi} = 0.3M_o$, while for $2 < M < 3.4$ Korkegi suggests that p_i/p is independent of Mach number. Goldberg's[105] and Holden's[106] measurements at Mach 6 and 11 respectively do not agree with the Korkegi correlation.

Studies with the emphasis on the heating in swept-shock interaction regions have been conducted by Neumann and Burke[107], Law[108], Token[109], and Scuderi[110] and Holden[111]. Figure 57 shows typical distributions of heat transfer and pressure along a streamwise cut through the interaction region together with nomenclature which is in conventional use. While the heat transfer and pressure distributions exhibit a uniform and monotonic increase through attached interaction regions, when the flow separates, distinctive plateau regions are formed in the heat transfer and pressure distributions, as depicted in Figure 57. As noted above, at low Mach numbers ($M = 2 \rightarrow 4$) and for adiabatic surfaces, a large body of data exists on the mean characteristics of swept-shock interactions. Strangely, this body of 3D data has been found to be in better overall agreement with the Hung and MacCormack[112], Horstmann[91], Shang and Hankey[90], Settles and Horstmann[92] solutions to the Navier-Stokes equations than the relatively less complex two-dimensional flow separation over a flat plate/wedge. These results are not as sensitive to the turbulence model and suggest that the gross features of the flows are controlled principally by invsicid effects.

In a corner flow, the swept-shock generated by the inclined fin impinges on the turbulent boundary layer in a plane perpendicular to the flat plate. The basic mechanism of pressure rise through the interaction is therefore controlled principally by the component of freestream Mach number normal to this shock ($M_o \sin\theta$). A highly simplified visualization of the viscous/inviscid interaction with flow separation is sketched in Figure 58. Here, we consider the flow in the plane normal to the plane of the shock to be similar to that in transonic flow. When flow separation occurs, a three-dimensional vortex is formed, the pressure in which is relatively constant at the "two-dimensional" plateau level, as we will show later. The streamwise distribution of heat transfer in this region is also found to be relatively constant, and indeed we and others using skin friction and oil flow measurements have correlated the first appearance of a plateau region in the heat transfer with a significant change in the flow structure which is linked with flow separation. In fact, Token[109] has shown that the McCabe[96] criteria, based on an examination of surface oil streaks in the neighborhood of flow separation, are less sensitive methods for detecting flow separation than observations based on changes in the heat transfer distribution with increased interaction strength. In a recent experimental study at Mach 11, Holden[111] used the incipient formation of a plateau in the heat transfer distribution, together with a marked increase in the fluctuation levels in the output of the thin film instrumentation, as marking the onset of flow separation. As shown in Figure 59 Holden's measurements indicated that in hypersonic flow over highly-cooled surfaces the turbulent boundary is more tenacious in resisting boundary layer separation than predicted by the methods derived by McCabe[96] and Korkegi[104]. Holden's measurements of the peak pressure ratio through the interaction and the plateau pressure rise are in better agreement with calculations based on an inviscid flow model in the 2D theory of Reshotko and Tucker[113] than the correlations of Scuderi[110] as shown in Figure 60. Holden found that, as in the studies of two-dimensional separated interaction regions, the peak heating can be related to the overall pressure rise by a simple power law relationship as shown in Figure 61. Figure 62 shows that the maximum pressure rise through the interaction region can be calculated with good accuracy from inviscid flow relationships. While there appears to be merit for the development of simple prediction methods in describing the flow in terms of the normal flow Mach number, this is clearly a gross oversimplification and it should be noted that the plateau pressure measurements obtained in the current study were relatively independent of $M_o \sin\theta$.

Skewed Shock/Boundary Layer Interaction

Another approach to exploring flow separation in regions of three-dimensional shock wave/boundary layer interaction is to begin with a two-dimensional or axisymmetric interaction and sweep this interaction (or introduce angle of attack for the axisymmetric case) to

progressively introduce crossflow into the interaction region. Experimental studies of this type have been conducted by Ericsson, Reding and Guenther[114], Settles and Perkins[115], and Settles and Teng[116]. Settles, who studied the interaction region over swept and unswept flat plate/wedge configurations in an adiabatic Mach 3 airflow, found that introducing crossflow increased the scale of the separated interaction region. Considerable effort was expended in this latter study to determine the Reynolds number scaling, and the length from the upstream tip of the wedge for the flow to become quasi-two-dimensional. However, the effect of changing the overall spanwise scale of the model on the scale of the interaction was not examined explicitly. The measurements of surface and pitot pressure through the interaction regions were in good agreement with solutions to the Navier-Stokes equations obtained by Horstman[91]; however, some key features of the flow were poorly predicted. It is known that agreement with pressure data is not the most definitive of tests. More recently Holden[106] performed studies of crossflow effects on the size and properties of the interaction region induced by a swept-oblique-shock incident on a turbulent boundary layer over a flat plate at Mach 11 and $R_{e_t} = 30 \times 10^6$. Experiments were conducted for two strengths of incident shock, the first ($\theta_{SG} = 12.5^o$) to generate a separated condition close to incipient separation, and the second ($\theta_{SG} = 15^o$) to generate a well-separated flow. Distributions of heat transfer and pressure as well as schlieren photographs of the unswept or two-dimensional flow condition and the 30 degree swept condition are shown in Figures 63 and 64. It is clear from the well defined plateau regions in the distributions of pressure and heat transfer, as well as the well defined separation shock in the schlieren photograph, that a well separated region, extending two inches in length, is induced beneath the stronger incident shock. The measurements made of the distribuiton of heat transfer and pressure beneath the well separated flow induced by both the 12.5 degree and the 15 degree shock generators swept at angles of 0 and 30 (shown in Figures 63 and 64) indicated that the induced crossflow has little effect on the size and characteristics of the interaction regions. If there is a perceptible effect, it is a decrease in the length of the separated region with increased crossflow. The significant differences between Holden's and Settles[92] measurements of the variation of interaction length with sweep angle and those obtained in these studies are shown in Figure 65. While Settles finds an almost threefold increase in separation length at sweep angles of 40 degrees, Holden found 10 percent reduction in this length. Further studies are required to resolve this issue.

Three-Dimensional Shock-Shock Boundary Layer Interaction

The heating rates generated in three-dimensional interaction regions by shock-shock interaction can pose serious problems for the designer of TPS. Heating levels up to two orders of magnitude larger than the stagnation point value can be generated at hypersonic speeds by shock-shock interaction over the leading edge of fins, inlets and structures connecting two vehicles. These regions of sharply peaked heating levels are accompanied by high pressures, and unlike the stagnation point their position cannot be defined with ease. Perhaps the most dramatic example of damage reuslting from shock impingement heating was that recorded on the ventral fin supporting a ramjet model on the X-15. At Mach 6.7, the heating resulting from shock-shock interaction caused a burn-through in the fin, as shown in Figure 66, which also graphically demonstrates the high gradients generated in such flows.

The first detailed investigation of the fluid mechanics of the shock-shock interaction was performed by Edney[117], who on the basis of a detailed schlieren study defined six distinct flow regimes which resulted from the orientation of the shock systems. Three classes of interactions are shown schematically in Figure 67 along with the typical levels of enhanced heating. Type IV interference, in which the shock-shock interaction generates a jet which impinges on the surface gives the greatest heating enhancement. Edney's Schlieren photographs of this interaction are shown in Figure 67 for the shock-shock interaction on a blunt fint. The Type IV flow structure for the unswept fin configuration, which is shown in Figure 67, exhibits a supersonic jet, bounded by shear layers, that impinges on the fin leading edge resulting in the highest heating levels. Because the shock layer flow is subsonic, the structure of interacting flow is not readily predicted. Similarly the shear layer flows are highly sensitive to the Reynolds number. The leading edge sweep has clearly a marked effect on the interaction heating as the studies of Hiers and Loubsky[118] and Gulbran[119] have demonstrated experimentally. The measurements of heating distribution obtained by Hiers and Loubsky[118] clearly show the magnitude of the impingement heating. Hains and Keyes[120] and Keyes and Morris[121] expanded on the Edney studies to provide correlations of the heating levels encountered in the various classes of interaction. These studies demonstrated a streng sensitivity to Reynolds numbers and were followed by studies by Birch and Keyes[122] who attempted to correlate conditions for transition in these flows. In general, the studies that have been conducted of shock-shock interaction were conducted at relatively low Reynolds numbers for limited ranges of Mach number. There remains a need for high Reynolds number studies in which detailed measurements are made of the distribution of heat transfer in fully turbulent interaction regions.

IX. COMPRESSIBILITY EFFECTS ON TURBULENT MIXING

While in supersonic and hypersonic flows constant pressure, turbulent boundary layers do not appear to be strongly influenced by compressibility effects, studies of the supersonic mixing between two coaxial streams suggest that there is a significant decrease in spreading rate with increased Mach number[123]. Similar effects have been observed in the turbulent near wakes of slender bodies travelling at hypersonic speeds[124,125,126]. Whether such an effect is associated with fundamental changes in the mechanism of turbulence production or dissipation (a turbulence compressibility effect) or is associated with the relative Mach number or density between the two streams remains to be determined. However such an effect has important implications for the performance of hypersonic ram jets where fuel (hydrogen)-air mixing will occur at supersonic and perhaps hypersonic speeds. It is clear from both the fundamental and practical viewpoint that an understanding of this phenomena is of key importance to the development of rational prediction techniques.

In their review of free shear layer mixing measurements, Birch and Eggers[123] concluded that there is a significant reduction in the spreading parameter with increased Mach number presenting their correlation of the measurements in a form reproduced in Figure 68. More recently Padova, et al.[127] have examined the coaxial mixing of non-reacting gas flows for relative Mach numbers up to 3 for density ratios up to 2.7; their measurements fall between the Birch and Eggers data and those of Maydew and Reed[128] who found little

variation of spreading parameter with Mach number. Currently there are a number of unresolved issues associated with the downstream effects of initial conditions; however a decrease in turbulent spreading rate has also been found in high Mach number turbulent wakes. It has been observed that in hypersonic flow the turbulent wake of slender bodies over which the boundary layer is fully turbulent grows at a significantly slower rate than a wake where transition occurs downstream of the rear stagnation point. Schlieren photographs suggest the existence of small scale turbulence in the wake behind the turbulent body, while when transition occurs in the wake larger eddies are observed as sketched in Figure 69. In his analysis of "low altitude" wake flows, Finson suggests that the weak growth of the large scale turbulence in the near wake of the turbulent body results from a damping of turbulence production by the small eddies transported from the boundary layer over the body. Others suggest that remnants of the turbulent boundary layer serve only to mask observation of the inner wake that they surround, and the intrinsic difference lies in the significantly different Mach number profile that exists across the wake in the two cases. Orenberger has suggested that the occurrence of slow wake growth is associated with a supersonic velocity defect across the wake. He suggests that when the largest eddy structures flow supersonically relative to the surrounding inviscid wake the compression waves which are generated act to dampen the lateral motion of the eddies. Recently Bushnell, et al.[129] have conducted numerical studies which demonstrate that the interaction between an eddy and a locally supersonic flow leads to eddy breakup through bification as sketched in Figure 70. One may conjecture that a similar analysis would show that the growth of large eddy structures would be inhibited by analogous mechanisms. In investigating such effects it is clear that we are attempting to understand the effects of compressibility on turbulent structure and diffusivity. It is also clear that if such effects are manifest in free shear layer mixing then they may also be important in separated flows induced by shock/boundary interaction and in flows with transpiration cooling at hypersonic speeds. This is an area where fundamental theoretical and experimental research is urgently needed.

X. CONCLUDING REMARKS

With the renewed interest in hypersonic vehicles whose design requirements are more complex and sophisticated than the essentially ballistic systems which have been developed to date, there has come the realization that the current predictive capabilities are inadequate in a number of important areas. While there has been significant increase in computing power during the past decade, relatively little progress has been made in the understanding and modeling of the fundamental mechanisms which must be incorporated into the machine codes. During the past decade fundamental research in hypersonic flow has almost stopped, and, in addition to the absence of work to develop new hypervelocity facilities, a number of hypersonic facilities have been destroyed. It is in the area of high altitude hypervelocity flight where real gas, non-equilibrium, viscous interaction, slip and catalytic wall effects are important, that the lack of ground test facilities is the most evident. While in the short term flight tests will help in obtaining measurements in the hypervelocitiy transition regime, the development of ground test facilities in which clean reacting airflows at velocities of up to 20,000 ft/sec are generated, should receive high priority. Facilities are also required in which turbulent flows can be studied on models in airflows at Mach numbers up to 20.

In the flow regime between free molecular and continuum flow where viscous interaction, non-equilibrium, surface slip and catalysis are important, there is a real need to obtain detailed flow field measurement in addition to those which can be obtained on the surface. These measurements, taken in an environment where there is non-equilibrium chemistry, would provide important information with which to model the conditions close to the wall in modifications to the Navier/Stokes equations to describe flows at the continuum end of the transition regime. In the laminar continuum flow at the lower altitudes, where non-equilibrium air chemistry can be embodied with Navier-Stokes codes, questions associated with catalytic wall effects still remain. However, Navier-Stokes solutions to the laminar flow over the Space Shuttle incorporating both real gas and viscous interaction effects would provide important insight into the modeling of these flows with less demanding techniques.

The prediction of boundary layer transition and characteristics of transitional flows in complex interaction regions is one of the most difficult and yet important problems in the design of hypersonic vehicles. In addition to the sudden changes which can occur in the aerodynamic performance of intakes and control devices when transition occurs, the thermal loads on the leading edges of swept wings and intakes when the boundary layer becomes turbulent may be a key feature controlling the aerothermal design. As discussed in the review, the dynamic loads generated in transitional regions of shock wave/boundary layer interaction may also lead to significant design problems. The tripping of the boundary layer at the lower altitudes by surface roughness, or blowing from a transpiration cooling system, is another important phenomenon. In this case, however, there is some reason to believe that it is possible to use transition measurements from ground test facilities to predict transition in flight. When transition occurs in or near regions of shock wave/boundary layer interaction as in the flow over indented noseshapes, these flows are not only difficult to describe theoretically but also sensitive to Mach number, Reynolds number and surface blowing and roughness. The use of wind tunnel measurements made under such conditions to evaluate a prediction technique must be handled with great care.

The design of ablative- or transpiration-cooling systems for components of a hypersonic vehicle is an area where a significant research effort is needed to develop new, more accurate prediction techniques. In addition to problems associated with the inherent three-dimensional structure of the transition process on ablative heat shields, defining the roughness height and surface characteristics of an ablating surface has yet to be successfully handled. The theoretical techniques used to describe the ablation of a heat shield in the presence of blowing and roughness are at best highly simplified, and the almost complete absence of experimental measurements on the effects of combined roughness and blowing in high Reynolds number flows over highly-cooled surfaces does not help this situation. Because of the rapid thinning of the boundary layer which occurs in regions of shock wave/boundary layer interaction, the effects of surface roughness can exert a strong influence on the local heating rate in these regions. Also the momentum deficit induced at the base of a rough wall boundary layer makes such a flow separate more readily when subjected to strong adverse pressure gradients. The influence of transpiration cooling on the development of a turbulent boundary layer in a shock interaction region is another problem which could be of importance in the design of ram jets for hypersonic propulsion.

In hypersonic flows, regions of shock wave-turbulent interaction are one of the most stressing aerothermal problems as well as one of the most difficult to compute accurately. At the heart of the problems associated with theoretical description of these flows is the description of the development of the turbulence at the base of the boundary layer as separation occurs and as the boundary layer undergoes a radical thinning in a recompression process where the pressure can rise two orders of magnitude over several boundary layer thicknesses. There are questions on compressibility effects in these flows and the effects of the intrinsic flow unsteadiness of separated regions. Do the unsteady distortions of the shock waves which traverse the boundary layer in the separation and reattachment regions contribute significantly to the turbulence generated in these flows? In fact, can these flows be described within the framework of the time or mass averaged Navier-Stokes equations? Are there Mach number effects on the separated shear layer mixing similar to those which are believed to exist in free shear layer mixing and turbulent wakes? It is clear that only through carefully directed and conducted experimental studies, involving detailed mean and fluctuation measurements in the flow field as well as on the surface, can the insight and information be generated to resolve these issues.

REFERENCES

1. Lukasiewicz, J., Experimental Methods of Hypersonics, Gas Dynamics Series, Vol. 3, Marcel Dekker Pub., NY, NY, 1973.

2. Stollery, J.L., Stalker, R.J., "The Development and Use of Free Piston Wind Tunnel" Proceedings 14th Internation Symposium on Shock Tubes & Waves, August 19-22, 1983.

3. Bird, G.A., "Low Density Aerodynamics," AIAA-85-0994, June 20, 1985, Williamsburg, VA.

4. Dunn, M.G. "Reaction Rate Constants for Ionized Air" Calspan Report No. AI-2187-A-1 April 1966.

5. Lewis, C.H., "Current Status of Computational Aerothermodynamics", AIAA-86-0229.

6. Zoby, E.V., "Analysis of STS-2 Experimental Heating Rates and Transition Data," JSR, Vol. 20, No. 3, May-June 1983, pp. 232-237.

7. Vidal, R.J., and Stoddard, F., "Measurements of Non-equilibrium Effects in Air on Wedge-Flat Plate Afterbody Pressures," Cal Report No. AF-1817-A-1, May 1965.

8. Maus, J.R., Griffith, B.J., Szema, K.Y., and Best, J.T., "Hypersonic Mach Number and Real Gas Effects on Space Shuttle Orbiter Aerodynamics," Journal of Spacecraft and Rockets, Vol. 21, March-April 1984, pp. 136-141.

9. Kogan, M.N., in Annual Review of Fluid Mechanics, Annual Reviews, Inc., Palo Alto, CA, 1973.

10. Vidal, R.J., and Bartz, J.A., AIAA Journal, Vol. 7, No. 6, June 1969, pp. 1099-1109.

11. Holden, M.S. "Theoretical and Experimental Studies of the Shock Wave-Boundary Layer Interaction on Curved Compression Surfaces" Paper presented at the ARL Symposium on "Viscous Interaction Phenomena in Supersonic and Hypersonic Flow," WPAF, OH 7-8 May, 1969.

12. Howarth, L., "The Propagation of Steady Disturbances in a Supersonic Stream Bounded on One Side by a Parallel Subsonic Stream," Proc. Camb. Phi. Soc. 1947, p. 44, Part 3.

13. Lighthill, M.J., "On Boundary-Layers and Upstream Influence. Part II. Supersonic Flows Without Separation," P.R.S.A., 1953, pp. 217 and 478.

14. Oswatitsch, K. and Wieghardt, K., "Theoretical Analysis of Stationary Potential Flows and Boundary-Layers at High-Speed, German Wartime Report, 1941." Translated as N.A.C.A. TM. 1189.

15. Glick, H.S., "Modified Crocco-Lees Mixing Theory for Supersonic Separated and Reattaching Flows," J. Aero. Sci., Vol. 29, No. 10, pp. 1238-1244, October 1962.

16. Crocco, L. and Lees, L., "A Mixing Theory for the Interaction between Dissipative Flows and Nearly Isentropic Streams," J. Aero. Sci., Vol. 19, No. 10, pp. 649-676, October 1972.

17. Honda, M., "A Theoretical Investigation of the Interaction Between Shock Waves and Boundary Layers," J. Aero/Space Sci. 25, pp. 667-678, November 1958, Japan Tokyo Univ. Rep. Inst. High-Speed Mech. 8, 1957, pp. 109-130.

18. Lees, L. and Reeves, B.L., "Supersonic Separated and Reattaching Laminar Flows: I. General Theory and Application to Adiabatic Boundary Layer-Shock Wave Interactions," GALCIT Tech. Report No. 3 (October 1963).

19. Holden, M.S., "An Analytical Study of Separated Flow Induced Shock Wave-Boundary Layer Interaction," Calspan Report No. AI-1972-A-3 (December 1965).

20. Cohen, C.B. and Reshetko, E, "Similar Solutions for the Compressible Laminar Boundary Layer with Heat Transfer and Pressure Gradient," NACA Report No. 1293 (1956).

21. Carter J.E., "Numerical Solution of the Supersonic Laminar Flow Over a Two-Dimensional Compression Corner," Lecture Notes in Physics, col. 19 Springer-Verlag, New York, 1973, p. 69.

22. Hung, C.M. and MacCormack, R.W., "Numerical Solutions of Supersonic and Hypersonic Laminar Flows Over a Two-Dimensional Compression Corner," AIAA Paper 75-2, January 1975.

23. Loiziansky, L.G., "Interference of Boundary Layers, No. 249," Trans. Central Aero-Hydrodynamical Inst. (Moscow) 1936.

24. Loiziansky, L.G., Bolshakov, V.P., "On Motion of Fluid in Boundary Layer Near Line of Intersection of Two Planes," NACA TM 1308, 1951.

25. Carrier, G.F., "The Boundary Layer in a Corner," Quart. Appl. Math, V. IV, N4, Jan. 1947, pp. 367-370.

26. Cooke, J.C., Hall, M.G., "Boundary Layers in Three Dimensions," Prog. in Aeronautical Sciences, Vol. 2, A. Ferri, D. Kuckemann & L.H. Sterne (eds.), The MacMillian Co., New York, pp. 221-282, 1962.

27. Stainbeck, P.C., "An Experimental Investigation at a Mach Number of 4.95 of Flow in the Vicinity of a 90° Interior Corner Aligned with the Freestream Velocity," Feb. 1960, NASA TN D-184 231 524.

28. Stainback, P.C., "Heat Transfer Measurements at a Mach Number of 8 in the Vicinity of a 90° Interior Corner Aligned with the Free-stream Velocity," Aug. 1964, NASA TN D 2417.

29. Stainback, P.C., Weinstein, L.M., "Aerodynamic Heating in the Vicinity of Corners at Hypersonic Speeds," Nov. 1967, NASA TN-D-4130.

30. Charwat, A.F. and Redekeopp, L.G., "Supersonic Interference Flow Along the Corner of Intersecting Wedges," AIAA J., Vol. 5, No. 3, Mar. 1967.

31. Watson, R.D. and Weinstein, L.M., "A Study of Hypersonic Corner Flow Interactions," AIAA Paper 70-227, 1970.

32. Kutler, P., Shankar, V., Anderson, D.A., and Sorenson, R.L., "Internal and External Axial Corner Flows for Integrated Ram/Scramjet Nacelles, Part I," NASA SP-347, Mar. 1975.

33. Reynolds, O., "An Experimental Investigation of the Circumstances Which Determine Whether the Motion of Water Shall Be Direct or Sinuous and of the Law of Resistance in Parallel Channels," Trans. Roy. Soc. (London) A174, 1883, pp. 935-982, Sci. Papers 2:51.

34. Schlichting, H., Boundary Layer Theory, 6th edition.

35. Mack, L.M., "Transition Prediction and Linear Stability Theory," in AGARD Conference Proceeding No. 224, "Laminar-Turbulent Transition," May 1977.

36. Stetson, K.F., "Laminar Boundary Layer Stability Experiments on a Cone at Mach 8, Part 3: Sharp Cone at Angle of Attack," AIAA Paper AIAA-85-492, January 14-17, Reno, NV.

37. Pate, S.R. and Schueler, C.J., "An Investigation of Radiated Aerodynamic Noise Effects on Boundary-Layer Transition in Supersonic and Hypersonic Wind Tunnels," AIAA Paper No. 68-375, April 1968.

38. Stainbeck, P.C., Fischer, M.C. and Wagner, R.D., "Effects of Wind-Tunnel Disturbances on Hypersonic Boundary Layer Transition," AIAA 10th Aerospace Sciences Meeting, San Diego, California, 17-19 January 1972.

39. Reda, D.C., "Boundary-Layer Transition Experiments on Sharp, Slender Cones in Supersonic Freeflight," AIAA Paper 78-1129, July 1978.

40. Potter, J.L., "Boundary-Layer Transition on Supersonic Cones in an Aeroballistic Range," AIAA Journal, Vol. 13, No. 3, March 1975.

41. Sheetz, N.W., Jr., "Free-Flight Boundary Layer Transition Investigations at Hypersonic Speeds," AIAA Paper No. 65-127, 2nd Aerospace Sciences Meeting, New York, N.Y., Jan. 1965.

42. Norkovin, M.V., "Instability, Transition to Turbulence and Predictability," Keynote Address to AGARD Symposium on Laminar-Turbulent Transition, Technical University of Denmark, Copenhagen, Denmark, 2-4 May 1977.

43. Reshotko, E., "Boundary-Layer Stability and Transition," Annual Review of Fluid Mechanics, Vol. 8, 1976, pp. 311-349.

44. Poll, D.I.A., "Boundary Layer Transition on the Windward Face of Space Shuttle During Re-Entry," AIAA 20th Thermophysics Conference, June 19-21, Williamsburg, VA, AIAA-85-0899.

45. Morkovin, M.V., "Instability Transition to Turbulence and Predictability," AGARDograph-236, July 1978.

46. Poll, D.I.A., Transition in the infinite swept attachment line boundary layer," The Aeronautical Quarterly, Vol. XXX, November 1979, pp. 607-629.

47. Stetson, K.F., "Nosetip Bluntness Effects on Cone Frustum Boundary Layer Transition in Hypersonic Flow," AIAA-83-1763, July 12-14, 1983, Danvers, MA.

48. Dirling Jr., R.B., "Asymmetric Nosetip Shape Change During Atmospheric Entry," AIAA Paper 77-779, 12th Thermophysics Conference, Albuquerque, NM, June 1977.

49. Finson, M.L., "An Analysis of Nosetip Boundary Layer Transition Data," AFOSR-TR-76-1106, August 1976.

50. Bishop, W.M., "Transition Induced by Distributed Roughness on Blunt Bodies in Supersonic Flow," AIAA Paper 77-124, 15th Aerospace Sciences Meeting, Los Angeles, California, January 1977.

51. Reda, D.C., Correlation of Nosetip Boundary-Layer Transition Data Measured in Ballistics-Range Experiments," AIAA Paper 80-0286 (AIAA Journal) Vol. 19, No. 3, March 1981, pp. 329-339).

52. Wassel, A.T., Shih, W.C.L., and Courtney, J.F., "Roughness-Induced Transition and Heat-Transfer Augmentation in Hypersonic Environment," AIAA Paper 84-0631, March 1984.

53. Batt, R.G., and Legner, H.H., "A Review of Roughness-Induced Nosetip Transition," AIAA Paper 81-1233, June 1981 (AIAA Journal Vol. 21, No. 1, Jan. 1983, pp. 7-22).

54. Poll, D.I.A., "The development of intermittent turbulence on a swept attachment-line including the effects of compressibility," The Aeronautical Quarterly, Vol. XXXIV, February 1983, pp. 1-23.

55. Welsh, W.E. "Shape and Surface Roughness Effects on Turbulent Nose Tip Ablation" AIAA Journal Vol. 8 No. 11 November 1970, pp. 1983-1989.

56. Abott, M.J., et al., "Unsteady Flow on Ablated Nosetip Shapes--PANT Series G Test and Analysis Report" Aerotherm Report 73-87, Project 7040, December 1973.

57. Holden, M.S., "Studies of the Effects of Transitional and Turbulent Boundary Layers on the Aerodynamic Perfomrance of Hypersonic Re-Entry Vehicles in High Reynolds Number Flow" Calspan Report No. AB-5834-A-2.

58. Holden, M.S., "Studies of Transitional Flow, Unsteady Separation Phenomena and Particle Induced Augmentation Heating on Ablated Nose Tips" AFOSR TR 76-1066, October 1975.

59. English, E.A., "Nosetip Recovery Vehicle Postflight Development Report" SAND75-8059, Sandia Laboratories, Livermore, CA, January 1976.

60. Voisinet, R.L.P., "Influence of Roughness and Blowing on Compressible Turbulent Boundary Layer Flow," Naval Surface Weapons Center, NSWC TR-79-153, June 1979.

61. Holden, M.S., "Studies of Surface Roughness Effects in Hypersonic Flow," Final Report, AFOSR, F49620-82-C-0026, October 1983.

62. Nikuradse, J., "Stromungsgeretze en rauken Rohren," VDI Forshuhngsheft No. 361, 1933, Translated as NACA TM 1292, 1950.

63. Schlichting, H., "Boundary Layer Theory," 4th Edition, McGraw Hill Book Co., New York, 1960.

64. Dvorak, F.A., "Calculation of Turbulent Boundary Layers with Roughness and Heat Transfer," AIAA Journal, 10, pp. 1447-1451, 1969.

65. Betterman, D., "Contribution a L'etude de la Couche Limite Turbulente le Long Plagnes Rugueuses," Rapport 65-5, Centre National de la Recherche Scientifique, Paris, France, 1965.

66. Lewis, M.J., "An Elementary Analysis for Predicting the Momentum - and Heat-Transfer Characteristics of a Hydraulically Rough Surface," J. Heat Transfer, 97, pp. 249-254, 1975.

67. Simpson, R.L., "A Generalized Correlation of Roughness Density Effects on the Turbulent Boundary Layer," AIAA Journal, Vol. 11, No. 2, pp. 242-244, 1973.

68. Lin, T.C. and Bywater, R.J., "The Evaluation of Selected Turbulence Models for High-Speed Rough-Wall Boundary Layer Calculations" AIAA Paper-80-0132, Pasadena, CA, 1980.

69. Finson, M.L. and Wu, P.K.S., "Analysis of Roughwall Turbulent Heating with Application to Blunted Flight Vehicles," AIAA Paper No. 79-0008, 17th Aerospace Sciences Meeting, 1979.

70. Goddard, F.E., Jr., "Effect of Uniformly Distributed Roughness on Turbulent Skin-Friction Drag at Supersonic Speeds," Journal of Aerospace Sciences, 26, pp. 1-15, 1959.

71. Dirling, R.B., Jr., "A Method for Computing Rough Wall Heat Transfer Rates on Reentry Nosetips," MDAC Paper WD 1778, AIAA 8th Thermophysics Conference, Palm Springs, 1973.

72. Reda, D.C., "Compressible Turbulent Skin Friction on Rough and Rough/Wavy Walls in Adiabatic Flow," Naval Ordnance Laboratory, Report No. NOLTR 74-34, Silver Spring, MD, 1974.

73. Lin, T.C. and Bywater, R.J., "The Evaluation of Selected Turbulence Models for High-Speed and Rough-Wall Boundary Layer Calculations" AIAA Paper-80-0132, Pasadena, CA, 1980.

74. Holden, M.S., "Shock Wave-Turbulent Boundary Layer Interaction in Hypersonic Flow," AIAA 10th Aerospace Sciences Meeting, San Diego, California, 17-19 January 1972, AIAA-72-74.

75. Holden, M.S., "Shock Wave-Turbulent Boundary Layer Interaction in Hypersonic Flow," AIAA 77-45.

76. Bogdonoff, S.M. and Kepler, C.E., "Separation of a Supersonic Turbulent Boundary Layer," J. Aero. Sci., 22, pp. 414-424 (1955).

77. Gadd, G.E., "Interactions Between Wholly Laminar or Wholly Turbulent Boundary Layers and Shock Waves Enough to Cause Separation," J. Aeronautical Sciences, Vol. 20, pp. 729-739, November 1953.

78. Green, J.E., "Interactions Between Shock Waves and Turbulent Boundary Layers," Progress in Aerospace Sciences, Vol. 11, pp. 235-340, Pergamon Press, Oxford, 1970.

79. Roshko, A. and Thomke, G. J., "Flare-Induced Separation Lengths in Supersonic, Turbulent Boundary Layers," AIAA Aerospace Sciences Meeting, Paper No. 75-6, 1975.

80. Law, C.H., "Supersonic Turbulent Boundary Layer Separation Measurements at Reynolds Numbers of 10107 and 108", AIAA Journal, Vol. 12, No. 6, June 1974, pp. 794-797.

81. Settles, G.S., Bogdonoff, S.M., and Vas, I.E., "Incipient Separation of a Supersonic Turbulent Boundary Layer at Moderate to High Reynolds Numbers," AIAA Paper 75-7, 1975.

82. Appels, C., "Incipient Separation of a Compressible Turbulent Boundary Layer," von Karman Institute Technical, Note 99, April 1974.

83. Chapman, D.R., Kuehn, D.M., and Larson, H.G., "The Investigation of Separated Flows in Supersonic and Subsonic Streams with Emphasis on the Effects of Transition," NACA Report No. 1356, 1958.

84. Kuehn, D.M., "Experimental Investigation of the Pressure Rise Required for the Incipient Separation of Turbulent Boundary Layers in Two-Dimensional Supersonic Flow," NASA Memo 1-21-59A, Feb. 1959.

85. Elfstrom, G.M., Coleman, G.T., and Stollery, J.L., "Turbulent Boundary Layer Studies in a Hypersonic Gun Tunnel," 8th Annual International Shock Tube Symposium, London, England, Jul. 1971.

86. Appels, C. and Richards, B.E., "Incipient Separation of a Compressible Turbulent Boundary Layer," AGARD Conference Pre-Print No. 168 on Flow Separation.

87. Spaid, F. W. and Frishett, J.C., "Incipient Separation of a Supersonic Turbulent Boundary Layer Including the Effects of Heat Transfer", AIAA Paper, 1971.

88. Knight, D.D., "Problems in Reconciling Computation and Experiment" 1985 Princeton University Workshop on the Structure of High-Speed Turbulent Boundary Layers.

89. Knight, D., Horstman, C.C., Shapey, B., and Bogdonoff, S., "The Flowfield Structure of the 3-D Shock Wave Boundary Layer Interaction Generated by a 20 degree Sharp Fin at Mach 3" AIAA-86-343.

90. Shang, J.S., Hankey, W.L., and Petty, J.S., "Three-Dimensional Supersonic Interacting Turbulent Flow Along a Corner," AIAA Paper 78-1210, July 1978; also AIAA Journal, Vol. 17, No. 7, July 1979, pp. 706-713.

91. Horstmann, C.C. and Hung, C.M., "Computations of Three-Dimensional Turbulent Separated Flows at Supersonic Speeds," AIAA Paper 79-2, January 1979.

92. Settles, G.S. and Horstmann, C.C., "Flowfield Scaling of a Swept Compression Corner Interaction--A Comparison of Experiment and Computation," AIAA-84-0096, 22nd Aerospace Sciences Meeting, January 9-12, 1984.

93. Holden, M.S., "Experimental Studies of Quasi-Two-Dimensional and Three-Dimensional Viscous Interaction Regions Induced by Skewed-Shock and Swept-Shock Boundary Layer Interaction" Paper presented at the AIAA 19th Thermophysics Conference Snowmass, Colorado 25-27 June 1984, AIAA Paper AIAA-84-1677.

94. Stalker, R.J., "The Pressure Rise at Shock-Induced Turbulent Boundary Layer Separation in Three-Dimensional Supersonic Flow," J. Aeronautical Science, Vol. 24, No. 7, July 1957, pp. 547.

95. Stanbrook, A., "An Experimental Study of the Glancing Interaction Between a Shock Wave and a Turbulent Boundary Layer," ARC CP 555, 1961.

96. McCabe, A., "The Three-Dimensional Interaction of a Shock Wave with a Turbulent Boundary Layer," Aeronautical Quarterly, Vol. XVII, August 1966, pp. 231-252.

97. Peake, D.J. and Rainbird, W.J., "The Three-Dimensional Separation of a Turbulent Boundary Layer by a Skewed Shock Wave and Its Control by the Use of Tangential Air Injection," AGARD CP-168, May 1975.

98. Oskam, B., Vas, I.E., and Bogdonoff, S.M., "Oblique Shock Wave/Turbulent Boundary Layer Interactions in Three-Dimensions at Mach 3, Part I," AFFDL-TR-76-48, June 1976.

99. Cousteix, J.A. and Houdeville, R., "Epaissement et Separation d'une Couche Limite Turbulente Soumise en Interaction avec un Choc Oblique," La Recherche Aerospatiale, No. 1, Jan./Feb. 1976, pp. 1-11.

100. Dolling, D.S. and Bogdonoff, S.M., "An Experimental Investigation of the Unsteady Behavior of Blunt Fin-Induced Shock Wave Turbulent Boundary Layer Interactions," AIAA-81-1287, 14th Fluid and Plasma Dynamics Conference, June 23-25, 1981.

101. Dolling, D.S. and Bogdonoff, S.M., "Upstream Influence Scaling of Sharp Fin-Induced Shock Wave Turbulent Boundary Layer Interactions," AIAA Paper 81-0336, AIAA 19th Aerospace Sciences Meeting, January 1981.

102. Dolling D.S. and Murphy, M., "Wall Pressure Fluctuations in a Supersonic Separated Compression Ramp Flowfield," AIAA-82-0986, AIAA/ASME 3rd Joint Thermophysics, Fluids, Plasma and Heat Transfer Conference, June 7-11, 1982.

103. Dolling, D.S., "Effects of Mach Number in Sharp Fin-Induced Shock Wave Turbulent Boundary Layer Interaction," AIAA-84-0095, 22nd Aerospace Sciences Meeting, Jan. 9-12, 1984.

104. Korkegi, R.H., "A Simple Correlation for Incipient Turbulent Boundary-Layer Separation Due to a Skewed Shock Wave," AIAA Journal, Vol. 11, No. 11, November 1973, pp. 1578-1579.

105. Goldberg, T.J., "Three-dimensional Separation for Interaction of Shock Waves with Turbulent Boundary Layers," AIAA Journal, Vol. 11, No. 11, November 1973, pp. 1573-1575.

106. Holden, M.S. "Experimental Studies of Quasi-Two-Dimensional and Three-Dimensional Viscous Interaction Regions Induced by Skewed-Shock and Swept-Shock Boundary Layer Interaction" Paper presented at the AIAA 19th Thermophysics Conference Snowmass, Colorado 25-27 June 1984, AIAA Paper AIAA-84-1677.

107. Newmann, R.D. and Burke, G., "The Influence of Shock Wave-Boundary Layer Effects on the Design of Hypersonic Aircraft," AFFDL-TR-68-152, USAF Flight Dynamics Laboratory, 1968.

108. Law, H.C., "Three-Dimensional Shock Wave Turbulent Boundary Layer Interactions at Mach 6," ARL TR-75-0191, June 1975.

109. Token, K.H., "Heat Transfer Due to Shock Wave Turbulent Boundary Layer Interactions on High-Speed Weapon Systems," AFFDL-TR-74-77, April 1974.

110. Scuderi, L.F., "Expressions for Predicting 3D Shock Wave-Turbulent Boundary Layer Interaction Pressures and Heating Rates," AIAA Paper 78-162, January 1978.

111. Holden, M.S. "Experimental Studies of Quasi-Two-Dimensional and Three-Dimensional Viscous Interaction Regions Induced by Skewed-Shock and Swept-Shock Boundary Layer Interactions" Calspan Report No. 7018-A-2 Report Covering Period 15 January 1982 - 31 July 1984 July 1984.

112. Hung, C.M., and MacCormack, R.W., "Numerical Solutions of Supersonic and Hypersonic Laminar Flows Over a Two-Dimensional Compression Corner," AIAA Paper 75-2, January, 1975.

113. Reshotko, E., and Tucker, M., "Effect of a Discontinuity on Turbulent Boundary Layer Thickness Parameters with Application to Shock Induced Separation," NACA TN3454, 1955.

114. Ericsson, L.E., Reding, J.P., and Guenther, R.A., "Effects of Shock-Induced Separation," Lockheed Missiles and Space Co., Sunnyvale, CA, L-87-69-1, July 1969.

115. Settles, G.S., and Perkins, J.J., "Upsteam Influence Scaling of 2D & 3D Shock/Turbulent Boundary Layer Interactions at Compression Corners," AIAA-81-0334, 19th Aerospace Sciences Meeting, Janaury 12-15, 1981.

116. Settles, G.S. and Teng, H.Y., "Flow Visualization of Separated 3D Shock Wave/Turbulent Boundary Layer Interactions," AIAA-82-0229, 20th Aerospace Sciences Meeting, January 11-14, 1982.

117. Edney, B.E., "Anomalous Heat Transfer and Pressure Distributions on Blunt Bodies in the Presence of an Impinging Shock," The Aeronautical Research Institute of Sweden, FAA-115 Report, February 1968.

118. Hiers, R.S. and Loubsky, W.J., "Effects of Shock-Wave Impingement on the Heat Transfer on a Cylindrical Leading Edge," NASA TN D-3859, Feb. 1967.

119. Gulbran, C.E., Redeker, E., Miller, D.S., and Strack, S.L., "Heating in Regions of Interfering Flow Fields," Part II, "Leading-Edge Shock Impingement," AFFDLM TR 65-49, Jan. 1967.

120. Hains, F.D., and Keyes, J.W., "Shock Interference Heating in Hypersonic Flows," AIAA Journal, Vol. 10, No. 11, pp. 1441-1447, Nov. 1972.

121. Keyes, J.W., and Morris, D.J., "Correlations of Peak Heating in Shock Interference Regions at Hypersonic Speeds," Journal of Spacecraft & Rockets, Vol. 9, No. 8, pp. 621-623, Aug. 1972.

122. Birch, S.F., and Keyes, J.W., "Transition in Compressible Free Shear Layers, Journal Spacecraft & Rockets, Vol. 9, No. 8, pp. 623-624, Aug. 1972.

123. Birch, S.F. and Eggers, J.M. "A Critical Review of the Experimental Data for Fully-Developed Free Shear Layer," NASA-SP-45.

124. Finson, M.L. "Hypersonic Wake Aerodynamics at High Reynold Numbers," AIAA Journal Vol. II No. 8, August 1973.

125. Orenberger, J., "Turbulent Near Wake Modeling Analysis For Reentry Application" BMD Report 29764-6002-RU-00, April 1977.

126. Legner, H.H., Finson, M.L. "On the stability of fine-scaled turbulent free shear flow," JFM (1980) Vol. 100 Part 2, pp. 303-319.

127. Padova, C. and Dunn, M.G. "Weak Shock Propagation into a Cross-Junction Against a Jet" Paper presented at the 14th International Symposium on Shock Tubes and Waves, Sydney, Australia 15-18 August 1983.

128. Maydew, R.C.; and Reed, J.F. "Turbulent Mixing of Axisymmetric Compressible Jets (in the Half-Jet Region) With Quiescent Air," Sandia Corp., Research Report SC-4764, March 1963.

129. Hussaini, M.Y., Collier, F., Bushnell, D.M., "Turbulence Alteration Due to Shock Motion," IUTAM Symposium on Shock Wave/Boundary Layer Interaction, Sept. 1985, Paris, France.

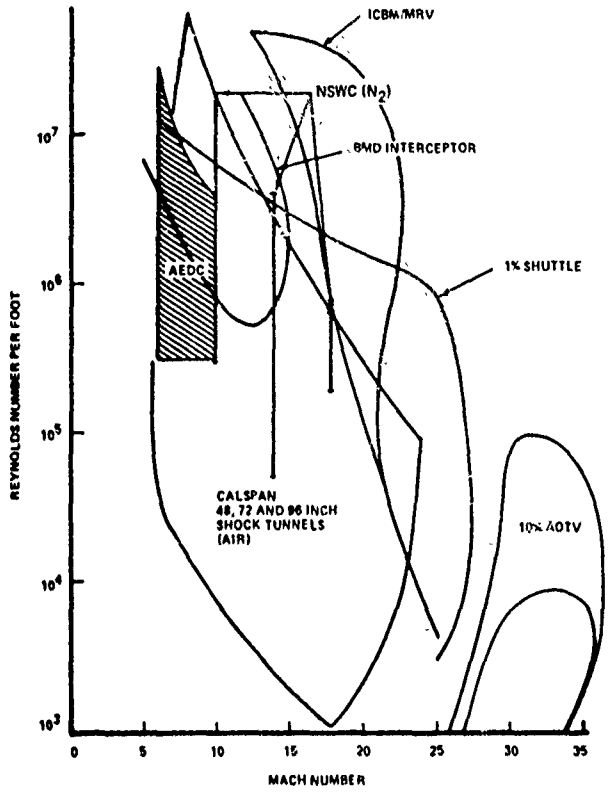

Figure 1 Performance Map of Current Hypersonic Facilities

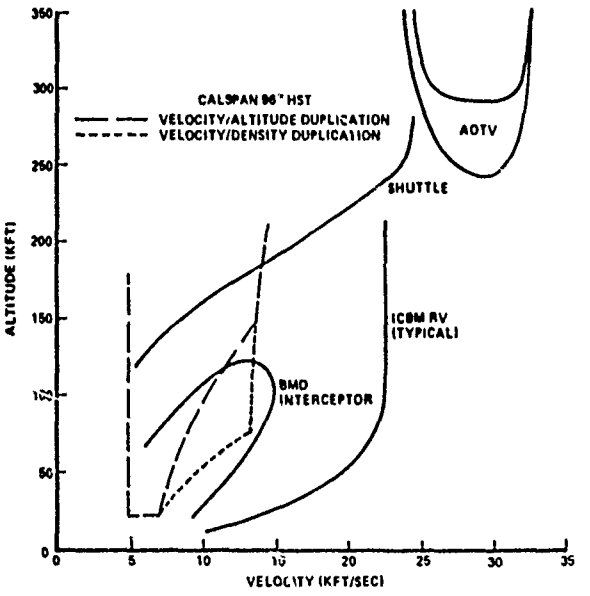

Figure 2 Velocity-Altitude Comparison of Flight Vehicles With Shock Tunnel Capability

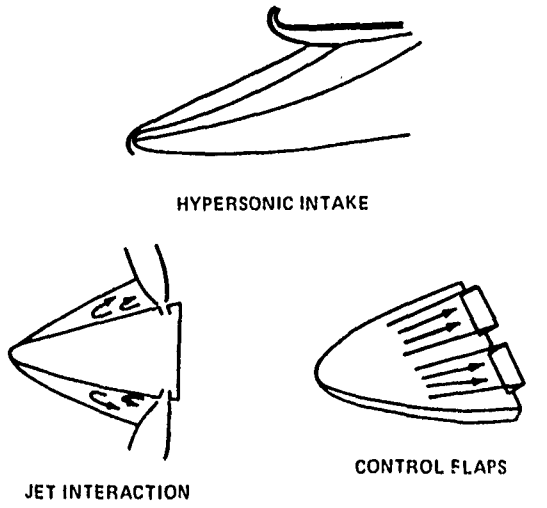

Figure 3 Problems Resulted From Laminar Viscous/Inviscid Interaction

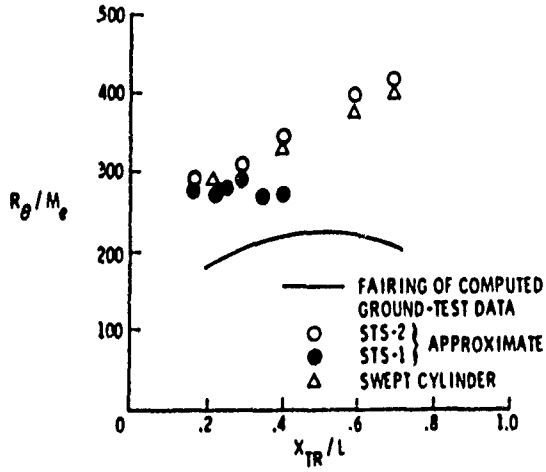

Figure 4 Comparison of Transition Criterion At Shuttle Flight and Ground-Test Conditions (Ref. 6)

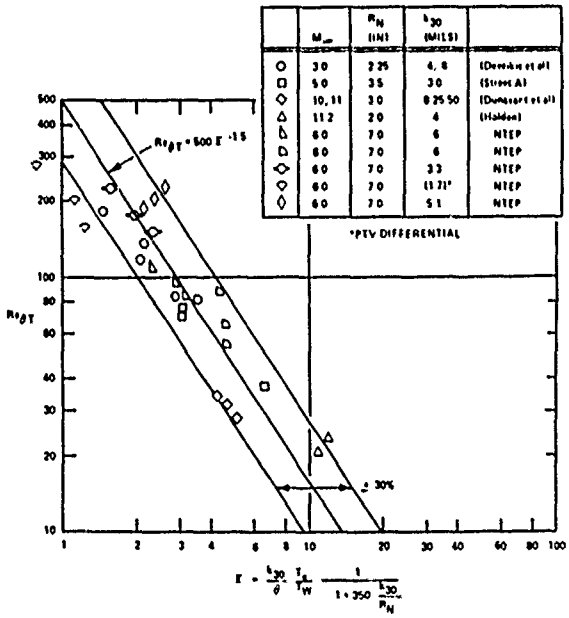

Figure 5 Batt's Transition Correlation (BMD-TR-81-58) (Ref. 53)

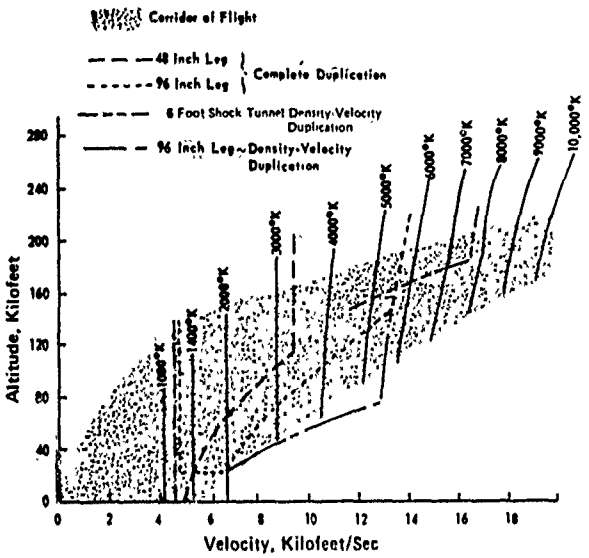

Figure 6 Performance Range of Calspan Hypersonic Shock Tunnel

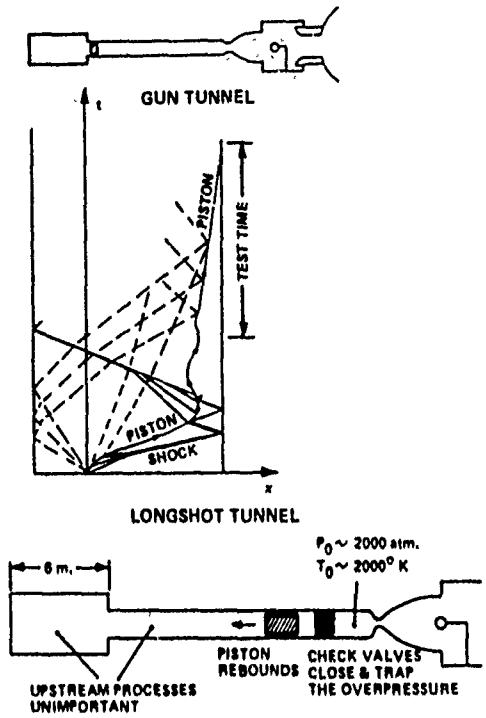

Figure 8 Gun Tunnel and Operating Cycle

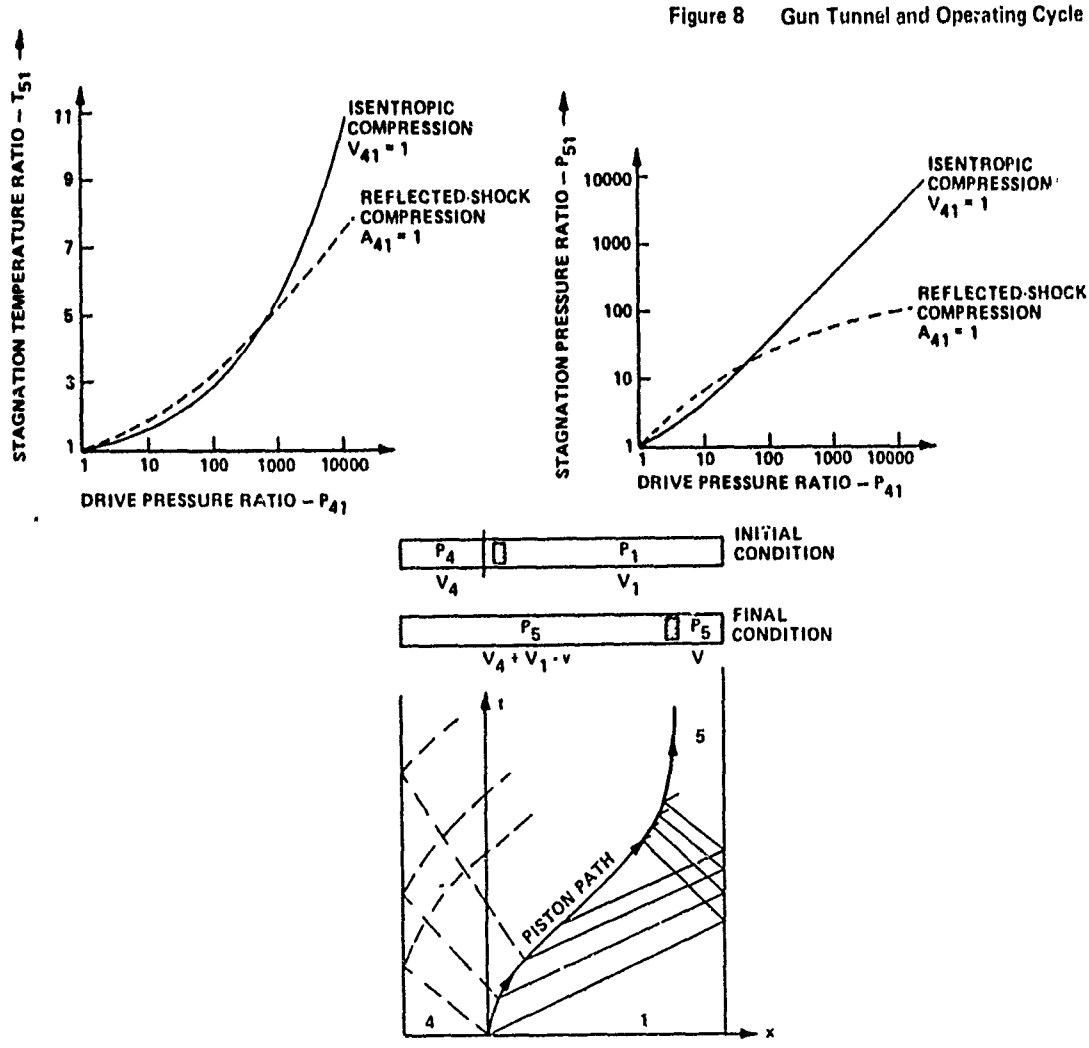

Figure 7 Isentropic Compression Tube (Ref. 2)

	PLACE	P_o ATM	T_o °K	M_∞	Re_d MILLIONS	NOZZLE DIA. D CMS	TEST TIME MS
SHOCK TUNNEL	CALSPAN/US	1300	8000	6.5 TO 20	0.02 TO 250	120	20 TO 0.7
STALKER TUBE	AUS	1000	8599	8	4	25	0.2
LONGSHOT	VK1/BEL	400	2400	15 TO 20	3 TO 1.5	15	40
GUN TUNNEL	IC/UK	130	1000	9.3	25	45	5

Figure 9 Comparison of Performance of Shock Tunnels and Free Piston Facilities

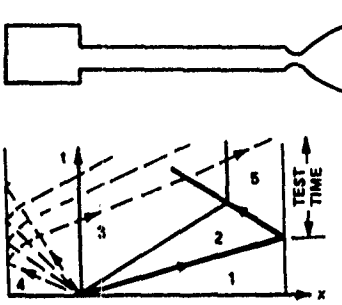

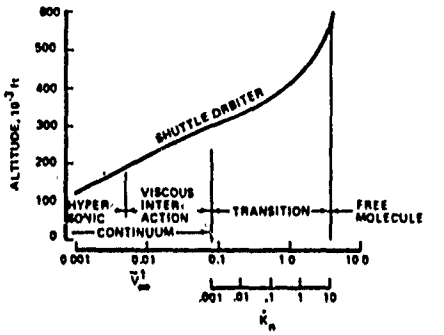

FREE PISTON SHOCK TUNNEL

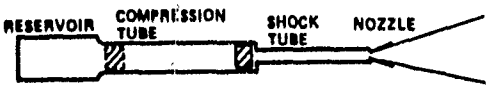

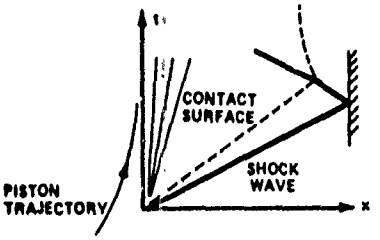

Figure 10 Shock Tunnel

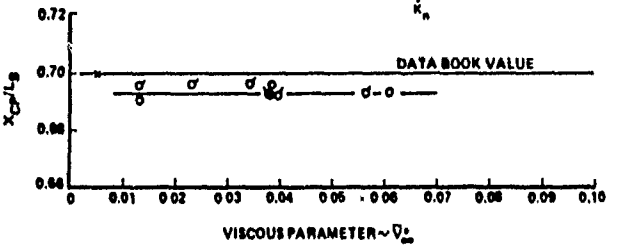

Figure 12 Comparison of Space Shuttle Orbiter Data From Calspan Hypersonic Shock Tunnel

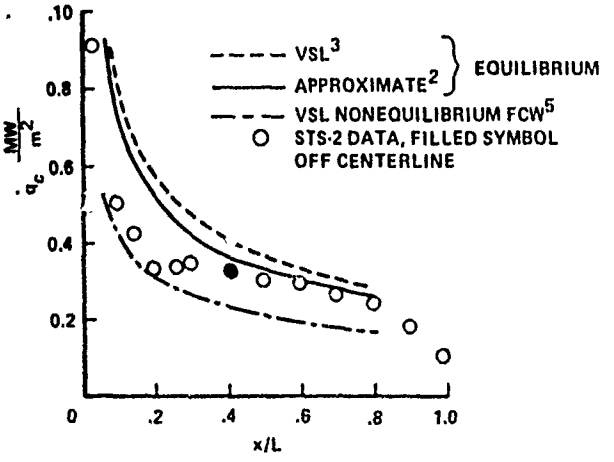

Figure 11 Comparison of Measured and Predicted Heating Rates for STS-2: (Zoby JSR Vol. 20 No. 3)

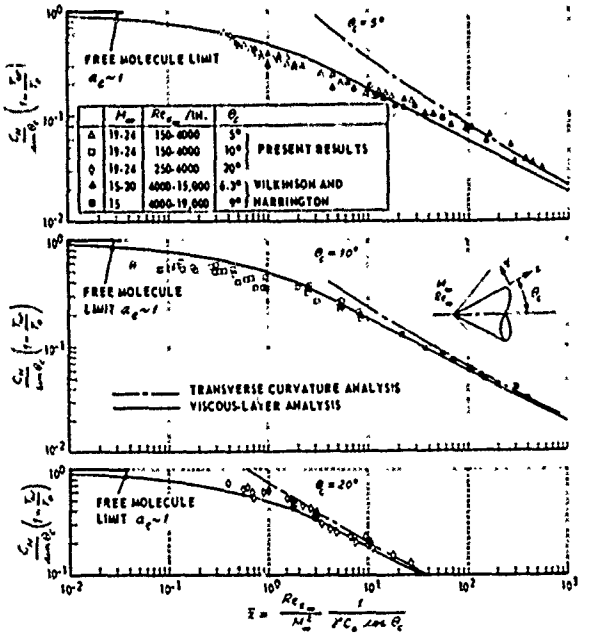

Figure 13 Comparison of Cone Heat Transfer with Viscous Layer Analysis (Waldron ARL66-0111)

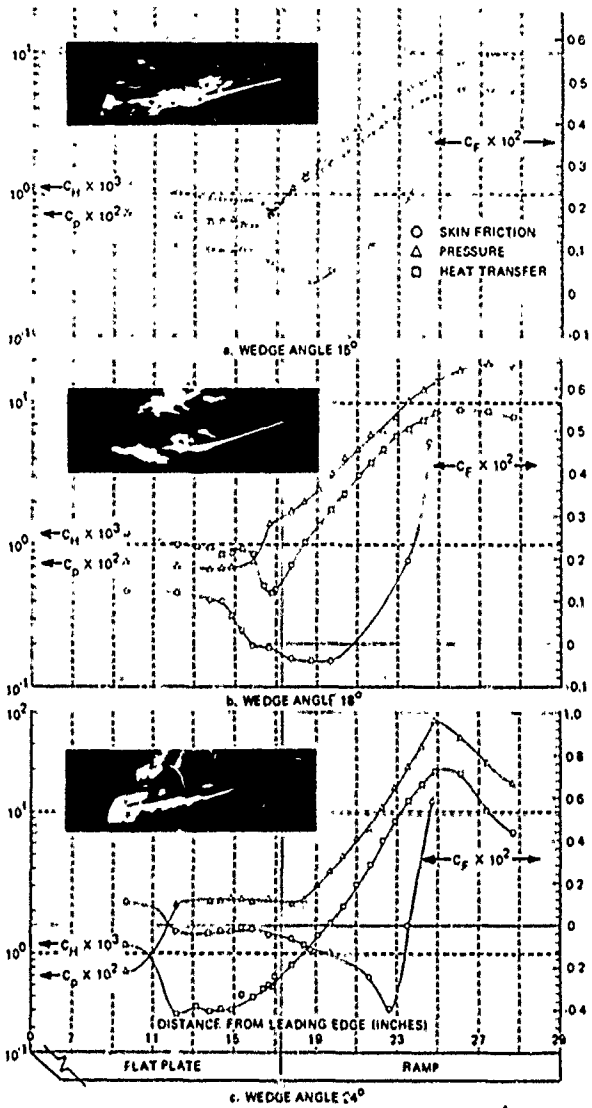

a) Sharp Leading Edge (M_∞ = 14.1, Re/FT = 7.2 x 10^4)

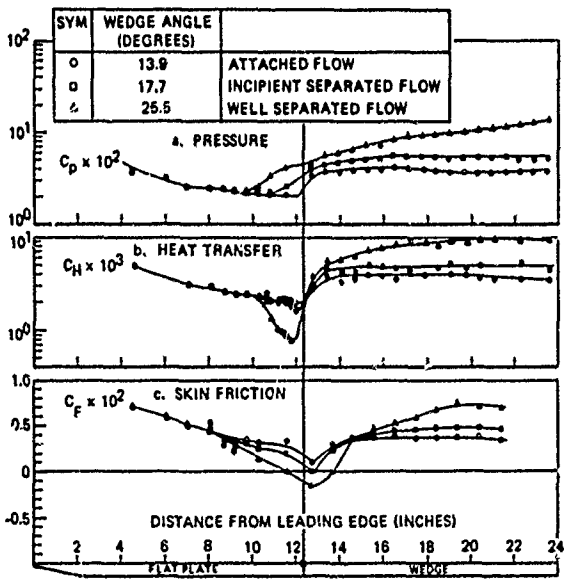

b) 0.71" Blunt Leading Edge (M_∞ = 19.8, Re/IN = 8.7 x 10^3)

Figure 14 Skin Friction, Heat Transfer, and Pressure Distributions on the Flat Plate-Wedge Models

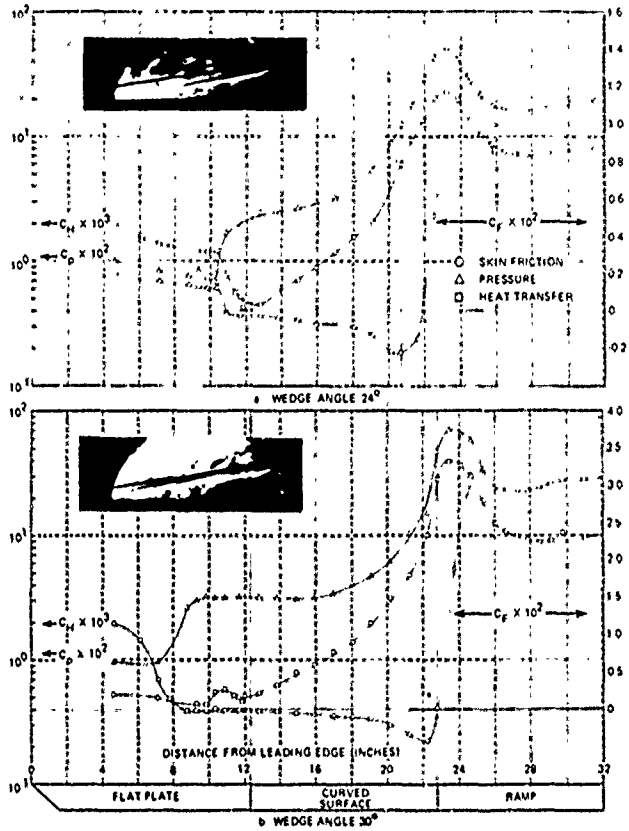

Figure 15 Skin Friction, Heat Transfer and Pressure Distributions on the Flat Plate - 20"R Cylindrical Arc-Wedge Models (Ref. 11)
(M_∞ = 14.0, Re/FT = 7.2 x 10^4)

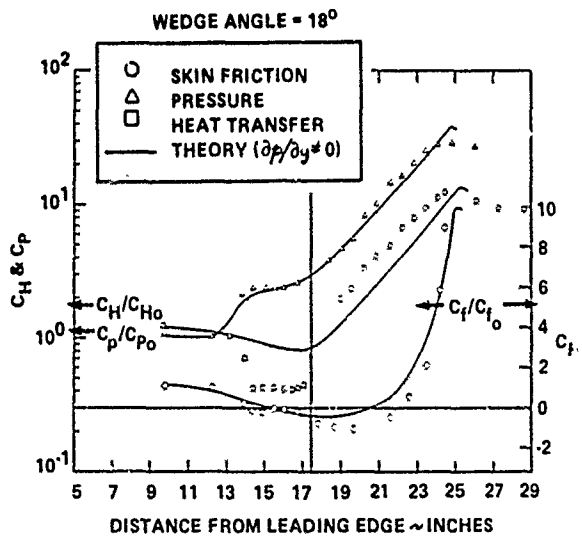

Figure 16 Comparison Between the Integral Solution and Experimental Measurements in a Well Separated Wedge-Induced Interaction Region (Ref. 11)

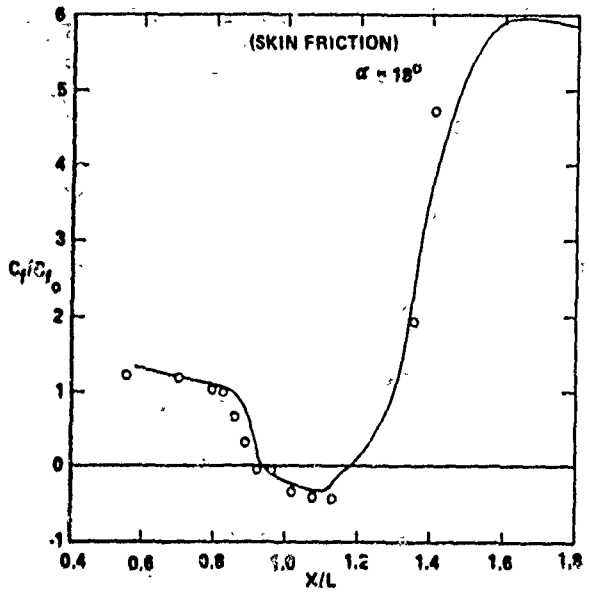

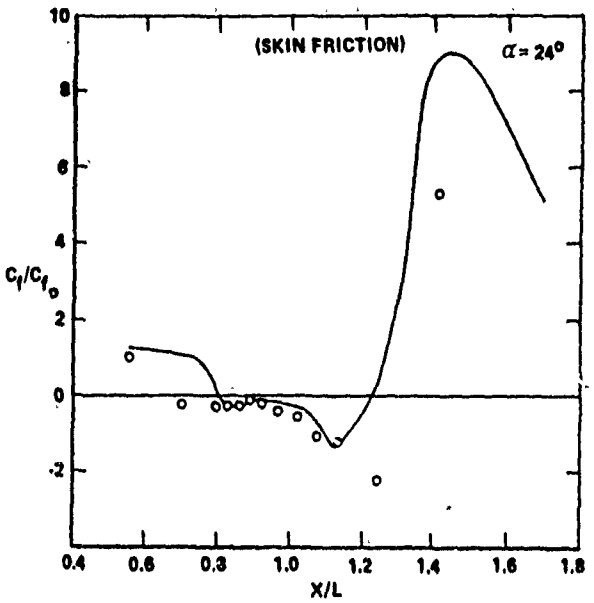

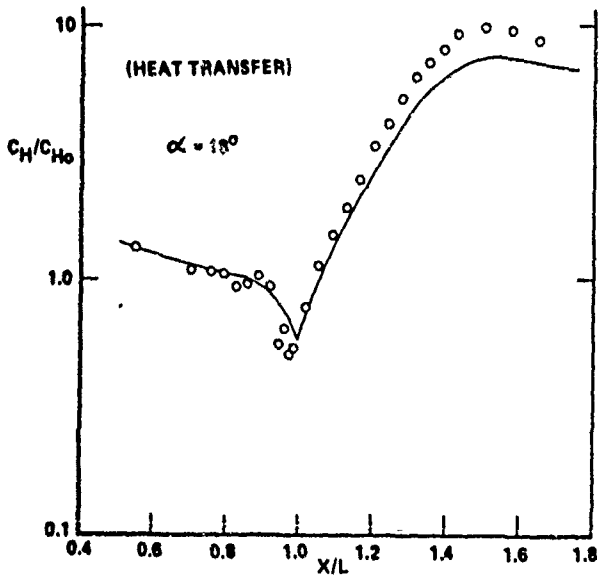

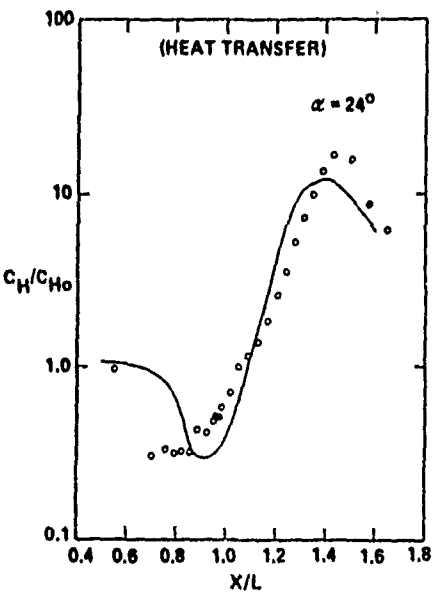

Figure 17(a) Comparison Between Experimental and Navier Stokes Solution for a Mildly Separated Flow (Ref. 11)

Figure 17(b) Comparison Between Experimental Measurements and Navier Stokes Solution for a Well Separated Flow (Ref. 11)

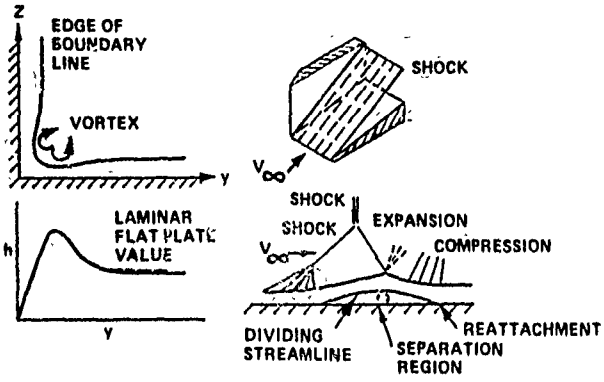

Figure 18 Typical Flow and Heat Transfer Laminar Corner Flows

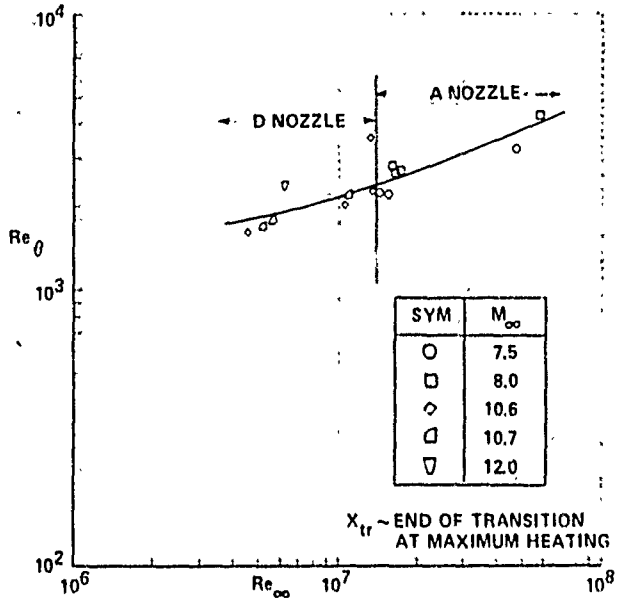

Figure 21 Correlation of Transition on Slender Cones Showing Effects of Tunnel Size

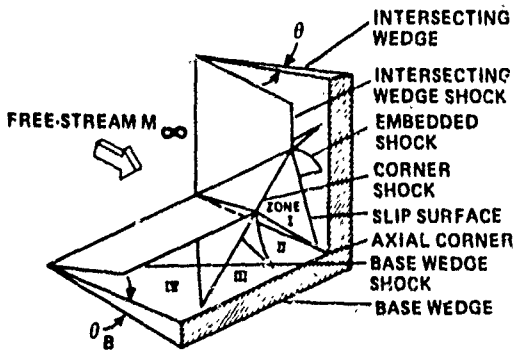

Figure 19 Schematic Representative of Model With Cross-Flow in Swept-Shock Laminar Boundary-Layer Interaction

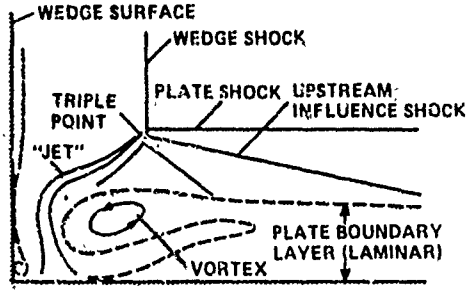

Figure 20 Shock-Wave Structure in Axial Corner Comprised of Two Intersecting Wedges

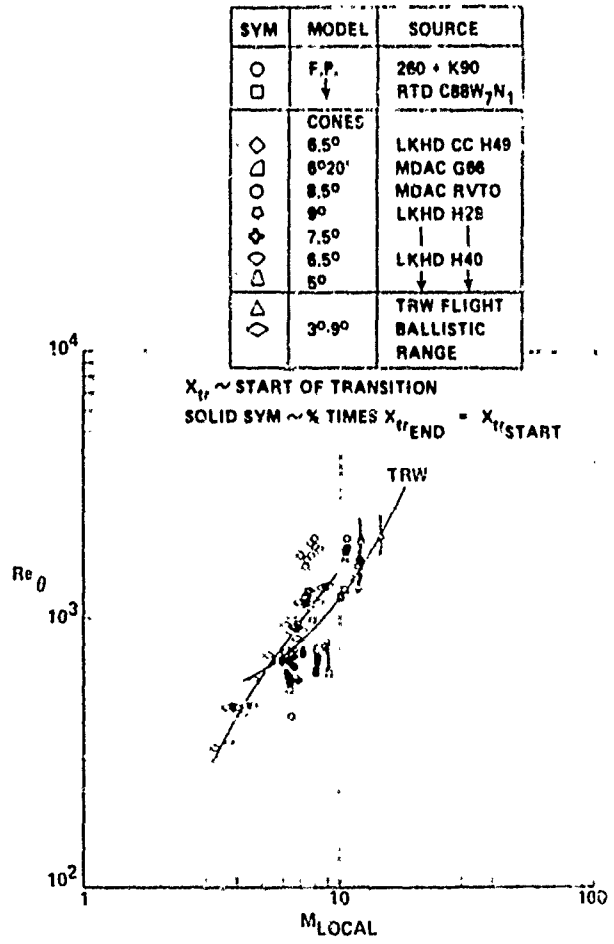

Figure 22 Correlation of Transition Measurements in Calspan Shock Tunnels with Ballistic and Downrange Measurements (Ref. 57)

SOURCE	SYM.	θ_c	M_∞	M_e	$(T_w/T_{ow})_o$	U_e^2/ν_e 1/SEC	FACILITY
REDA	○	5°	4.4	4.2	.22	$.28 - 1.66 \times 10^{11}$	RANGE
POTTER	— —	10°	5.0	4.3	.19	$.42 - 5.27 \times 10^{11}$	RANGE
	— —	10°	2.3	2.1	.52	$.17 - 1.00 \times 10^{11}$	RANGE
SHEETZ	□	5°	5.0	4.8	.19	$1.40 - 1.71 \times 10^{11}$	RANGE
PRESENT STUDY	▲	6°	13.2	10.2 – 10.5	.14	$.34 \times 10^{11}$	SHOCK TUNNEL

PRESENT RESULTS ARE PRIMARY-RAY DATA ($\theta < 46°$)
CORRECTED FOR $\theta > 0°$, $\alpha > 0°$, AFTER POTTER
—— LEAST-SQUARES FIT OF PRIMARY-RAY DATA, $\left(\frac{U_e}{\nu_e}\right) > 10^6$/IN.

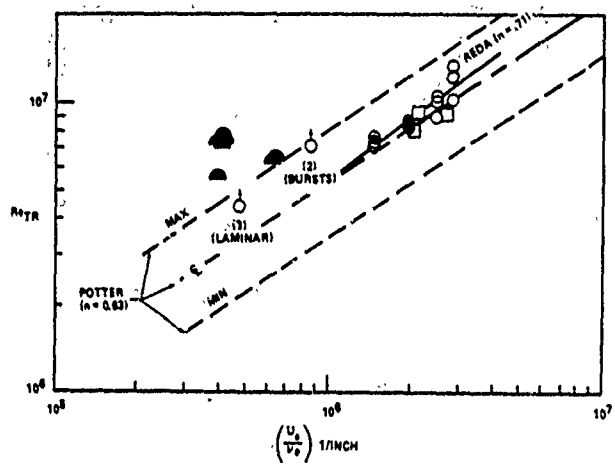

Figure 23 Transition Reynolds Number vs. Unit Reynolds Number; Present Data vs. Potter and Sheetz (Ref. 57)

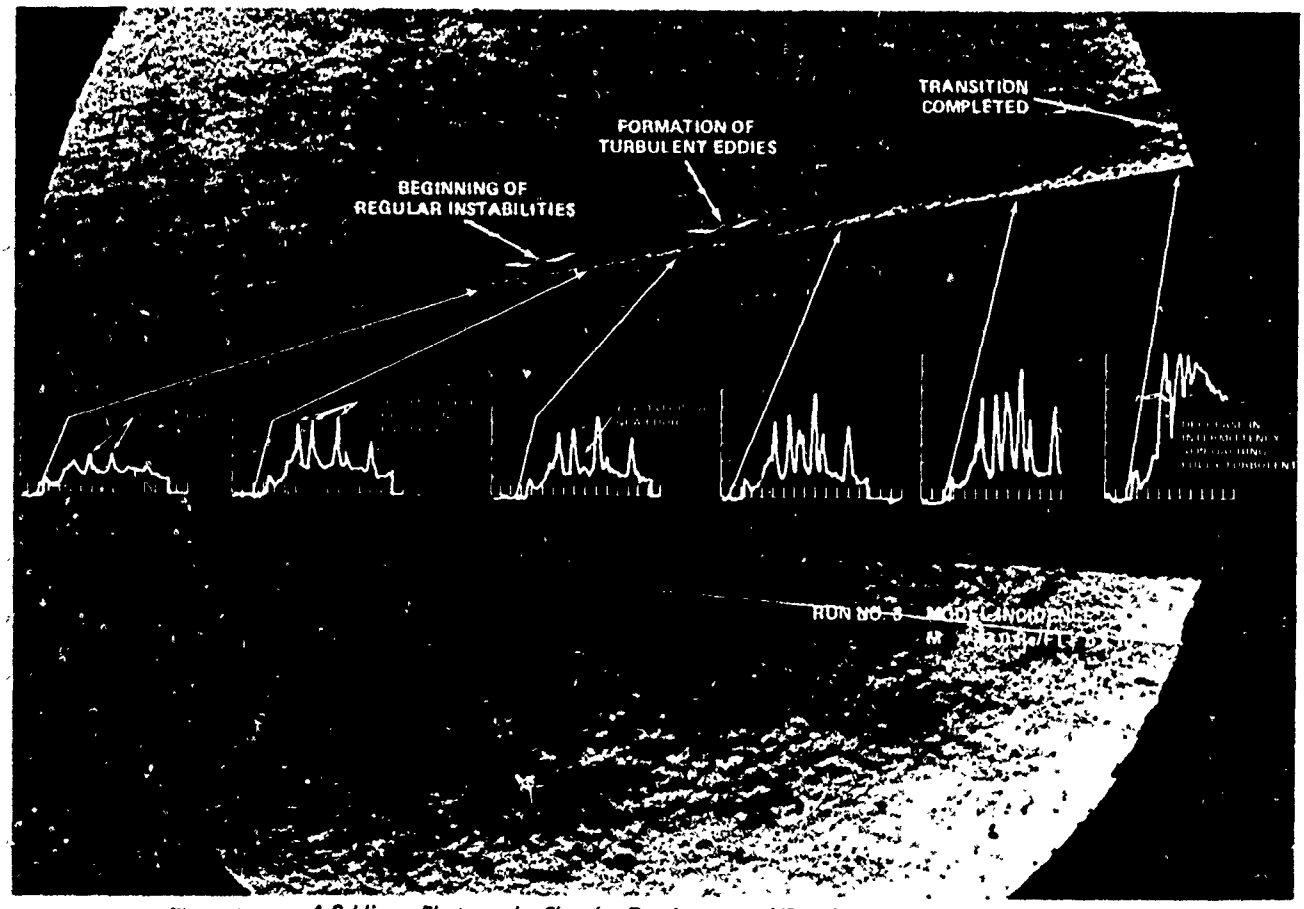

Figure 24 A Schlieren Photography Showing Development of Transition of a Conical Boundary Layer in Hypersonic Flow (Ref. 57)

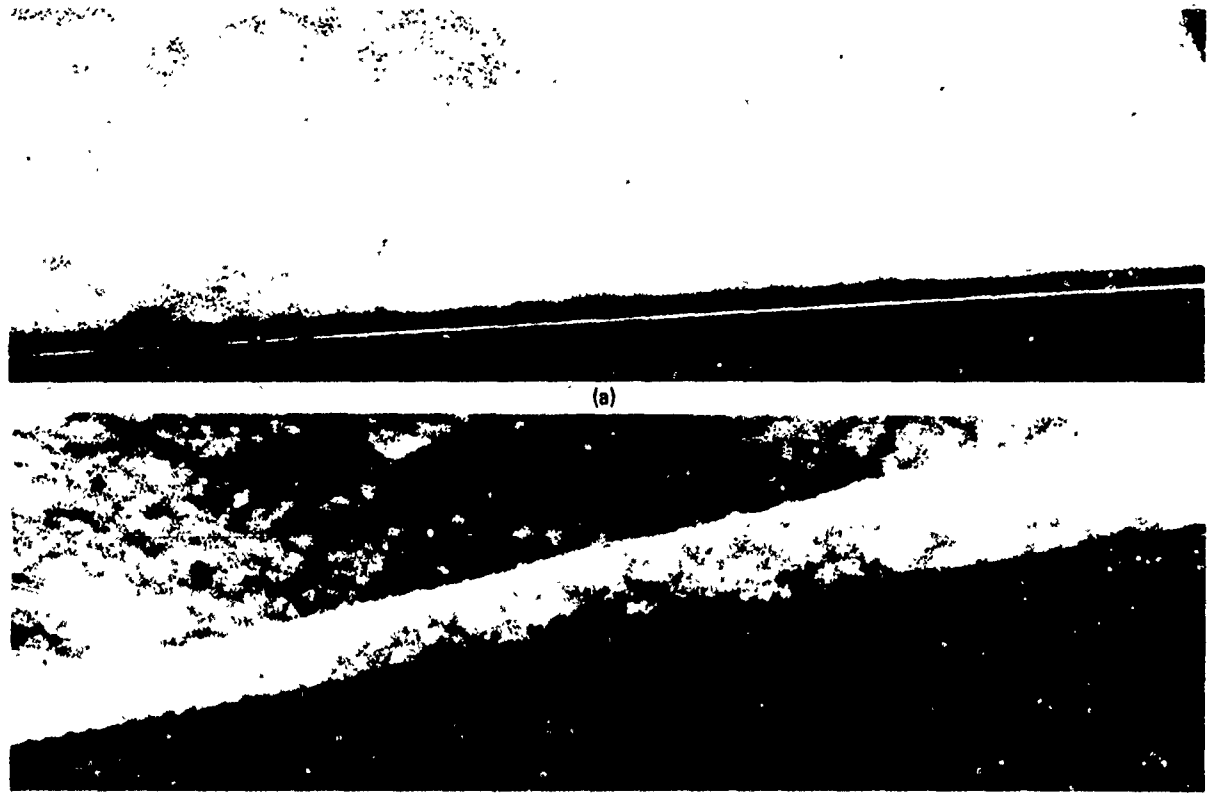

(a)

(b)

Figure 25 Schlieren Photographs of "Wave-Like" Instabilities (Ref. 57)

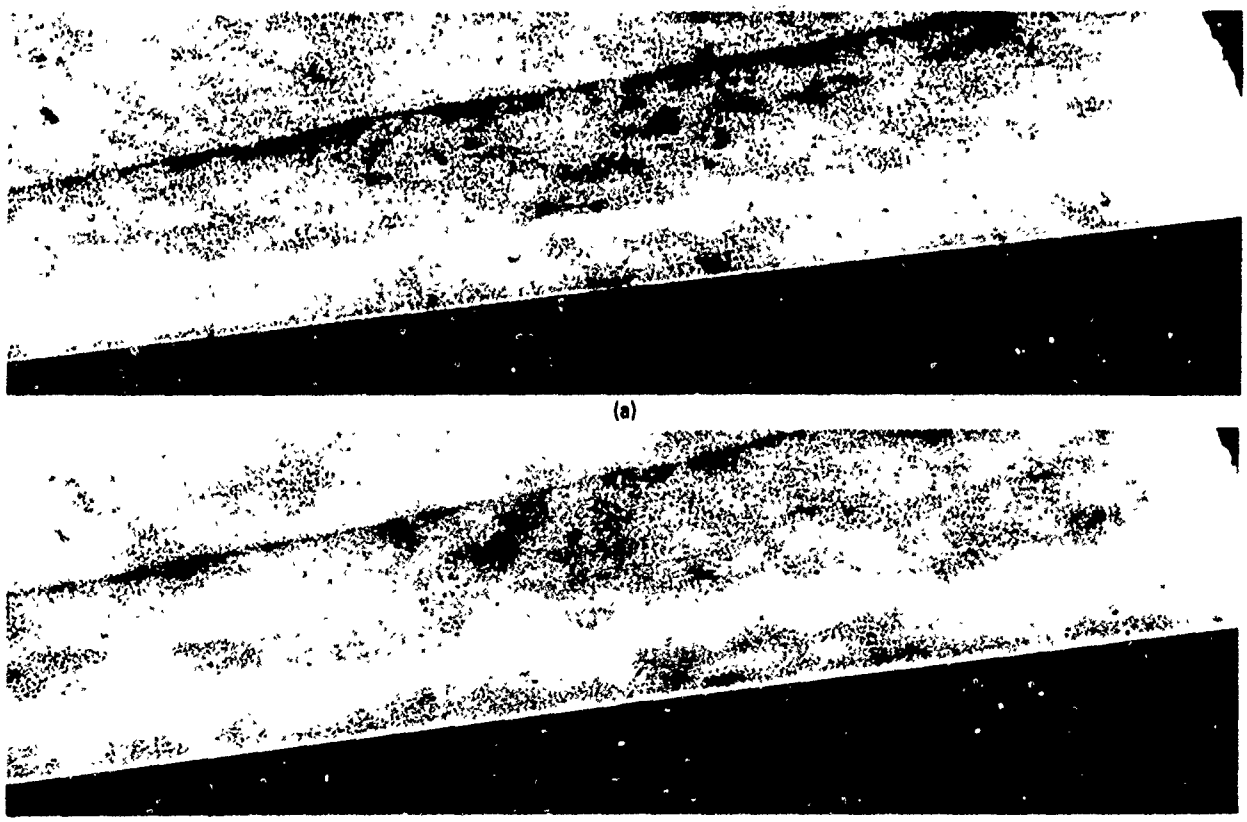

(a)

(b)

Figure 26 Schlieren Photographs of Gross-Instability Region (Ref. 57)

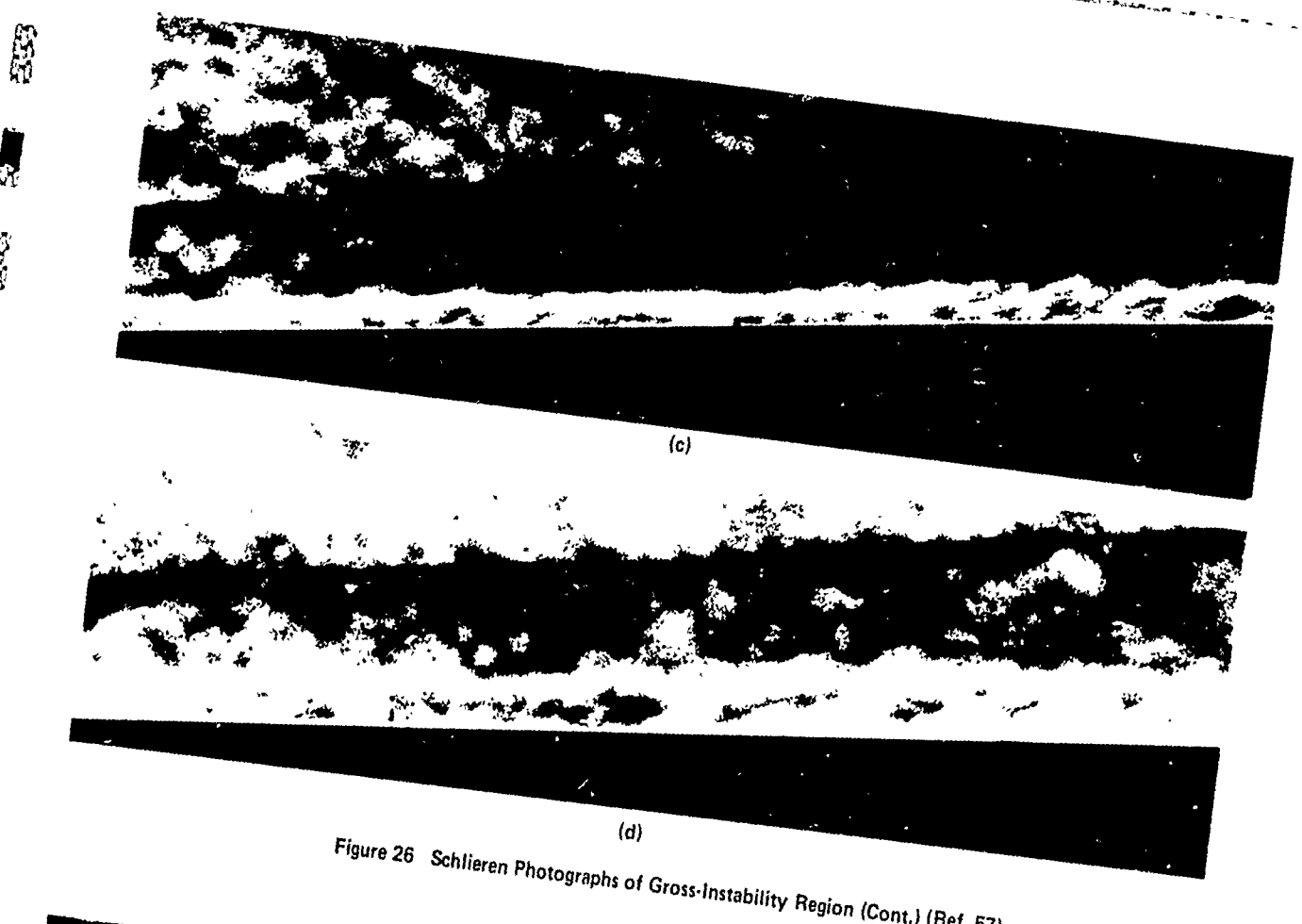

(c)

(d)

Figure 26 Schlieren Photographs of Gross-Instability Region (Cont.) (Ref. 57)

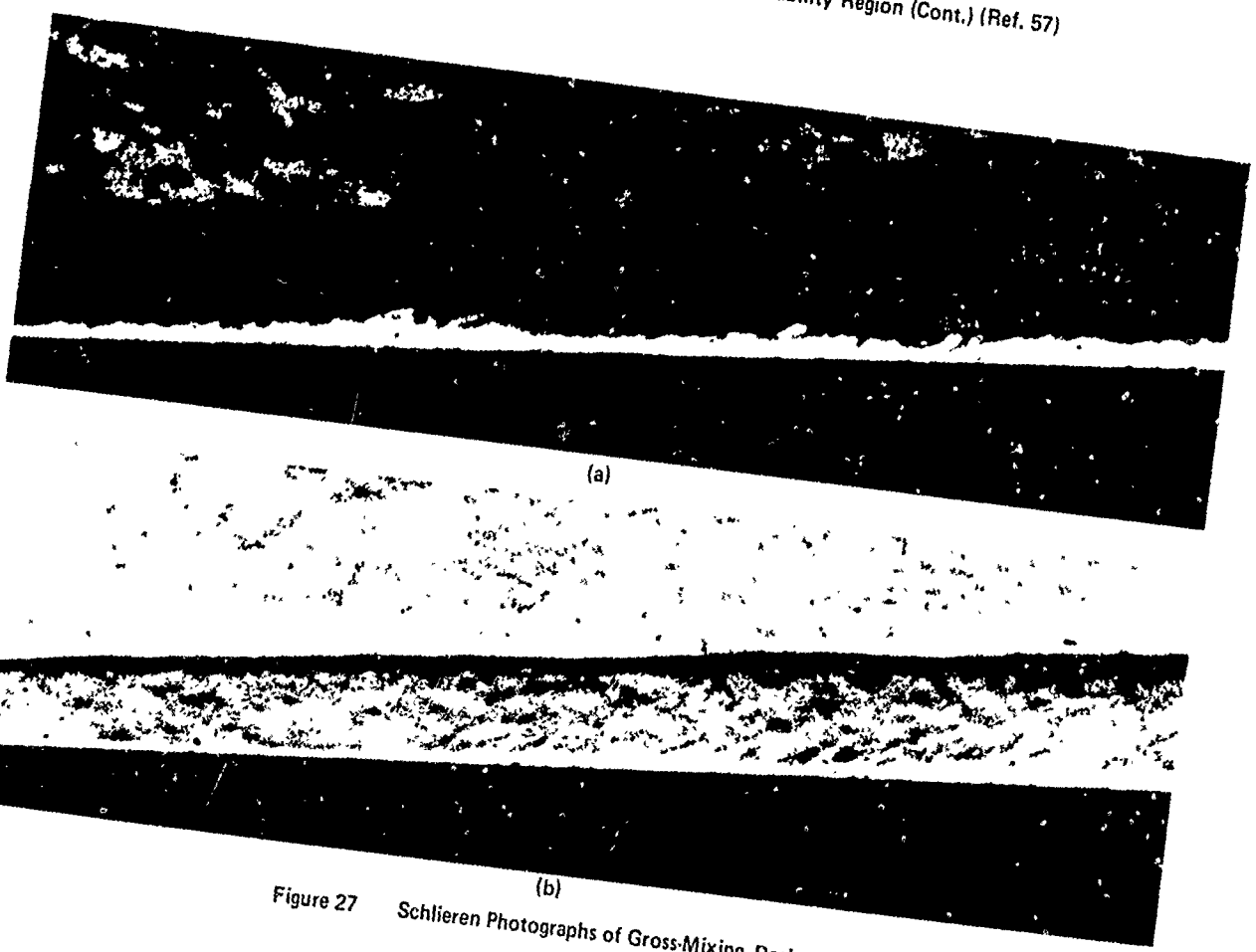

(a)

(b)

Figure 27 Schlieren Photographs of Gross-Mixing Region (Ref. 57)

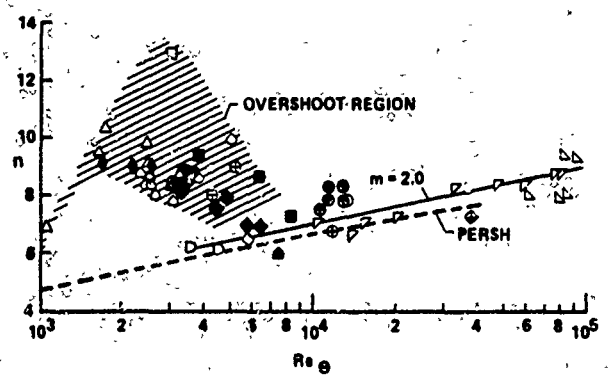

Figure 28 Variation of n with Re_θ for Flat Plates, Cones, and Hollow Cylinders (Ref. 61)

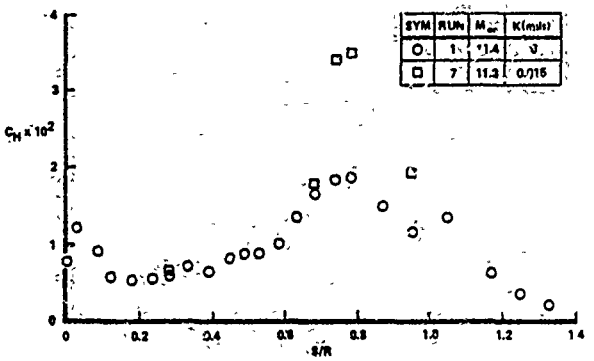

Figure 31 Influence of Surface Roughness on the Heating Distribution ($M = 11.4$ $Re_D = 12 \times 10^6$)

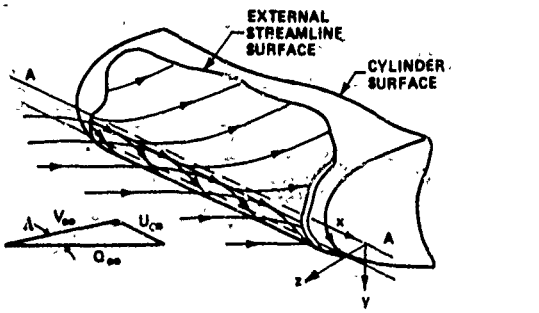

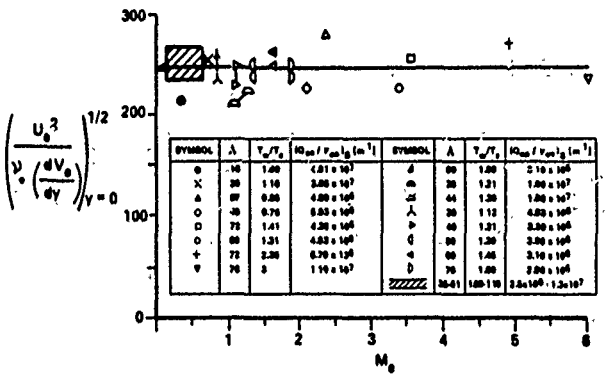

Figure 29 Dependence of R_* Upon Edge Mach Number For Rough Surfaces, After Poll (Ref. 44)

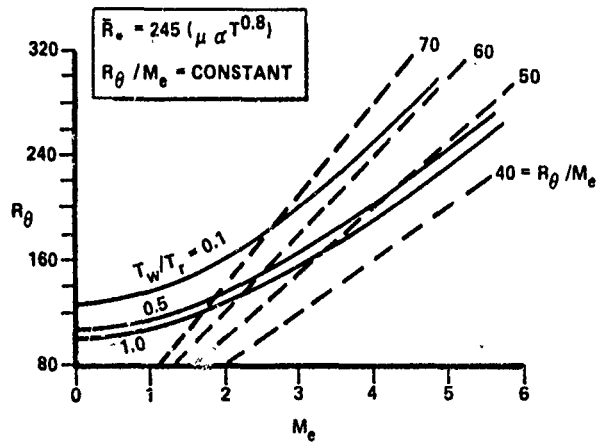

Figure 30 Transition Correlation on Rough Leading Edge, After Poll (Ref. 44)

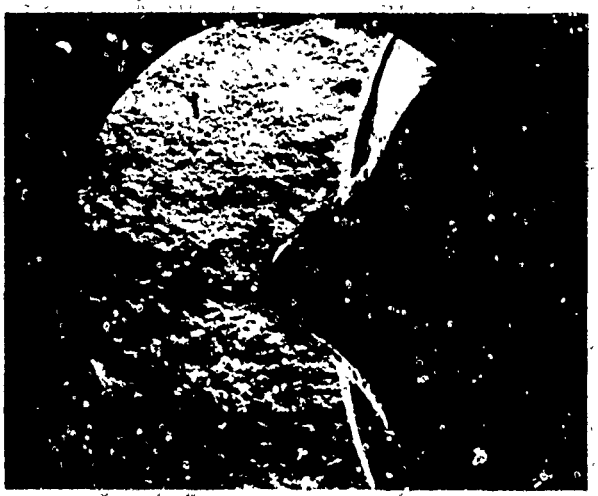

(a) K = 0

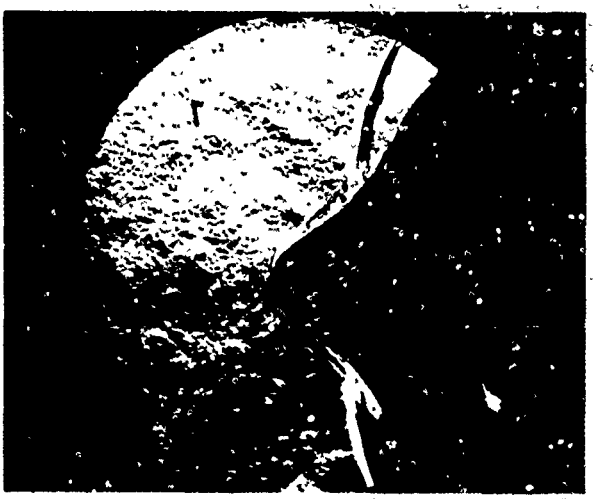

(b) K = 15 MILS

Figure 32 Influence of Surface Roughness on the Flow Field on Indented Nosetips (Ref. 61)

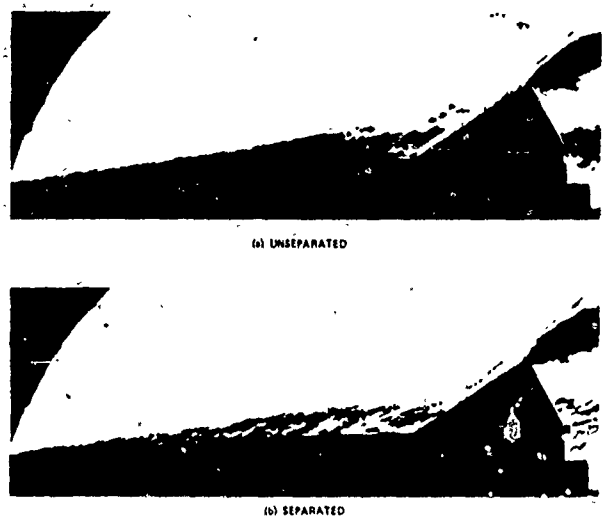

Figure 33 Flow Over the Rough MRV Configuration With a 30^{0} Flap Deflection

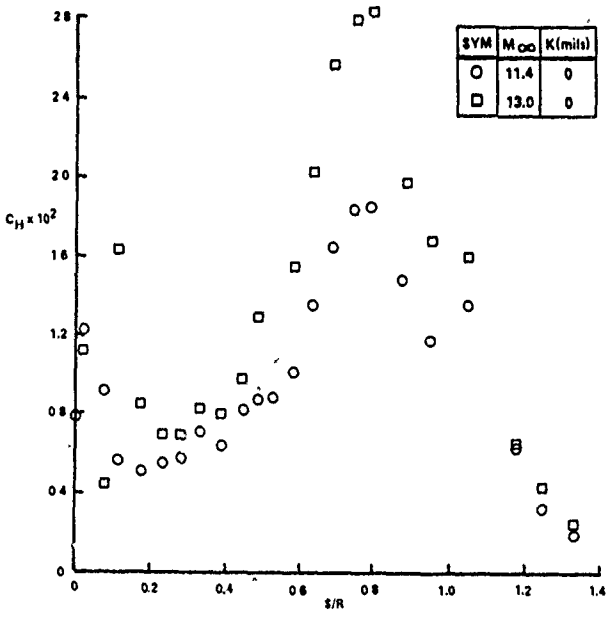

Figure 34 Influence of Mach Number on the Distribution of Heating to the Smooth Model

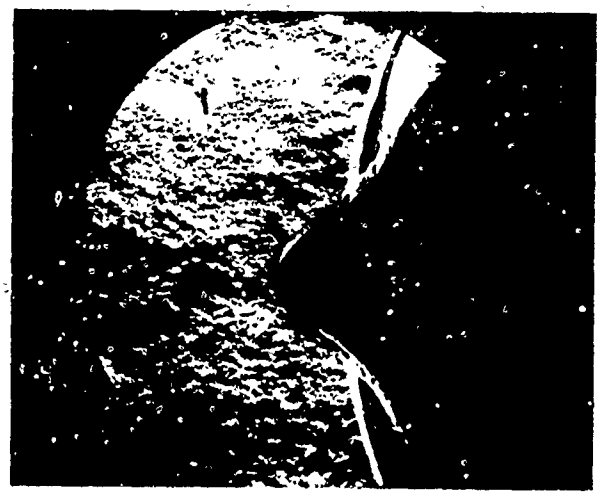

(a) MACH 11

(b) MACH 13

Figure 35 Effects of Mach Number on Flow Pattern Over the Indented Nosetips (Ref. 61)

Figure 36 Installation of NRV Heat Transfer and Pressure Model in 96" Shock Tunnel

Figure 37 Schlieren Photograph of the Flow Over the NRV Heat Transfer and Pressure Model (M = 11.3 Re/FT = 10 x 10^6)

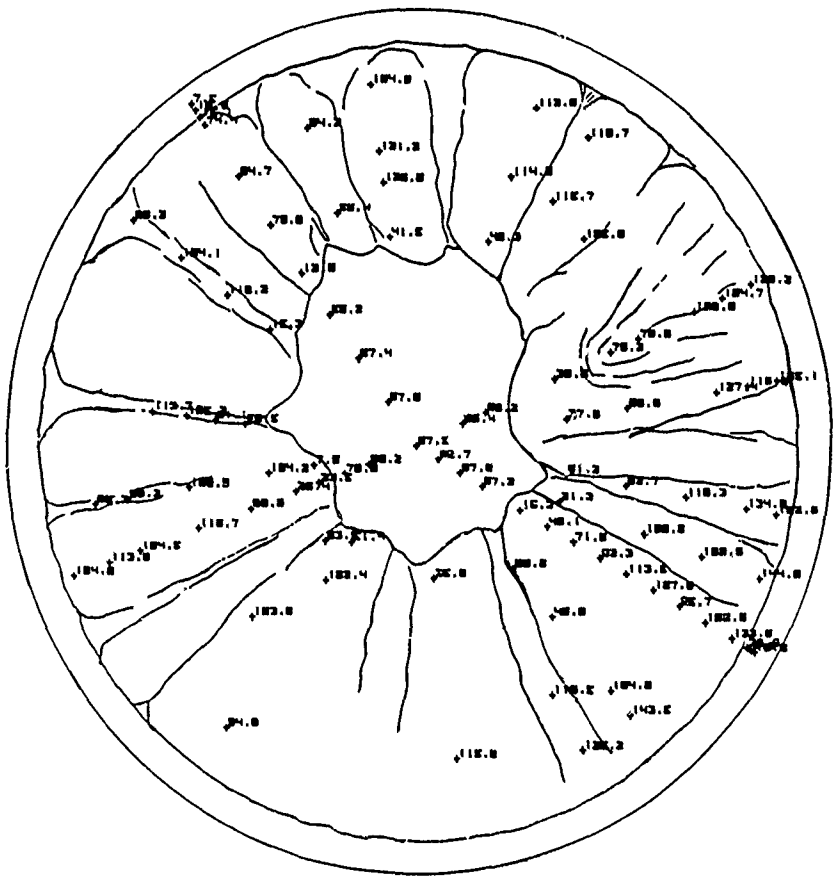

Figure 38 Heat Transfer Distribution Over the NRV Configuration – M = 11, Re/FT = 10 x 10^6, $\alpha = 0^o$ (Ref. 57)

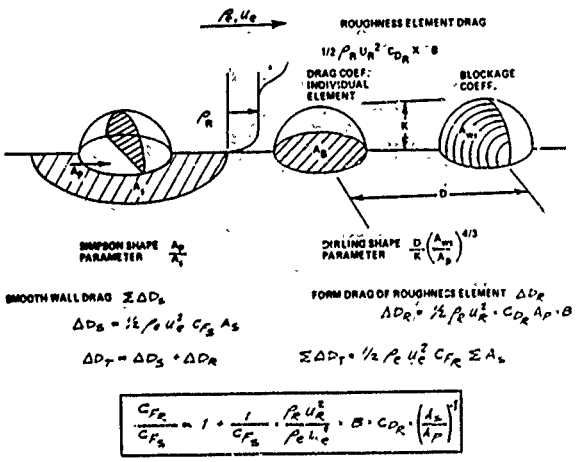

Figure 39 Simplified Drag Model for Rough-Wall Skin Friction

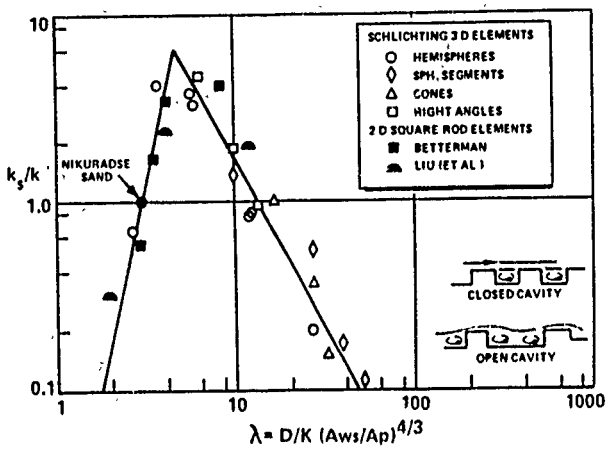

Figure 40 "Effective" Roughness Correlations For Differing Roughness Geometries and Spacings

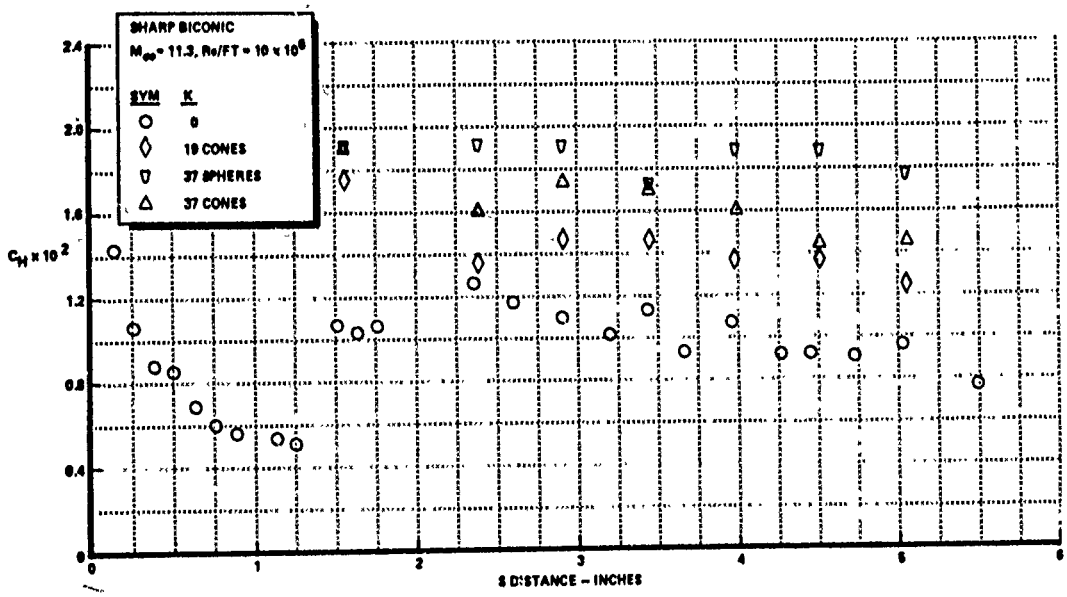

Figure 41 Heat Transfer Measurements on the Sharp Biconic Configuration Showing the Importance of Roughness Shape and Spacing Effects on Roughness-Induced Augmentation Heating (Ref. 61)

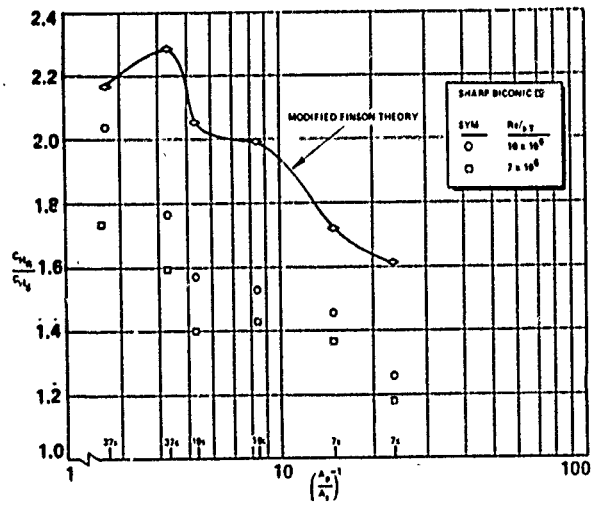

Figure 42 Correlation of Patterned Roughness Heating on Sharp Biconic Nosetips in Terms of Effective Windward Area (A_p/A_s)

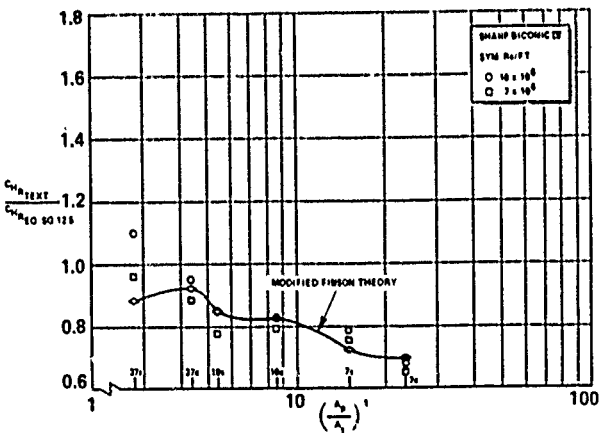

Figure 43 Correlation of Effective Roughness Heating Parameter For Sharp Biconic Nosetips in Terms of the Effective Windward Area Parameter (A_p/A_s)

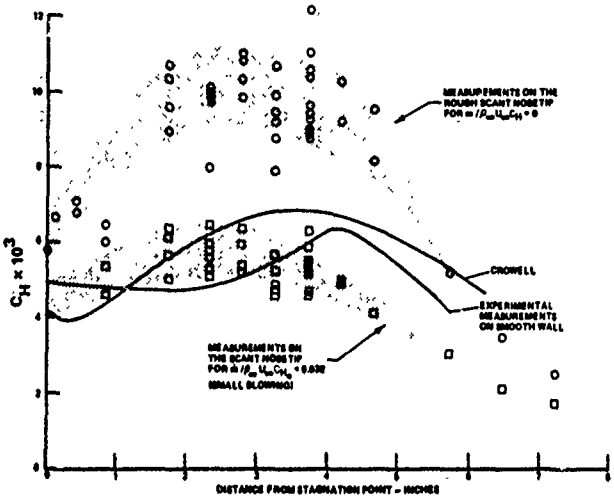

Figure 44 Heat Transfer Measurements on Scant and Smooth Hemispherical Nosetip Showing How Small Blowing Brings Down Heating Levels To Smooth-Wall Values

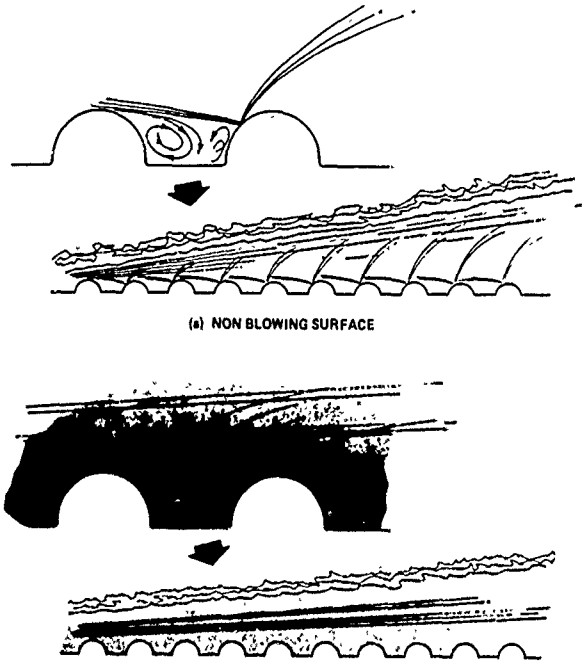

Figure 46 Schematic Diagrams of the Flow Structure Between and Above the Roughness Elements on Blowing and Non-Blowing Surfaces

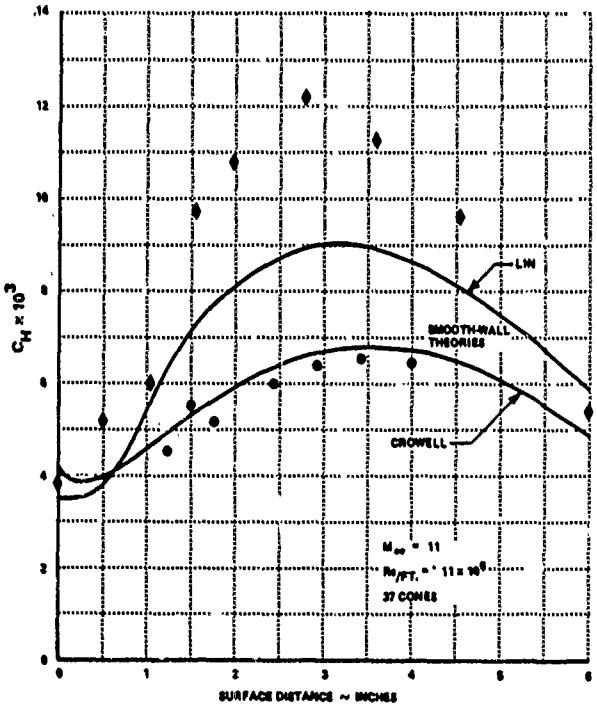

Figure 45 Comparison Between the Turbulent Theories of Lin & Crowell for Smooth-Wall and Rough-Wall Measurements of Holden on 12" Diameter Hemisphere (M = 11.2, Re_D = 11 x 10^6, K = 12.5)

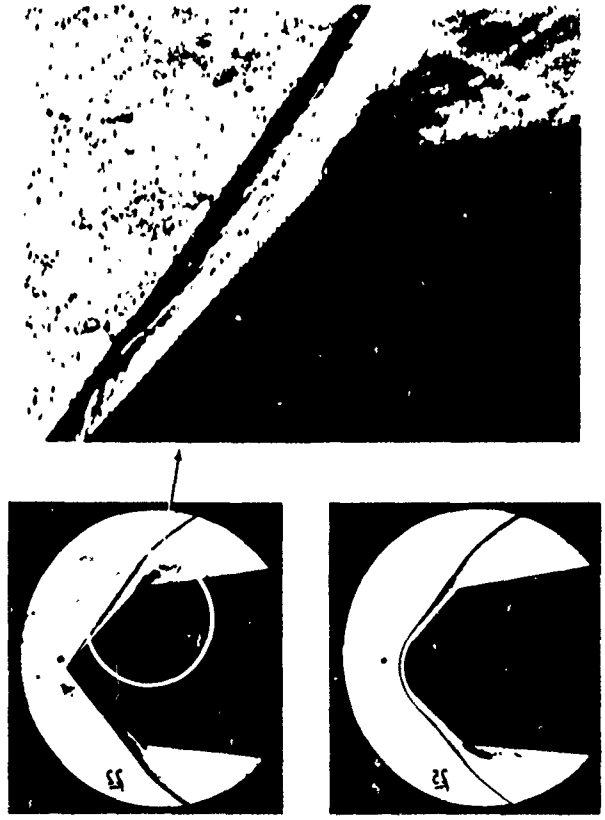

Figure 47 Schlieren Photographs of the Flow Over the Sharp Biconic Nosetip Showing the Individual Shocks for the Roughness Elements (Ref. 61)

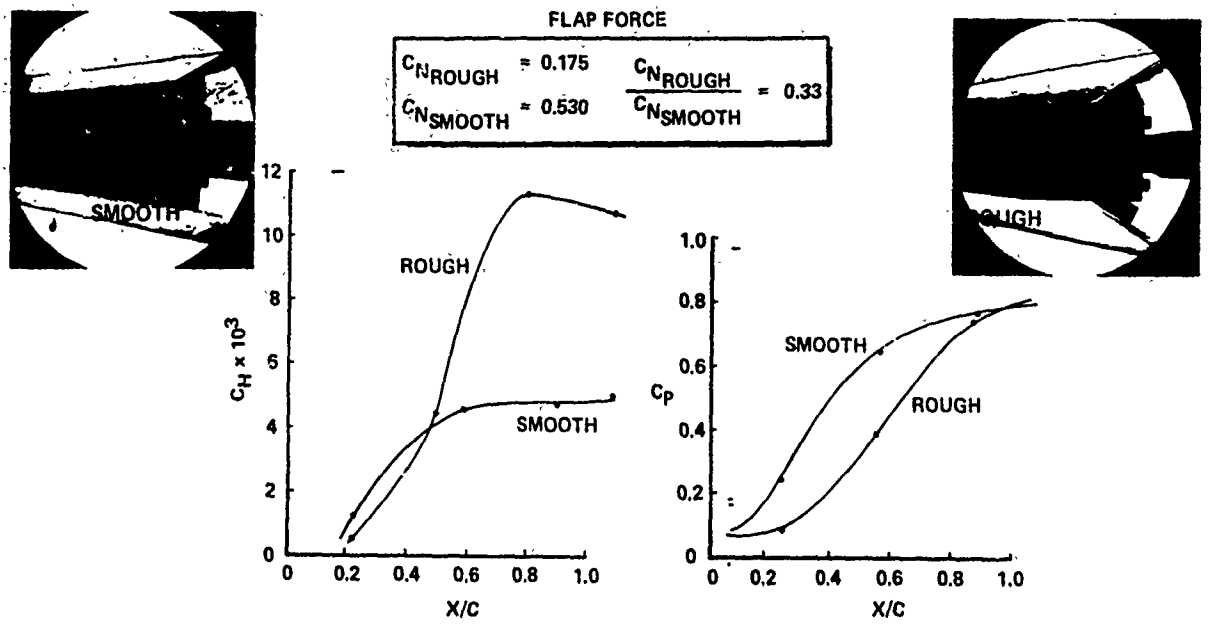

Figure 48 Effect of Surface Roughness on Flap Forces, Heating and Pressure

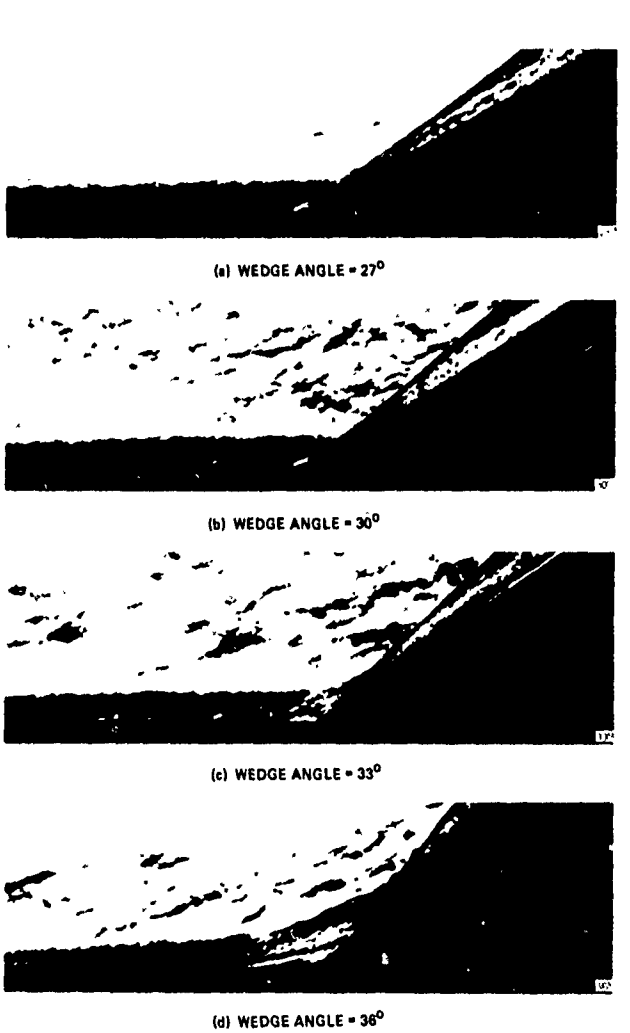

(a) WEDGE ANGLE = 27°

(b) WEDGE ANGLE = 30°

(c) WEDGE ANGLE = 33°

(d) WEDGE ANGLE = 36°

Figure 49 The Development of a Wedge-Induced Separated Flow (M_∞ = 8.6 Re_L = 22.5 x 10^6) (Ref. 75)

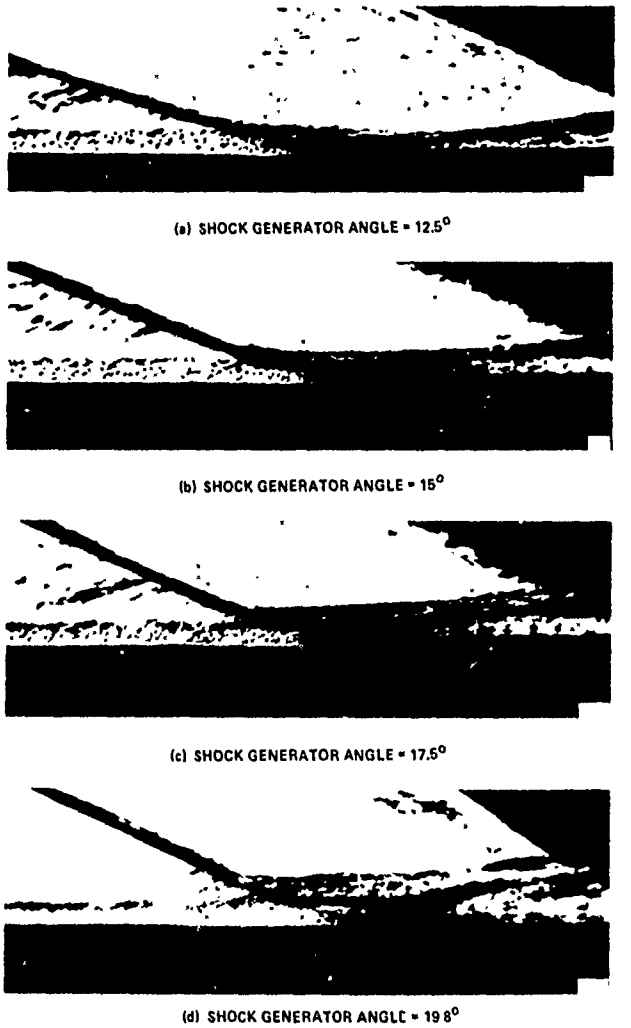

(a) SHOCK GENERATOR ANGLE = 12.5°

(b) SHOCK GENERATOR ANGLE = 15°

(c) SHOCK GENERATOR ANGLE = 17.5°

(d) SHOCK GENERATOR ANGLE = 19.8°

Figure 50 The Development of a Shock-Induced Separated Flow (M_∞ = 8.6 Re_L = 22.5 x 10^6) (Ref. 75)

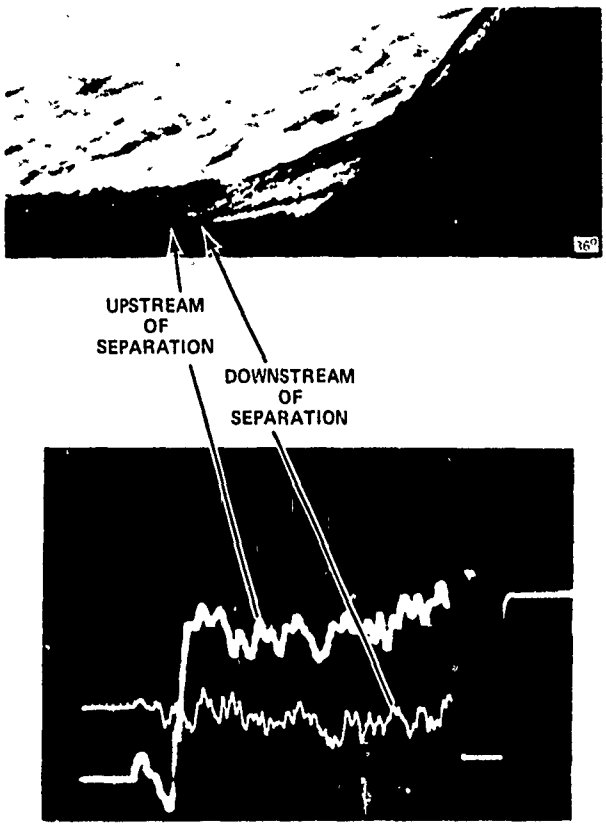

Figure 51 Output From Skin Friction Gages in the Separation Region

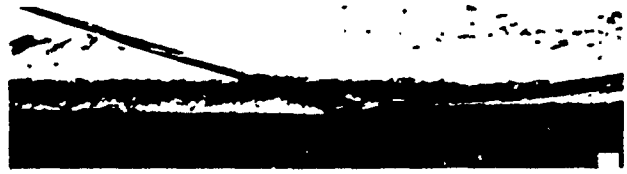

Figure 53 Incipient Separation at Mach 6.5 and $R_{e_L} = 27 \times 10^6$

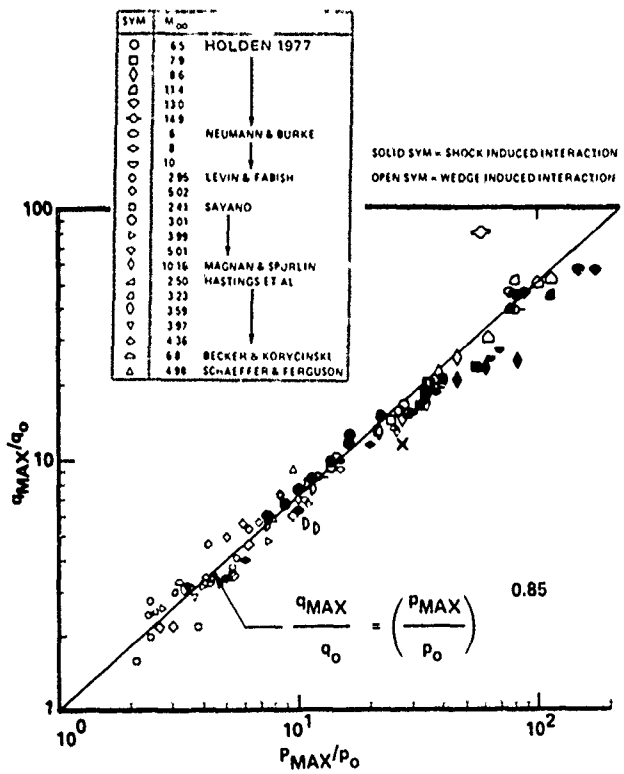

Figure 52 Correlation of Maximum Heating Rate in Wedge - And Externally-Generated Shock-Induced Turbulent Separated Flows (Ref. 75)

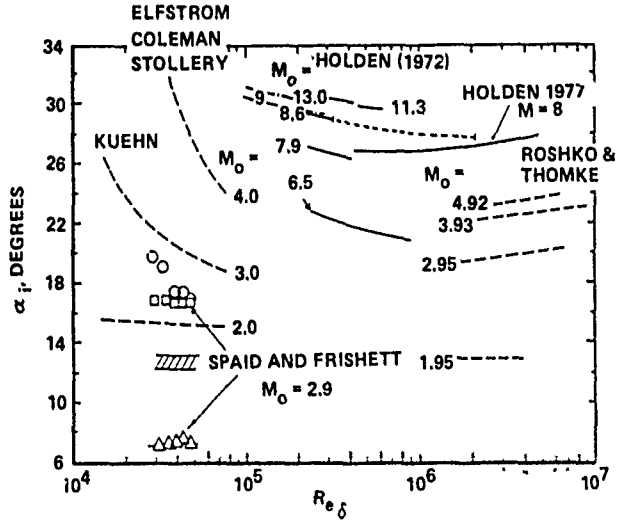

Figure 54 Wedge Angle to Induce Incipient Separation

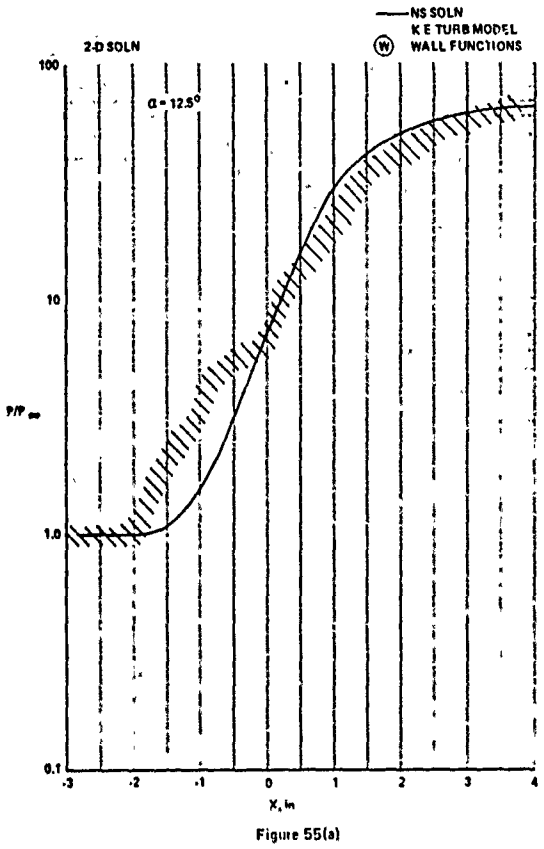

Figure 55(a)

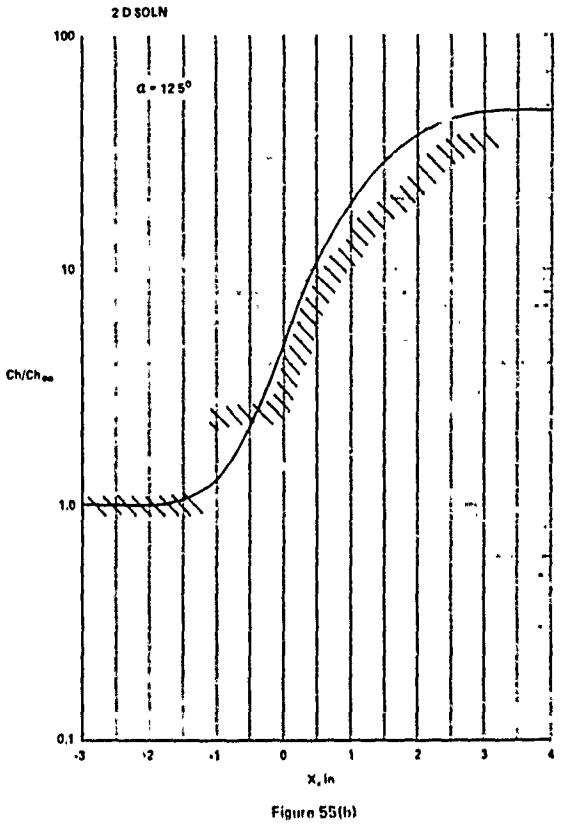

Figure 55(b)

Figure 55 Comparison Between Navier-Stokes Solution and Experiment for a Mildly Separated Flow

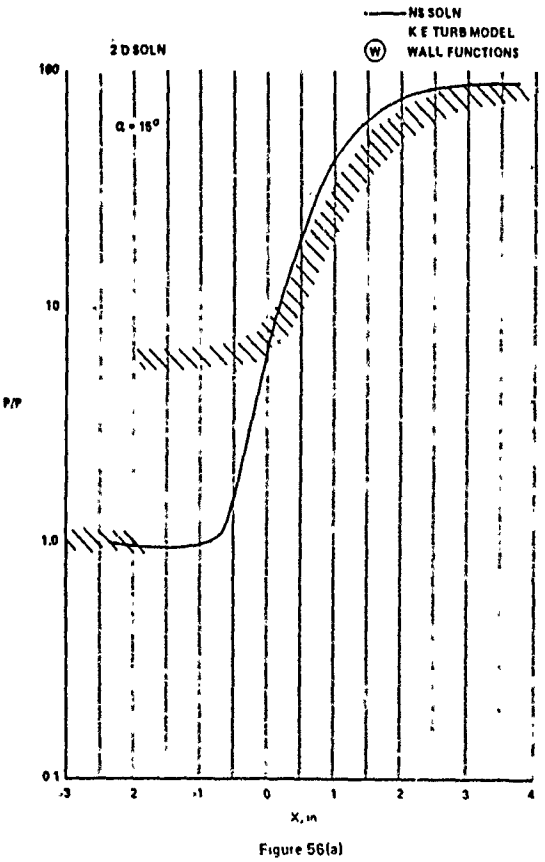

Figure 56(a)

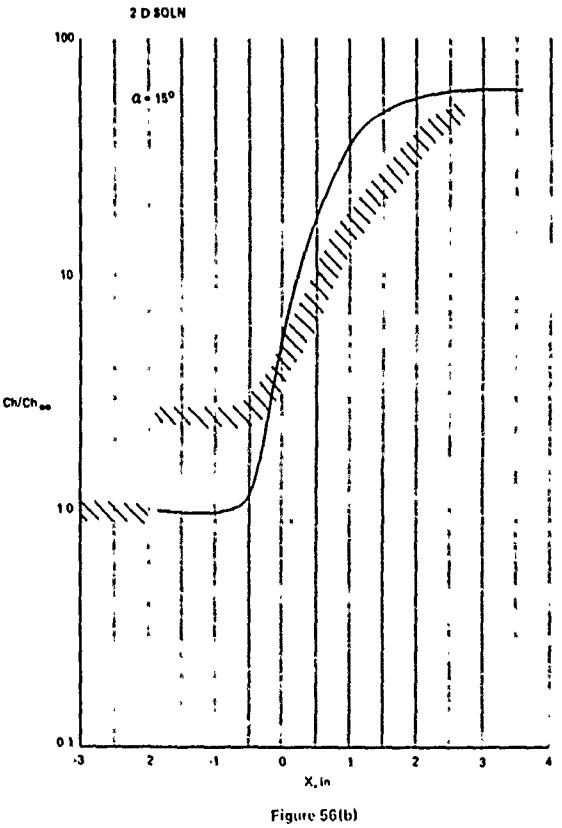

Figure 56(b)

Figure 56 Comparison Between Navier-Stokes Solution and Experiment for a Well Separated Flow

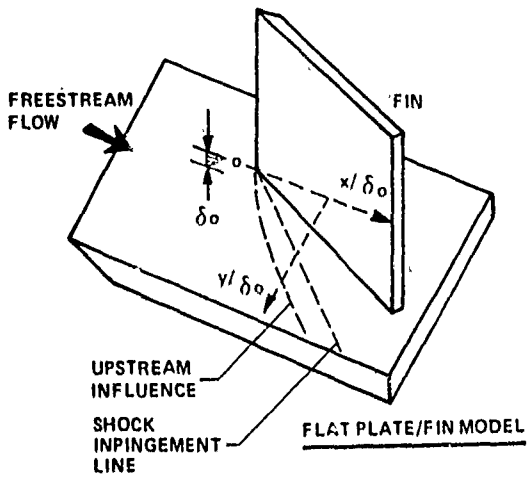

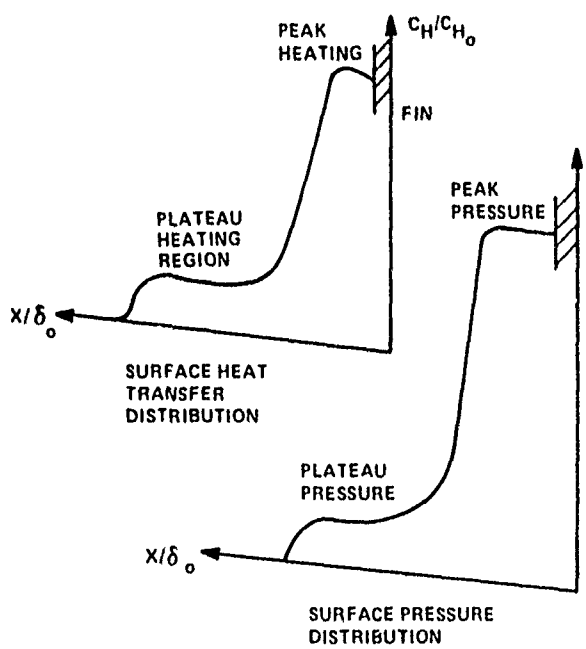

Figure 57 Typical Surface Heating and Surface Pressure Distributions Through Swept Shock/Turbulent Boundary Layer Interaction

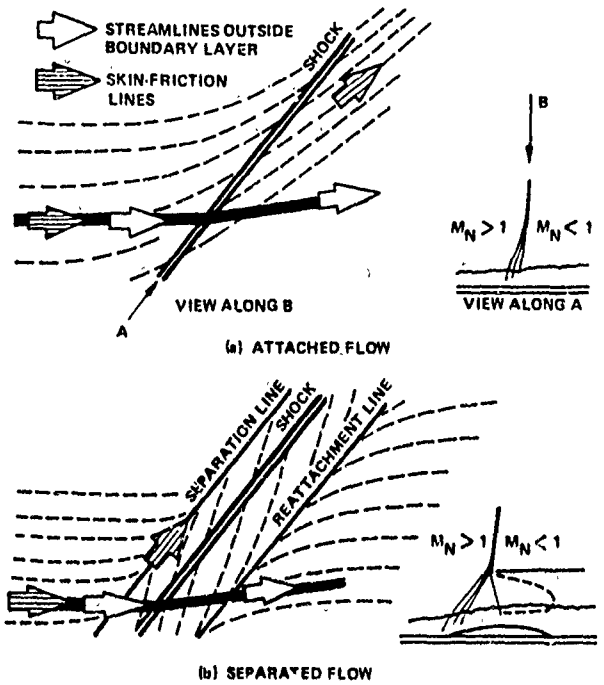

Figure 58 Schematic Representation of Attached and Separated Regions in Swept-Shock/Boundary Layer Interactions

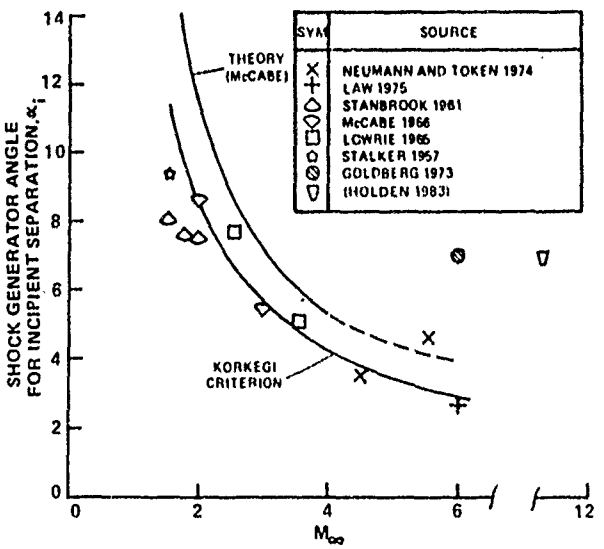

Figure 59 Variation of Shock Generator Angle to Induce Incipient Separation with Mach Number (Ref. 56)

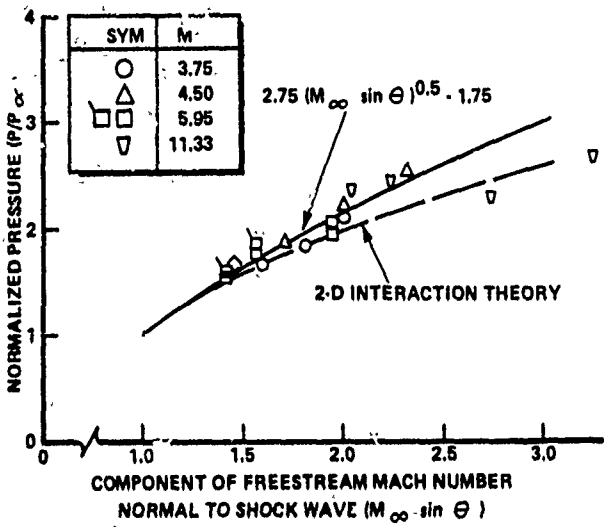

Figure 60 Correlation of Plateau Pressure Measurement From Swept-Shock Interaction Studies (Ref. 106)

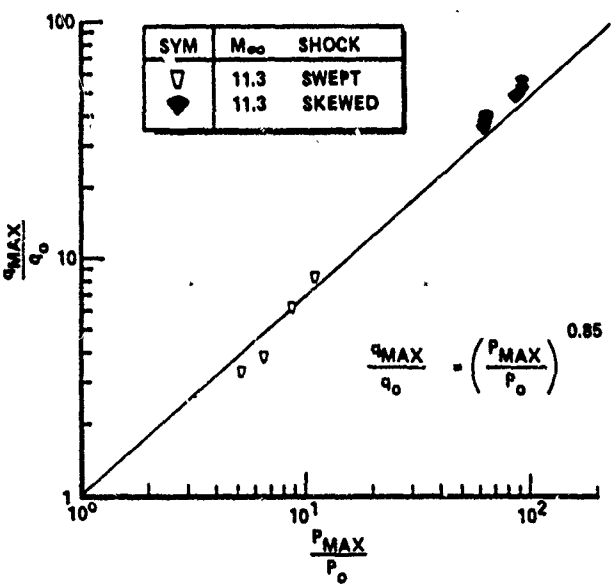

Figure 61 Correlation of Peak Heating Rates in Skewed- and Swept-Shock Interaction Regions

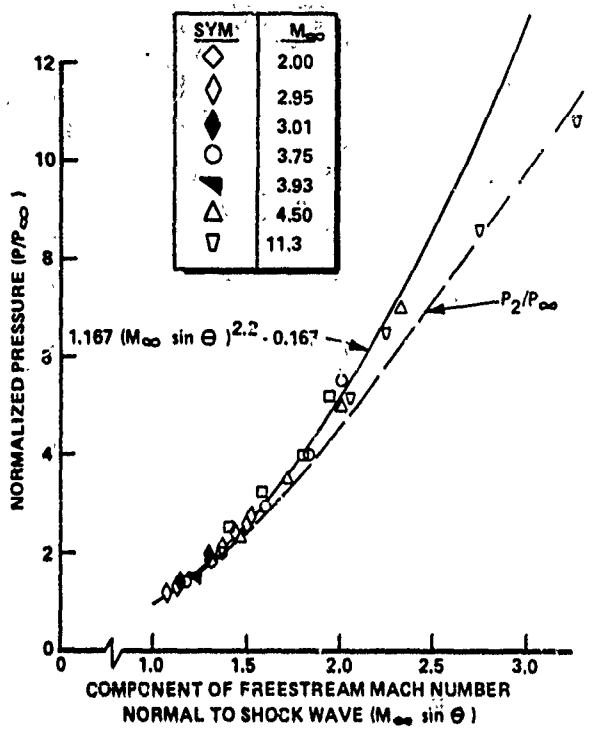

Figure 62 Correlation of Maximum Pressures Recorded in Swept-Shock Interaction Regions

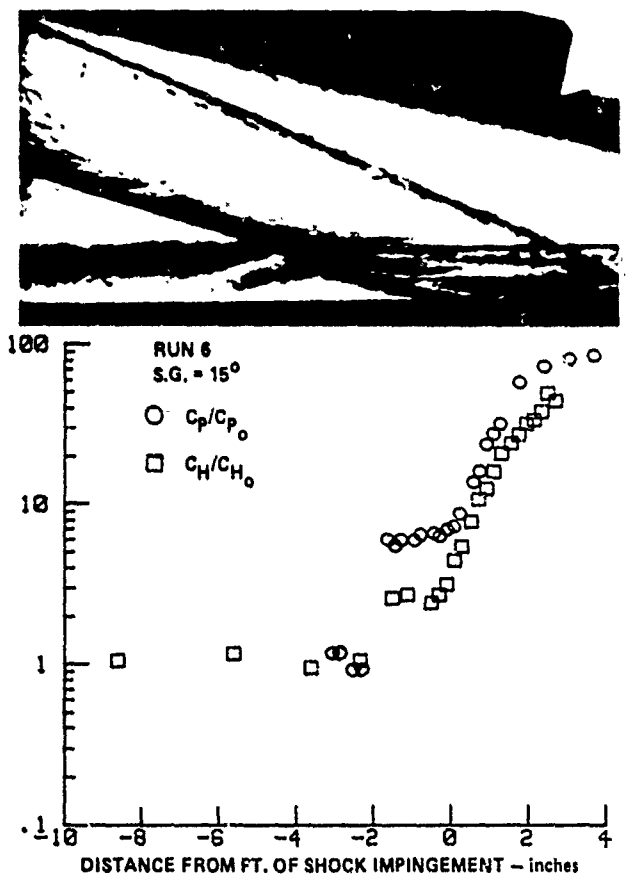

Figure 63 Streamwise Distributions of Heat Transfer and Pressure Through Skewed-Oblique-Shock Boundary Layer Interaction ($\theta = 15^{\circ}$ $\psi = 0^{\circ}$)

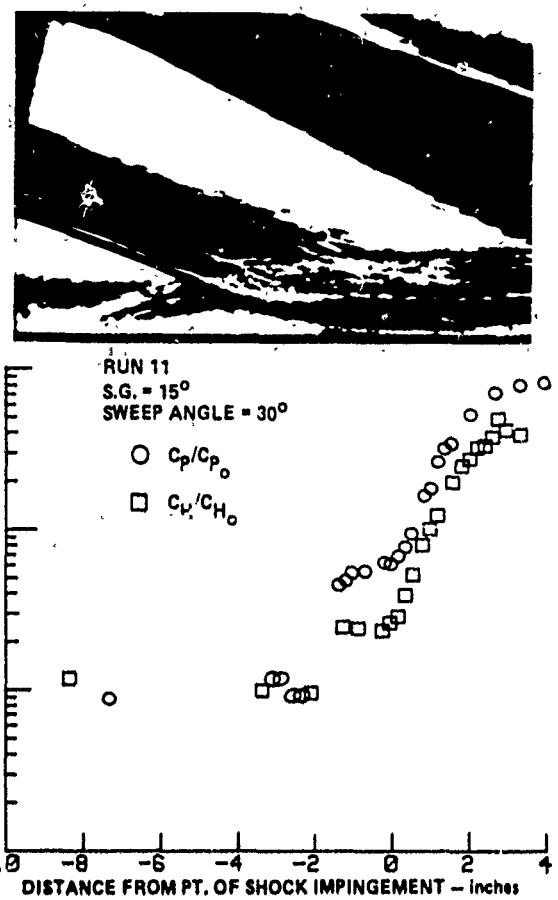

Figure 64 Streamwise Distribution of Heat Transfer and Pressure Through Skewed-Oblique-Shock Interaction ($\theta = 15^o$ $\psi = 30^o$)

SYM	GEN/WED	SOURCE	Re_x
○	16°	SETTLES, PERKINS AND BOGDONOFF	18.7×10^6
□	16°	↓ (M = 3)	10.7×10^6
◇	12.5°	HOLDEN STUDY	50×10^6
△	15°	↓ (M = 11)	50×10^6

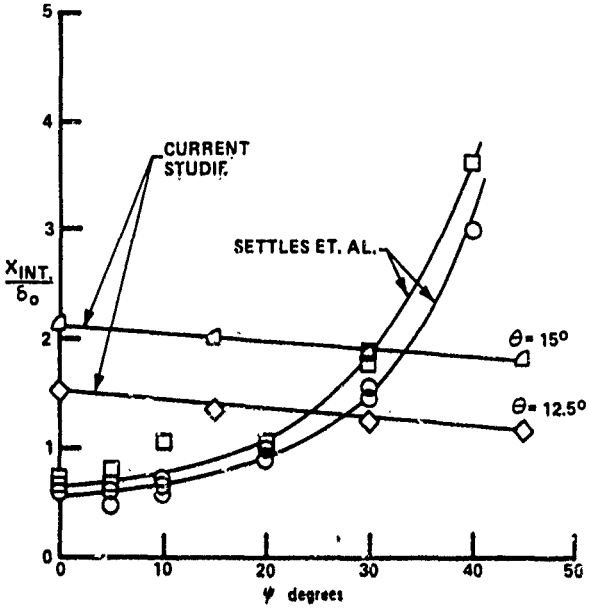

Figure 65 Variation of Streamwise Extent of Interaction Ahead of Shock Impingement (or Corner) with Sweep Angle (Ref. 106)

Figure 66 Damage Resulting From Shock Impingement on Vertical Support

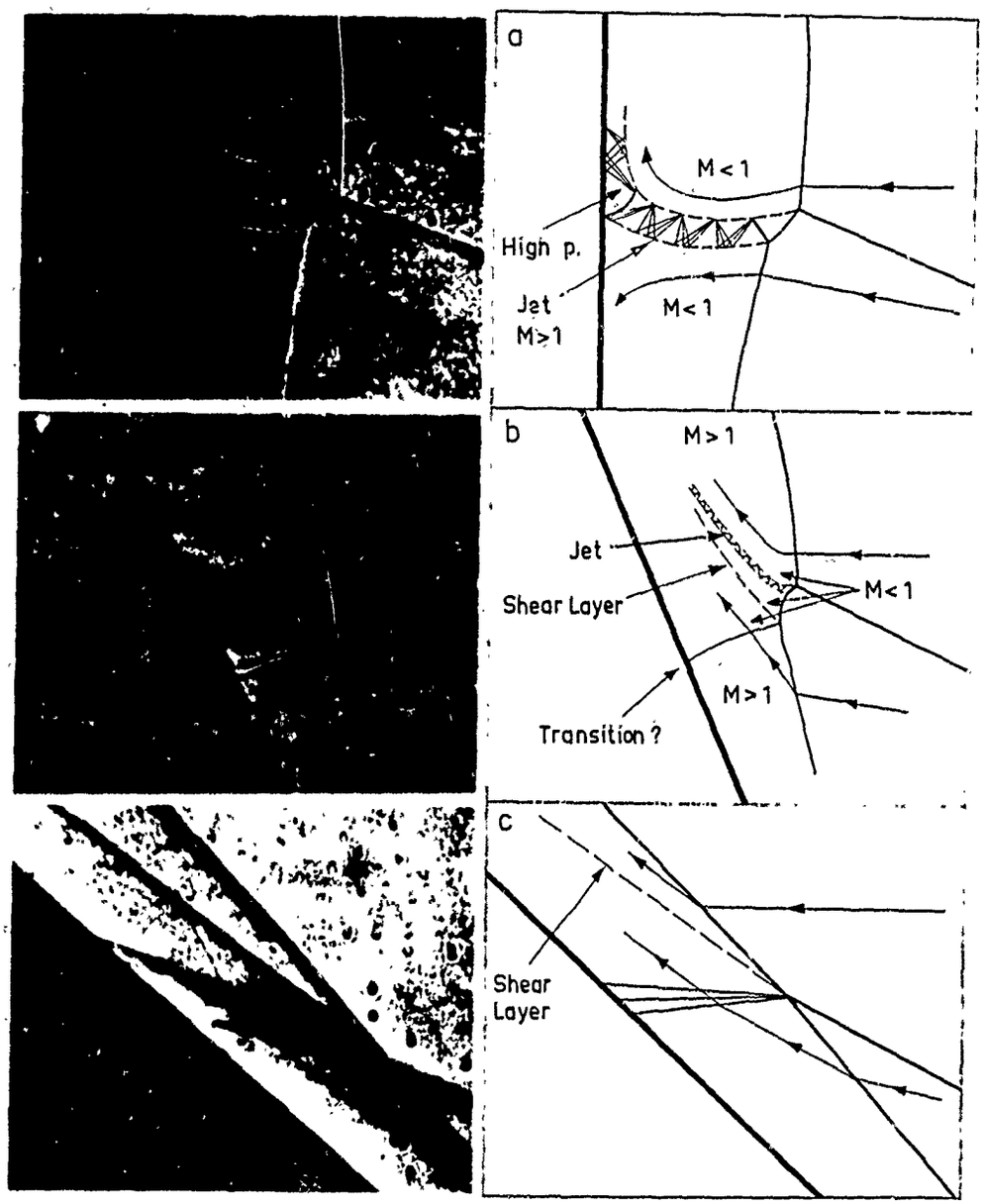

Figure 67 Edney's Photographs Showing the Effect of Varying Sweep Angle of Cylindrical Fin. a. Type IV Interference. b. Type V Interference. c. Type VI Interference. M = 4.6 $\xi = 5^{o}$ (Ref. 117)